



HAL
open science

GANIL Scientific Annual Report 2023

P. Roussel-Chomaz, Fanny Farget

► **To cite this version:**

P. Roussel-Chomaz, Fanny Farget. GANIL Scientific Annual Report 2023. GANIL. 2024. hal-04780854

HAL Id: hal-04780854

<https://hal.science/hal-04780854v1>

Submitted on 13 Nov 2024

HAL is a multi-disciplinary open access archive for the deposit and dissemination of scientific research documents, whether they are published or not. The documents may come from teaching and research institutions in France or abroad, or from public or private research centers.

L'archive ouverte pluridisciplinaire **HAL**, est destinée au dépôt et à la diffusion de documents scientifiques de niveau recherche, publiés ou non, émanant des établissements d'enseignement et de recherche français ou étrangers, des laboratoires publics ou privés.

Public Domain



GANIL

**GRAND ACCÉLÉRATEUR
NATIONAL D'IONS LOURDS**

Scientific annual report

2023



CONTENTS

01 INTRODUCTION	5
I. A FEW WORDS FROM THE GANIL MANAGEMENT	5
II. KEY NUMBERS	7
III. COMMUNICATION AND OUTREACH	9
IV. ENVIRONMENTAL REPORT	11
V. ACTIVITIES IN TECHNOLOGICAL TRANSFER	13
02 SCIENTIFIC RESEARCH	15
I. STRUCTURE, ASTROPHYSICS, REACTION AND SPECTROSCOPY	17
II. PHYSICS OF HEAVY AND SUPERHEAVY NUCLEI	20
III. FISSION AND REACTIONS	23
IV. FUNDAMENTAL INTERACTIONS AND DARK SECTORS	26
V. DOSIMETRY, APPLICATIONS AND NUCLEAR DATA	28
VI. CIRIL	30
03 OPERATION, TECHNOLOGICAL RESEARCH AND DEVELOPMENT	31
I. EXECUTIVE SUMMARY OF ACCELERATOR AND EXPERIMENTAL AREAS OPERATION	33
II. ION BEAM AND RADIOACTIVE ION BEAM DEVELOPMENTS	37
III. PHYSICS OF ACCELERATORS	41
IV. EQUIPMENTS FOR BEAM ACCELERATION, TRANSPORT AND DIAGNOSTICS	45
V. AUTOMATS AND COMMAND CONTROL	48
VI. ACHIEVEMENTS IN MECHANICS	51
VII. DETECTION AND LASER FOR PHYSICS	54
VIII. DATA ACQUISITION	59
IX. MANAGEMENT AND ORDERING OF INSTALLATIONS	61
X. STATUS OF SCIENTIFIC AND ACCELERATOR PROJECTS	63
04 EXPERIMENT REPORTS	73
I. NFS	75
II. VAMOS	95
III. LISE	99
IV. D1-HE	109
V. D1-SME	115
VI. IRRSUD	125
VII. ARIBE	145
05 ANNEXES	163
I. PUBLICATION LIST	165
II. CONFERENCE LIST	171
III. COMMITTEES	172
IV. ORGANISATION CHART	181



40th GANIL anniversary

I. A few words from the GANIL management

Forty years after the first experiment, a new dynamic is shaping GANIL.

A large renovation program for the cyclotrons (CYREN) has been proposed in 2022 for a realization in the years to come, strengthening a long-term future of the cyclotron scientific program. In June 2023, the Minister of Research and High Education confirmed the interest in maintaining GANIL installation at the fore-front level, allocating a dedicated significant budget. This long-term commitment supports for a great part the exotic beams of SPIRAL1, which are of the outmost importance for the DESIR hall, of which the construction site was inaugurated in 2023 after the official authorization.

The beam-line for the transport of exotic beams of SPIRAL1 to DESIR has been assembled and tested before its future implementation planned in 2025.

CYREN is already going on with a new prototype validated for the power supplies of the magnets and a refurbishment of the CSS1 vacuum system.

Looking ahead, new beams are under development at GANIL.

On the side of cyclotrons, the newly accelerated ^{232}Th beam allowed to enlarge the domain of fission studies at VAMOS.

For the first time, ^8Li beam was provided at SPIRAL1, accelerated with CIME and decelerated in a dedicated installation in the G2 experimental hall to meet astrophysical nuclear reaction conditions. Further developments of SPIRAL1 beams are going-on to prepare for the future.

On the side of the LINAC, heavy-ion beams of Argon and Oxygen were accelerated through the 26 cavities of the LINAC and the ion-source has received a large program of optimization for its reliability and for recycling of the rare isotopes in the plasma chamber.

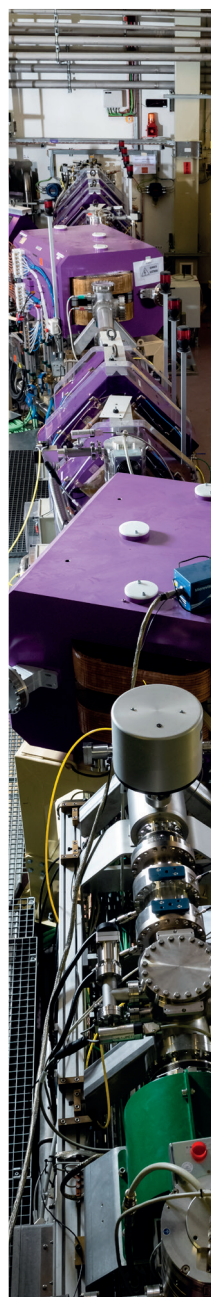
To prepare for a further enlargement of the heavy ion beams accelerated by the LINAC, and increase their intensities, NEWGAIN project entered its construction phase.

Preparing for the parallel operation of the LINAC and the cyclotrons, the LINAC was tuned for the first time in the main control room, and the cryogenic system of EXOGAM detection set-up was doubled.

The LINAC beam diagnostics have followed in 2023 an important upgrade to adapt to the heavy-ion beams of S³. The rotating target station of S3 was tested, as well as SIRIUS, the instrumentation for the study of super-heavy isotope spectroscopy. S3-LEB completed its off-line commissioning and optimization of its performances, and prepared its moving to S3 hall.

In 2023, the GANIL nuclear physics scientific Community applied to more than 3500 hours of beam-time, and only half of these experiments could be approved, showing a strong request on the cyclotron and LINAC beams. The results of the previous experimental campaigns were intensively discussed during the GANIL colloquium in Soustons, in September 2023, where more than 100 participants contributed.

GANIL is proud to contribute to important scientific publications with high impact : more than 120 articles were published in 2023 related to GANIL experiments. GANIL is also contributing to young researchers training, in particular with more than 95 PhD theses presently under preparation based on data obtained at GANIL.



II. Key Numbers 2023

Resources

- State subsidy: 12,8M€
- Normandie Region: 1,2M€
- ANR: 2,8 M€
- Europe: 0,4 M€
- Other: 0,9 M€



Staff

300



Expenditures

- Operation: 10 M€
- Investment: 8,1 M€



Publications

121



Visitors

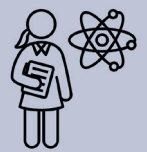
884

(general public)



Experimentation

301 Experimenters
103 Scientific visitors
5 Long-term visiting
scientists



Operating hours

Cyclotrons: 3046 h
LINAC: 1774 h
SPIRAL1: 167 h
Beam on target:
4600 h



Internships

38 interns
27 doctoral students
16 post-docs



Partners

6 international agreements
6 european contracts



Consumption

Electricity: 27 GWh
Gas: 2 GWh
Water: 20 000 m³



Accepted experiments

PAC: 241 UTs
IPAC: 416 UTs

(Acceptation rate: 58%)

Number of experiments

8 nuclear physics
48 interdisciplinary
physics
23 industrial
applications

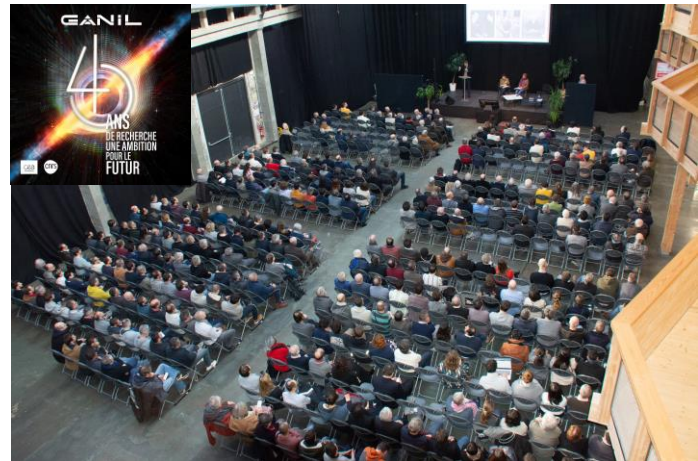


III. Communication and outreach

40th GANIL anniversary

March, 2nd

On March 2, 2023, GANIL celebrated 40 years of the laboratory's first experiment with more than 400 participants. This anniversary was an opportunity to celebrate a rich history of research at the dawn of a new phase in the development of scientific programs thanks to very intense ion and neutron beams.



Brochure on the DESIR public inquiry

April, 24th

GANIL produced a communication brochure for the public inquiry concerning the modification of INB 113 in order to include the DESIR project.

Ministerial visit to GANIL to address the development of future projects

June, 9th

On June 9, 2023, Sylvie Retailleau, Minister for Higher Education and Research, and Agnès Pannier-Runacher, Minister for Energy Transition, visited the GANIL facilities. On this occasion, Sylvie Retailleau announced €40 million for GANIL's projects funding, in particular the renovation of the cyclotrons (CYREN project) and the DESIR project, thanks to an investment made possible by the Research Programming Act. The NEWGAIN project will also benefit from this funding.



GANIL thesis prizes awarded to Chloé Fougères and Lukas Madauss

September, 28th

For the first time, two GANIL thesis prizes were awarded this year. The first went to Chloé Fougères for her thesis at GANIL under the supervision of François de Oliveira, entitled « Understanding the cosmic abundance of ^{22}Na : lifetime measurements in ^{23}Mg », and the second to Lukas Madauss for his thesis entitled « Structurally modified two-dimensional materials for membrane applications », at the University of Duisburg-Essen under the supervision of Marika Schleberger.



Science festival

October, 13th, 14th, 15th

On the occasion of the three days science festival, organized by the Ministry of Research and Higher Education, several scientific demonstrations, two conferences, games and stands were made by GANIL the Caen science village. The science festival on average attracts a very general public.

Festival of Normandie's excellence

October, 20th, 21st, 22nd

GANIL participated in the 3 day exhibition displaying excellence of the region of Normandy, organized by the Region of Normandy. Here the researchers, engineers and technicians presented the activities of through scientific demonstrations and games to a very broad public. This exhibition had ~40000 visitors.

Inauguration of the DESIR construction site

November, 10th

On November 10, 2023, GANIL inaugurated the construction site of the new DESIR experimental room during a ceremony which welcomed nearly 250 people. This experimental hall for very low energy nuclei will link GANIL's two accelerators, the cyclotrons and the linear accelerator, using the ion beams produced by each of them.



Exhibition "150 years of particle accelerators"

November, 17th and 18th

On the occasion of the 150th anniversary of the French physics society, GANIL presented the exhibition "150 years of particle accelerators". The public discovered the world of particle accelerators through fun, spectacular and intriguing experiments!

Master's Day

November, 18th

As every year, GANIL organised the "Master's Day". This event aims at presenting the PhD opportunities offered at GANIL for Masters students from all Universities in France. This is combined with extensive visits to the accelerators and detectors. More than 120 students participated at the master's day.

GANIL open days

December, 2nd

GANIL welcomed more than 600 visitors and 110 pupils during its open days. Guided by researchers, engineers and technicians, the visitors discovered the installation from the ion sources to the experiment rooms.



IV.Environmental report

1. Radioactive releases

The nuclear facility GANIL is under supervision of the French Nuclear Safety Authority (ASN), which gave in 2015 the authorisation for atmospheric radioactive emission with limits for cyclotrons and spiral2 facility (see table below). GANIL carries on-going monitoring in both chimneys and each month, GANIL reports on the quantity of radioactivity released to the Authority.

GANIL	Tritium (Bq)	Noble gas (Bq)	Iodines (Bq)	Other β and γ emitters (Bq)
Annual limit for GANIL cyclotrons	2.10E+09	3.27E+10	1.94E+08	9.70E+12
Release in 2023	7.32E+07	8.34E+09	2.87E+05	6.85E+11
% release in percentage of the annual limit in 2023	3.5%	25.5%	0.15%	7.1%

GANIL SPIRAL2	Tritium (Bq)	Noble gas (Bq)	Iodines (Bq)	Other β and γ emitters (Bq)
Annual limit for SPIRAL2	6.50E+09	2.20E+12	5.00E+05	1.40E+12
Release in 2023	1.06E+09	3.33E+10	1.09E+05	4.96E+11
% release in percentage of the annual limit in 2023	16.3%	1.5%	21.8%	35.4%

All along the years, the releases were low and complied with the annual authorized limits.

The dosimetry due to those releases in 2023 is estimated up to 2 μ Sv for a representative population living at 500 m from GANIL.



2. Environmental monitoring

The radiological monitoring of GANIL's environment is defined by the regulation and the ASN. Certified laboratories analyse each month 80 to 90 samples of air, water, plants and milk. Once a year, some soil samples and agricultural products are also analysed. GANIL has two air monitoring stations. On-going irradiation monitoring are carried on with detectors in those stations and dosimeters around the site and in towns near GANIL. All the radiological values are available in the official website for the radiological environmental monitoring in France: <https://www.mesure-radioactivite.fr> (available in English).



During 2023, the daily global beta radioactivity measured in aerosols are due to the natural environmental radioactivity. All the other results are under the detection limits excepted a few rainwater measurements of global beta emitters staying nevertheless inside natural level standards.

The activity and releases of GANIL's facility do not involved any increase of radioactivity in its environment.

3. Non radioactive releases

The main risk concerns the cooling towers of GANIL's and SPIRAL2's facilities releasing steam. The monthly water analysis showed the absence of legionella bacteria in water.

GANIL's activities do not induce specific conventional pollutant release in the atmosphere. The sole releases are due to the heating system burning gas and the burning of diesel for the periodic tests of electric generators needed for safety. The quality of the effluent are controlled regularly and meet the standard values.

Few years back, GANIL took some measures to restrict the release of perfluorocarbon gas used in detectors. The loss of those gases were of 8 kg in 2023 which represent 52 tons equivalent carbon dioxide and were less than in 2022. GANIL will continue to study how to reduce the release of such gases.

4. Liquid effluents

Wastewater are transferred to the public sewerage system (20 525 m³ yearly). Accredited laboratory analyses the quality of wastewater 4 times a year with radiological and chemical tests. All the measured parameters were under the limits required by the Nuclear Safety Authority and the local public department for water.

In 2023, about 8 m³ of effluents containing less than 100 Bq/L of tritium were transferred to the public sewerage system, corresponding to a total of 240 kBq of tritium representing 24% of the authorized limit.

5. Wastes

Dangerous wastes were produced in 2023 in smaller amount than during 2022 on GANIL site recovering the usual production excepted for asbestos-containing wastes coming from asbestos removal operation.

Three campaigns occurred for the conditioning of radioactive wastes including one concerning historical electronic wastes containing dangerous compounds. These operations occurred in a new dedicated room equipped for this purpose.

V.Activities in Technological Transfer

GANIL is participating to Regional, National and European Economic Networks.

1. Service to industries

Industrial applications using stable ion beams focus today on microporous membrane production by irradiating polymer films with heavy ions, on the tests of electronic components to study their behavior and resistance under irradiation and biology under irradiation in collaboration with CIMAP.

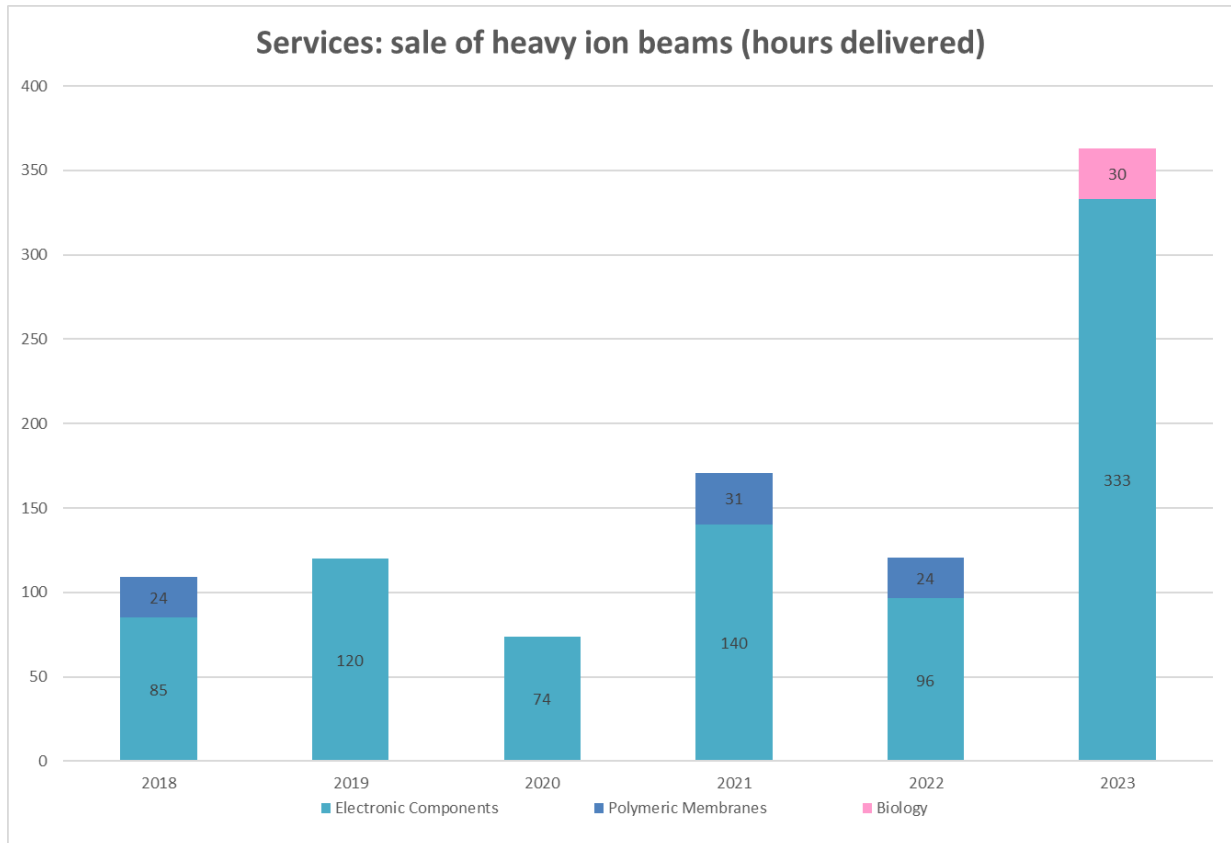


Figure 1: Sales of heavy ion beams

This second type of application is presently undergoing a strong rise of activity due to the development of “new space” activities, as shown in Figure 1. Companies dealing with the aerospace industry have developed programs of component certification with the use of GANIL beams. The beam time dedicated to these various applications is billed to the user at an hourly rate. CNES asked GANIL to propose solutions to improve access to GANIL’s beams for the space industry community. This idea led to the launch of the emergence phase of the SAGA (Space Applications at Ganil Accelerators) project.

GANIL is present at european conferences such as RADECS (Radiation and its effect on Systems and Components) and RADNEXT (RADiation facility Network for the EXploration of effects for indusTry and research) and at national meetings (RDV CARNOT) that foster links between academics and industrial partners. With its scientific and technological expertise, GANIL also acts as a relay enhancing the transfer of its employee skills to industrial companies and their applications.

2. Technology transfers in 2023:

- Beam profile monitor with regional company PANTECHNIK
- Patent on mechanical structure for specific aluminium vacuum pipes with national company STIRWELD
- A glove box project for the NFS experiment hall has been built around an industrial collaboration validated in 2023 for development of new types of adaptable gloveboxes for radioactive sample manipulation with national company IDEALEX

This collaboration has been the subject of grant applications for academic/industry R&D collaboration in the Normandy and Occitania regions. These grants cover almost all the investment and the costs of 2.3 FTEs.

Differents various collaboration agreements have been studied in 2023.

They are related to various domains that reflect the variety of techniques and scientific specialties of GANIL:

- BOREALES Energy (Normandy)
Case studies of applications of their innovative energy storage system to save energy
- INSTITUT DE RECHERCHES GEOLOGIQUES ET MINIERES (Cameroun)
Development of environmental radiation protection equipment

In more upstream research, connection to industrial partners exist in the fields of Artificial intelligence for monitoring complex and multi-parameters systems as accelerators.





02

SCIENTIFIC RESEARCH:

Internal activities and user experiments

I. STRUCTURE, ASTROPHYSICS, REACTION AND SPECTROSCOPY

The STARS group leads experimental research in the fields of nuclear structure and nuclear astrophysics using heavy-ions collisions and high-resolution charged particles and gamma-rays spectroscopy. The group is involved at high level in the development and running of state-of-the-art instruments such as AGATA(γ), EXOGAM(γ), PARIS(γ), MUGAST/GRIT(lcp), ACTAR (active target) and NEDA(n). Members of the group have high responsibilities in the nuclear physics international community (AGATA project Manager, NuPECC chairman, RESANET GDR chairman, GANIL beam coordinator, leader of the European astrophysics schools of the Chetec-Infra project). The publications presented in the following are the result of PhD work supervised or co-supervised by a member of the group.

1. Elucidating the nature of the proton radioactivity and branching ratio on the first proton emitter discovered ^{53m}Co

The observation of a weak proton-emission branch in the decay of the 3174-keV ^{53m}Co isomeric state marked the discovery of proton radioactivity in atomic nuclei in 1970. Here we show, based on the partial half-lives and the decay energies of the possible proton-emission branches, that the exceptionally high-angular momentum barriers, play a key role in hindering the proton radioactivity from ^{53m}Co , making them very challenging to observe and calculate. Indeed, experiments had to wait decades for significant advances in accelerator facilities and multi-faceted state-of-the-art decay stations to gain full access to all observables. Combining data taken with the TASISpec decay station at the Accelerator Laboratory of the University of Jyväskylä, Finland, and the ACTAR TPC device on LISE3 at GANIL, an international collaboration measured their branching ratios as $b_{p1} = 1.3(1)\%$ and $b_{p2} = 0.025(4)\%$. These results were compared to cutting-edge shell-model and barrier penetration calculations. This description reproduces the order of magnitude of the branching ratios and partial half-lives, despite their very small spectroscopic factors.

[Luis G. Sarmiento, Thomas Roger et al Nature Communications volume 14, Article number: 5961 (2023)]

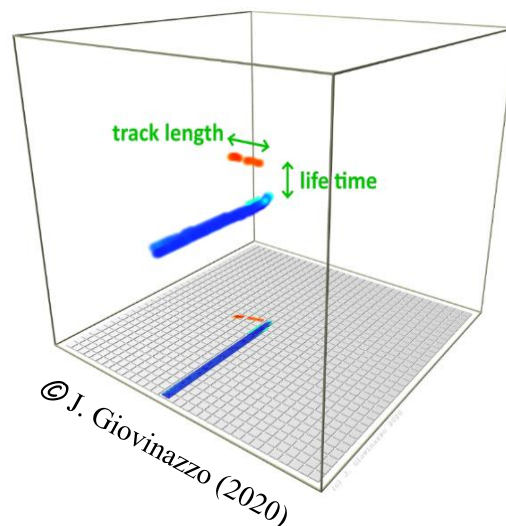


Figure 2: 4D decay of very exotic isotopes in ACTAR

2. Search for ^{22}Na in novae supported by a novel method for measuring femtosecond nuclear lifetimes

Classical novae are thermonuclear explosions in stellar binary systems, and important sources of ^{26}Al and ^{22}Na . While γ rays from the decay of the former radioisotope have been observed throughout the Galaxy, ^{22}Na remains untraceable. Its half-life (2.6 yr) would allow the observation of its 1.275 MeV γ -ray from a cosmic source. However, the prediction of such an observation requires good knowledge of its nucleosynthesis. The $^{22}\text{Na}(p, \gamma)^{23}\text{Mg}$ reaction remains the only source of large uncertainty about the amount of ^{22}Na ejected. Its rate is dominated by a single

resonance on the short-lived state at 7785.0(7) keV in ^{23}Mg . Here, we performed a combined analysis of particle-particle correlations and velocity-difference profiles to measure femtosecond nuclear lifetimes. The application of this method to the study of the ^{23}Mg states, places strong limits on the amount of ^{22}Na produced in novae and constrains its detectability with future space-borne observatories. Chloé Fougère obtained for this work the 2023 GANIL thesis prizes.

[Chloé Fougères, François de Oliveira Santos et al, Nature Communications volume 14, 4536 (2023)]

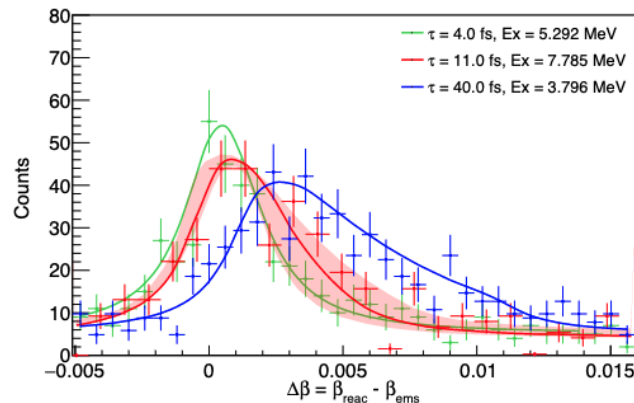


Figure 3: Velocity distribution for different excited states. The profile is used to determine sub-ps nuclear lifetime

3. High-Precision Spectroscopy of ^{20}O Benchmarking *ab-initio* Calculations in Light Nuclei

The excited states of unstable ^{20}O were investigated via γ -ray spectroscopy following the $^{19}\text{O}(d,p)^{20}\text{O}$ reaction at 8 A.MeV. By exploiting the Doppler shift attenuation method, the lifetimes of the 2^+_{2} and 3^+_{1} states were firmly established. From the γ -ray branching and $E2/M1$ mixing ratios for transitions deexciting the 2^+_{2} and 3^+_{1} states, the ($E2$) and ($M1$) were determined. Various chiral effective-field theory Hamiltonians, describing the nuclear properties beyond ground states, along with a standard USDB interaction, were compared with the experimentally obtained data. Such a comparison for a large set of γ -ray transition probabilities with the valence space in medium similarity renormalization group *ab initio* calculations was performed for the first time in a nucleus far from stability. It was shown that the *ab initio* approaches using chiral effective field theory forces are challenged by detailed high-precision spectroscopic properties of nuclei. The reduced transition probabilities were found to be a very constraining test of the performance of the *ab initio* models.

[I. Zanon, E. Clément et al. Phys. Rev. Lett. 131, 262501 – (2023)]

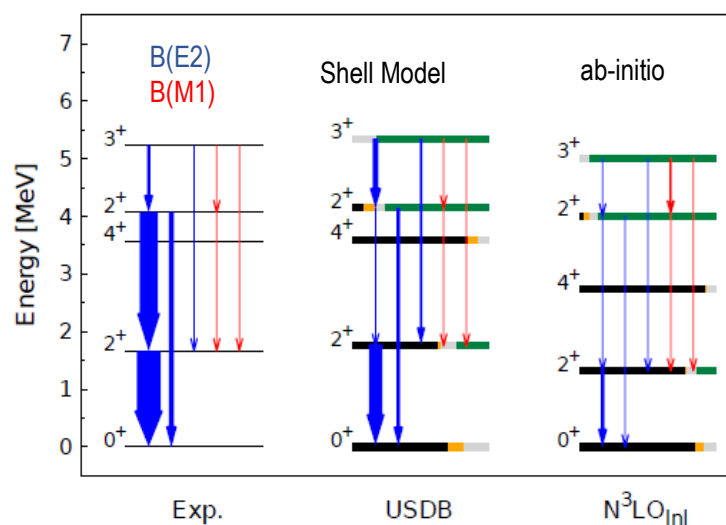


Figure 4: Comparison of the transitions probabilities in ^{20}O between experimental data, Shell model calculations and state-of-the-art *ab-initio* calculations

4. N=16 Magicity Revealed at the Proton Drip Line through the Study of ^{35}Ca

The last proton bound calcium isotope ^{35}Ca has been studied for the first time, using the $^{37}\text{Ca}(p,t)^{35}\text{Ca}$ two neutron transfer reaction. The radioactive ^{37}Ca nuclei, produced by the LISE spectrometer at GANIL, interacted with the protons of the liquid hydrogen target CRYPTA, to produce tritons t that were detected in the MUST2 detector array, in coincidence with the heavy residues Ca or Ar. The atomic mass of ^{35}Ca and the energy of its first $3/2^+$ state are reported. A large $N=16$ gap of 4.61(11) MeV is deduced from the mass measurement, which together with other measured properties, makes ^{36}Ca a doubly magic nucleus. The $N=16$ shell gaps in ^{36}Ca and ^{24}O are of similar amplitude, at both edges of the valley of stability. This feature is discussed in terms of nuclear forces involved, within state-of-the-art shell model calculations. Even though the global agreement with data is quite convincing, the calculations underestimate the size of the $N=16$ gap in ^{36}Ca by 840 keV.

[L. Lalanne, O. Sorlin et al. Phys. Rev. Lett. 131, 092501 (2023)]

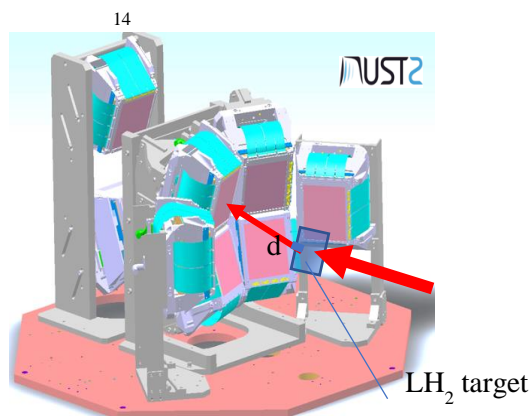


Figure 5: The MUST2 setup with the liquid hydrogen target CRYPTA

5. The AGATA project

GANIL is an important partner of the AGATA collaboration; The Project Manager is part of the STARS group and the GTA group is in charge of the trigger and clock distribution of the Phase 2 Project. GANIL hosts the Operation Cost of the collaboration and contribute to 50% of the French share. The achievement of phase 1, the review of the performances and the technical design of phase 2 have been published in a dedicated topical issue in EPJA. GANIL physicist have been part of the guest editorial board and leading authors of several contribution

[The European Physical Journal A, AGATA: Advancements in Science and Technology, Nicolas Alamanos, Maria Jose Garcia Borge, Angela Bracco, Emmanuel Clement, Andres Gadea, Wolfram Korten, Silvia Leoni and John Simpson (2023)]

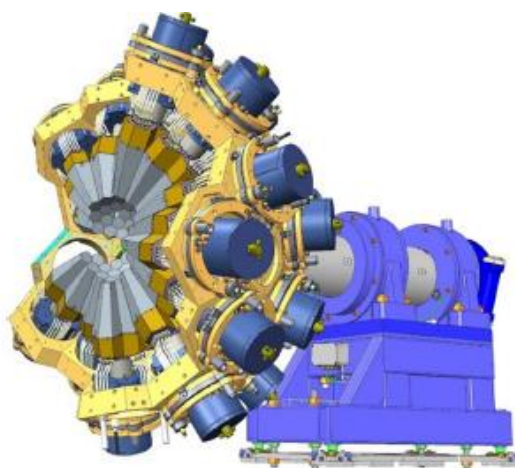


Figure 6: The AGATA array at LNL since 2021

II. PHYSICS OF HEAVY AND SUPERHEAVY NUCLEI

The main research topics of the PHASE group are the studies of nuclear structure and reaction mechanisms from the proton drip line to the end of the periodic table. These studies are based on laser and decay spectroscopy, and mass spectrometry.

The group is in charge of developing the state of art spectrometer (S^3) and the associated new instrumentation (SIRIUS and LEB).

1. Commissioning of the S^3 Target Station at LISE2000

In order to sustain the very high intense heavy ion beams accelerated by the LINAG, a specific target station for stable material was designed and built few years ago and mainly financed by a CPER (Contrat Plan Etat Région Normandie). This station consists of a vacuum chamber equipped with two large wheels and a set of instrumentation for monitoring the target integrity and the beam characteristics, i.e. beam spot profile, intensity and time structure [1].

Until 2022, all the components of the target station were developed and tested separately, and it was essential to evaluate the whole system under realistic irradiation conditions. In July 2023, few UTs of a $^{20}\text{Ne}^{3+}$ beam at 4.5 MeV/u up to 1.8 μA , was delivered to the LISE2000 beam line where the target station was installed.

Firstly, the intensity on the Faraday cup, used to protect the targets during beam tuning, was measured at low intensities, up to about 30 Watts. The response was found to be proportional to the beam intensity monitor of the cyclotron.

The synchronization of the wheel with the beam time-structure was then checked. To avoid irradiating the target frames and to optimize the irradiation of the material effective surface, a user defined signal controls the cyclotron chopper. The signal time-structure was set using an absolute encoder and a National Instrument compact RIO controller with a LabVIEW interface. The count rate of a barium fluoride scintillator, sensitive to gamma radiation emitted by the interaction of the beam with the frames or target material, was used to adjust the delay and the width of the synchronization signal. In addition, an optical switch and a hall effect sensor were positioned on a small toothed wheel fixed on the rotating arm in order to get a redundant signal for each revolution.

The integrity of 16 different targets mounted on the upstream wheel was checked by three methods: alpha particle energy loss, particle scattering and transmission of an electron beam. The working principle and the systems are described in [2] [3] and illustrated in Figure 7. The S^3 target station is equipped with an electron gun from STAIEB industry, whose control and command was developed to remotely configure its energy and intensity, as well as the deflection sequence according to the wheel rotation signal. In addition, a current/voltage converter was designed to measure the electron current output signal from the Faraday cup.

All the signals, i.e. from the silicon detectors, the BaF2 scintillator, the electron Faraday cup and the deflector, the wheel rotation, are processed, digitalized and time-stamped by a dedicated NUMEXO2 module. The data obtained make it possible to display the various observables, either their count rate or their energy, along the target. All tests were performed at a speed between 0 to 1000 rpm. Up to about 2 μAe of incoming beam intensity, the obtained spectra were as expected. In addition, a two-dimensional image of each target was obtained, currently at low resolution with on-line data. This display allows to distinguish thin and thick targets and pinholes of less than 1 mm in diameter.

In conclusion, with these beam conditions, we were able to validate the response of the heavy-ion Faraday cup, the synchronization of the beam with the wheel rotation, the detection systems and the data acquisition. Following the feedback from this test, some feedthroughs have been enlarged and added in order to facilitate the access to connections. The station has been moved to S^3 and will be commissioned with a LINAG beam in fall 2024.

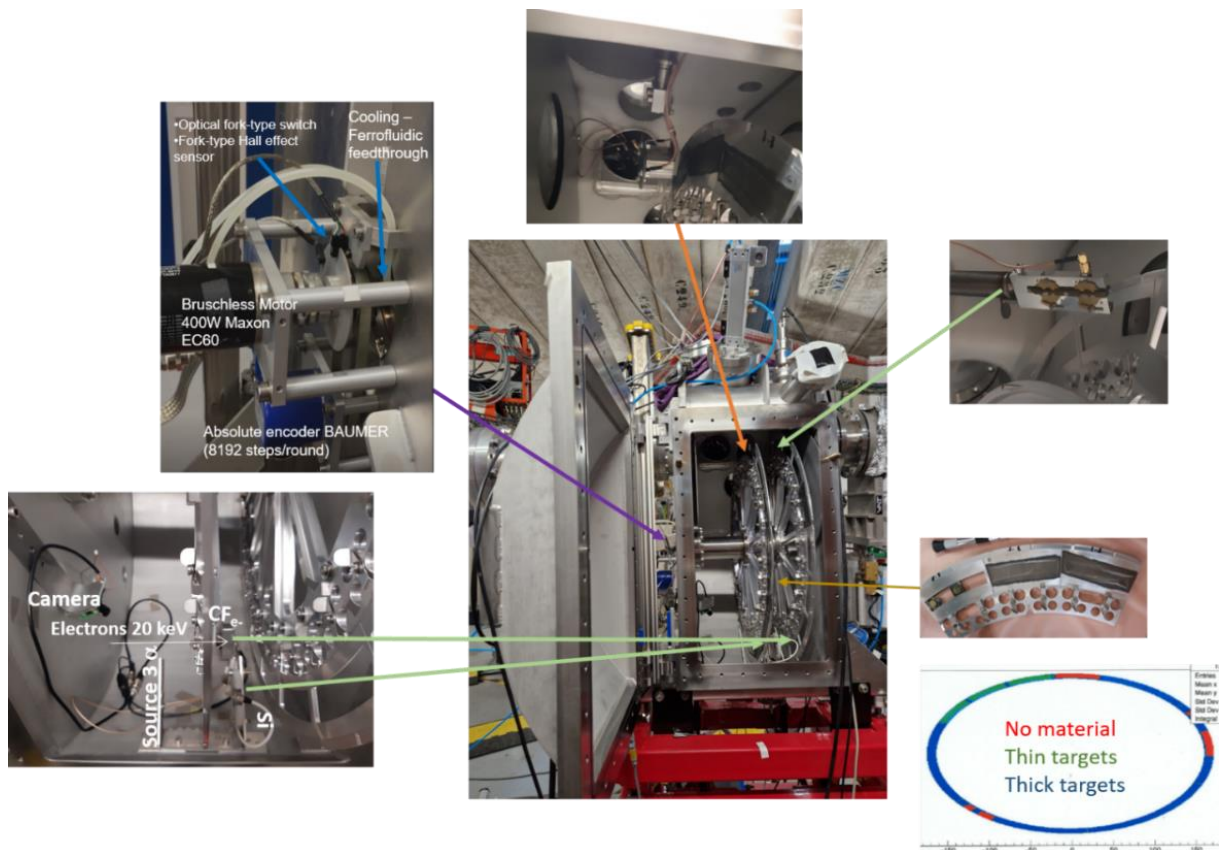


Figure 7: S^3 target station

Reference

- [1] C. Stodel, J.-F. Libin, C. Marry, F. Lutton, M.-G. Saint-Laurent, B. Bastin, J. Piot, E. Clément, S. Le Moal, V. Morel, J.-C. Thomas, O. Kamalou, G. Grémont, C. Spitaels, H. Savajols, R. Hue, P. Gangnant, M. Authier, A. Drouart, A. Van Lauwe, E. Lamour, J. Kallunkathariyil, C.-O. Bacri, V. Petitbon-thévenet, H. Lefort and F. Pellemoine, "High Intensity targets stations for S^3 ," *Journal of Radioanalytical and Nuclear chemistry*, vol. 305, no. 3, pp. 761-767, 2015.
- [2] C. Stodel, "Methods of Targets' Characterization," *EPJ Web of conferences*, vol. 229, p. 02001, 2020.
- [3] J. Kallunkathariyil, C. Stodel, C. Marry, G. Frémont, B. Bastin, J. Piot, E. Clément, S. Le Moal, V. Morel, J.-C. Thomas, O. Kamalou, C. Spitaels, H. Savajols, M. Vostinar, F. Pellemoine and W. Mittig, " S^3 Target Monitoring with an Electron gun," *AIP Conference Proceedings*, vol. 1962, no. 1, p. 030019, 2018.

2. Commissioning of SIRIUS

SIRIUS (Spectroscopy and identification of Rare Isotopes Using S^3) is a detection setup at the focal plane of S^3 designed for the alpha, gamma, conversion electron and fission spectroscopy of superheavy nuclei. The detector was built in collaboration between GANIL, IRFU, IPHC and IJCLab and assembled in GANIL in March 2021.

In June 2023 we performed an online test of the setup in the IRRSUD beamline in order to validate the system under beam conditions and test the time-of-flight measurement. The test used a 0.28 MeV/u ^{238}U beam from the C02 injector cyclotron in order to mimic the energy deposition of the recoiling nuclei produced in fusion-evaporation reactions. The acquisition system was able to take data with the implantation detector and the tracker detector up to 1000 Hz.

The time of flight is measured between the emissive foil of the Tracker and the Double-Sided Silicon strip Detector (DSSD) where the ions are implanted. The Tracker consists of a Secondary Electron Detector (SeD) with Mylar emissive foil placed at 45° with respect to the beam axis. The time signal of the SeD and the signals of the DSSD are sent into a NUMEXO digitizer where the signal is recorded at 200 MHz and timestamped with 100 MHz clock. The time of flight was measured between the timestamps of the SeD and DSSD and corrected with the trigger point reconstructed on digitized each signal. This measurement provided a time of flight resolution of 2.06 ns FWHM.

In addition to the timing, the Tracker also has a 1mm FWHM position resolution. This allows tracking individual ions at the focal plane of S^3 and enhance the mass resolution of the spectrometer. The trajectories of the ions between the SeD and the DSSD were reconstructed during the test. Figure 8 shows the projection of the trajectories on the horizontal plane.

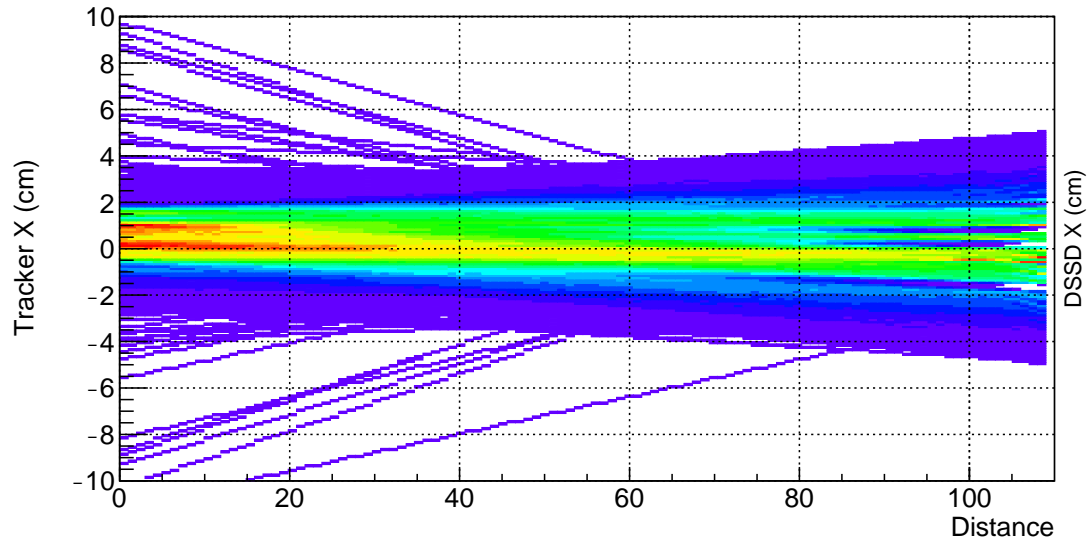


Figure 8: Tracking of individual ions between the Tracker and the DSSD of SIRIUS.

III. FISSION AND REACTIONS

The FIRE (Fission & REactions) group is principally concerned with the study of nuclear dynamics, its interplay with nuclear structure, and its use to better constrain the underlying effective nuclear interactions and their extrapolation towards an equation of state for dense matter. The members of the group are at the forefront of research into topics ranging from nuclear fission to multifragmentation and beyond. As such, the members of FIRE are also responsible for two major instruments of GANIL used in this field, namely the VAMOS++ spectrometer and the coupled INDRA-FAZIA charged particle arrays.

1. Experimental evidence of the effect of nuclear shells on fission dissipation and time

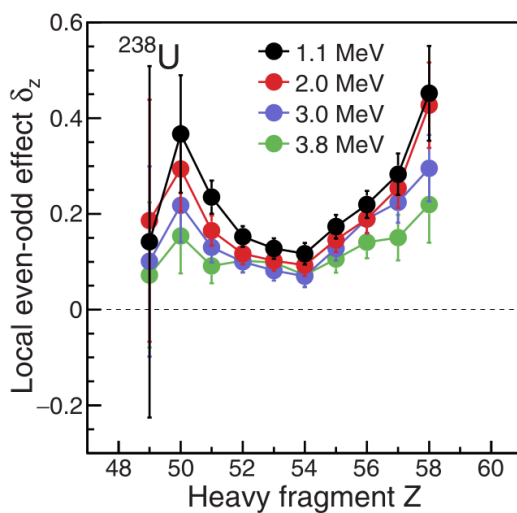


Figure 9: Evolution of local even-odd effect as a function of heavy fragment Z and excitation energy above the barrier (see text)

More than 80 years after its discovery, nuclear fission is still one of the most complex physical processes we can observe in nature due to the interplay of macroscopic and microscopic nuclear properties that decide the result. An example of this coupling is the presence of nuclear dissipation as an important ingredient that contributes to drive the dynamics and has a clear impact on the duration of the process. However, different theoretical interpretations, and scarce experimental data make it poorly understood. Thanks to data obtained from transfer-induced fission reactions between a ^{238}U beam and a ^{12}C target, measured in inverse kinematics with the VAMOS++ large-acceptance magnetic spectrometer, we achieved the first experimental determination of the dissipation energy in fission as a function of the fragment split, for three different fissioning systems. The amount of dissipation was obtained through the measurement of the relative production of fragments with even and odd atomic numbers with respect to different initial fission energies (see Figure 9). The results reveal a clear effect of particular nuclear shells on the dissipation and fission dynamics. The analysis of the relative production of even- and odd- Z fragments shows a clear influence of nuclear structure in the dissipation process and fission dynamics: fission is faster when producing fragments with spherical shell $Z = 50$, but slower and more dissipative when fragments are near the octupole-deformed shell $Z = 52$.

→ D. Ramos, M. Caamano, F. Farget, C. Rodriguez-Tajes, A. Lemasson, C. Schmitt *et al.*, *Phys. Rev. C* **107**, L021601 (2023)

2. Experimental study of isospin transport with $^{40,48}\text{Ca}+^{40,48}\text{Ca}$ reactions at 35A MeV

The nuclear equation of state (NEoS) of bulk nuclear matter over a wide range of densities, temperatures and neutron-to-proton asymmetries remains a major issue in modern nuclear physics and astrophysics. Heavy-ion collisions are a unique tool to probe the NEoS at finite temperature under laboratory-controlled conditions, especially to constrain the density dependence of the symmetry energy $E_{\text{sym}}(\rho)$ of the NEoS. With this aim, isospin transport in heavy-ion collisions around the Fermi energy has been measured with the coupling of the VAMOS high-acceptance spectrometer and the INDRA charged-particle multidetector. Two main contributions to isospin

transport phenomena are generally distinguished: *isospin diffusion*, taking place whenever an isospin gradient is present and inducing isospin equilibration, and *isospin drift*, driven by density gradients, leading to the neutron enrichment of lower-density regions.

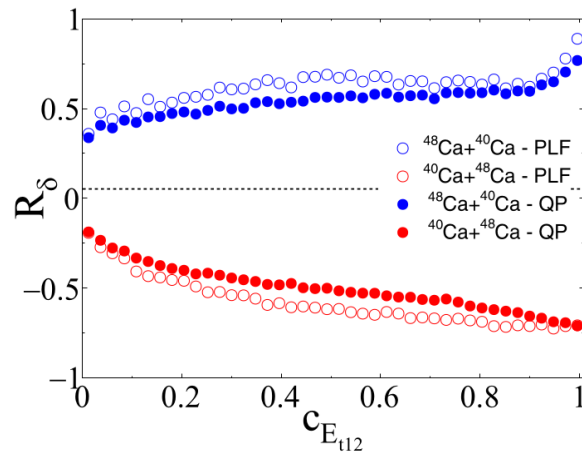


Figure 10: Isospin transport ratio for PLF/QP produced in isospin-asymmetric reactions as a function of centrality ($c=0$ corresponds to head-on collisions). The closer the upper & lower branches, the greater the degree of isospin equilibration.

Using isotopically-identified projectile-like fragments (PLF) measured with VAMOS and selected light-charged particles (LCP: $Z = 1,2$) measured in coincidence with INDRA, the properties of the initial highly-excited quasiprojectile (QP) have been estimated on an event-by-event basis using a novel reconstruction method. Using the asymmetry $\delta = (N-Z)/A$ of either PLF or QP as isospin-sensitive observable and the total transverse energy of LCP for centrality sorting, the isospin transport ratios demonstrate a clear increase of isospin equilibration with increasing centrality, due to isospin diffusion between projectile and target. Isospin drift has also been evidenced through an enhancement of the mean neutron-to-proton ratio of LCP emitted in the mid-velocity region, for the reactions using same- δ projectile-target combinations where isospin diffusion is expected to be negligible.

→ Q. Fable, A. Chbihi, J.D. Frankland *et al.* (INDRA Collaboration), *Phys. Rev. C* **107**, 014604 (2023)

3. Quasiprojectile breakup and isospin equilibration at Fermi energies: Potential indication of longer projectile-target contact times

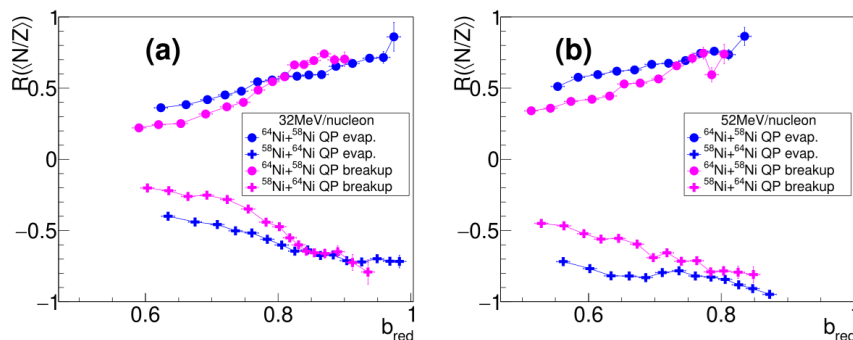


Figure 11: Comparison of isospin transport ratio centrality dependence ($b=0$ corresponds to head-on collisions) between binary exit channels leading to a QP evaporation residue (QP evap) or the QP breakup channel, for 32A and 52A MeV reactions. In each case the distance between the upper and lower branch is related to the distance from isospin equilibration.

In our previous analysis of data from the first INDRA-FAZIA campaign (Ciampi *et al.*, 2022), the topic of isospin equilibration in the reactions $^{58,64}\text{Ni}+^{58,64}\text{Ni}$ at 32 and 52 A.MeV was addressed by considering the most dominant reaction channel for semiperipheral and peripheral reactions: a binary exit channel resulting in the production of two main fragments, the quasiprojectile (QP) and the quasitarget (QT), accompanied by lighter ejectiles, such as neutrons, LCPs, and intermediate mass fragments (IMFs). Along with the binary exit channel, a ternary (or quaternary) outcome is also possible: in this case, one (or both) of the heavy products may break up into two smaller fragments, in a fission-like process. When the characteristic timescale of this process is short (around or

below 1 zs) the breakup process has been linked to a dynamical origin. In this new analysis, isospin equilibration has been studied for the QP breakup channel, using the isospin transport ratio for the neutron-to-proton ratio of the QP reconstructed from its daughter fragments. Evidence was found that, for the same reaction centrality, a higher degree of relaxation of the initial isospin imbalance is achieved in the breakup channel with respect to the binary channel, possibly indicating the indirect selection of specific dynamical features. An interpretation based on different average projectile-target contact times related to the two exit channels under investigation was proposed, with a longer interaction for the breakup channel. The time information has been extracted from Antisymmetrized Molecular Dynamics (AMD) simulations of the studied systems coupled to the statistical decay code, GEMINI++: the model calculations appear to support the present hypothesis.

→ C. Ciampi, S. Piantelli, G. Casini, A. Ono, J.D. Frankland *et al.* (INDRA-FAZIA Collaboration), *Phys. Rev. C* **108**, 054611 (2023)

Inverse-Kinematics Fission with PISTA at VAMOS++

The Particle Identification Silicon Telescope Array (PISTA) has been developed and installed at VAMOS as collaboration between FIRE group and CEA/DAM. The array of 8 ΔE -E telescopes composed of highly segmented silicon detectors aim at achieving isotopic identification of light charged particles from He to O. The goal is to obtain a precise characterization of the incoming channel of a fission reaction induced by multi-nucleon transfer reactions in terms of fissioning system identification and event-by-event initial excitation energy measurement. The PISTA detector was operated for the first time in a experiment studying the fission of actinides produced in reaction of ^{238}U beam at Coulomb energies on ^{12}C target. Fissioning systems ranging between U and Cm were isotopically identified by detecting in PISTA the target-like recoils from He up to Carbon isotopes as shown in Figure 12. The achieved resolution in excitation energy is better than 1 MeV FWHM. In addition, for each fission reaction, one of the fission fragments was fully characterized using the magnetic spectrometer VAMOS++ and associated detection equipment.

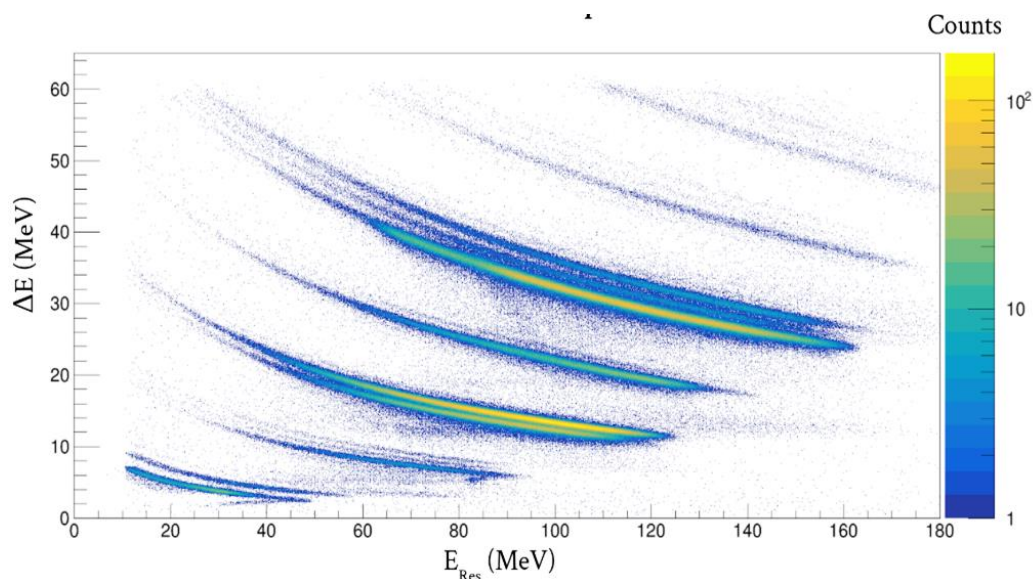


Figure 12: Light charged ΔE -E particle identification in PISTA from He to Carbon. The good separation between the 3 isotopes of Carbon, ^{12}C , ^{13}C and ^{14}C reflects the high identification capability of the detector. [PhD work of L. Begue-Guillou]

IV. FUNDAMENTAL INTERACTIONS AND DARK SECTORS

The Fundamental Interactions and Dark Sectors (FINDS) group is looking for evidence of New Physics thanks to precision measurements scrutinizing the decay or de-excitation of radioactive nuclei. It presently encompasses the MORA and New JEDI experiments, precision measurements of branching ratio and half-lives of 0^+ to 0^+ β emitters, and the search for a dark decay channel in the decay of ${}^6\text{He}$ [1]. In 2023 a proposal to the PAC was accepted to evaluate the contribution of isospin symmetry-breaking forces to the 0^+ to 0^+ superallowed Fermi β -decay of the ${}^{18}\text{Ne}$ nucleus at the SPIRAL facility and should be scheduled in 2025.

1. The Matter's origin from RadioActivity (MORA) experiment

MORA is looking for a possible evidence of charge and parity CP symmetry violation in the nuclear beta decay of ${}^{23}\text{Mg}^+$ and ${}^{23}\text{Ca}^+$ laser polarized ions [1]. A large CP violation is required to explain the matter-antimatter imbalance observed in the Universe. The MORA experiment is using an innovative polarization technique, which combines the high efficiency of ion trapping with the one of laser orientation. It is currently taking data using ${}^{23}\text{Mg}^+$ beams delivered by the IGISOL [2] facility, at the Accelerator Laboratory of the University of Jyväskylä. A strong isobaric contamination by ${}^{23}\text{Na}^+$ ions (${}^{23}\text{Na}:{}^{23}\text{Mg} \sim 1000$), originating from the IGISOL gas cell components, has so far limited the statistics acquired. Despite this limitation, a polarization proof-of-principle has been attempted at the end of 2022. The analysis of this experiment was undertaken during the first semester of 2023. The results were presented during two PhD defences [3,4]. The analysis showed that a contamination of at least a factor of 10 lower is needed to realize the proof of principle in reasonable time (a few days of data-taking). The defences were also displaying in details the otherwise good performances of the MORA apparatus: 10% trapping efficiency, detection (Figure 13) and laser polarization system working nominally, good overall production of ${}^{23}\text{Mg}$ from the IGISOL facility, up to a few 10^5 pps for 10 μA of 30 MeV protons on the thin Mg target. The experimental efforts of 2023 concentrated on reducing possible traces of Na in the target by producing at GANIL different Mg thin foils or MgO crystals, baked and or coated with BaO to reduce potential surface ionization of this alkali element. One on line test was realized

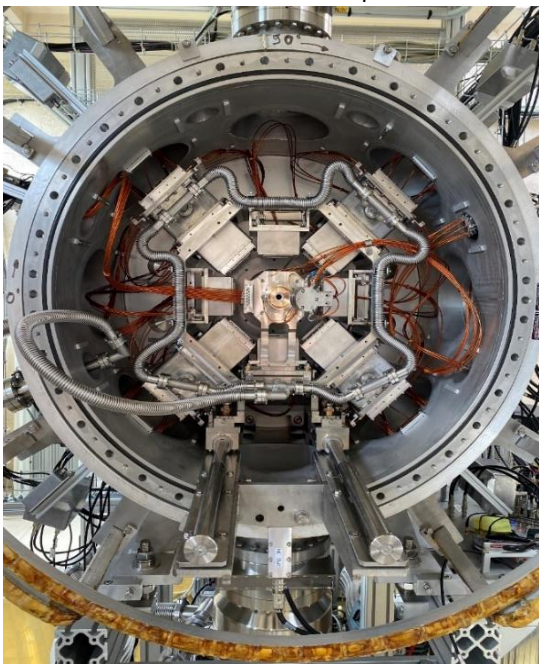


Figure 13 : The MORA detection setup around the trap, in the center. The chamber diameter is about 1m.

References

- [1] P. Delahaye et al., «The MORA project,» *Hyp. Int.*, vol. 240, p. 63, 2019.
- [2] I. D. Moore et al., "Towards commissioning the new IGISOL-4 facility," *Nuclear Instruments and Methods in Physics Research B*, vol. 317, p. 208, 2013.
- [3] N. Goyal, Detection of beta decay in laser oriented trapped radioactive isotopes for the MORA project, PhD of the university of Caen, 2023
- [4] S. Dumas-Tschopp, Recherche de violation de CP avec MORA : mise en service de l'installation et premières expériences, PhD thesis of the university of Caen, 2023
- [5] H. P. Mumm et al., «New Limit on Time-Reversal Violation in Beta Decay,» *Phys. Rev. Lett.*, vol. 107, p. 102301, 2011

2. New Judicious experiments for Dark sectors Investigations (New JEDI):

In 2023, lecture notes concerning the New JEDI project have been published [1]. The focus was set on the ^8Be data analysis aiming to study the existence of the hypothetical X17 boson, from the experiment carried out at the ANDROMEDE facility (see Figure 14). In practice, algorithms have been developed to check the proper data synchronization between channels and between digitizers (via the Numexo fusion mode), to identify and to correct the data for dead time. Two soft methods have been developed to reconstruct coincidences between the plastic detectors. Results are compatible with the one recorded using an additional analog electronic chain. We studied

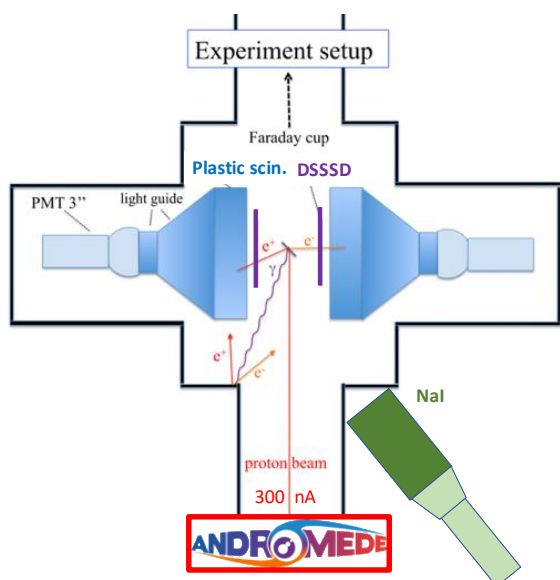


Figure 14: New JEDI experimental setup at ANDROMEDE

also the lepton-nucleons elastic scattering formalisms: quantum-relativistic (Mott) model versus classical (Rutherford). Finally, we made an independent study of the ^8Be anomaly spectrum from ATOMKI group. We studied the Internal Pair Creation process formalism (IPC) and the Boson emission formalism (X17). We developed tools based on simulations, to fit and interpret the ^8Be spectrum including IPC, X17 and other contributions, such as the scattering of leptons on nuclei. This work was done in collaboration with Prof (Hon) Tibor Kibédi from the Australian National University. One PhD student, 2 master students and a bachelor student worked on all these aspects. In addition, in October 2023, we performed a complementary experiment at the iThemba LABS facility. The aim of this experiment is to check the existence and the impact of additional nuclear physics effects in the ^8Be quantum system and to see to what extent it impacts the result concerning the X boson.

References

[1] B. Bastin, J. Kiener, I. Deloncle, A. Coc, M. Pospelov, J. Mrazek, L. Lamia, on the Behalf of the New JEDI collaboration, EPJ Web of Conferences 275, 01012 (2023).

3. Search for a neutron dark decay in ^6He

The 1 % discrepancy with a 4.4σ between beam and bottle experiments measuring the neutron lifetime has triggered many interrogations within the physics community. In 2018, Fornal and Grinstein suggested that this difference could be the consequence of a new decay channel involving dark matter particle(s) in the final state. Following this idea, Pfützner and Riisager listed radioactive nuclei whose decay could be sensitive to this channel, among which ^6He :

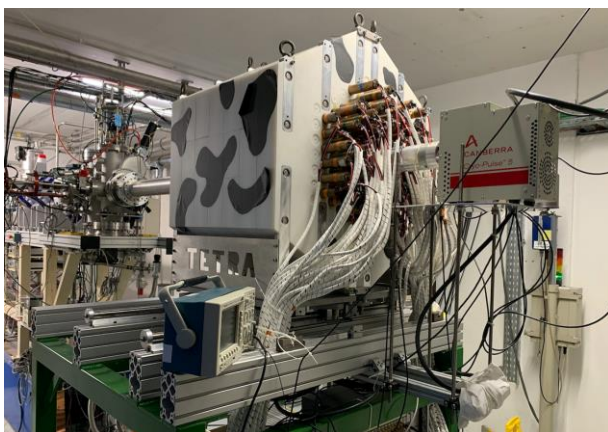


Figure 15 : The TETRA detector used in 2021.



where a free neutron and DM particle noted χ are emitted, would be a unique signature to look for a potential dark decay as there are no neutron emissions in a standard ^6He decay from its ground state. ^6He probes about 75 % of the open mass range for χ to be a DM candidate. In 2021, the high efficiency neutron detector TETRA (Fig. 3) was used to look for this specific dark decay at LIRAT with a 10^8 $^6\text{He}/\text{s}$ beam. The data analysis, concluded in 2023, allowed us to put a stringent upper limit for the branching ratio, at $\text{Br}_\chi \leq 4 \times 10^{-10}$, which is about 5 orders of magnitude lower than previously estimated.

M. Lejoubioux et al., Phys. Rev. Lett. 132, 132501 (2024)

V. DOSIMETRY, APPLICATIONS AND NUCLEAR DATA

The activity of the research group DOSADO in 2023 was mainly focused on 3 topics related to cancer treatment and neutron-induced reactions.

1. Radiotherapy and dosimetry

In 2018, the number of people in France who had cancer in their lifetime was around 3.8 million. Their risk of developing a second cancer is on average 36% higher than the risk of cancer in the general population. In this context, reducing side effects and improving quality of life after treatment have become a major issue in cancer research. DOSADO group works particularly on two treatment modalities to address this challenge: pencil-beam scanning proton therapy (PBS-PT) and targeted alpha therapy (TAT).

PBS-PT consists of irradiating the tumor volume with a large number of thin proton beams, whose position, energy and intensity are adapted to deliver the prescribed dose distribution. The delivery technique combined with the Bragg peak dose deposition allows a better sparing of normal tissues than X-Ray radiotherapy and thus a reduction of the risk of radiation-induced cancer. However, quality assurance of PBS-PT treatments is complex, especially for small target volumes ($< 3 \times 3 \times 3 \text{ cm}^3$). A 3D scintillation dosimeter was finalized in 2023 and an experimental program was completed at the Cyclhad protontherapy center. It provided data currently under analysis to perform 3D dose reconstruction.

TAT consists of injecting the patient with a radiopharmaceutical that specifically targets biomarkers of the cancer cells or their immediate environment. In TAT, it is radiolabelled with alpha-emitting radioisotopes. The short range and the high ionization density of alpha particles allow for high dose deposition in cancer cells while sparing surrounding tissues. In this domain, the DOSADO group has two main contributions. The first one deals with the study of the production of alpha-emitting radioisotopes, and in particular of ^{211}At to increase its production efficiency. This research program was funded by the REPARE ANR program that will end in March 2024. In 2023, the ^{210}At contaminant production cross section was measured. It is reported in a collaboration report and will be published in the near future. The principal activity was the design of a high-power solid Bismuth target and the first in-beam tests in September 2023. The second contribution of DOSADO to TAT deals with the study of the treatment biological effects at the cell level. In this context, a new detection system and a deconvolution method were developed by A. Doudard during his PhD, which he defended in September 2023. This work was published in *Med. Phys.* and presented in two international conferences.

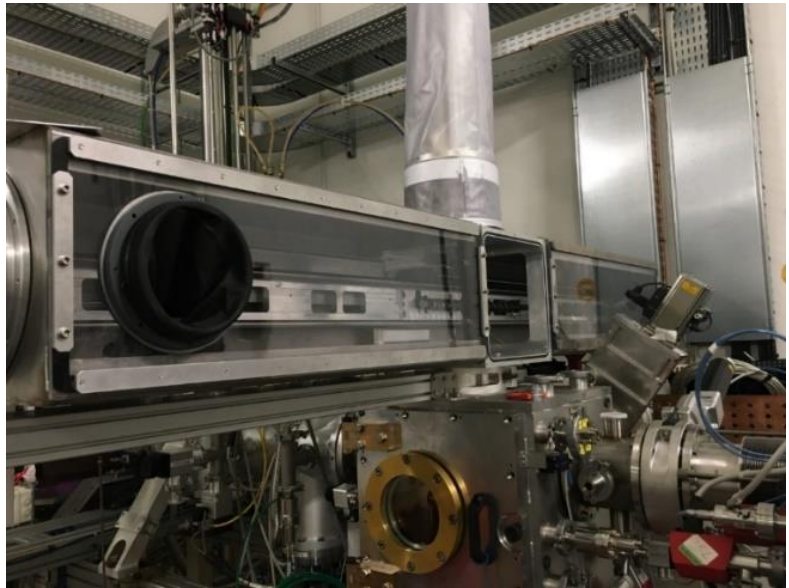


Figure 16: High power solid Bismuth target installed in the converter room of NFS.

2. FALSTAFF

2023 was a busy year for the FALSTAFF collaboration, with a scientific activity shared equally between:

- FALSTAFF's experimental program;
- The project of building the second arm of the spectrometer.

As for the experimental program, first we analyzed the data of the E814_20 experiment, which was performed at NFS in fall 2022 on the neutron-induced fission of ^{235}U . The analysis is still going on to achieve publishable results

on the dependence of the fission-fragment mass-yields on the incident-neutron kinetic energy, closely linked to the excitation energy of the fissioning system. The existing GEANT4 FALSTAFF simulations were improved to allow a better detector calibration. The data analysis results will be compared to GEF and FIFRELIN predictions, filtered by the GEANT4 simulation. Second, we have designed and proposed a second experiment for FALSTAFF at NFS on the study of the neutron-induced fission of ^{237}Np . This proposal was recommended by GANIL-SPIRAL2 PAC and will be run in October 2024.

We consolidated the project of building the second arm of FALSTAFF. This second arm will allow measuring in coincidence both fission fragments and performing, event by event, mass, energy and charge balances. Such balances are key observables for fission and fragment-deexcitation models. In addition, we submitted a proposal for funding to the French ANR (Agence Nationale de la Recherche) for the first five years of the scientific program of FALSTAFF. The construction of FALSTAFF second arm started and will allow us to reach our nominal goal with this detector.

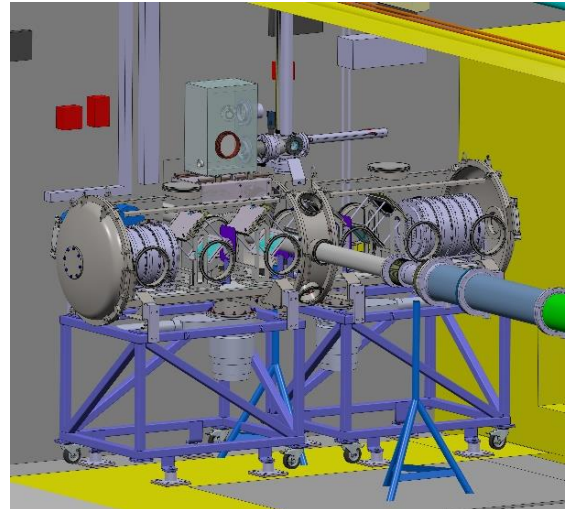


Figure 17: The two-arm fission-fragment spectrometer FALSTAFF installed on the neutron line of SPIRAL2/NFS. The detectors of both arms have been made feasible by transparency of the vacuum vessels. (Scale: The beam pipe is at 1.5 m from the floor)

3. Studies on neutron-induced reaction with Medley at GANIL

The MEDLEY detector (see Figure 18) is designed to measure the doubly differential cross sections of light charged particles (LCP) emitted in neutron-induced reactions. It consists of 8 telescopes, each consisting of 2 silicon junctions and a Cesium iodide crystal. The ΔE - ΔE -E technique is used to identify charged particles (p , d , t , α and ^3He), measure their time-of-flight and determine the incident neutron energy. Cross sections up to about 40 MeV can be measured at the NFS facility. These cross sections are fundamental quantities for research in many fields, including neutron dosimetry in aerospace, medical applications, radiation effects in electronics and, most importantly, the development of fusion energy.

In addition to feeding the nuclear databases, the results of these experiments will be used to test and improve the models used in the Talys code. Indeed several models, as optical potential, pre-equilibrium and statistical de-excitation models, are needed to properly describe these reactions. Since 2021, several experiments have been carried out at NFS: LIONS, GARIC and GARROS to study carbon, chromium and iron respectively.



Figure 18: The MEDLEY detector with its 8 telescopes

The spokesperson of these experiments is D. Tario from Uppsala University. In 2024 a new experiment will be performed on Copper and the spokesperson is I. Ipatova from UKEA. The analysis and interpretation of the results is the subject of Lucas de Arruda's PhD thesis (jointly supervised by the University of Caen-Normandie and the University of Uppsala). In addition to the LCP production cross section, the neutron spectrum and flux can be determined using a CH_2 target and detecting the scattered protons.

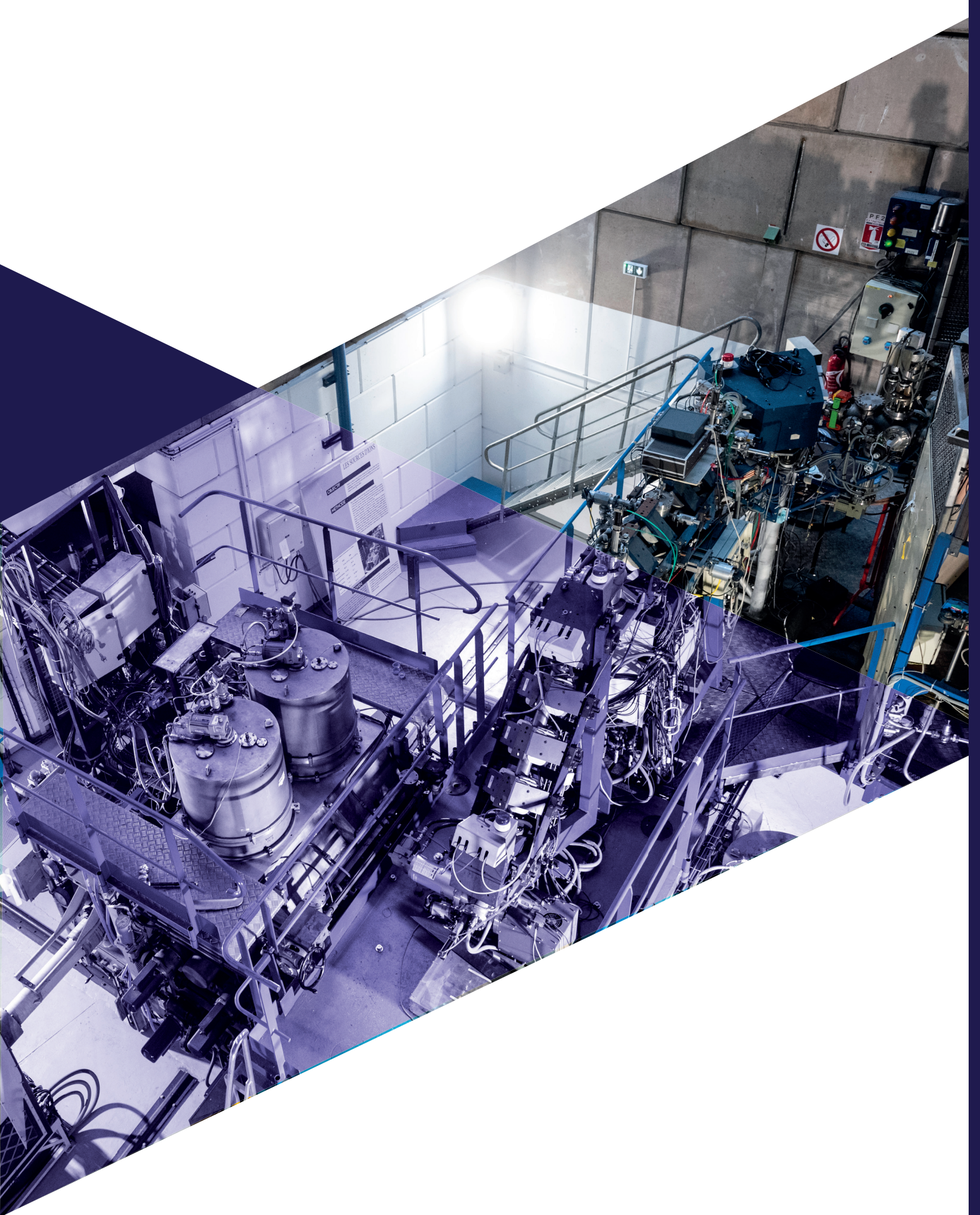
VI.CIRIL

Interdisciplinary research has been part of the GANIL facility's scientific ambition since its inception. The platform for hosting interdisciplinary researches is the CIRIL platform, which runs the beamlines (D1-HE, D1-ME, IRRSUD and ARIBE) for non-nuclear physics and their equipments, develops new devices requested for experiments, manages the proposal selection process of the local interdisciplinary program advisory committee (IPAC) and schedules the interdisciplinary physics beamtimes accepted through scientific committees. Today, up to 4 simultaneous experiments can be hosted using the 4 beamlines corresponding to each step of the ion acceleration at GANIL (ion source: ARIBE, C0 injector: IRRSUD, CSS1: ME, CSS2: HE). This multi-user configuration enables different interdisciplinary research communities to meet up, leading to the emergence of new projects. Simultaneous use of the lines is only possible thanks to the very specific configuration of the GANIL, with its 3 cyclotrons (C0, CSS1 and CSS2) in cascade (for HE, SME and IRRSUD) and the presence of two C0 injector cyclotrons. Thanks to parallel operation for several users, interdisciplinary research has access to beam times comparable to, or even superior to, nuclear physics.

In addition, *in-situ* characterization techniques have been developed using state-of-the-art online techniques such as X-ray diffraction, IR/Visible/UV emission/absorption photon spectroscopy, gas analysis, mass spectrometry, time-of-flight measurements or electron spectroscopies. Devices for low-temperature and/or high-temperature irradiation, under ultra-high vacuum or in a controlled atmosphere have also been built, expanding the range of studies using accelerated ions. The construction of the biology sample preparation laboratory, ARIA with the newly IBISA accreditation, has improved the facilities for radiobiology experiments and attracted new experimenters. We will install in 2024 the new IRRSUD command/control program and we will develop a new MIRRPLA multi-beam chamber that will be open to the community in 2026.

If the topics that interdisciplinary physics covers have continually evolved as a result of expanding possibilities (beamlines and on-line instrumentation) and the emergence of new subjects, to date, GANIL's beams remain highly attractive to the interdisciplinary community for which the main physics themes are: materials science applied to inorganic materials, materials science applied to organic materials, astrochemistry or astrophysics, radiobiology and atomic and molecular collision physics.

The collection of experiment reports (see part 04-VI) summarizes the scientific objectives carried out in 2023.



03

OPERATION, TECHNOLOGICAL RESEARCH AND DEVELOPMENT

I. EXECUTIVE SUMMARY OF ACCELERATOR AND EXPERIMENTAL AREAS OPERATION

Since 2019, GANIL operation concerns the LINAC as well as the cyclotrons. The first beam was ejected from CSS2 forty years ago, while SPIRAL1 first radioactive beam is 23 years old. The LINAC is still in a commissioning phase for S³ beams, but also, for the second year, in operation for experiments in NFS (Neutrons For Science) for nuclear physics, nuclear data and also for nuclear medicine development. For the first time, the operation teams have tuned the LINAC from the main control room. Compared with 2022, the shutdown began sooner than usually, in mid-November, due to energetics strains in the world. Therefore, the time available for physics in NFS was decreased. Fortunately, failure rate of the cyclotrons facility in 2023 has been improving compared to 2022. More than 1900 hours are dedicated for beam time in cyclotrons experimental areas.

1. GANIL operation status

Over the almost last 30 years, cyclotrons beam time shows a peak in 2005 and a decrease since 10 years due to the construction and operation of SPIRAL2 (Figure 19).

Since 2019 yet, LINAC operation is to be added to cyclotron operation. Total physics beam time is more than 2500 hours in 2023. Moreover, we have parallel beam-time delivered to SME (600 hours), IRRSUD (1305 hours) and ARIBE (790 hours) operation. This corresponds to a total available beam-time for experiments of more than 4600 hours. During next years, the parallel operation of cyclotrons and LINAC will be considered to increase available time for experiments.

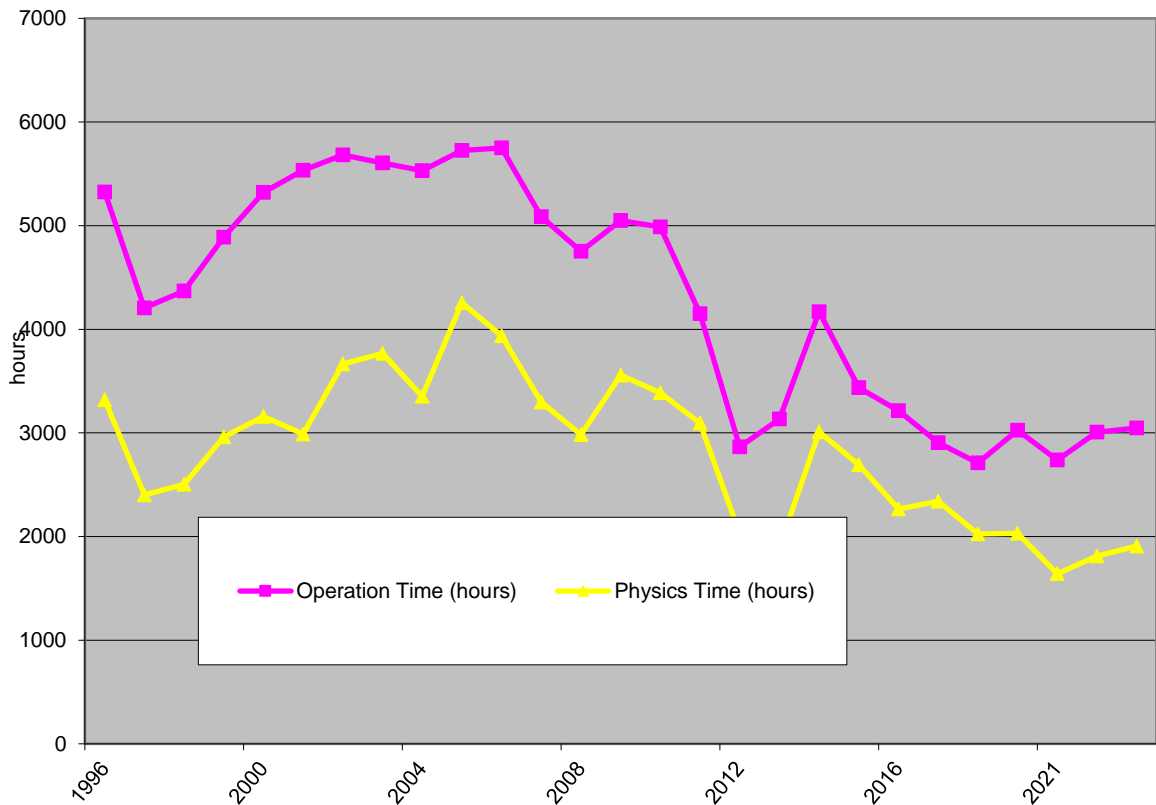


Figure 19: Cyclotrons Beam time available for physics since 1996.

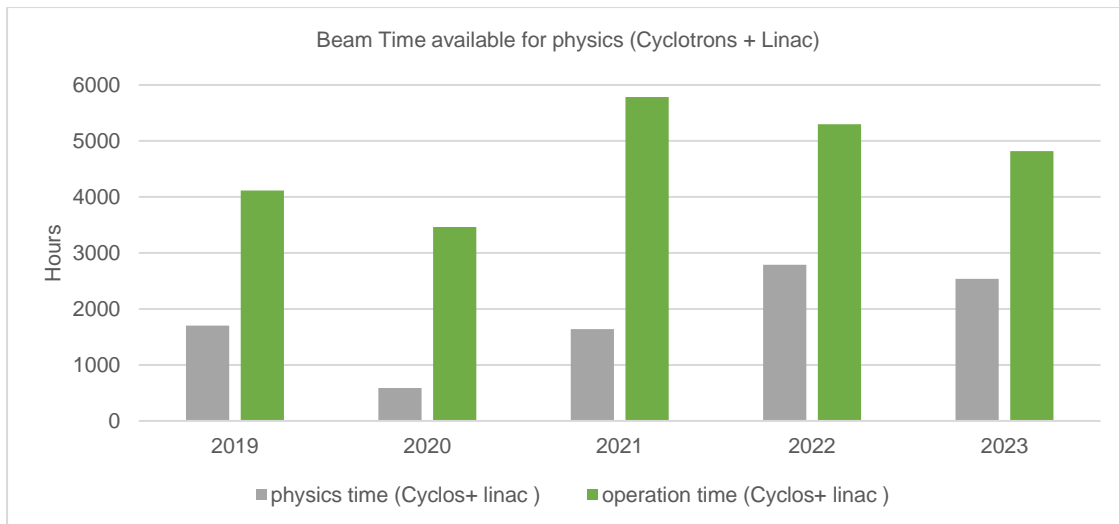


Figure 20: Beam time available for physics (Cyclotrons + LINAC).

2. 2023 cyclotrons operation

The accelerator failure rate is much better, with a notable improvement in 2023 (Figure 21), compared to 2022 when a high failure rate due to water leaks inside the machine was observed.

Nevertheless, the failure rate of the recent last years of an 40 year old machine combined with the high-level of demands at the PAC (Physics Advisory Committee)- still claims the need of the CYREN (Cyclotron Renovation) project, a major renovation plan of the cyclotron facility to operate the facility 20 years more.

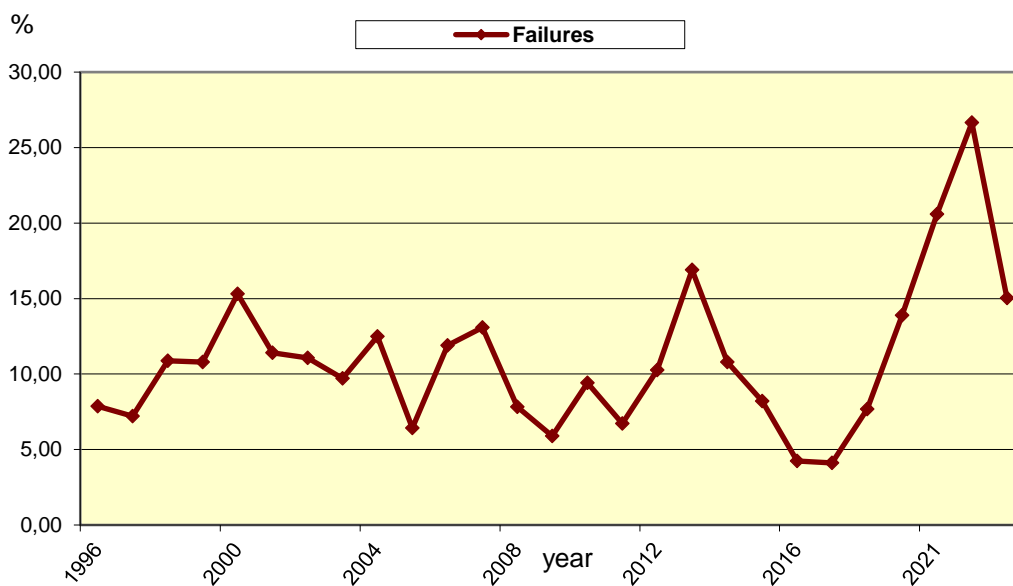


Figure 21: Cyclotron failure rate since 1996

The accelerator tuning rate is at 14%, to be compared to 10% in 2022 and 16% in 2021. Difficulties of tuning have been analysed to be related not to new beams but to experiments needing high intensity, like SPIRAL1 radioactive beams (^{19}O and ^{20}O).

Because of a dedicated time for improving the beam delivery, the part of the machine studies rose up to 6% (2% in 2022). This time for machine studies is related to developments for radioactive beams at SPIRAL1 (see Radioactive Beam Developments in this report) but also to some tests dedicated for SPIRAL2 (production of radioisotopes for medical use in NFS or high-power target development for S^3) in mid-2023.

Significant increase of beam-time for interdisciplinary physics or industrial application follow 2022 technical failures during which these programs had been cancelled to preserve nuclear physics experiments (Figure 22).

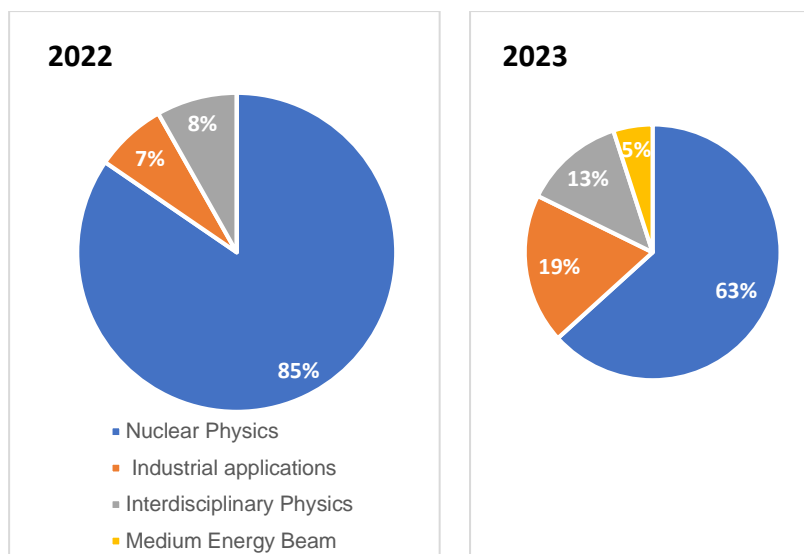


Figure 22: Main Beam Use (High and Medium Energy)

Concerning nuclear physics, LISE (D3/D4/D6) (fragmentation of CSS2 beams and SPIRAL1) is still the most requested experimental area with the cyclotrons beam, right before G1 (fusion reactions or fission studies with CSS1 beams and SPIRAL1).

3. 2023 LINAC Operation

With NFS the only experimental facility in operation, the LINAC schedule is shared between physics, improvement of the tuning methods and tools, and beam development for S³.

D⁺, ⁴He²⁺ have been tuned for NFS in 2023, as well as two beams with ratio $q/A=1/3$ for S³ : ¹⁸O⁶⁺ and ⁴⁰Ar¹⁴⁺ were both accelerated to 7 MeV/u.

Machine studies are related to tests of new tuning methods, beam diagnostics or RF tests, control-command tests.

On the LINAC the tuning time has decreased, going from 20% (in 2022) to 15% (in 2023), demonstrating better control of the accelerator. However, the failure rate (Figure 23) was quite high, increasing from 8 to 19% (mostly RF failures concerning the RFQ).

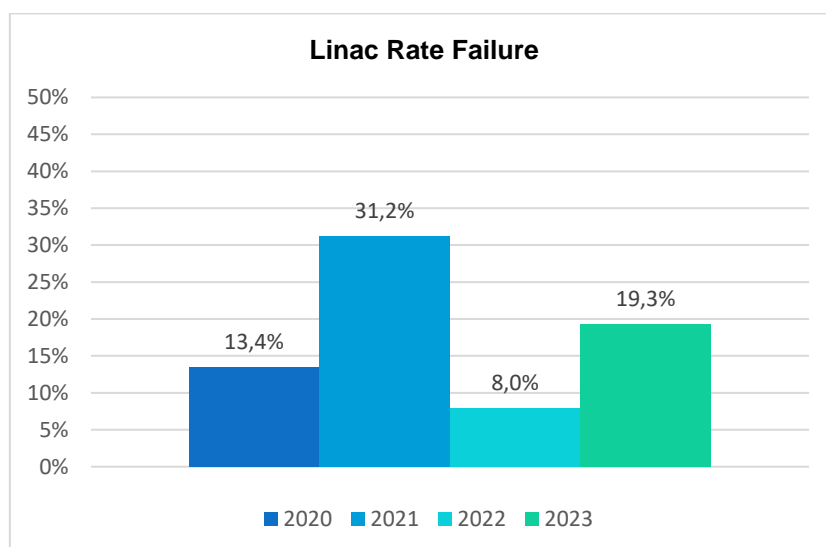


Figure 23: Failure rate (LINAC and NFS)

Five experiments have been proceeded and a new static converter for neutron production from deuteron beam (1,5 kW) has been commissioned. One of this experiment (REPARE) involved $^4\text{He}^{2+}$ beam to produce Astatine 211, an experiment of research and development for nuclear medicine.

However the number of physics hours in NFS compared to 2022 has decreased (about 345 hours less) because of the shutdown of LINAC on mid-November (3 weeks less compared to 2022) having limited the number of experiments. In addition, one experiment had to be cancelled due to technical difficulties of the experiment: E856_22 with 42UT allocated by the PAC.

A machine study dedicated on the tuning method has replaced E856.

II. ION BEAM AND RADIOACTIVE ION BEAM DEVELOPMENTS

1. ECR ion sources production on Cyclotron and SPIRAL2 facilities

New beam: ^{232}Th

In the context of requests for a ^{232}Th beam (LOI10-20, E849_21), the Target and Ion Source group has developed this new beam.

It is produced from a compound of $^{232}\text{ThF}_4$, for which the safety, security radioprotection group has been in charge of the supply.

The characterization of the compound and the tests carried out on the ECR4 ion source allow to validate this new beam, in terms of intensity, stability and charge state required for an acceleration to 6.1 MeV/u.

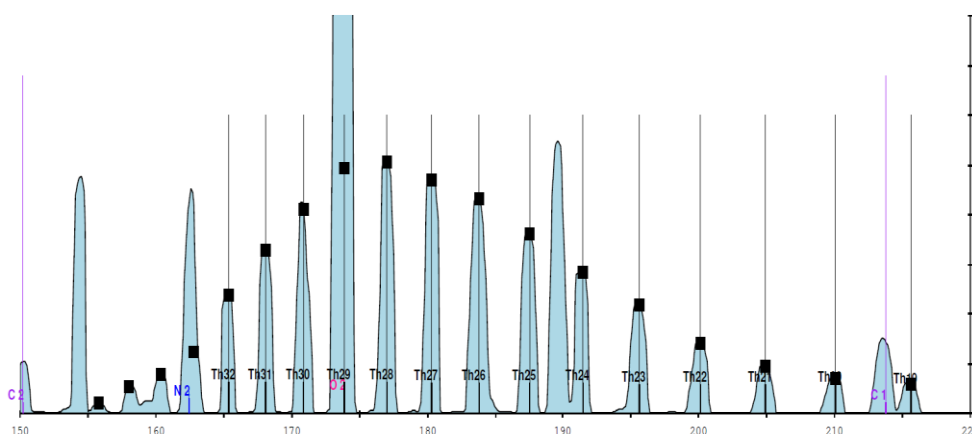


Figure 24 : Thorium beam charge states at the extraction of ion source.

Finally, this new beam was programmed for the start of RUN1 2024 on the cyclotron facility. The intensity delivered by the ion source was around $2\mu\text{Ae}$ (for the 30+ charge state) throughout the 15 days with good stability and without interruption. ThF_4 consumption was very low.

High intensity ^{50}Cr beam

The E805_20 experiment required a ^{50}Cr beam with a high intensity over a long period. This experiment was programmed in April 2023.

To meet this requirement, the Target Ion Source group team worked with the IPHC team to produce the beam. The best method for obtaining an intense medium charge state for a stable, long-duration beam is to use the MIVOC method. This technique is based on the production of a volatile compound including the atom of interest. For ^{50}Cr beam, the molecule is $^{50}\text{Cr}(\text{C}_{10}\text{H}_{10})$ (or $\text{Cp}_2^{50}\text{Cr}$).

The IPHC team is specialised in producing syntheses with enriched isotopes. This compound has a high vapour pressure, which makes it easy to inject into the ion source.

The plasma of the ECR ion source breaks down the molecule and ionises the atom of interest.

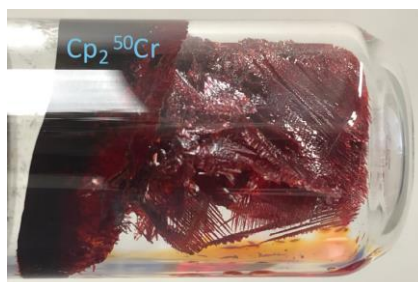


Figure 25 : Synthesis of $\text{Cp}_2^{50}\text{Cr}$ produce by IPHC Team

Finally, a sample of 1gr of $\text{Cp}_2^{50}\text{Cr}$ allows to produce 35UT of $15\mu\text{Ae}$ of $^{50}\text{Cr}^{10+}$

2. SPIRAL2 injectors : Upgrade for heavy ion source.

Heavy-ion source: Phoenix V3

The phoenix V3 ion source is installed since 2020 at the LINAC injection and is dedicated to the production of ions with $A/Q < 3$. During the commissioning of the ion source at GANIL, it presented reliability problems (high voltage, pollution, metallization of insulators) and temporary technical adjustments were made to meet production requirements. In 2023, new devices were developed to improve the ion source and its reliability.

In the same time, the development of the metal beam continued, in particular with the testing of a recycling technique, with the aim of obtaining a $^{48}\text{Ca}^{16+}$ beam with optimized consumption. During this test, we observed the appearance of a hole in the tantalum liner inserted into the plasma chamber. This hole is the signature of a radial confinement problem produced by the permanent magnet hexapole. Given this weakness of the magnetic field, the hot electrons of the plasma of the source ECR have an output path other than the extraction of the source. The energy associated with this electron leakage creates a local heating zone that pierces the liner.

Studies have been carried out on the hexapolar permanent magnet to solve this problem. After measurements and simulations, some of the magnets in the hexapole were changed and we finally found a broken magnet at the origin of the magnetic field instability. The hexapole has been repaired and the magnetic field is now uniform.

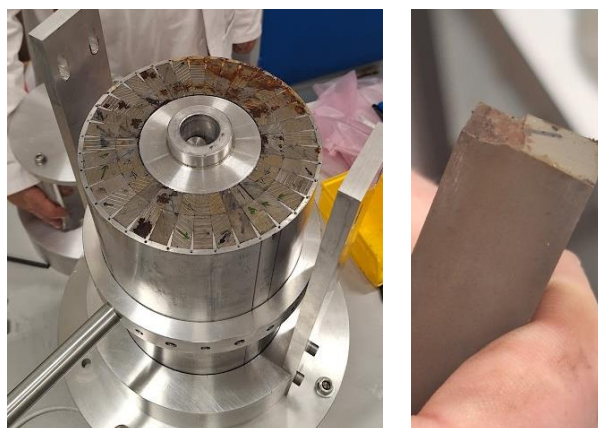


Figure 26 : left : Magnetic structure of hexapole. Right : Broken magnet

During the winter 2023, all modifications of ion source were done, including the installation of the new devices for reliability and the ion source restart in June 2024.

3. SPIRAL1 : Radioactive ion beam development

TULIP project

In July 2023, a ^{20}Ne beam at 4.5 MeV/u beam delivered by the GANIL cyclotrons was used to test a second TULIP Target Ion Source System (TISS) to verify the results obtained in March 2022 on the production rates of $^{74-78}\text{Rb}^+$ ions and the particularly short atom-to-ion transformation time observed. Additional isotopes were observed. Rates were improved compared to 2022 (see table).

Rb Mass Number	Half-life $T_{1/2}$	Production Rates	
		March 2022 ^{22}Ne 4.5 MeV/u	July 2023 ^{20}Ne 4,5 MeV/u
74	64,8ms		1,7E+01
75	19 s		1,5E+04
76	36,8 s	3,8E+03	2,5E+04
77	3,9 mn		1,6E+05
78*/78	5,7 /17,7 mn	5,8E+04	6,8E+04

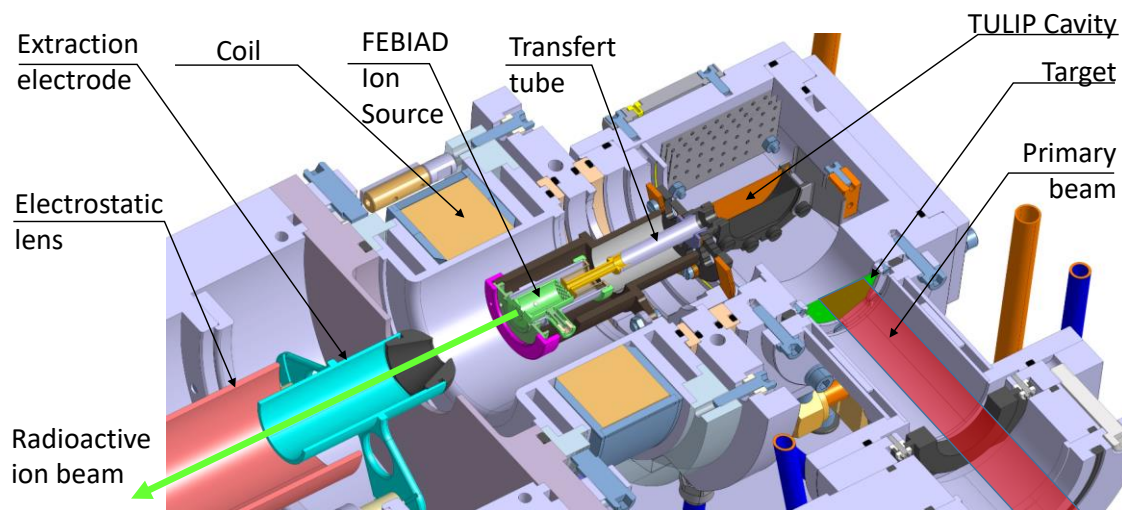
Table 1 : Comparison between yields 2022/2023

The atom-to-ion transformation time showed two components. One of them is long enough to partly explain the low production rate of the ^{74}Rb (65 ms).

An analysis of the production process highlighted several possible improvements : 1 - an increase of the TISS temperature to speed up the release of the radioactive atoms out of the cavity, 2 - an optimization of the primary beam energy to favor the production of ^{74}Rb nuclei, and 3 - an improvement of the primary beam intensity.

To insure the ability of the target to sustain the primary beam intensity and power, a rotating target is under development. Mechanical parts are under construction for a first test in fall 2024.

The main objective of the TULIP project is to deliver a TISS able to produce metallic ions in the region of the ^{100}Sn nucleus. For this purpose, the TULIP cavity developed for alkali ion production has been associated to the GANIL FEBIAD (see Figure) for its high performances. The first off-line tests will be performed by July 2024.



A detailed description of this development is given in the PhD thesis of V. Bosquet, defended in June 2024

TISS MonoNaKe

MonoNaKe is a TISS dedicated to the production of radioactive alkali ions, from Li to Rb. After an on-line test performed in spring 2023, technical improvements and tests have been done off-line to compare the performances of two ionizing materials, *i.e.* Pt and graphite. Regarding their respective physico-chemical features, Pt should offer better performances. Surprisingly, ionization efficiency was better in graphite. A first on-line test with a primary beam of ^{13}C at 60 MeV/u has provided intensities of $\sim 1\text{E}+7$ pps of $^8\text{Li}+$ and of $\sim 1\text{E}+5$ pps of $^9\text{Li}+$. As the primary beam intensity was lower than expected, one can consider a room for progress and a post-accelerated beam of $^9\text{Li}+$ as realistic.

A MonoNaKe TISS equipped with a graphite ionizer was thus used to deliver post-accelerated ions of $^8\text{Li}+$ at 1.2 MeV/u to the E864_22 experiment in June 2024. The intensity was higher than demanded ($> 1\text{E}+4$ pps).



Figure 27 : Photo of Graphite and Platinum ioniser

Li is the most difficult alkali to ionize. The ionization obtained for Li ensures a better ionization efficiency for all the other alkali. Moreover, it suggests the possibility of ionizing other elements like alkaline-earth elements while conserving an ionization selectivity. Such test will be performed by spring 2025.

TISS FEBIAD

In april 2023, a stable beam of ^{50}Cr at 72 MeV/u was sent into a FEBIAD TISS in order to produce radioactive chromium isotopes. Due to the unexpected exhaustion of the primary beam sample, the experiment was cut short and the beam power was reduced to about 1/30 of the expected value. Nevertheless, the experiment was a success as it was possible to estimate the rates for the new beams $^{48,49}\text{Cr}$ and ^{50}Mn and for other several previously measured beams of Cl, Ar and K. These rates can be reasonably extrapolated to higher primary beam power or other available primary beams with higher production cross sections (see table 2 showing the rates in pps per W of primary beam and the expected rate with the GANIL beam yielding the highest production in the target).

We also observed radioactive molecules of AlF and HCl, which could be used in the future for selective extraction of a given species. A small amount of CF_4 was injected into the TISS after irradiation, allowing to create several diatomic or triatomic fluoride ions with Be, C, Al, Mg.

Isotope	rate ^{50}Cr /W (pps)	Extr. best beam (pps)
^{50}Mn	3.5E+02	2.1E+05
^{49}Cr	2.5E+04	1.5E+07
^{48}Cr	1.2E+04	7.0E+06
^{45}K	1.1E+02	5.8E+06
^{44}K	1.3E+03	2.2E+07
^{43}K	1.5E+04	1.1E+08
^{43}Ar	2.5E+01	6.7E+05
^{42}K	1.0E+05	3.3E+08
^{41}Ar	2.7E+03	1.5E+07
^{41}Cl	1.6E+01	2.8E+05
^{40}Cl	1.7E+02	1.5E+06
^{39}Cl	1.9E+03	1.2E+08
^{38}K	2.3E+04	2.5E+08
$^{38\text{m}}\text{Cl}$	9.4E+01	2.2E+06
^{38}Cl	1.2E+04	2.7E+08
^{37}K	4.8E+02	5.3E+06

Table 2: Rate/W of primary beam, measured during experiment and rate extrapolated with the best primary beam

III. PHYSICS OF ACCELERATORS

This report presents new projects started on cyclotrons in order to improve GANIL capacity to deliver beams, in terms of intensity, energy range, or availability. The nominal energy for heavy ions has been reached this year in the SPIRAL 2 LINAC. Theoretical studies on beam dynamics and machine studies in the linac are also described. Artificial intelligence applications for accelerators are also investigated in the frame of a European effort.

1. CYCLOTRONS

Increase of the energy range available on the IRRSUD beamline

The energy range accessible on the IRRSUD beamline is currently between 0.27 and 0.99 MeV/u. However, potential users at the CIMAP laboratory have expressed their interest in very low energy ions and filling an energy zone not accessible at GANIL, between the energies available on ARIBE and those of IRRSUD.

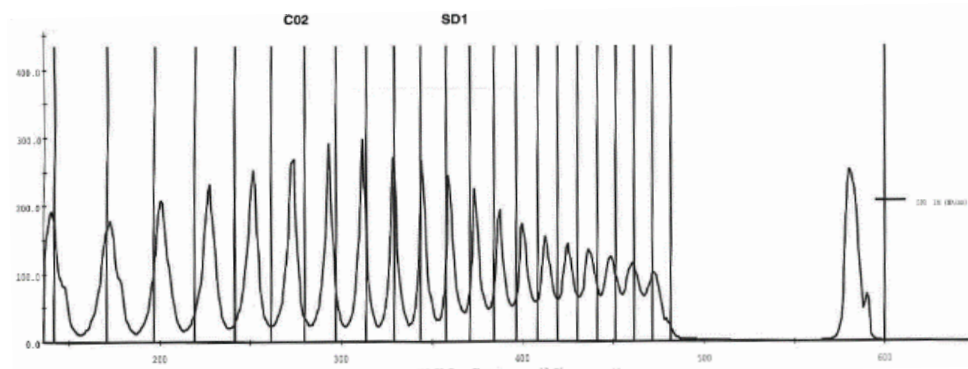


Figure 28 : $^{18}\text{O}^{2+}$ beam turn inside the C02 in harmonic 5 with an HF voltage of 25.05 kV.

The EM133 machine study was carried out with success in guiding approximately 500 nA of an $^{18}\text{O}^{2+}$ beam at an energy of 0.108 MeV/u at the C02 exit in harmonic 5, with an efficiency of 10.6%. The beam optimized in harmonic 5 appears to be usable (intensity and quality in L1 beamline) by physicists on IRRSUD. This $^{18}\text{O}^{2+}$ beam at 0.108 MeV/u also represents the lowest energy ever achieved with the GANIL cyclotrons (Figure 28).

Prospective study of new beamlines in G4 for the SAGA project

Among the various users who come to GANIL, tests of electronic components under heavy ion beam irradiation are carrying out for space industrial applications, and their requests for beam time have recently increased significantly. The objective of the SAGA project (Spatial Applications Ganil Accelerators) is thus to improve accessibility to industrialists to the means of irradiation with heavy ions at GANIL. One solution would be to create new high-energy beamlines.

The idea of carrying out simultaneous experiments to maximize the scientific impact of the GANIL accelerator was successfully deployed at GANIL on the medium energy (SME in 1990) and low energy (IRRSUD in 2003) beamlines. These projects have made it possible to significantly increase the productivity of the laboratory (in terms of number of hours of experience per year) and its scientific impact. This currently allows GANIL to regularly carry out three experiments in parallel on IRRSUD, SME and High Energy.

As part of the emergence of the SAGA project, we studied the possibility of creating new high-energy beamlines, to be allocated mainly for industrial applications, in order to increase their beam time without increasing the operating time of GANIL. One of the solutions considered consists of partially degrading the high energy beam in order to create a distribution of charge states, to separate, and to guide these charge states and the primary beam towards different beam lines.

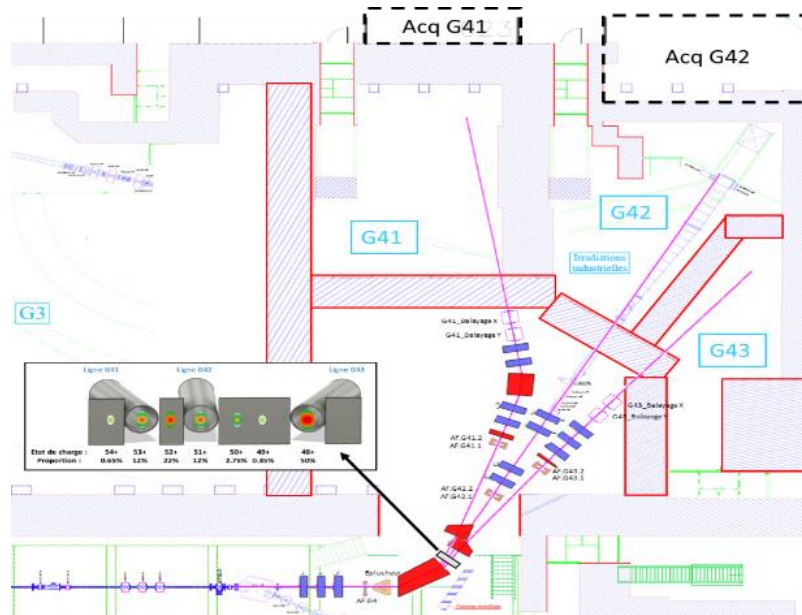


Figure 29: Proposal for the implementation of lines G41, G42 and G43 for the realization of 3 experiments in parallel. The G42 beamline corresponds to the one currently used by industrialists in G4.

The study considers to have 3 beamlines in parallel operation in room G4 (Figure 29). To do so, the two 30° deviation dipoles of the fishbone would be replaced by one of 60° and a removable degrader would be positioned at its entrance. This partial degrader would make it possible to create a distribution of charge states, while maintaining an adjustable proportion of primary beam. At the exit of the dipole, the degraded beams whose Brho will be lower than that of the primary beam, will find themselves deflected towards the inside of the bend with an exit angle directly dependent on their Brho.

Although this proposal is feasible from a beam optics point of view, if retained within the SAGA project it will require extensive feasibility studies from an infrastructure and safety perspective. This particular configuration, although complex to achieve, would nevertheless bring numerous benefits. It would make it possible to carry out three experiments in parallel by having equipment (diagnostics and intensity controls) and independent access from one room to another. These different aspects could thus meet the demands of industrialists, and could also benefit to scientific research more widely (interdisciplinary physics, detector tests, etc.).

Improving a cyclotron injector with a new ECR Ion Source

Two options have been proposed to Accelerator Advisory Committee in 2024 to improve the cyclotron beam intensity. (1) A new ECRIS PHOENIX-V3 developed at LPSC Grenoble, could be installed at the GANIL cyclotrons. Presently the axial injection of C02 cyclotron is relatively inefficient. This, coupled with the growing needs for high intensity beams at GANIL, adds to the difficulty in the optimization of the beam schedule. (2) Another relatively easier choice, requiring a lower manpower and budget (but with a lower performance) could be envisaged by installing a Grenoble Test Source “GTS” (like the one available at ARIBE). Such a choice would need almost no modification of the beam line (same voltage, same inflector). The intensity gain being lower, it would be more effective to put this GTS source on the HV platform of C01.

Radioactive Beams around 1 MeV/u in G21

The GANIL-SPIRAL1 facility has delivered Radioactive Ion Beams (RIBs) for 20 years. The post-accelerator, the Cyclotron CIME, delivers purified radioactive beams with a good transmission (15%-30%) from 1.8 MeV/u to 15 MeV/u. Attempts have been made to deliver beams at 1.2-1.8 MeV/u with a very low transmission (~ 1%). Figure 30 shows the new set-up in G21 for nuclear astrophysics with ACTAR in G21. The new set-up has been validated in June 2024 with an intense radioactive beam ^8Li at 1.2 MeV/u.

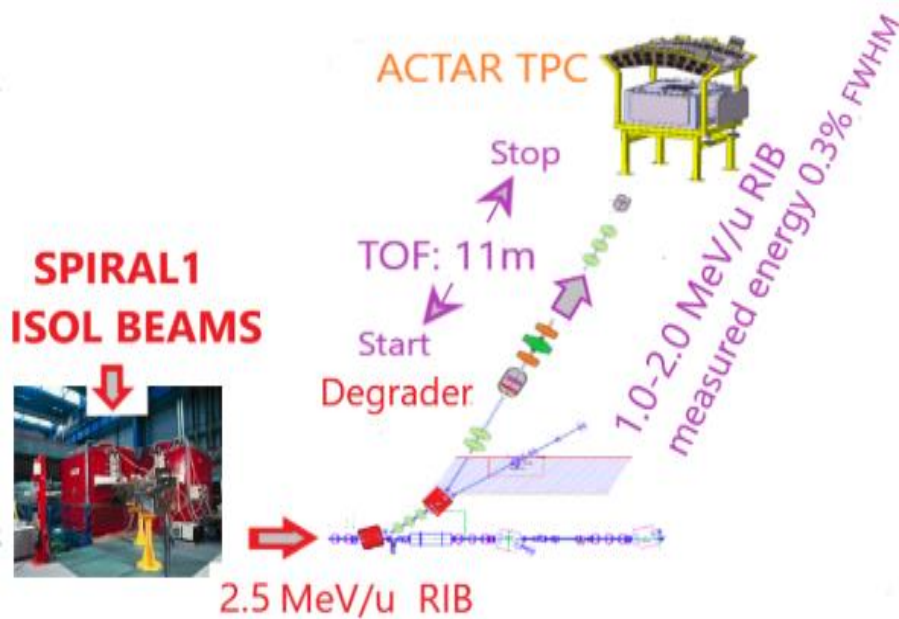


Figure 30: Principle of the degraded beam. Energy degradation of the beam will increase a lot the energy dispersion (+1-2% σ_ϵ). Therefore, a measurement of the energy of each particle is required (TOF).

2. LINAC

Linac tuning with a missing cavity

In the most recent study without CMA6 cavity, a $900 \mu\text{A}$ $^4\text{He}^{2+}$ beam was accelerated to 64 MeV instead of the nominal value of 80 MeV. Nevertheless, a 2 kW total beam power was transported to the beam dump with a transmission of 99% (Figure 31). The beam-loss increase in the HEBT confirms the reduction of the longitudinal acceptance in the studied case. Considering the importance of the study to assess the reliability of the LINAC, the need of a dedicated tool to facilitate the calculation of new parameters in case of a cavity failure, and the advantage of being able to conduct tests for its development, the Accelerator Physics group participates to the REFILL project with LPSC Grenoble and other international laboratories. The goal of the collaboration is to improve the reliability of linacs. The first phase plans to develop models, simulations tools that can be adaptable to different high power linacs such as SPIRAL2, ESS, JPARC, MYRRHA/MINERVA, ADS linacs...

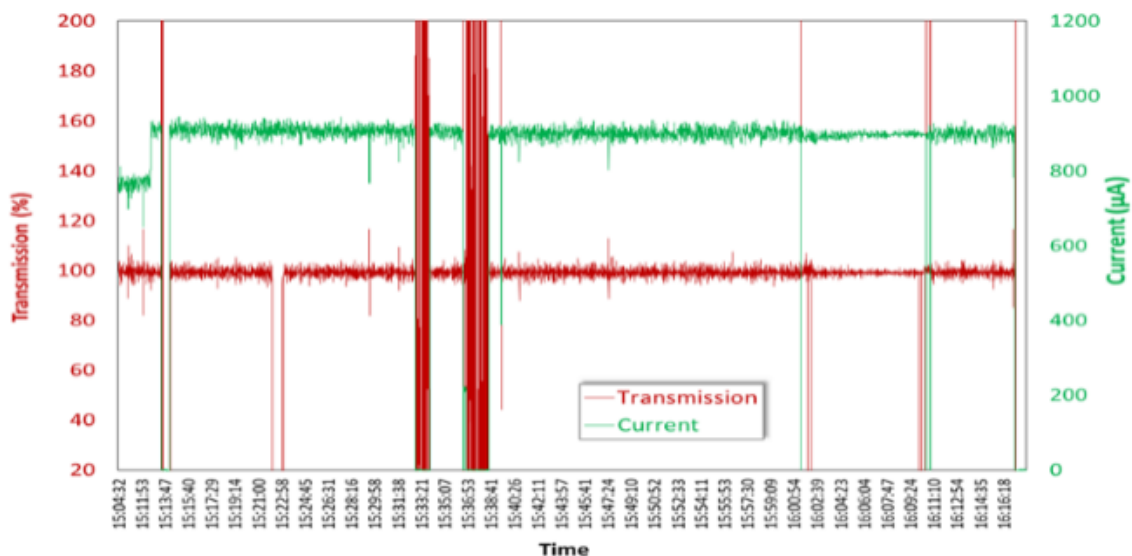


Figure 31: Transmission (red) and current (green) evolutions of a $900 \mu\text{A}$ $^4\text{He}^{2+}$ beam without CMA6.

Heavy ions at nominal energy

Figure 32 presents the results of the first heavy ion acceleration to 14.5 MeV/u. A power ramp-up to 2 kW with a $^{18}\text{O}^{6+}$ beam at 14.5 MeV/u was performed to qualify the tuning.

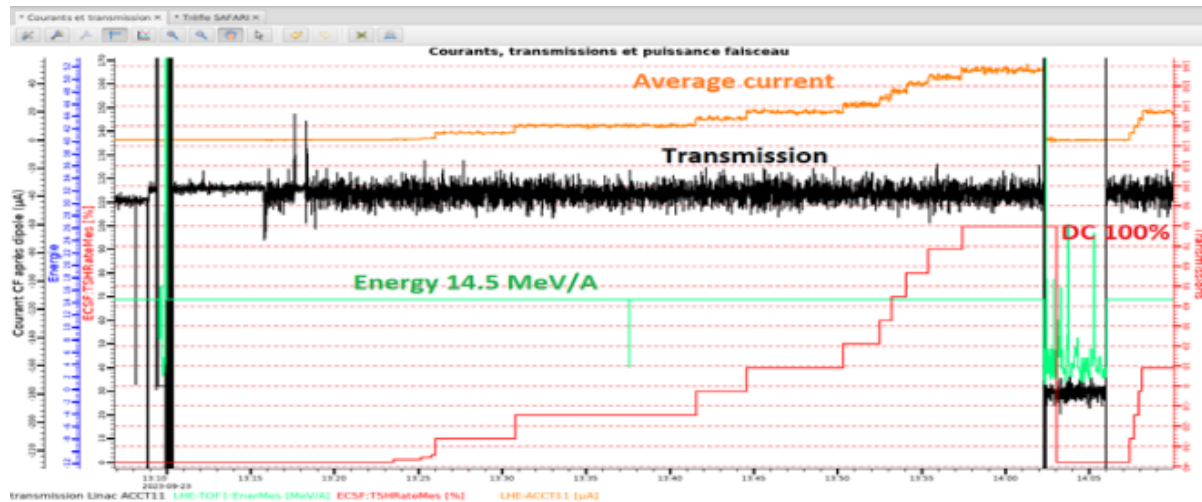


Figure 32: Power ramp up of 50 μA $^{18}\text{O}^{6+}$ beam: Energy (green), transmission (black), average current (orange) and duty cycle (red).

Beam physics studies

Two studies were recently done for a better understanding of the longitudinal beam dynamics with high-gradient accelerating fields and to increase the accelerating gradient in the first linac cavities. The first one deals with the excitation of the 4th-order resonance ($\sigma_{\parallel} = 90^\circ$) leading to strong longitudinal emittance growths and acceptance reductions, even at low space-charge. In the second one, a new optimized definition of the synchronous phase allowing improving the linac performances was proposed. Already implemented in TraceWin it was successfully used to optimize the SPIRAL2 linac tuning for heavy ions up to $A/Q = 7$.

Artificial intelligence for accelerators

Artificial Intelligence for particle accelerators is increasing every year, improving reliability of related research infrastructures. GANIL started investigating some applications of these advanced techniques in the SPIRAL2 linac. At the same time, GANIL has taken a central place in structuring and coordinating a national and European effort towards a synergetic approach to develop, deploy and disseminate the use of these techniques and bring optimisation and reliability to the next level. At GANIL, the work on AI applications at the accelerator division started with the study of a virtual heat load observer for SPIRAL2 superconducting cavities. A PhD funding allowed to continue this exploratory work.

IV. EQUIPMENTS FOR BEAM ACCELERATION, TRANSPORT AND DIAGNOSTICS

1. Improvement of the precision of measurement of the SPIRAL2 BPM

The Beam Position Monitors (BPM) are beam diagnostics installed in the quadrupoles of the hot sections of the SPIRAL2 LINAC. Twenty BPMs and their instrumentation chain measure the following characteristics: beam position, ellipticity (a characteristic of the transverse shape), and beam phase.

The four electrodes of a BPM pick up the electric field induced by the bunch of ions from the beam. The generated signal is periodic and can be decomposed in harmonics, mainly at the accelerator frequency ($f_1=88.0525$ MHz) and at its double frequency ($f_2=176.105$ MHz). The level of the signal is mainly due to the beam intensity, its energy and the considered harmonics

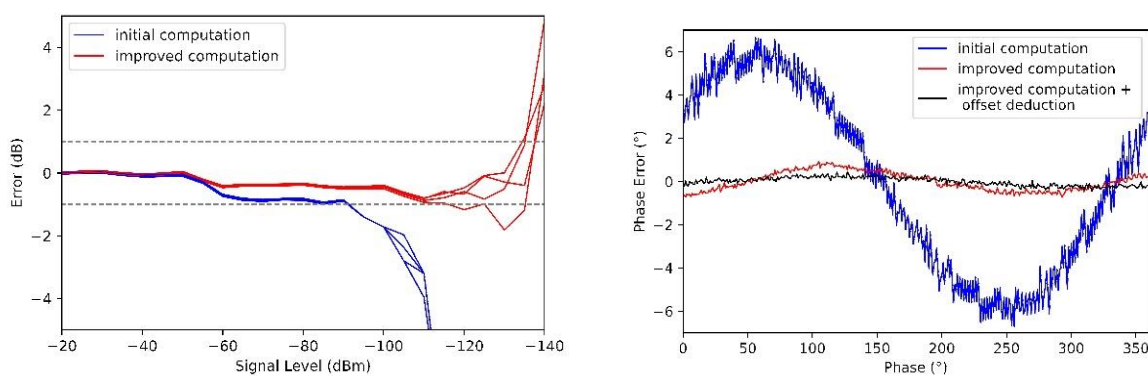


Figure 33 : Left : Error of the measurement of level for the four channel as a function of the input level before and after the modifications of the algorithms. Right : Error of the phase measurement as a function of the phase of the signal equivalent to a $1\mu A$ beam.

Improvement of the instrumentation chain has been previously done (see 2022's report), making possible to measure beam characteristics with an intensity down to $50\mu A$, namely signal power down to -90 dBm. Below this intensity, the measurement precisions deteriorate quickly. Future beams of S^3 , including those of Newgain, could have an intensity below this value. It is thus important to increase the dynamic of measure toward the low levels of signal. This improvement was achieved by modifying the digital signal processing.

The acquisition chain is composed of an analog acquisition followed by a digitization. The digital signals are then processed in a programmable electronic component (FPGA). The data is transmitted to a computer card (CPU) for further digital processing and publication to the network.

We have undertaken modifications to the digital processing code embedded in the FPGA chip and the CPU. The graphic in Figure 33 shows the error of the signal level measurement for different signal levels. One can see the increase of the measure range: the measured error is in the range of ± 1 dBm for signals levels down to -110 dBm, i.e. a beam intensity less than $1\mu A$.

These modifications have shown similar improvements for the phase measurement. Changes were also done in the CPU to deduce parasitic signals (for example perturbation signals from the voltage of the cavities) from the real signal (see Figure 33).

All these improvements are now to be confirmed in real case during future machine studies. Laboratory studies have also shown that improvements could be achieved by enhancing the regulations that are taking place in the FPGA.

2. Safety plan for RFQ1 amplifier operation

The RFQ1 (Radio Frequency Quadrupole) is an essential part of the linear accelerator SPIRAL2, bunching and initially accelerating the ions so that they enter the first superconducting cavity at an energy and phase compatible with the operation of subsequent cavities.

This RFQ operates at room temperature, and requires the injection of an RF wave @88.0525MHZ supplied by four 60kW amplifiers. More precisely, four waves of the same frequency are recombined inside the RFQ.

The RFQ1 requires a maximum accelerating voltage of 114kV for heavy ions ($Q/A=1/3$), and a lower voltage (of the order of 50 to 85 kV) for deuterons and protons. Maximum voltage can only be reached when all 4 amplifiers are switched on, whereas it is possible to operate with 3 amplifiers to deliver proton and deuteron beams.

Since the first power tests of this equipment, a number of failures have affected its operation. In particular, the tetrode tubes of the amplifiers, 2 out of 4 of which have already been replaced, as well as various power components that were replaced or repaired (preamplifiers, dimmers, HV power supply, cooling circuits, sensors, etc...). Over time, we have been able to deploy a limited plan for upgrading certain elements, and purchasing a large number of spare components. However, this strategy does not guarantee 100% availability of these amplifiers, which could jeopardize SPIRAL2's heavy-ion delivery to the spectrometer S³. In addition, the cost of the main components (Tetrodes) is incredibly rising, since the production of tetrodes tubes is becoming a niche market. In 2023, the division and the group decided to work on a medium-term plan to secure operations, which mainly involved adding a solid-state amplifier, with the aim of significantly reducing the time needed to return to operation in the event of a major failure. This additional amplifier would then be connected in place of the failed one, using coaxial lines. Furthermore, the modular architecture of a solid-state amplifier makes the occurrence of a major failure less likely, as we observe with LINAC superconducting cavity solid-state power amplifiers.

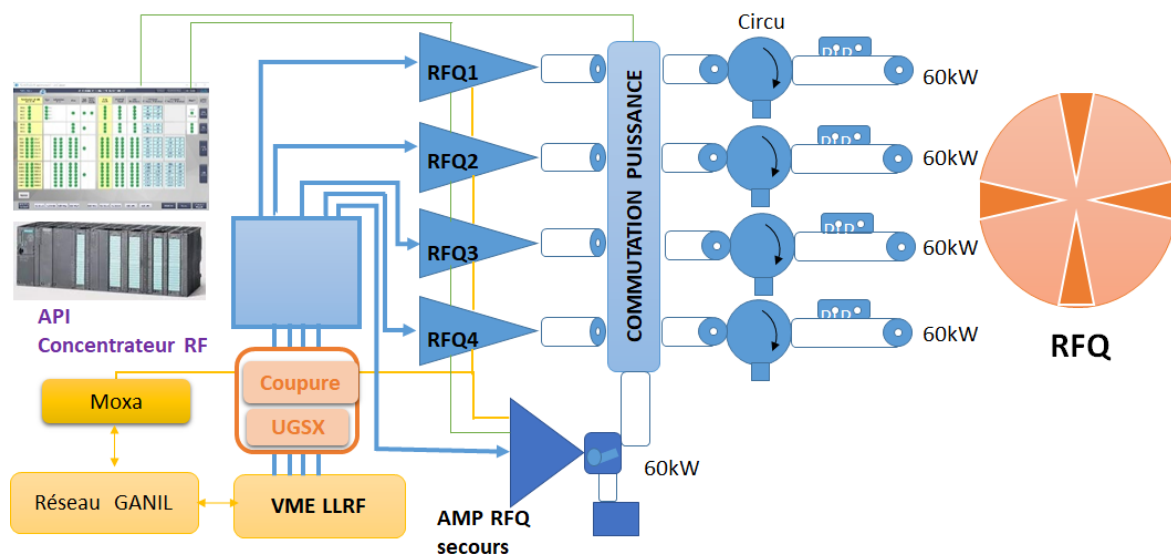


Figure 34: RFQ signal architecture with the spare RF Amplifier

During the year, we were able to define the layout of the future crate within the existing amplifier rooms, and identify the requirements in terms of electrical power and cooling (which must remain compatible with what is available in that room). We also had to imagine the structure and estimate the cost of an RF switching grid (see Figure 35, example of coaxial RF power lines), and define the overall architecture of the system with regard to control and feedback signals (see Figure 34).

We have also considered the various possible configurations with respect to the existing Master-Slave concept, and the consequences on the test plan of this 5th amplifier.

We were able to draw up a provisional schedule to make the validation of the future amplifier compatible with SPIRAL2's operating schedule.

Once the broad outlines have been established, we have been able to work on the specifications for the future 5th amplifier, whose main features will be shared with the RFQ2 solid-state amplifiers (Newgain project). The call for tender has been issued, and bids received.

We should work in 2025-2026 to validate the first solid-state power amplifier 40kW for RFQ2 at GANIL, and then the 60kW 5th amplifier for RFQ1. Sharing the same technologies between this 5th amplifier and the 4 of RFQ2 (with $Q/A=1/7$) will result in savings in terms of spare parts costs, ease of implementation, and reactivity in the case of potential failures



Figure 35: Exemple of RF power distribution

V.AUTOMATS AND COMMAND CONTROL

1. Realization in the experimental areas

REPURE project

The REPARE project aims at validating the experimental procedure to produce innovative radio-isotope for medical applications. The important radioactivity induced in the irradiation of materials need a complete automatic hand-off handling of the targets. Creation of an electrical cabinet and a control box equipped with a ET200SP PLC and two SINAMICS CU310 drives to allow the unloading of multiple targets after beam irradiation.



Figure 36: REPARE's automation management

Autofill of Liquid Nitrogen for Germanium detectors

Germanium detectors are an important instrumentation for GANIL users who hunt nuclear structure of rare species. In 2022, we designed a prototype of mobile cabinet able to cool up to 16 germanium detectors. Following the success of this project, in 2023, we duplicated this prototype to have a second one. It allows us to have one on the GANIL original installation and one on LINAC's experiment areas.



Figure 37: Left :Picture of the new Programmable Logic Controller. Right : Supervision of the Autofill Cabinet

Automation and electrotechnical renovation of the D5 experiment room

Previously, automatism of vacuum, insertions and all the equipments around INDRA / FAZIA confines was drive with an APRIL brand PLC. In collaboration with the technical coordinator of D5 experience area, we have renovated the electrical engineering and automatism of D5 by using a S7-1500 PLC.



Figure 38: PLC before renovation



Figure 39: New electrical cabinet



Figure 40: New PLC

2. CYREN

Renovation of the vacuum automation of the L3 line and the CSS2 cyclotron

As part of the CYREN project, the renovation of the original GANIL automation systems continues with the renovation of the vacuum automation systems and the Human-Machine Interface (HMI) of the L3 line, composed of seven vacuum chambers and the CSS2 cyclotron.

Previously controlled by S5-135U PLC (programmable logic controller) which are now obsolete, the vacuum equipment is now managed by S7-1500 PLC. This allows to improve the diagnostic, modernize the communication protocol and improve the drive of vacuum equipments.



Figure 41: L3 and CSS2 PLC

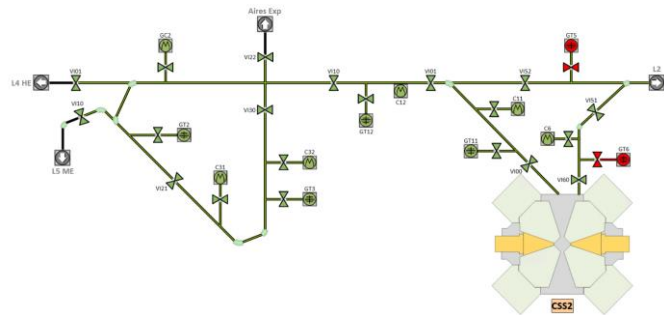


Figure 42: L3's vacuum supervision

Renovation of CIME vacuum controller



Figure 43: CIME's PLC

The CIME vacuum controller has also been revamped with an S7-1500 CPU. This controller also manages the regulation of the new cryopanel cooling system. This renovation is part of the modification of the cooling system of the CIME northern cryostat. Deployment will continue on the southern cryostat when the tests will be validated.

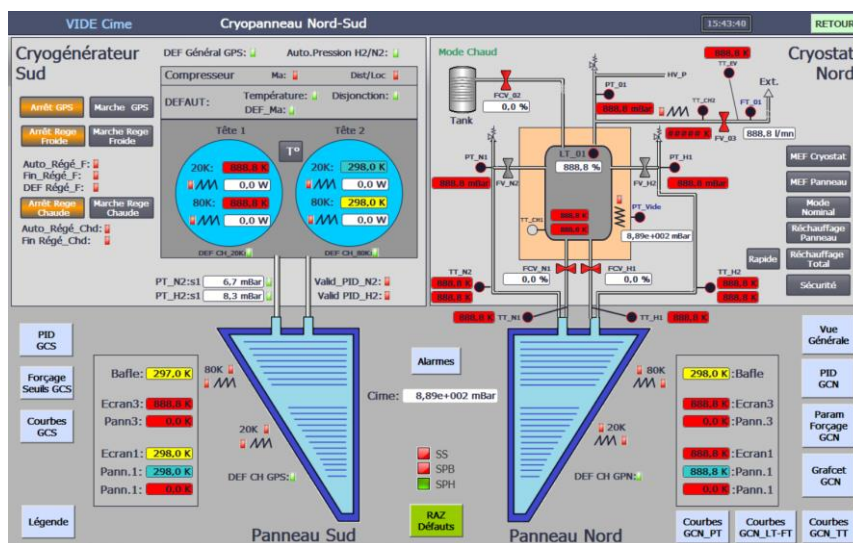


Figure 44: CIME's HMI

3. Organization of G2CA activity

Open Project

G2CA's activity is cross-functional, the automation and IT teams each handle around 400 tasks per year to provide other technical groups solutions for connecting and controlling their equipment.

Since 2023, the group uses the Open Project tool to organize activity. This tool makes it possible to formalize requests, prioritize them in relation to each other and track them, the tool also makes it possible to keep the history of processing a task and sharing information with team members and needs holders. It is a tool that promotes collaboration and allows to have an AGILE approach and apply some simple LEAN rules such as visualizing and limiting tasks in progress in order to positively impact the flow of deliveries.

VI. ACHIEVEMENTS IN MECHANICS

This chapter describes some of the achievements of the Mechanics group of GANIL.

1. S³ Stable target station modification

A stable target station was manufactured for the S³ project a few years ago, and it was tested with beam for the first time in 2023. These tests permitted to define some necessary improvements on the design of the station, including manufacturing modifications. These modifications were not especially difficult, but considering the dimensions of the station, it was not possible to use the numerical machining center. In this context, the GANIL machine shop used conventional milling machine.



Figure 45: Measurements and Manufacturing

2. S³ Electrical dipole feedthrough integration

The S³ electrical dipole designed by IJCLAB was mounted and integrated in the S³ room in 2021. This operation did not include the feedthrough that were not manufactured yet. As the feedthrough were supplied at the beginning of 2023, the GANIL mechanical team, with the collaboration of IJCLAB, finalized the global assembly of the electric dipole.



Figure 46: Feedthrough

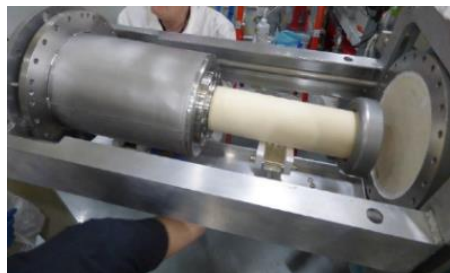


Figure 47: Integration tool



Figure 48: Feedthrough integrated

3. REPARE first beam test

The high power irradiation station designed by GANIL in the context of the REPARE project, with the goal to produce up to 100 GBq of ^{211}At in 8 hours of He beam irradiation, has been installed at the mid of 2023 in the NFS facility to permit the first tests with beam, and the first production of ^{211}At . Installation and first tests included all the mechanical skills (design, manufacturing, mounting and alignment), and needed an important global coordination to result to experiment with others professions.

These first tests did not permit the final validation of the irradiation station, but made it possible to understand different problems, and to launch global design and manufacturing improvements before the next tests under beam in 2024.



Figure 49: REPARE in NFS facility

4. EXOGAM in NFS

To allow the E838_21 experiment in NFS, an EXOGAM structure was designed, calculated to stand seisms, manufactured, installed and aligned in 2023. The design was constrained by the NFS facility, but this equipment was designed to be installed also in the G21 experimental room.

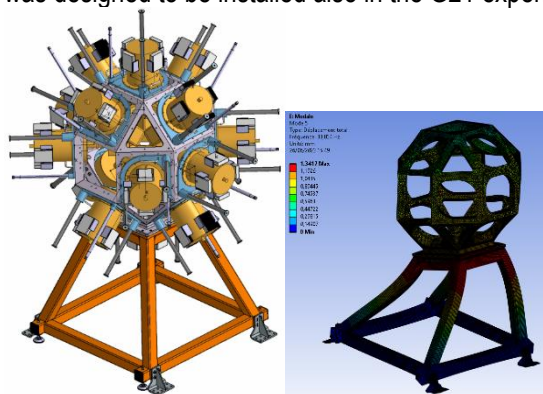


Figure 50: Design and seism calculation



Figure 51: Manufacturing and assembly

5. Building Information Management

Considering the evolution of the Building Information Management (**BIM**) in terms of conception, digital twin, building manufacturing, maintenance, data retention, life cycle and so on..., the design office started a reflection to integrate this new way of working. Indeed, all building and infrastructure companies are engaged in this direction already, and GANIL could have an interest to do the same. That is why a BIM FORUM was organized at the end of 2023.

Its goal was to well understand what is the BIM, what are the advantages, and what is necessary in terms of organization, manpower, skills and budget.

6. Phoenix ion source optimized injection

In the goal to improve the reliability of the polarized disk of the Phoenix ion source injection, a design was launched in 2021 to permit the cooling of this disk, and to optimize its materials and its dimensions.

This equipment was supplied in 2023, and it involved different manufacturing technique as 3D metal printing, bi-material brazing, machining, bending...



Figure 52: Design

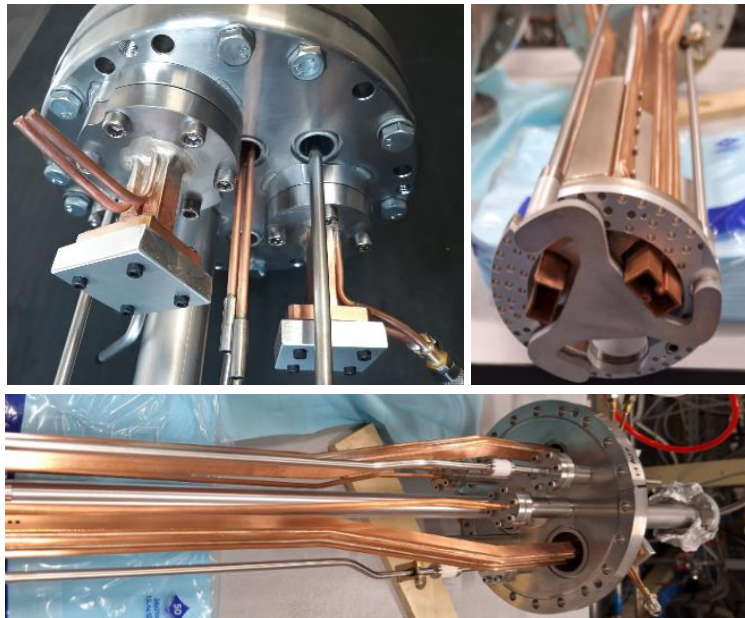


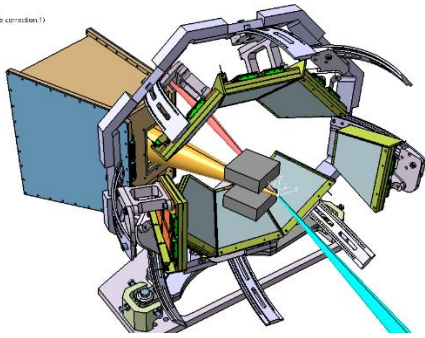
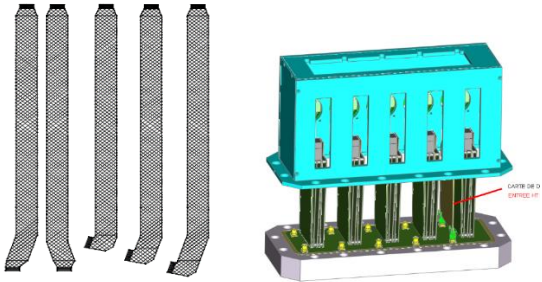
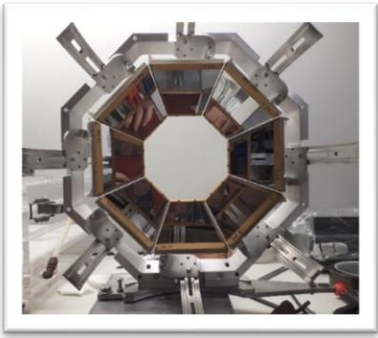
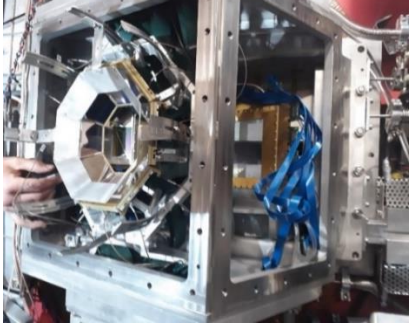
Figure 53: Manufacturing

VII.DETECTION AND LASER FOR PHYSICS

1. First use of PISTA in the VAMOS 2023 campaign

PISTA (Particle Identification Silicon Telescope Array) is a highly integrated telescope array with high granularity. It is used to study transfer-induced fission reactions in inverse kinematics to detect light ejectiles from the target. The first stages of PISTA are 100 μm thick single-sided silicon-strip detectors, while the second stages are 1 mm thick single-sided silicon-strip detectors, both with trapezoidal shape. The PISTA detection system measures the angle and the energy of the target-like recoils, which enable the proper characterization of the fissioning system in mass, atomic number and excitation energy. The detector is placed 10 cm from the target position, which permits to detect emitted nuclei from 30° to 60° .

PISTA is a project financed by CEA/DAM/Bruyère le chatel and GANIL. Only two years have been necessary to design, integrate and optimize the detector system and all has been ready in time for the 2023 campaign in G1, which was a real challenge.

<p>1/ Design of the system:</p> 	<p>2/ Routing of specific cables and interface vacuum Flex kapton circuit of 1200 channels connected to MMR electronics by specific interface</p>  <p>Cables Interface</p>
<p>3/ Assembling</p> 	<p>4/ Integrate in target point G1</p> 

Credits: G.Frémont

2. S³LEB

The S³ Low Energy Branch (S³LEB) has been mounted and intensively commissioned off line at the LPC Caen labory during the last past years and resulted in 3 PhD thesis in 2023 [1,2,3]. High resolution narrow-band in-gas jet laser spectroscopy of stable Erbium isotope was performed, achieving a spectral resolution of 268MHz as well as isotope shift and hyperfine constants measurements. These results were published in [4]. However, the resolution attained at S³-LEB indicates a jet with Mach number 4.5 whereas a Mach number of 8.5 was expected. In order to diagnose jet formation, the technique of Resonance Ionization Spectroscopy flow mapping, where the excitation step laser frequency is scanned along the gas jet, was used (see Figure 54). After implementing several improvements as realignment of the lasers, reduction of the laser power to avoid power broadening, correction of the pressure reading and fine tuning of the background pressure, a resolution of 206MHz could be obtained,

which corresponds to Mach number 6.8, as shown in Figure 55 [5]. Further investigations will be necessary in order to further improve these results.

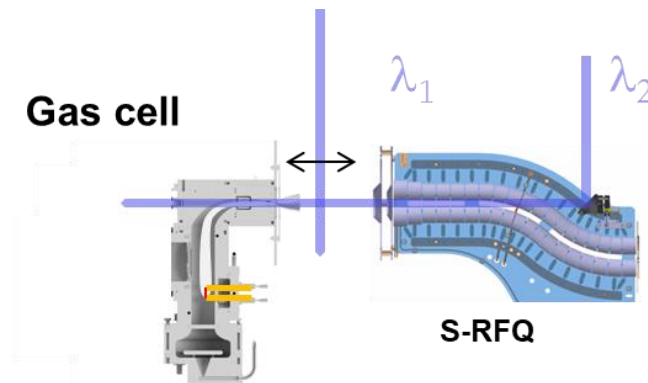


Figure 54: Scheme of gas cell and gas jet with scanning of the position of the probe laser beam.

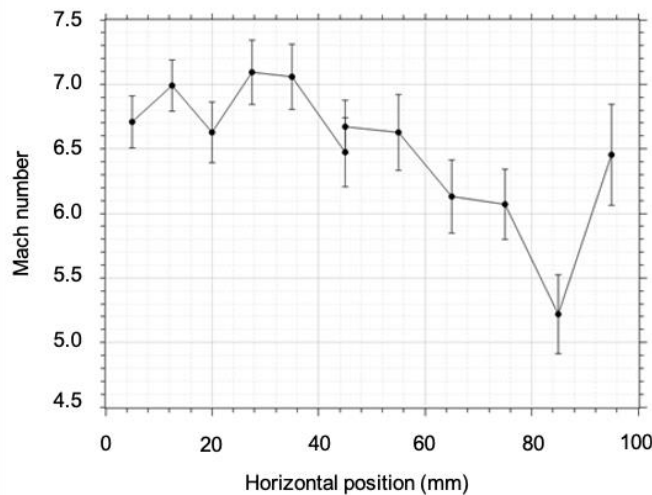


Figure 55: Deduced Mach number as a function of the horizontal position of the probe laser beam in the gas jet after optimization.

Another result deduced from ref [4] is that the ionization scheme involving the 415.2 nm first step is very efficient for Erbium and reasonably sensitive to hyperfine constants measurements. However it provides very small isotope shifts that prevents to deduce the changes in charge radii with a good precision. Therefore, search for other transitions better suited for laser spectroscopy was performed and the transition 408.8nm was found to have much larger isotope shifts, as shown in the Figure 56 [6]. This new transition will be used for the isotope shift measurement of Erbium during the on-line commissioning at S³.

Finally, the TiSa based laser system for laser spectroscopy purposes at S³LEB is being improved with the development of a new direct diode pumped continuous wave Ti:sapphire cavity as shown in Figure 57 [3]. Such a cavity has a wide wavelength scanning range, and is to be used as a seed for the injection-locked lasers. It will replace the cw external cavity diode lasers with limited tuning range that currently act as the seed source, while being cheaper than commercially available cw Ti:sapphire lasers.

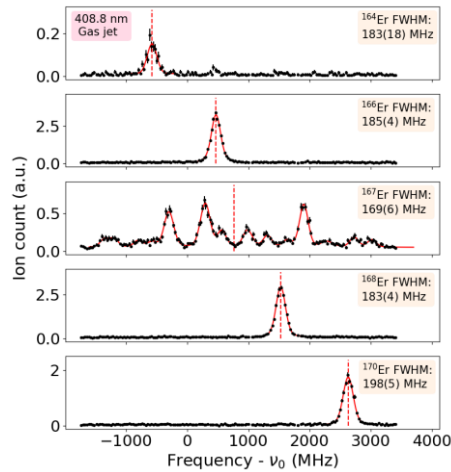


Figure 56: Isotope shifts and hyperfinesplitting of natural Er isotopes obtained with the 408.8nm first step transition in gas jet.



Figure 57: New direct diode pumped continuous wave Ti:sapphire cavity under development for S³LEB .

- [1] PhD thesis of A. Ortiz Cortes, GANIL/JYU (2023) <https://theses.hal.science/tel-04508679>
- [2] PhD thesis of J. Romans, KU Leuven (2023) <https://lirias.kuleuven.be/4071124&lang=en>
- [3] PhD thesis of A. Ajayakumar, GANIL (2023), <https://theses.hal.science/tel-04483471>
- [4] A. Ajayakumar et al., NIMB 539, 102-107 (2023)
- [5] Private communication, PhD thesis of F. Ivdikov, KU Leuven
- [6] Private communication, PhD thesis of W. Dong, IJCLab

3. INDRA-FAZIA

During 2023 the INDRA-FAZIA collaboration has launched some developments in order to improve the experimental set-up.

The full INDRA silicon detectors upgrade has been completed and installed. Combined with the new INDRA electronics it allows better isotopic identification up to Z~9-10. We also completed some maintenance on Caesium Iodide CsI(Tl) crystals where photomultipliers were unglued.

In addition, we also started some new works with the old ionisation chambers of INDRA. We have investigated two solutions. First a renovation of the existing one at GANIL, see Figure 58 and second, some new developments and upgrade at LPC Caen. The goal is at least to benefit from two of them, covering rings 6-7 and rings 8-12 for the next INDRA-FAZIA campaign in 2025.

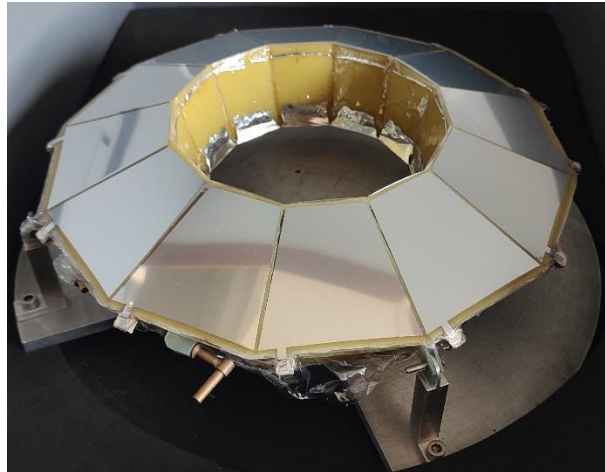


Figure 58 : Ionisation chamber of INDRA covering the rings 6 and 7, renovated at GANIL.

The FAZIA collaboration has also launched some R&D on very thin silicon detectors ($\sim 25 \mu\text{m}$) for low energy experiments (with Spiral 1&2 beams for example), see Figure 59. A thin first layer will reduce considerably the detection thresholds as Pulse Shape Analysis for identification (PSA) is (so far) impossible under $\sim 50 \mu\text{m}$, which is the case for standard FAZIA telescopes.

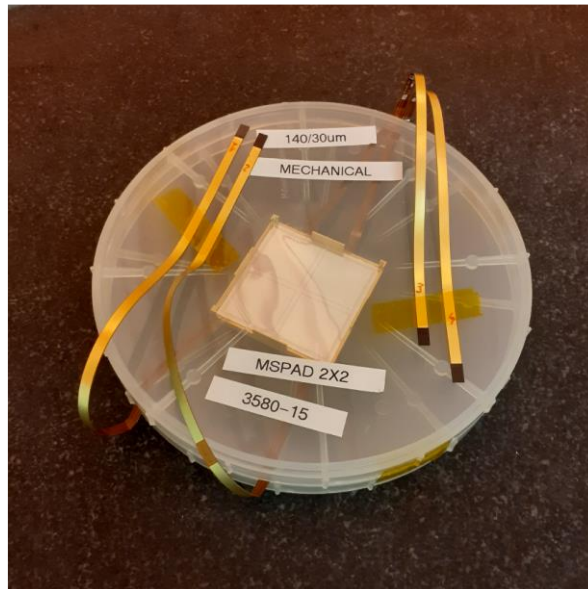


Figure 59 : Prototype of very thin silicon detectors of FAZIA. The PAD covers the first layer of 4 telescopes.

These developments on new thin silicon detectors will enlarge in the future the capabilities of FAZIA to perform in various range of beam energies and thus additional domain of physics. They use the single PAD technology which consists of using the same silicon matrix for four telescopes all together thus reducing dead zone in between them. This technique could be later reasonably used for the standard thicknesses (300, 500 and $750 \mu\text{m}$) of FAZIA silicon detectors.

We have also developed a new device to monitor the beam intensity and to be able to measure cross sections for physics analyses. It is composed of four plastic detectors read by photomultipliers and sent as scalers in the INDRA Data Acquisition system (DAQ). They are mounted in circle downstream of the INDRA-FAZIA apparatus at very low angle (1.6°) around the beam axis, see red arrow on Figure 60.



Figure 60 : INDRA (left)-FAZIA (right) apparatus in D5 at GANIL, the red arrow indicates the location of the beam detectors monitor downstream the beam line, behind the 12 FAZIA blocks.

Those plastic detectors and the electronic chain behind have been validated in G4 using parasitic Xe and Kr beams devoted to industrial applications in spring 2023. Plastic detectors are fast and sustain large counting rates, so are well adapted for this task.

In parallel of detector developments, we have also updated the whole command and control for vacuum control and target loader.

VIII. Data Acquisition

1. Experiments support

Support to experiments is an important mission of the acquisition technics group. It corresponds to 30% to 50% of the group's activity. The experiments E839, E805, E815, E843, E850, S³ target and Sirius tests, Tulip, E838, E802, E858... have used GANIL Acquisition developed and maintained by the group. The group provides support in the preparation of electronics, the triggering systems, the configuration of digitizers, the implementation of user accounts and associated softwares. On-call duty was carried out for more than 1600 hours.

2. SMART

2023 is a key year for the SMART project in terms of results. SMART (Sfp connectivity and Microtca for Advanced Remote Trigger) is a new time-stamping and selective trigger system. The architecture, built according to the MicroTCA standard, uses a tree configuration with a single HUB card and up to 16 ROUTERS to reach 240 digitizers called END POINTS. These modules exchanging data at 4 and 2 Gbit/s are connected by high-performance copper cables, or optical fibers for distances that can exceed 100 meters. This device allows the synchronous distribution of a 100 MHz clock to each END POINT and a timestamping system where each clock of each END POINT is capable of tagging data buffers on 48 bits/10 ns with a temporal error of +/- one LSB. Further testing is still underway and the second step is the validation of trigger processing. At the same time, phase 2 of the SMART project, called SMART_MCH was launched at the end of 2022 and a prototype design started in 2023, it will double the number of controlled END POINTS going from 240 to 480 mainly for the needs of the AGATA detector. It will also permit to upgrade the SMART board toward an independant complete trigger module.

3. VTC

By the end of 2023, a new trigger using VME bus standard has been validated and proposed for physics experiments. This VME module from CAEN company is based on an INTEL/ALTERA FPGA. A full firmware has been developed at GANIL in order to propose this board to physicists who want to control a full VME data acquisition system. In particular, a CENTRUM interface has been implemented in the FPGA to allow a synchronization by the GANIL BEAST modules.

4. Negma and REActif

The NEGMA project (NEw Generation of Multifunction ADCs) was subject to an audit by external experts (Engineers and researchers). Following this meeting, the concept based on the ZCU216 evaluation KIT (see Figure 61) was validated. We created a Front-End card to adapt our signals to the dynamics of the kit. The first tests are very encouraging. Several parts of the project have been validated. Currently we are working on the transmission of data to JETSON (HACKtif prototype based on JETSON compact computer) in order to allow the visualization and analysis of the data.



Figure 61: ZCU216 evaluation kit with a front-end board for input signals

The REActif project (signal processing on embedded GPU) aims at implementing the signal processing algorithms using a computer language (e.g. energy calculation in C++) more flexible and more responsive. The signal can come for instance from a digitizer (eg NEGMA). On the hardware side, the prototype of the HACKtif card (See Figure 62) was produced, integrated into a 1U NIM module, and on the software side, the REAssemble data aggregator permits to collect the processing outputs of several HACKtif cards.

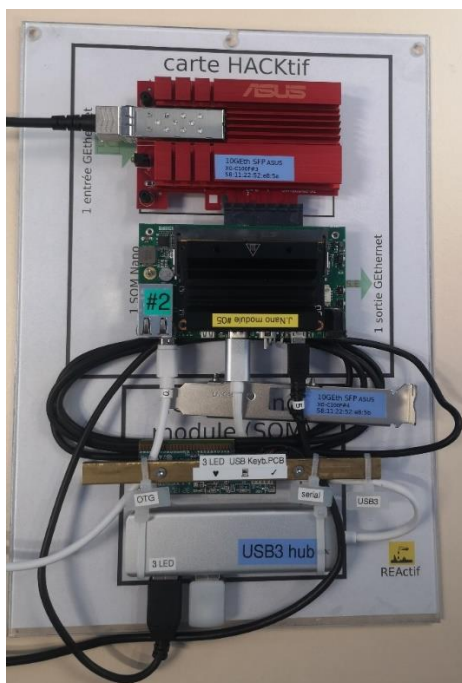


Figure 62: HACKtif card

5. DAQ up

The year 2023 marks the beginning of developments aimed at renovating the data acquisition system for physics experiments. Preliminary work began with (in collaboration with the G2I) a server package facilitating the simple and rapid installation of tools and software and also with the implementation of development and implementation tools, in continuous integration thanks to the IN2P3 GitLab platform.

IX. Management and ordering of installations

1. NFS

New Beryllium converter

The first neutron beam produced by irradiation on a static Beryllium target, (Figure 63), cooled by water in Copper support, has been produced in the converter room of NFS.

The converter has been tested with a D^+ ion beam of maximum intensity $42 \mu A$. The temperature produced by the beam was controlled and compared to the simulation. The flux measured on the MEDLEY detector was close of $5.10^7 \text{ n/cm}^2/\text{s}$ for the maximum power of 1680W.

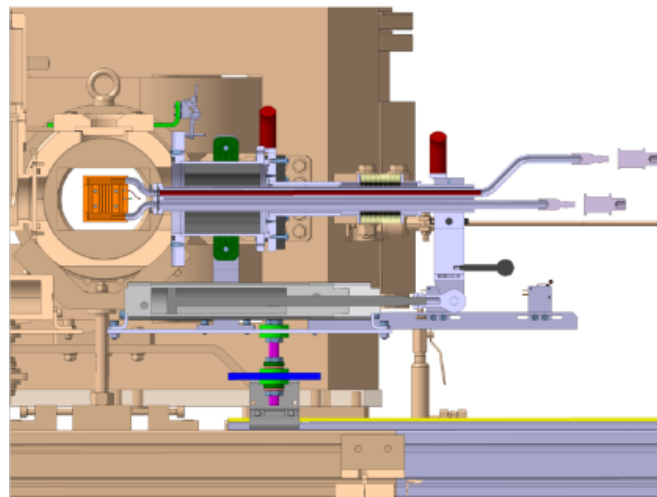


Figure 63: : Target in the ion beam axis

It was shown that the orientation of the incoming beam to the neutron beam axis influences the neutron beam. If the D^+ beam has a little angle with the theoretical beam axis, then the neutron beam is also with an angle compared to the expected axis. A really good adjustment of the incoming primary beam with profilers is essential. It is also measured that the design of the support with some Cu behind the Be reduces the flux of around 20% compared to the simulation.

REPARE in NFS

REPARE was installed in the converter room of NFS (Figure 49) to study the Astatine production on Bi plates irradiated by 7 MeV/u He ions. A first session of tests have shown that some adjustments were necessary. To optimize the integration in the irradiation line, some changes have been made. In particular, the Elcom chassis of NFS (Figure 64) was cut as it was on the way to install REPARE with only one movement axis. It induced that the support of the line was shifted and a new mechanical component was added.

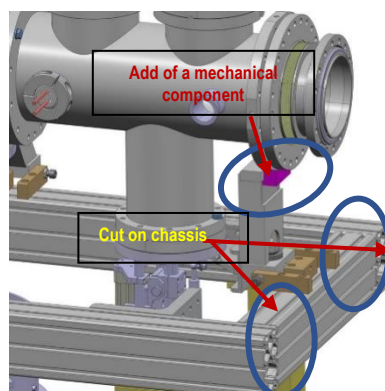


Figure 64: Modifications of the line NFS

2. NEW G21

Modifications on G21 line

The G21 beam line (Figure 65) has just been completely overhauled to transport low-energy radioactive beams (1MeV/u to 2MeV/u).

The project took place over 5 months with the contribution of many persons supervised by G2 technical coordinator. The new beam line makes it possible to slow down the beams of the CIME cyclotron while measuring the energy of each particle with a great precision.

With this new device, the SPIRAL1 beams have an energy close to that of nuclei in stars. It is now possible to reproduce as close as possible the stellar nuclear reactions in the laboratory.

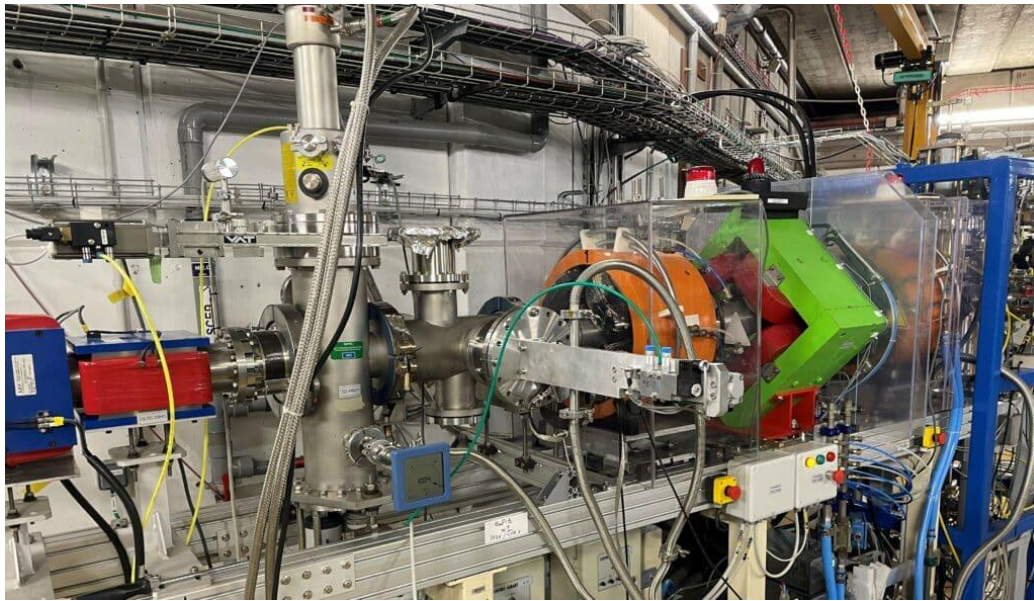


Figure 65: Beginning of the line, with an energy degrader (thin sheet) and a detector to measure the time of flight of ions hitting the active target of ACTAR TPC 10 meters further. Thereby it is possible to measure the energy of each event.

X. Status of scientific and accelerator projects

1. DESIR

Presentation



Figure 66: Schematic view of the future desir building, between spiral1 and spiral2 buildings

DESIR (Disintegration, Excitation and Storage of Radioactive Ions) will be the new "low-energy" experimental hall for GANIL and SPIRAL2. It will receive radioactive beams produced by SPIRAL1 and S³. The experiments carried out there will enhance our understanding of the fundamental rules governing the structure of atomic nuclei. These experiments will be based on the following three pillars of low energy experiments: the study of radioactive decay modes, laser excitation and storage in traps.

- Radioactive decay studies can be used to determine the lifetime and the structure of nuclei. These parameters are key to understanding the synthesis of chemical elements in stars.
- Laser excitation provides information on the shape, magnetic and quantum properties of nuclei.
- Storage of ions in electromagnetic and optical traps to determine their mass or study their decay with high precision.

DESIR building and infrastructure

The first half of 2023 was dedicated to preparing the construction site for the DESIR installation (see Figure 67). Clearing operations were carried out to free up space for the future site base and the extension of the Nuclear Base Installation (INB) perimeter necessary for the construction of the installation. These operations were carried out by implementing the recommendations of the Environmental Authority given in March 2023. The fire water, wastewater and rainwater networks circulating in the area of the construction site were diverted, and the area itself stripped and fenced to make the construction site closed and independent.



Figure 67: Compilation of pictures of the DESIR construction site preparation in 2023

In the second half of the year, general earthwork operations began as soon as the building permit was obtained. They continued with the digging of the construction site to a depth of around ten meters (level -3), so as to allow the future connection of the DESIR installation to the buildings of the SPIRAL2 installation and to those of the original GANIL facility. Once the drainage operations were carried out, the design of the rafts of the junction rooms with the existing installations and the DESIR experimental hall were carried out. The end of the year was marked by the raising of the sails of the premises on levels -3 and -2 of the junction block with the SPIRAL2 installation and the drilling of the first of the common emergency exits with the existing installations at the level of the SPIRAL2 experimental room S³.

The construction site for the DESIR installation on the GANIL site was inaugurated on November 10th, 2023 during an event gathering the supervisory bodies of the laboratories involved in the project, local and territorial authorities, as well as the various stakeholders of the project.

Safety licensing

The favorable report of the Environmental Authority for the DESIR licensing paved the way for the launch of the required Public Inquiry, the terms of which are set by prefectural decree. The investigation took place between the end of April and the end of May 2023. It concerned the 22 municipalities located within a 5 km distance to the INB and was instructed by an investigating commissioner mandated by the Administrative Court of Caen. Its favorable opinion led to the publication of the building permit for the DESIR installation at the end of June 2023. The decision endorsed by the Prefecture of Calvados marked the end of a long instruction process of administrative authorizations that begun in March 2022 with the submission of the Modification Authorisation Request (DAM) file to the Ministry of Ecological Transition and to the Nuclear Safety Authority. This process will end with the publication of the decree authorizing the modification of the INB 113-GANIL, expected in 2024.

In the meantime, the nuclear safety group of the DESIR project has started compiling the Commissioning Request (DMES) file for the installation, the second of the two major administrative files necessary for operation. Its preparation requires taking into account changes in the GANIL installation since its last safety review and data from the DESIR Preliminary Safety Report in the INB 113-GANIL Safety Report.

Quality

The GANIL Quality unit is responsible in close collaboration with the Nuclear Safety group of the compliance, by the various stakeholders of the project, of the safety-quality requirements of the project. Following the Project Management Plan issued in 2022, the Quality Safety Management Plan of the project was reviewed and validated in 2023. The unit was heavily involved in 2023 in monitoring the execution of the building construction work and in the installation of the beam process equipment in the premises of GANIL. In order to improve the document management within the framework of the project, "Quality Information" was regularly produced and distributed to the project's technical groups.

Beam process

Two of the thirty identical sections that will constitute the DESIR transport beam lines were assembled at LP2iB and GANIL (see Figure 68). At LP2iB, two complete vacuum chambers were assembled with the aim of validating the principles of the automated management of the pumping and the online insertion of the beam diagnostic equipment. At GANIL, it is a first complete "head of series" section of transport line that was mechanically assembled in the premises of GANIL at their interface with DESIR in order to test the assembly procedures. Corrections and technical adjustments were validated in order to ease the integration of similar equipment for the entire DESIR transport beam lines. The commissioning of this first definitive beam transport section is planned beginning of 2025. It will be an opportunity to test full-scale and in real operating conditions the equipment of the DESIR transport beam lines as well as the remote control systems and adjustment procedures required for commissioning the entire installation.



Figure 68: Picture of the assembly of the transport beam line from the SPIRAL 1 facility towards DESIR.

Beam preparation and purification devices

Characterizing the performance of the high resolution separator dedicated to the purification of ion beams delivered to DESIR experimental devices requires studying its optical properties at high orders. For this purpose, an upgraded version of an emittance-meter was installed at the exit of the HRS presently commissioned at LP2iB. This allows now a much more sensitive and faster measurement of optical aberrations to characterize the HRS. New magnetic probes including Hall probes have also been installed in the HRS magnets to facilitate and accelerate the measurement of their magnetic field. The developments made in recent years and the performances of the device have been the subject of two publications in Nuclear Instruments and Methods in Physics Research Section B.

The performances of the double Penning trap PIPERADE, dedicated to the purification of ion beams used in DESIR as well as to very precise measurements of the mass of nuclear species, were tested at LP2iB using the Phase-Imaging Ion-Cyclotron Resonance technique. Simulations and programming work has been carried out to facilitate the implementation of this technique, which offers the highest precision in measuring the mass of trapped ions. The diaphragm between the two traps has also been reduced, which made possible to significantly improve the precision of the device: by minimizing the gas leaking from one trap to the other on the one hand and by reducing the anharmonicities of the electric field in the traps on the other hand.

Experimental process

The MORA device (see section 02|IV.-1.) is currently being tested at the University of Jyväskylä, Finland, pending transfer to the DESIR facility.

The MLLTrap device will be operated at the ALTO installation of IJCLab before its use at DESIR. The commissioning of the ion beam transport section from ALTO to MLLTRAP was carried out between May and July 2023. All the electrostatic elements (quadrupoles, steerers, deflectors) were tested with a stable beam produced by the ALTO ion source.

The assembly and wiring of the deceleration electrodes of the radiofrequency quadrupole ensuring the cooling and pulsing of the ion packets injected into the double Penning trap of MLLTrap were carried out during the summer of 2023. The Penning traps were installed in the vacuum tube (aligned with the field lines of the superconducting magnet) and placed under vacuum.

In parallel, the construction of a system for recovering the Helium evaporated while keeping the superconducting magnet cold was started. Such a system will be deployed at the DESIR installation, with the aim of reducing the operating cost of MLLTrap and PIPERADE, both powered by liquid Helium. A technical study was also launched at IJCLab to develop a system for recovering helium evaporated when filling the cryogenic chambers of superconducting equipment.

2. S³ Installations and test

Introduction

Almost every S³ equipment is now in the caves and the main part is installed and completely or partially qualified (Figure 69).

This involves specific skilled and committed Ganil personnel in several fields, with key contributions from collaborating institutes at CEA and CNRS.

However serious issues arose on the testing of the SMTs in 2023: the newly received SMT did not behave nominally and the cold box was out of order the main part of 2023, preventing from properly diagnose the SMTs. The cold box was eventually fixed by Air Liquide at the end of 2023 but too late for meaningful progress on this topic.

At the end of 2023 and beginning of 2024, an important investigation campaign, within Ganil and with committed and effective help from CEA and CNRS, allowed us to decide, organize and schedule effective an action plan.

Future commissioning phases (spectrometer, Low Energy Branch, SIRIUS) have been now defined by the collaboration.

The exhaustive lists of prerequisites for beam commissioning (as well for equipment readiness and for safety requirements) are identified with assigned responsible personnels and due dates.

Three milestones with three bunches of prerequisites for three consecutive commissioning beam configurations have been identified.

S³ Installation

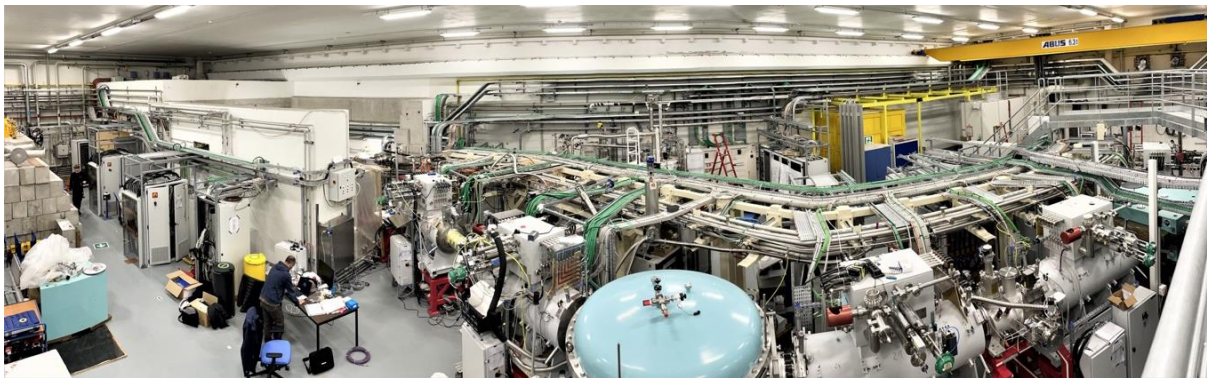


Figure 69: S³ Experimental area

The installation phase of the spectrometer is still in progress, but around 90% of the main operations is completed. In 2023, the program was disturbed by two liquefier breakdowns, which did not permit to progress as foreseen in terms of SMT electric and cryogenic tests, and then in terms of installation.

In parallel, a global installation review, in several meetings, was organized with all the GANIL task responsible persons involved in the project, with the goal to get a detailed picture of all the technical works and tests remaining before beam commissioning. This review has identified more than 800 action items, and a follow-up has been set up to finalize the installation program in time, considering the different S³ milestones.

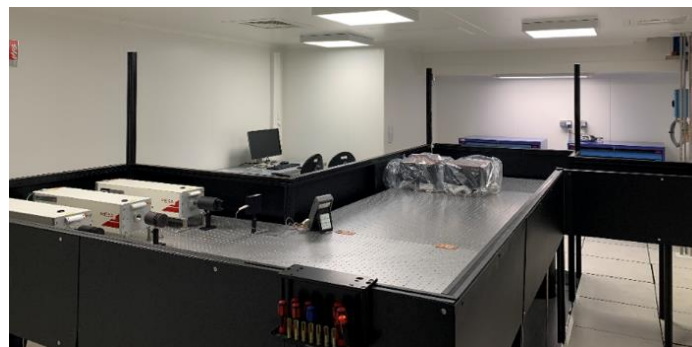


Figure 70: S³ TiSa laser room

Infrastructure:

- Power and signal cables connection between equipment's and command and control cabinets are finalized,
- TiSa Laser room is finalized (Figure 70),
- Both HEPA filters plates for the future decay circuit of the LEB/REGLIS3 project are manufactured and installed,
- 80% of the concrete wall openings closed,
- The two Cryogenic lines branches have been installed at the beginning of 2023

Spectrometer and physic equipment:

- Last SMT (#7) delivered and installed at a test position,
- Dipoles D11 and D41 seismic-proof installed and connected (hydraulically / electrically),
- SMT positions 5, 6 and 7 seismic-proof installed and connected (hydraulically / electrically) ,
- Electric Dipole installed with its two feedthroughs (GANIL + IJCLAB), and connected
- Diagnostics box (last object of the spectrometer line upstream the detection setups) installed,
- LEB REGLIS3 project line partially installed (LPC Caen + GANIL + IJCLAB),
- Upstream beam line mechanical section finalized, including the stable rotating target station (Figure 71)

Main Tests:

- Qualification of the vacuum and the command & control for: upstream beam line vacuum section, beam dump vacuum section and SMT5 to SMT7 vacuum section,
- Validation of the UGA and UGSx systems,
- First tests for the electrical dipole and its power supplies,
- Cryogenic lines tests,
- SMT cryogenics cabinet's connections and validation (IRFU).
- Some SMT cryogenic and electric SMT partial tests,



Figure 71: Upstream Beam Line

Commissioning of S³ superconducting magnets and associated cryogenic plant

The acceptance and commissioning of S³'s superconducting magnets was marked by numerous difficulties related to cryogenics, but also by the identification of magnet-specific problems that had not been observed on equipment previously tested.



Figure 72: CERNOX temperature monitor on HTS current leads.

Since the delivery of the S³ superconducting magnets, the cryogenic installation and, above all, the distribution line had been operating in partial mode, enabling one or two magnets to be electrically qualified simultaneously. However, as the system had been designed for 7-magnet control, it was difficult to regulate, leading to uncertainties about the behaviour of the magnets due to non-constant cryogenics.

In 2023, the cold box turbines experienced several episodes of stoppage and breakage, which could be attributed to maintenance (outsourced to Air Liquide).

In July 2023, the project received the last magnet (SMT#7) from Cryomagnetics (Oak Ridge, USA).

In November 2023, the team was able to carry out tests on the SMT#5 and SMT#6 magnets, with results that unfortunately differed from previous tests. Operating limitations of the order of 300A (out of a nominal 465A) were observed on several quadripolar coils. These limitations seem correlated with temperature increases in the lower part of the current conductors.

It has been possible to validate the operation of the 3D bench to align SMT#5 cold mass inside the cryostat. It should be noted that in 2023, these tests were carried out with the yokes removed from the magnets, a decision taken in view of previous alignment results, which were not fully reproducible in the presence of the yokes.

Unfortunately, the final highlight was the discovery, after SMT warm-up, of a broken power wire inside SMT#6. This will inevitably lead to the need to open the magnet's helium cryostat for repair.

2023 results led the project and the funding agencies (CEA / CNRS) to organize a review of cryogenics and superconducting magnets to be held in 2024, with the aim to validate and consolidate a strategy for cryogenics and magnets.

3. NEWGAIN

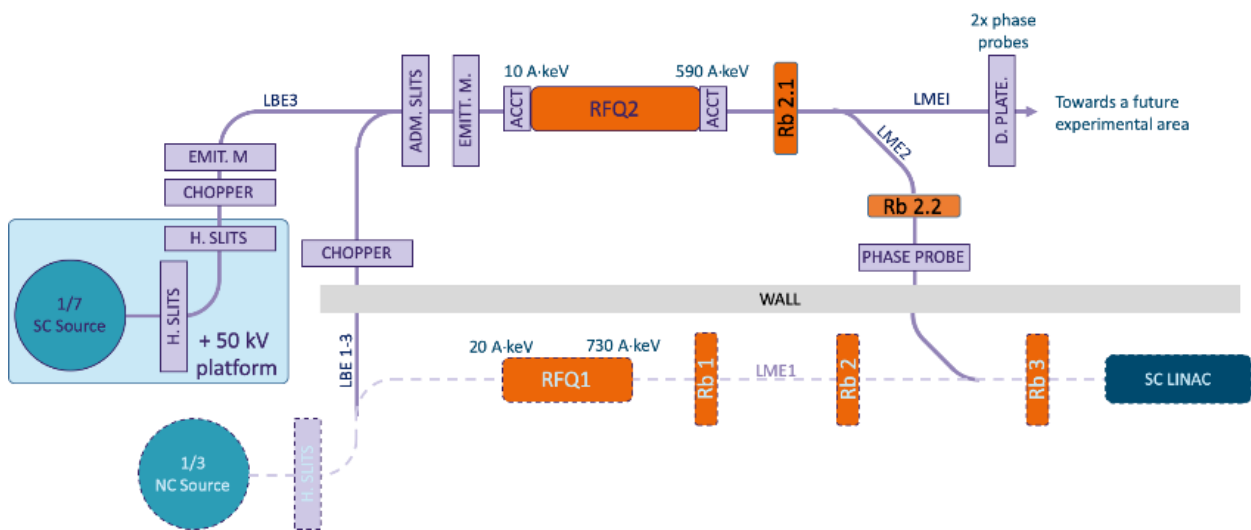


Figure 73: Schematic diagram of the new injector

The NEWGAIN project (NEW GAnil INjector) aims to construct a second injector $A/q=7$ to produce very intense heavy-ion beams up to uranium, well beyond the performance of the existing injector of the SPIRAL2 linear accelerator. With the addition of this new injector, the SPIRAL2 LINAC will deliver, within its energy range of operation, the most intense beams in the world over a large variety of ions (ranging from protons to uranium). The second injector is designed to be fully compatible with the existing facility and to further enhance its ‘multi-user’ capabilities. It is composed of the following:

- A high-performance superconducting ion source (1/7 SC Source)
- A first low energy beam transport line (LBE3) connecting the superconducting ion source to the Radio-Frequency Quadrupole (RFQ2).
- A second low energy beam transport line (LBE1.3) connecting the existing ion source PHOENIX V3 ($A/q=3$) to the RFQ2
- An RFQ2 that will accelerate heavy ions up to the injection energy for the superconducting LINAC
- A medium energy beam line (LME2) connecting the RFQ2 to the LINAC, with a possibility to send the medium energy beam (via LME1) to a future experimental area (to be defined).

A schematic diagram of the new injector is presented in Figure 73.

The NEWGAIN project preliminary design phase started on May 7th 2020, and the detailed design phase started in June 2021. In April 2023 started the construction phase.

The project is organized through a broad national collaboration, involving a large number of French laboratories from CEA/DRF/IRFU and CNRS/IN2P3.

As a reminder, the production and validation of the consortium agreement for the Equipex (funding of 13,7M€ out of 20M€ for equipment for the Construction phase) was completed in September 2022, and the consortium agreement signed by all partners was submitted to the ANR in December 2022.

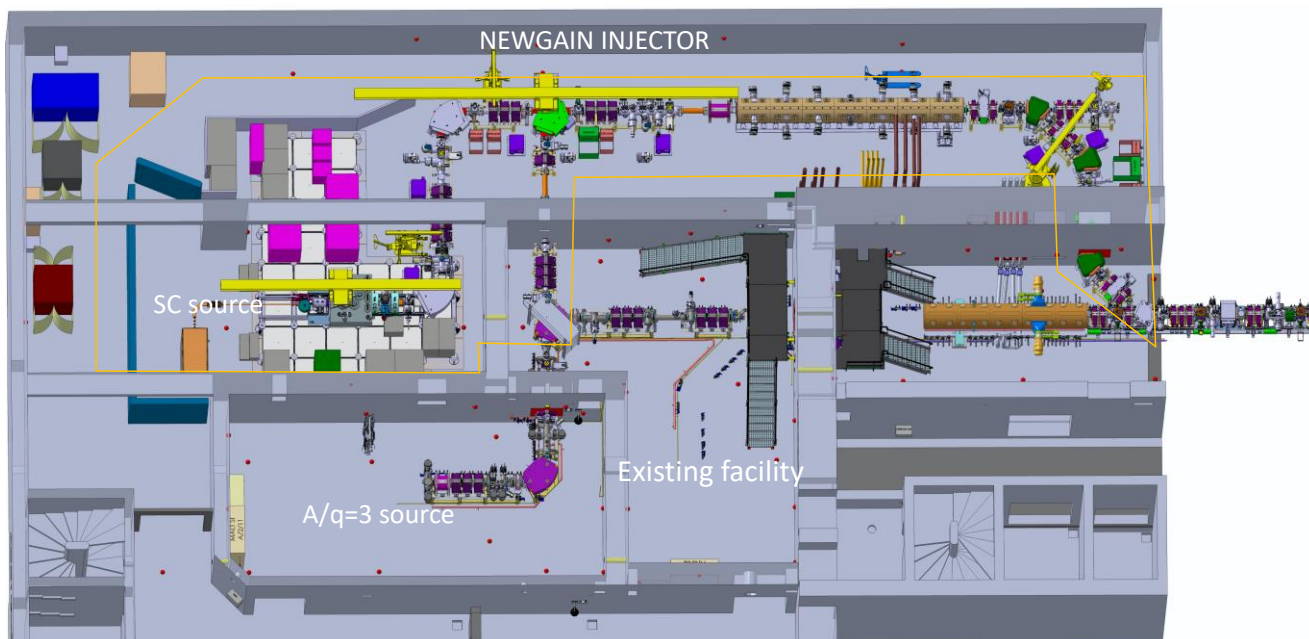


Figure 74 :View of the injector integrated inside the existing cave and with the existing beam lines

In 2023, the technical specifications being well established and the technical configuration consolidated, the technical specifications for numerous equipments could begin allowing the launch of consultations for vacuum equipments, power supplies for magnets, power amplifiers as well as than the first magnets which are the quadrupoles. This is facilitated by the fact that the design of NEWGAIN relies heavily on the one of SPIRAL2. Even if modifications or improvements resulting from feedback from the operation of SPIRAL2 are necessary, the expressions of need concerning previous products are well known. Copper for the RFQ has been procured, so that manufacturing can begin in 2024.

The configuration of the transmission lines is being finalized and should be finalized in early 2024. Any modification made to the design of these lines will be subject to a specific modification and monitoring procedure. Safety studies concerning modifications to the existing walls of the SPIRAL2 building are in progress and the technical specifications have been drawn up to assist the project owner in the design and construction of works (emergency exits, wall crossings) and infrastructure modifications.

Concerning EIP equipments (Equipment classified as Important for Protection), X emissive equipments (RFQ and combiner cavities) as well as modifications to the existing walls of the SPIRAL2 building, part of the equipment is under the declaration regime. A strategy for submitting safety files to the ASN is currently being studied to enable GANIL to optimize the phasing of the 3 files.

In December 2023, a review of the detailed design of the superconducting magnet of the ASTERICS source (1/7 SC Source) took place.

4. CYREN (CYclotrons RENovation) Project: Refurbishment of the GANIL cyclotron facility

In order to allow the continuation of experimental programs in nuclear and interdisciplinary physics, to provide exotic beams to the new installation DESIR that will be in operation in 2027, refurbishment project has been launched.

The project CYREN (CYclotrons RENovation) consists of refurbishing the GANIL cyclotron facility that are 40 years old. The perimeter integrates:

- the cyclotrons, beam lines and the experimental areas
- the infrastructure and utilities
- the safety, security, radioprotection systems

The objectives are to maintain the facility in operational conditions for at least 20 years and to optimize the manpower for maintenance after refurbishment.

A preliminary project was launched in 2022 to identify different refurbishment scenarios including all the equipment and system in the CYREN perimeter. The main topic for the cyclotrons is the RF cavities for the two separated sector cyclotrons (SSC). The risk analysis defined two different scenarios (baseline and complete), one where a new cavity is produced and the old one stands as a spare, the other where all 4 cavities are changed.

These scenarios were presented to the CEA/DRF and CNRS/IN2P3 Board of Directors and Scientific Council in 2023. Initial recommendations call for a more in-depth study of the renovation of the 4 cavities to find the best technical solution compatible with resources and accelerator scheduling. A specific pre-project for the renovation of RF cavities will be launched in January 2024 to propose and then select the refurbishment strategy.

The study and implementation schedule for this project is based on 5 to 8 years, depending on the scenario.

Furthermore, funding requests have been made and partial but substantial funding has been obtained in 2023 from the State-Region Plan contract 2023-2027 and the French Ministry of Research and Education. Discussions between France and Germany took place in 2023 to complete the CYREN project funding scheme.

Studies and achievements of the CYREN project in 2023:

- It can be noted that, for the power supplies of cyclotrons and experimental caves, a prototype (see Figure 75) of power supplies for magnets is produced and validated at GANIL. This solution is based on commercial power supplies integrated into a cabinet. The prototype was connected to magnets and the electrical performances (in stability and control) were validated.



Figure 75: Prototype of power supplies refurbished for magnet

- The CSS1 vacuum system (primary and secondary pumping and automation) is refurbished
- The studies and the call for tenders for the refurbishment of the control system of the 90kV high-voltage station are carried out



04 | EXPERIMENT REPORTS



I. NFS

Beam was delivered to NFS between September and November 2023. The year 2022 was marked by the failure of the rotating converter. It was no longer rotating and the maximum permitted power was 400W. While waiting for the rotating converter to be repaired, a static water-cooled beryllium converter was designed and built by the CEA/IRFU and GANIL design offices. This new converter was successfully used for experiments in 2023. Six experiments and detector tests were run.

The E802 and E858 experiments with the MEDLEY detector, spokesperson D. Tarrío from the University of Uppsala, on which Lucas Dearth, a PhD student at GANIL, is working. These experiments are a continuation of those carried out in 2021 and 2022.

The E838 experiment, spokesperson E. Clément (Ganil), deal with the study of ^{56}Ni produced in the $^{58}\text{Ni}(n,3n)$ reaction. It was possible thanks to the energy spectrum of the NFS, which extends up to 40 MeV. This is the first time that the EXOGAM detector was installed in the NFS experimental area. The smooth running of the experiment shows that the room is suitable for the use of gamma multidetectors.

The E835 experiment, spokesperson V. Blideanu (CEA/DRT), aimed to measure the cross-section of reactions induced by neutrons on the following elements: stainless steel, Pb, Cu, C and Al. The activation method was used. The sample was irradiated near the converter and then sent by the pneumatic sample transfer system to a gamma spectroscopy station. For this measurement, the pneumatic transfer system, previously used only for ion irradiation, was adapted for neutron irradiation by NPI staff from Rez (Czech Republic).

The REPARE experiment was particularly important in 2023, not because of the amount of beam time used, but because of the amount of work required to set up and dismantle the device in the converter room. The aim was to produce ^{211}At with an alpha beam impinging on a bismuth target in the REPARE device. The first test went perfectly, but the irradiation a week later was a failure. Bad adjustment of the beam power resulted in partial melting of the target and alpha contamination of the REPARE chamber. There is no consequences in terms of contamination of the facility are because the ^{211}At period (7.4 hours) is short. The feedback will be used to re-run the experiment under optimal conditions in September 2024.

The E856 experiment was scheduled in November 2023. Its objective was to study fission and (n,xn) reactions on Pu-239. An active target consisting of a fission chamber containing 6 mg of Pu-239 was placed in the center of the SCONE detector. A first experiment was performed in 2022 with a U-238 target. A problem at the beginning of the experiment destroyed the windows of the fission chamber and some of the plutonium deposits were spread in the beam pipe in the time-of-flight room. This stopped the experiment and had a significant impact on the availability of the NFS experimental area.

In addition to the experiments mentioned above, detector tests were carried out. The characteristics of NFS, the energy and time structure of the beam and the dimensions of the NFS room make it a unique facility for this type of measurements. A MONSTER detector, already used the previous year during the E833 experiment, was tested by a team of Spanish physicists from CIEMAT. Two teams, one from CEA/DAM and the other from IRSN, used the NFS neutron beam to characterize paraterphenyl and stilbene-based neutron detectors. One team of CEA/Cadarache tested SiC detectors in the converter room of NFS. Physicists from CEA/Cadarache have tested two SiC detectors in the convector room in parallel with experiments running in the time-of-flight room to study these detectors exposed to an intense flux of high-energy neutrons.

A team from CEA/DAM irradiated an electronic board close to the converter during the physics experiments. The flux and energy of the neutrons delivered by NFS are particularly interesting for studies of the behavior of electronic components under neutron irradiation. This activity will be continued and in 2024 a dose monitoring system will be tested.

The NFS facility is operating correctly, and the beam delivered is in line with forecasts. A permanent effort of adaptation is necessary to control the problems of exploitation which are of 2 orders:

1. The NFS operating period is short, but concentrated in just 2 months. Periods without beam, which would allow experiments to be set up and dismantled, are short and very rare, making it difficult to carry out and sequence experiments.
2. Activation levels in the converter room are very high and any manipulation in this room, whether for installation (eg REPARE) or repair, is difficult, further complicating the operation of the facility.

1. Measurement of the light output function of crystalline organic scintillators as a function of incident neutron energy

Date: September 13-18, 2023

Spokeperson and co-authors

David DENIS-PETIT¹, Benoit LAURENT¹, Xavier LEDOUX², Gabrielle LELAIZANT¹, Laurent LOPEZ¹

¹CEA DAM DIF, 91297 ARPAJON, France

²GANIL, 14076 CAEN, France

Abstract

A new fast neutron detector, designed as an array of crystalline organic scintillators (made of stilbene or para-terphenyl), is being developed in order to avoid some limitations of ³He-based neutron detectors, whose constraints limit to the sole detection of thermal neutrons and then need a moderator to detect fast neutrons. These detectors are often used to characterize unknown radioactive material not only in homeland security applications but also in the fields of radioactive waste characterization, neutron dosimetry or accelerator management. Organic scintillators being sensitive to both neutrons and gamma rays, a major issue arises from the need for distinguishing these events and using this opportunity as a good complement to ³He-based detectors. After addressing this issue thanks to the usual Pulse Shape Discrimination (PSD) method, different performances have been investigated for both types of crystals, in particular their Light Output Functions (LOF). The current setup is composed of an array of organic scintillators (seven detectors of two different sizes) that have been combined to count neutrons emitted by known sources. In order to fully characterize the different scintillators, a wide energy range has been studied thanks to the GANIL-NFS facility. On another hand, the intense flux of the NFS facility has also enabled to test the saturation limits of the experimental setup. Getting access to the facility during its assays was really useful for our experiment which did not need more than few hours of data acquisition and enabled parallel settings.

Experiment report

All the detectors had previously been calibrated, first by using both neutron and gamma sealed sources, and then, through monoenergetic neutron beams produced at the 4MeV CEA facility. Nevertheless, the energy range was limited at a maximum energy of few MeV - less than 14 MeV (and without any energy point between 6 and 14 MeV). Therefore, only the first part of the continuous energy spectra of usual spontaneous fission sources of interest, such as ²⁵²Cf or different uranium and plutonium isotopes, had been investigated. The NFS facility was the only solution in order to constrain the calibration parameters in the highest part of energy spectra (until 20 MeV). Indeed, the NFS high time resolution enables to address neutron energies ranging from few hundreds of keV and tens of MeV and then to fully characterize our different stilbene and para-terphenyl crystals following a Time-Of-Flight (TOF) data analysis.

Experimental setup

The beam was pulsed for TOF measurements, with a period of 4543 ns to allow the slowest neutrons to reach the detector (approx. 0.21 MeV) before the gamma photons of the next pulse. The neutron beam itself is produced by the deuteron break-up reaction on a thick beryllium converter, while the deuteron beam is delivered by a linear accelerator. The neutron spectrum extends higher than at the CEA 4MeV accelerator, up to 40 MeV, with a maximum yield at approximately 14 MeV. This experiment was thus implemented to extend the range of neutron energies formerly investigated.

Both stilbene and para-terphenyl crystals have been characterized. Moreover, two different crystal sizes have been investigated: a cylinder of dimensions Ø1" x 0.5" and another cylinder of dimensions Ø75mm x 50mm, each encased in an aluminium housing. A total of seven detectors are presented in TAB. 1. These detectors were obtained fully integrated, and five of them can be seen in FIG. 1.

Crystal type	Crystal dimensions	Aluminium housing thickness	Photomultiplier	Number of detectors	Detector name(s)
Stilbene	Ø1" x 0.5"	1.5 mm	Hamamatsu R6094	2	S1-1 & S1-2
Stilbene	Ø75mm x 50mm	1 mm	Photonis XP53X2B	1	S3-1
Para-terphenyl	Ø1" x 0.5"	1.5 mm	Hamamatsu R6094	2	P1-1 & P1-2
Para-terphenyl	Ø75mm x 50mm	1 mm	Photonis XP53X2B	2	P3-1 & P3-2

TAB. 1: Description of the seven detectors. The names are the ones that will appear throughout the paper



FIG. 1: Picture of 5 of the 7 detectors (from left to right: P1-2, S1-2, P1-1, S1-1, S3-1)

Data acquisition

In each setup, data acquisition was performed with a CAEN V1730SB digitizer [2], with 16 data acquisition channels, 14-bit resolution, a 2-V maximum digitization window and a 500 MHz sampling rate. The Digital Pulse Processing – Pulse Shape Discrimination (DDP-PSD) firmware uses the digitized signals to generate other values of interest, with the CoMPASS software [3]. The recorded data are, among others, time of event detection (picosecond timestamp, using Constant Fraction Discrimination for each pulse), long gate integral (integral of the signal over its entire duration) and short gate integral (integral of the beginning of the signal). All data in this work was processed and analyzed using the ROOT [4] framework. The high voltage for the detector photomultipliers (PMTs) was provided by CAEN V6533 [5] boards.

The location of our scintillator and data acquisition device is shown in FIG. 2.



FIG. 2: Picture of the GANIL NFS experimental hall

Each detector was placed individually in the beam trajectory, and two digitizer channels were used: one for the detector, and the other for the beam pick-off signal. The Time-Of-Flight (TOF) spectrum in FIG. 3 is built from the time difference between the two signals.

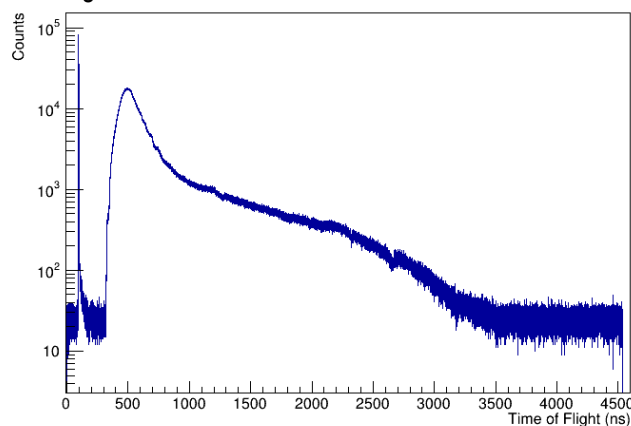


FIG. 3: TOF spectrum, with the gamma peak (left) and the following neutrons

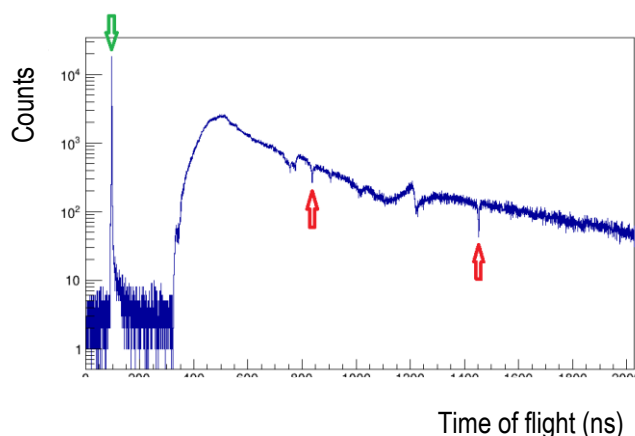


FIG. 4: TOF spectrum with carbon screen, showing the gamma peak (green) and the two cross-section resonances (red).
Left: 6.295 MeV resonance; right: 2.078 MeV resonance

For TOF experiments, a precise knowledge of the flight path distance for neutrons is necessary. To this end, a carbon screen was placed in the beam, and a TOF spectrum was measured (FIG. 4). The carbon cross-section presents relatively sharp resonances to neutrons, including at 2.078 and 6.295 MeV [6]. Using the time difference ΔT between the gamma peak and the resonance energies (E_n) in the TOF spectrum, the distance D can be determined. A time difference of $\Delta T = 1358.85$ ns between the gamma peak and the 2.078 MeV resonance, the distance between source and detector was found to be $D = 28.93$ m.

Based on the knowledge of the neutron flight distance and of the TOF spectrum, it is possible to determine the energy of each neutron event.

Results

It is then possible to subdivide the resulting neutron energy spectrum for each detector (example in FIG. 5 for one of them: P3-2) into smaller bins, and extract the Pulse Height Distributions (PHDs) of neutrons corresponding to the selected energies. FIG. 6 shows these PHDs, with the uncertainty showing the width of each selected energy bin.

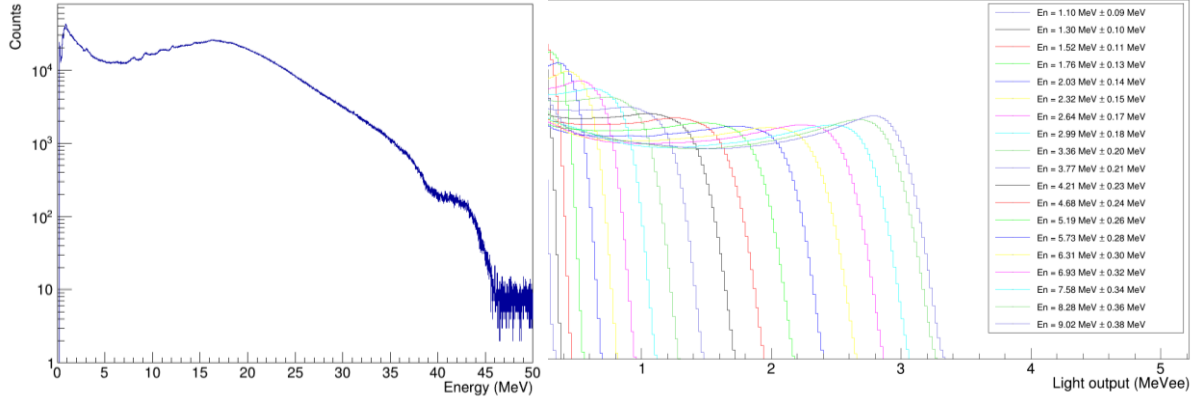


FIG. 5: P3-2 detector neutron energy spectrum at GANIL NFS

FIG. 6: P3-2 neutron PHDs for energies ranging 1.1 - 9.0 MeV

The light output functions are ultimately extracted from the mean of each Gaussian fit of the PHDs' derivative, and shown in FIG. 6. A possible empirical formula to fit the LOFs is [7]:

$$L(E_p) = AE_p - B(1 - e^{-CE_p})$$

Where A, B and C are fit parameters, $L(E_p)$ is the light output in MeVee and E_p is the recoil proton energy. Such an expression takes into account the exponential rise at the beginning of each LOF, and becomes linear for higher energies, those reachable only thanks to the NFS facility. Fit parameters for the seven detectors have been assessed from these measurement. FIG. 7 shows these LOF, compared to other works concerning similar detectors [8-11].

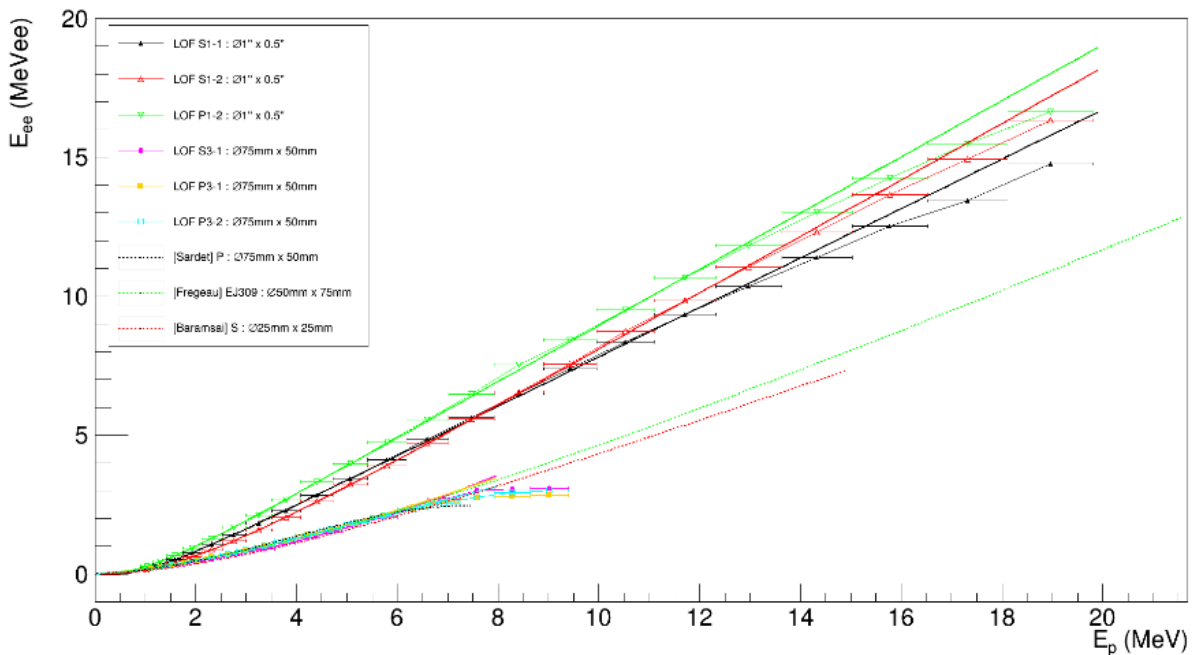


FIG. 7: LOF of the detectors determined at GANIL NFS

These response functions are in good agreement with each other and with the works of Baramsai [10] for stilbene, Sardet [9] for para-terphenyl and Frégeau [8] for another organic scintillator (liquid EJ309), at least concerning the thicker detectors. Between the data for the 50mm-thick detectors and other works for organic scintillators, the difference is less than 0.2 MeVee in the entire energy range, but there is a higher discrepancy for the 0.5"-thick detectors. As expected, for the 0.5"-thick detectors, a higher light output was measured, due to a lesser self-attenuation in the crystal [11].

We would like to sincerely thank the NFS facility team for having enabled us to get access to the beam in order to complete our study over the whole energy range of interest.

Legend

LEDOUX, X. et al., First beams at Neutrons For Science, EPJA (2021), vol. 57, no. 8
CAEN – Tools for Discovery, CAEN V1730SB digitizer (2019), www.caen.it/products/v1730/
CAEN – Tools for Discovery, CoMPASS software (2020), www.caen.it/products/compass/
CERN, ROOT – Data Analysis Framework (2021), root.cern
CAEN – Tools for Discovery, CAEN V6533 board (2019), www.caen.it/products/v6533/
NEA, JEFF-3.3, Incident neutron cross-section for carbon, 2017
KORNILOV, N. V. et al., Total characterization of neutron detectors with a ^{252}Cf source and a new light output determination, NIM A (2009), vol. 599, no. 2-3, pp. 226-233
BARAMSAI, B. et al., Fast Neutron Spectroscopy with Organic Scintillation Detectors in a High-Radiation Environment, NASA, Glenn Research Center (2020)
FREGEAU, M. O. et al., Light response and efficiency calibration of EJ309 liquid scintillator between 3 and 45 MeV, NIM A (2019), vol. 941
SARDET, A., Spectres en énergie des neutrons prompts de fission : optimisation du dispositif expérimental et application à l' ^{238}U , Université Paris-Saclay, Saclay (2015)
ENQVIST, A. et al., Neutron light output response and resolution functions in EJ-309 liquid scintillation detectors, NIM A (2013), vol. 715, pp. 79-86

2. GARIC – GAs pRoduCtion In Chromium by neutrons and GARROS – GA pRoduCtion in iROn by neutrons

Experiment number: E802 and E858

Date: October 2023

Spokeperson and co-authors

Diego Tarrío¹ (spokeperson), Lucas de Arruda Serra Filho^{1,2}, Xavier Ledoux², Stephan Pomp¹, Diego Ramos², Ali Al-Adili¹, Mattias Lantz¹, Ivan Kodeli³, Iuliia Ipatova³, Udomrat Tippawan⁴, and the Medley Team.

¹Uppsala University, Sweden; ²GANIL, France; ³United Kingdom Atomic Energy Agency, UK; ⁴Chiang Mai University, Thailand.

Abstract

Two experiments have been recently done to study the light-ion production in neutron-induced reactions in natural chromium and in natural iron, using the white neutron beam of NFS and the Medley setup. Those reactions are relevant for applications in materials for fusion devices and for fission reactors. The data analysis is ongoing, and the goal is to get double-differential cross-sections on the production of light-ions, as a function of neutron energy. The identification of light ions (p , d , t , ^3He , and α) is based on energy losses in three-element telescopes.

Experiment report

These two experiments deal with studies on emission of light-ions in reactions induced by neutrons in chromium and in iron. The goal is to provide with double differential cross-sections for the production of light-ions, with respect to emission angle and to energy of the emitted ion, as a function of neutron energy.

The motivation for these measurements stands on the use of those elements as components in structural materials in fission and fusion reactors. Exposure to highly intense neutron fluxes produces the formation of light ions (protons, deuterons, tritons, ^3He , α -particles...). These ions, which are isotopes of hydrogen and helium, represent defect impurities in the lattice. With high temperatures, these impurities migrate through the lattice, creating gas bubbles of hydrogen and helium that can cause swelling and embrittlement in the material, thus degrading its mechanical properties. As a consequence, and in order to calculate the lifetime of structural components, it is required to have a good knowledge on the production cross-sections for light-ions. The lack of a comprehensive set of experimental data on light-ion production cross-sections for these elements, which also covers a continuous and wide neutron energy range, motivates the need for these experiments.

The experiments have been done in October 2023 at NFS using the so-called Medley setup (see Figure 1), designed for detection of charged particles over a wide dynamic range. It consists of eight three-element telescopes mounted inside a 240-mm high cylindrical evacuated chamber with inner diameter of 800 mm. Each telescope consists of two fully depleted ΔE silicon surface barrier detectors (SSBD) and a CsI(Tl) crystal. The back-end part of each crystal is connected to a read-out diode. The setup had been used at quasi-monoenergetic neutrons beams at the currently dismantled TSL facility in Uppsala. In order to be able to use it at a white neutron beam, as the one provided at NFS, the original setup has been upgraded to incorporate time-of-flight capabilities in the detectors. For that, new readout preamplifiers have been developed by GANIL.

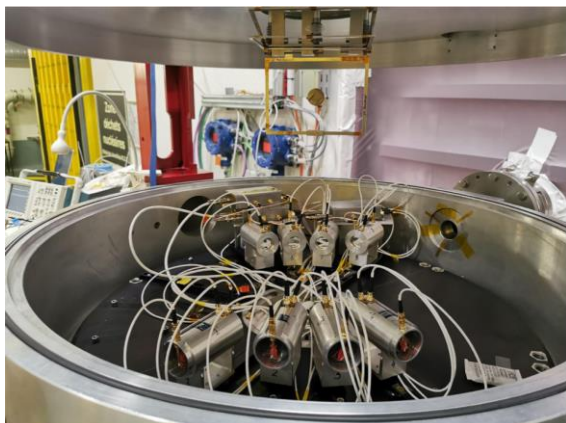


Figure 1: Inner view of the Medley chamber. The eight telescopes are pointing to the central part of the chamber. A circular target can be seen in the upper side, attached to the lid.

Different targets have been used in these experiments and, being exposed to the beam one at a time. The targets are samples of natural Cr and Fe. For each of them, two different samples have been used: In the case of Fe, the circular samples were 25 mm in diameter, and with thicknesses of 5 μm and 15 μm . For Cr, the samples were squared, with 18 mm in side length, and thicknesses of 15 μm and 75 μm . Moreover, and because of their fragility, the Cr samples were attached to a 150- μm thick polyester backing. Therefore, another target consisting on an empty polyester backing has also been used to account for the effect of the backing in the Cr measurements. Moreover, a good knowledge on the neutron flux is also required to provide to deduce absolute values of the production cross-sections. Therefore, circular targets of CH_2 and C have been also used to measure the neutron flux using neutron-proton elastic scattering on H.

By measuring the energy deposited by each light-ion in the different detectors of a telescope, it is possible to detect it and to identify it, in an event-by-event basis. Moreover, its detection in the second silicon of a telescope produces a time signal which is used as a “start” for the time-of-flight, and the next pulse produced by the LINAC is used as a “stop” signal. The time difference between these two signals corresponds to the time-of-flight of the neutron which produced the reaction and, therefore, its kinetic energy is determined. A correction taking into account the time required by the ion to travel from the target to the telescope is also applied, since its velocity is deduced from the kinetic energy (measured as the energy deposited in the telescope) and the mass of the ion, which is known because of the identification achieved with the ΔE - ΔE -E technique.

The identification of the light-ions is based on the different energy deposition of different particles in the detectors of the telescope, following what is called the ΔE - ΔE -E technique. Figure 2 shows a subset of data on the correlation between the energy deposited in the first silicon ΔE_1 , in the second silicon ΔE_2 (left figure) and between ΔE_2 and the energy deposited in the scintillator ΔE_3 (right figure) for the telescope placed at 20° . The good energy resolution of the setup allows to distinguish between the different light-ions (p, d, t, ^3He , α) produced in the C target

By plotting the energy loss in each of the three elements of the telescope, it is possible to identify the different light-ions produced. Figure 2 shows, using a fraction of the collected statistics of statistics, the correlation between the energy deposited in the first silicon ΔE_1 , in the second silicon ΔE_2 (left figure) and between ΔE_2 and the energy deposited in the scintillator ΔE_3 (right figure) for the telescope placed at 20° . The good energy resolution of the setup allows to distinguish between the different light-ions (p, d, t, ^3He , α). This figure corresponds to the C target, but similar plots have been obtained with all the targets.

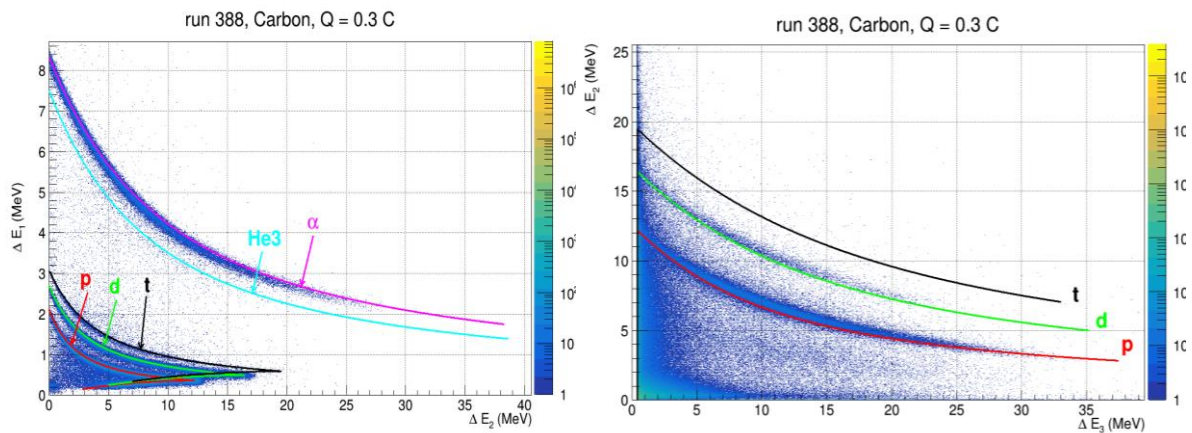


Figure 2: Energy deposited by light-ions in the telescope placed at 20° . Left: Energy deposited in the first silicon (ΔE_1) vs. energy in the second silicon (ΔE_2). Right: Energy deposited in the second silicon (ΔE_2) vs. energy deposited in the CsI (ΔE_3) by those ions with enough energy to pass through the second silicon. The continuous lines represent simulation results from KaliVeda.

As a consequence, it is possible to identify the light-ion produced in each event, and to associate it with the energy of the neutron which has produced it. The analysis of the data is currently ongoing and is expected that double-differential cross-sections for the production of light-ions in Cr and Fe will be obtained.

This work has received funding from the European Union’s research and training programme under grant agreements with numbers 847552 (SANDA), 847594 (ARIEL) and 101057511 (EURO-LABS). Part of this work has been carried out within the framework of the EUROfusion Consortium, funded by the European Union via the Euratom Research and Training Programme (Grant Agreement No 101052200 — EUROfusion). It has also received funding from the European Union’s 2020 research and innovation programme under grant agreement No 101008126, corresponding to the RADNEXT project. Funding from the Swedish Centre for Nuclear Technology (SKC) has been also received.

3. Measurement of the neutron induced activation in materials: improvement of nuclear reaction models and decay data libraries for the specific case of radiotherapy accelerators

Experiment number: E835_21

Date: November 1-2, 2023

Spokeperson and co-authors

Valentin Blideanu (CEA)

Clément Besnard-Vauterin (CEA)

Xavier Ledoux (GANIL)

Jaromir Mrazek (Nuclear Physics Institute of the Czech Academy of Sciences)

Benjamin Rapp (CEA)

Abstract

The aspect of induced radioactivity and waste management for the particle accelerators is currently not properly addressed. There is an increasing demand by accelerator operators to waste management agencies and regulatory authorities to provide the appropriate solutions to this problem. This is particularly true for electron linear accelerators used in radiotherapy for which the activation level is expected to be relatively low when compared to other facilities from the nuclear industry, due to the activation occurring via secondary neutrons created in photo-nuclear reactions. These reactions are usually characterized by a high energy threshold, around 10 MeV for most of the elements, creating neutrons which can further activate the materials only for some operating regimes of these accelerators involving high electron energies. However, without a rigorous methodology able to accurately determine the activation level and the contributions from particular radio-isotopes, no well-grounded decision can be taken on the management of the generated waste.

Methodologies based on Monte-Carlo simulations coupled with activation calculation codes are often used to address this issue since they are able to provide the complete radioactive inventory in each part of the accelerator whose geometry can be modeled with a high level of details. Calculation tools capabilities in terms of accuracy in simulating nuclear reactions at the origin of the materials activation must be however tested against experimental data. The present work focusses on this aspect by producing new macroscopic data in terms of activity induced by neutrons in the materials commonly present in medical electron LINACs allowing to estimate the precision than can be achieved by a fully calculation-based methodology.

Experiment report

Samples of six materials in their natural isotopic compositions, (carbon, aluminum, steel, copper, tungsten and lead), selected for being abundantly present in the components of medical electron accelerators, were irradiated under the neutron flux produced at NFS in a particular configuration. The angle of 90 degrees has been selected as the best compromise allowing an enough decrease of the contribution from fast neutrons from the deuteron break-up while preserving a reasonably high neutron flux which would have been much lower at higher backward angles.

After being exposed in the converter room to neutrons with energy distribution as discussed above and at an average flux of the order 10^9 neutrons/cm²/sec (for deuteron beam intensities of around 20 μ A) for a duration of 15 minutes, the samples were quickly transferred through a pneumatic system to the TOF area in front of a *Canberra coaxial n-type liquid nitrogen cooled* hyper pure germanium (HPGe) detector for the measurements of the γ spectra. Data acquisition began approximately 15 seconds after the irradiation ended, allowing the measurement of contributions from short-lived radio-isotopes. This is illustrated by the identification in the γ spectra of the radio-isotope ¹⁶N (half-life of 7.13 seconds), produced by the ¹⁶O(n,p)¹⁶N reaction in the air trapped inside the sample containers.

For the carbon sample no data above the background has been recorded suggesting that no radioactive isotope is created in significant amount in this material when exposed to a neutron energy distribution typical for a medical electron LINAC. The identification of the radio-isotopes from the energies of the peaks in the spectra for the activated samples has been performed based on state-of-the-art nuclear data library developed in the frame of the DDEP project (Decay Data Evaluation Project) and maintained and continuously updated by LNHB.

The experimental set-up has been simulated using the MCNP6.2 code with a detailed geometry model taking into account all the elements present in the converter room strongly influencing the flux and the energy distribution of neutrons: the concrete shielding with walls, roof and ceiling, the magnets of the deuteron beam line, the neutron collimator separating the converter cave from the TOF hall. The simulations result in terms of 2D neutron flux map allow the neutron flux and its energy distribution at the exact location where the samples were irradiated to be determined. The neutron energy distribution has been calculated with MCNP6.2 using the specific CCFE scheme with 709 energy groups, allowing further activation calculations to be performed with the FISPACT-II code using the option of neutron-induced reactions cross-sections from the TENDL library.

FISPACT-II allows to accurately reproduce the irradiation and decay sequences as they were recorded during the experiments. Based on the neutron flux value and the energy distribution previously calculated by the simulations with the MCNP6.2 code at the sample location and considering the known irradiation duration, it uses the energy-dependent cross-section values from the TENDL library to calculate the yields of radio-isotopes produced in each sample by the neutron-induced nuclear reactions on the stable nuclei present in its initial composition. Decay data libraries are further used to calculate the weight of these radio-isotopes at the time after the sample irradiation corresponding to the γ spectrometry measurements. The calculations predictions, thus simulating as accurately as possible the real experimental conditions, can then be directly compared to the data obtained by the experiments performed in this work.

The analysis of the results has been done for each sample individually. The example we are discussing in detail here concerns the case of copper, as it is a material which can generally be always found in particle accelerators. Several radio-isotopes were identified in the γ spectrum acquired after neutron irradiation of the copper sample, created from both ^{63}Cu and ^{65}Cu natural isotopes through various neutron-nucleus reaction channels as discussed below. In order to test the accuracy of the calculation by the code FISPACT-II of the radio-isotopes production probability, we further analyzed the corresponding neutron-induced reactions cross-sections behavior and compared the values from the TENDL library used by FISPACT-II with the data available in the literature.

Among the three neutron-induced reactions on the ^{63}Cu natural isotope producing measurable radio-isotopes given our irradiation times, the available experimental cross-sections found in EXFOR database for the reactions $^{63}\text{Cu}(n,\gamma)^{64}\text{Cu}$ and $^{63}\text{Cu}(n,2n)^{62}\text{Cu}$ are relatively abundant and the evaluated cross-sections from TENDL library show globally a good agreement despite discrepancies being identified in some neutron energy domains. In the case of the other possible reaction $^{63}\text{Cu}(n,2p)^{62}\text{Co}$ no data was found in the literature which doesn't allow to test the accuracy of the cross-section values from TENDL library in this particular case.

Concerning the reactions on ^{65}Cu , experimental cross-sections are available for all of them and the evaluated values from the TENDL library are in some cases in significant disagreement, namely for the reaction $^{65}\text{Cu}(n,\alpha)^{62}\text{Co}$, for the reaction $^{65}\text{Cu}(n,p)^{65}\text{Ni}$ at neutron energies below 10 MeV and for the reaction $^{65}\text{Cu}(n,\gamma)^{66}\text{Cu}$ in the thermal neutrons region. A very good agreement was found on the other hand for the reaction $^{65}\text{Cu}(n,2n)^{64}\text{Cu}$.

Provided the good knowledge of the neutron flux and its energy distribution as well as the sample composition and the irradiation-decay sequences when calculating the radioactivity induced by neutrons in the samples with the FISPACT-II code, the main source of uncertainty affecting the calculations results is related to the reaction cross-sections used to determine the probability of production of each radio-isotope. The experimental conditions in which the samples were irradiated at NFS and subsequently analyzed by γ spectrometry are well known and faithfully reproduced in the simulations performed in this work as discussed in the beginning of this section. The next step was the estimation of the calculation accuracy based on the comparisons related to the neutron-induced reactions cross-sections, between the values from the TENDL library used by FISPACT-II and the experimental data.

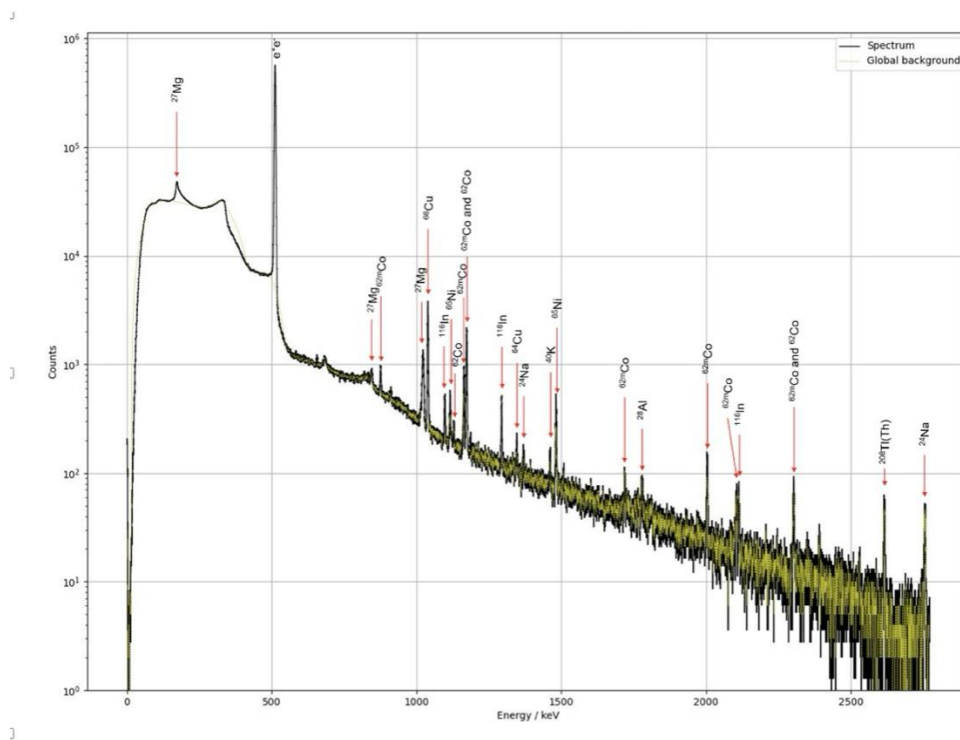
An article bringing together all the results of this first experiment at NFS will be submitted very soon to Nuclear Instruments and Methods in Physics Research B.

The first measurements performed using neutrons produced at the NFS facility presented in this work are related to the case of medical electron LINACs, but they must be seen as the first stage of a broader scientific program to be continued in the future. Other specific needs can be considered, related to the deep study of neutron-induced activation for other extensively used accelerator-based applications such as cyclotrons for the production of isotopes for nuclear medicine. Large-scale research facilities using particle accelerators such as synchrotrons and spallation sources also have specific needs in terms of neutron-induced activation, especially when considering the large quantities of materials used. On this aspect, we demonstrated that the neutron beams available at NFS offer enough flexibility in terms of energy distribution, considering the kinematics of the reactions used for their production, to cover a wide range of application related needs in terms of neutron-induced radioactivity.

Legend



Picture of the inside of the converter cave showing the experimental configuration



The γ spectrum measured for the copper sample after neutron irradiation at NFS (right)

4. Detector response characterization at a wide energy neutron range

Experiment number: Test MONSTER

Date: September 17-18, 2023

Spokeperson and co-authors

T. Martínez¹, D. Cano-Ott¹, A. Pérez de Rada Fiol¹, V. Alcayne¹, E. Mendoza¹, J. Plaza¹, A. Sánchez-Caballero¹, D. Villamarín¹, D. Doré², P. Miriot-Jaubert², M. Vandebrouck² and I. Matea³

¹CIEMAT, Madrid, Spain

²CEA DRF/Irfu/DPhN, Saclay, France

³IJCLab, Orsay, France

Abstract

The characterization of the neutron response of detectors in the energy range from a few 100 keV up to tens of MeV is needed to provide accurate results in many applications where the detection of fast neutrons plays an important role. This is the case of β -delayed neutron spectroscopy of exotic nuclei, nuclear reaction studies, the inspection and characterization of nuclear materials, homeland security applications, and neutron dosimetry in hadron therapy treatments.

Experiment report

Introduction

Organic liquid scintillation detectors have been traditionally used for fast neutron spectroscopy due to their high intrinsic efficiency, fast response, and the ability to distinguish between detected neutrons and γ -rays by pulse shape analysis. The characterization of the neutron response in the energy range from a few hundredths of keV up to tens of MeV is needed to provide accurate results in nuclear technology applications as well as in nuclear structure phenomena.

The determination of the neutron light output of the scintillators as a function of the incident neutron energy is required for obtaining the efficiency of the detectors over a broad neutron energy range. This is achieved by including the light output functions in detailed Monte Carlo simulation codes [Sch02] and through the validation of the simulations with accurate measurements.

The MODular Neutron time-of-flight SpectromETER (MONSTER) [Gar12, Mar14], based on BC501A and EJ301 liquid scintillators, has been designed for β -delayed neutron spectroscopy and other applications like (α, n) and neutron-induced reactions. A first characterization of the light output response in MONSTER detectors for neutron energies up to 14 MeV was performed at PTB and CEA/DAM facilities. The contribution to the light output response due to n-p recoil cross section and $^{12}\text{C}(n, \alpha)$ and $^{12}\text{C}(n, n')3\alpha$ reactions channels were validated with NRESP and GEANT4 codes [Gar17].

At higher neutron energies ($E > 20$ MeV), other break-up reactions, such as $^{12}\text{C}(n, p)$ and $^{12}\text{C}(n, d)$, also contribute to the response. These reactions are not accurately implemented in state-of-the-art codes, and therefore specific light output calibration measurements are needed when small uncertainties are required for neutron energies above 20 MeV. In this context, a characterization measurement of the neutron response in the range of 1 MeV up to 40 MeV has been performed at the NFS facility [Led21] of GANIL.

Experimental methods

At NFS, a neutron beam with a wide energy range was generated through the $^9\text{Be}(d, n)$ reaction. A primary deuteron beam at 40 MeV impinging on a thick beryllium target provided neutrons with a continuous spectrum thanks to the deuteron break-up reactions. According to the estimated reaction yield, neutron energy range, flight distance, and detector count rate it was necessary to work at a repetition rate below 88 kHz, both to avoid overlap of neutrons from successive bunches and to keep a reasonable neutron count rate. For that, the LINAC frequency (88 MHz) was reduced by a factor of 1000 to 1500 using the bunch selector at the RFQ element. The LINAC RF signal was used to provide the start signal for the determination of the neutrons' time-of-flight (TOF). The beam current was

measured with a faraday cup placed close to the target. The signal provided by a current integrator module was also registered, to be used for normalization.

Several detectors have been irradiated to study their response to neutrons of such energies. Four MONSTER detectors, which combine two types of module design and two kinds of PMT models, and a small EJ315 (deuterated benzene) detector, which is used in neutron capture cross section measurements at the n_TOF facility of CERN. The detectors were placed at the end of the TOF Hall at a flight path distance of ~30 m from the target and at 0 degrees (Figure 1).

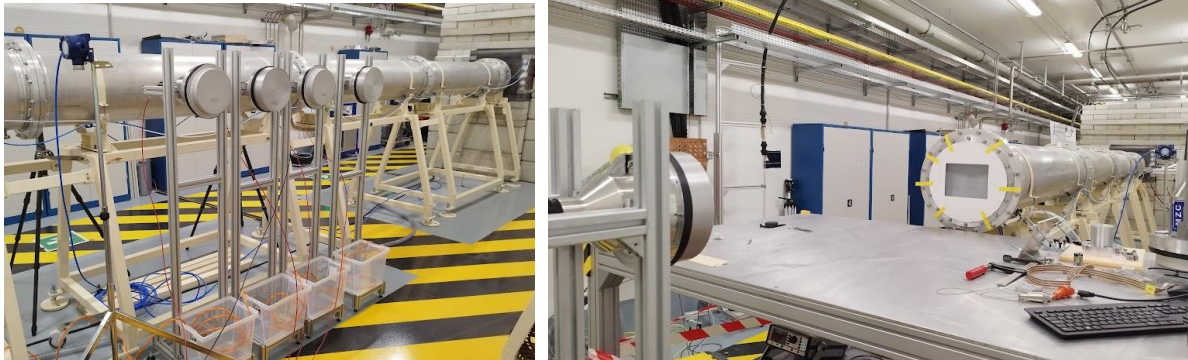


Figure 1. (Left) Four MONSTER cells used in this test. (Right) Detector placed at the irradiation position.

The detector signals, as well as the RF and current signals, were registered with the Digital data Acquisition System (DAISY), a custom digital DAQ system developed at CIEMAT. It is based on ADQ14DC digitizers from Teledyne SP Devices with 14 bits vertical resolution, 1 GHz sampling rate, and 4 channels [Vi23]. The system integrates custom pulse shape analysis software to perform an online analysis of the signals.

Results and discussion

A preliminary analysis of the measurement performed with the MONSTER detectors is presented in this section. Linearity and light calibration

The light calibration of the detectors was performed with ^{22}Na and ^{88}Y gamma-ray sources that only covered a small energy range. Thus, the linearity of the detectors over the whole range of interest was checked with data from (d,n) reaction runs. As can be seen in Figure 2, the area of the signals is proportional to their amplitude over the whole energy range of interest, confirming the linearity of the detector response.

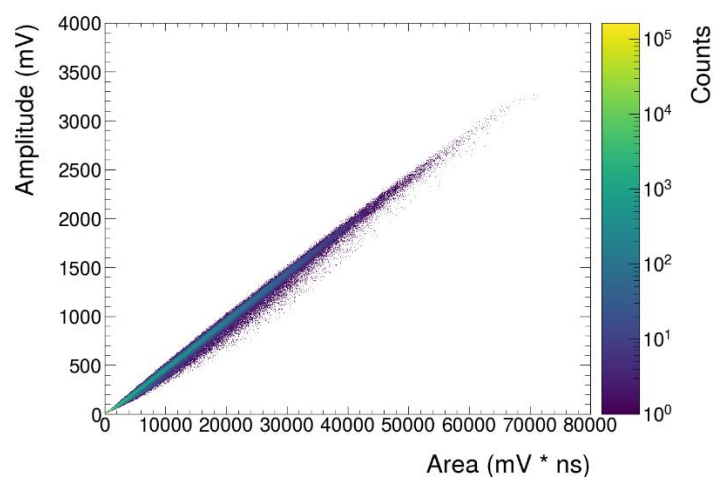


Figure 2. Amplitude of the signals registered during (d,n) reaction runs with MONSTER M3 detector as a function of their area.

Confirming the linearity of the detectors allowed to extend the calibration performed with γ -ray sources to the whole energy range of interest.

Time-of-flight spectrum

To obtain the TOF spectrum of the neutrons, a selection of the neutron events on the PSD vs light spectrum was performed. In the left part of Figure 3, the selected events are shown. Events corresponding to the detection of γ -rays are filtered out with the excellent discrimination capabilities of MONSTER detectors. In this figure, lower values of PSD correspond to events where the scintillation light has been produced by reactions of the neutrons with the hydrogen in the liquid, while higher values of PSD correspond to light emitted after reactions with heavier ions. On the right side of the figure, the corresponding clean neutron TOF spectrum is shown.

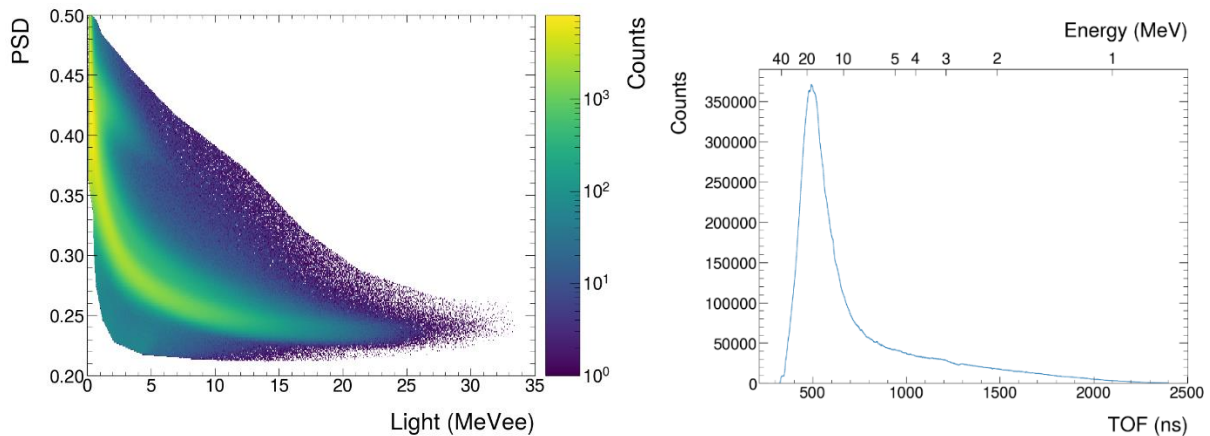


Figure 3. (Left) PSD vs light spectrum of the selected neutron events. (Right) Neutron TOF spectrum.

To determine the real flight path of each detector, necessary for the TOF calibration, a measurement with a carbon sample placed between the target and the detector was performed. The resonances of the carbon observed in the TOF spectrum were used to perform a fit and obtain the distance of each detector from the target.

Detector response function

With a clean and calibrated neutron TOF spectrum, the TOF technique can be applied to obtain the detector response to neutrons of different energies. Cuts at different TOF values have been applied in the neutron TOF spectrum to obtain the detector response function to neutrons of different energies. Some of the response functions obtained can be seen in Figure 4. In this figure, it can be observed that different structures appear on the response functions as the neutron energy increases.

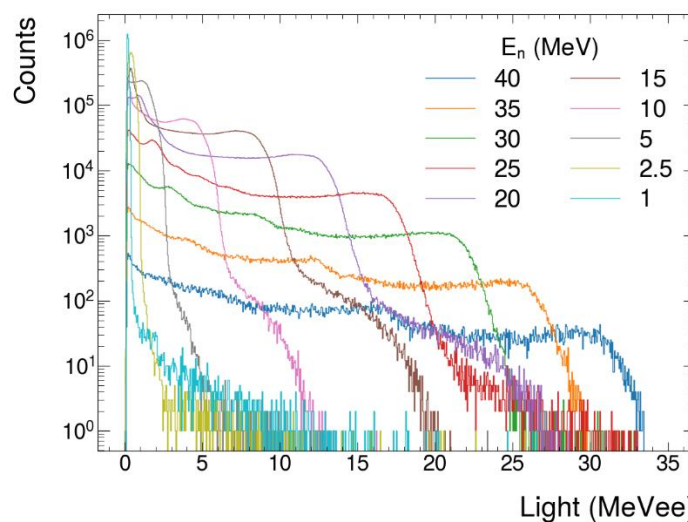


Figure 4. Response functions of MONSTER for neutrons of different energies.

The structures that appear at higher neutron energies correspond to the different reaction channels that open as the energy of the neutrons increases. The evolution of these structures can be seen more clearly by checking the

PSD vs light spectrum with a selection of the neutron TOF (i.e. energy). Figure 5 shows this spectrum for neutrons of 20 and 30 MeV, where the different structures can be clearly differentiated as banana-like shapes.

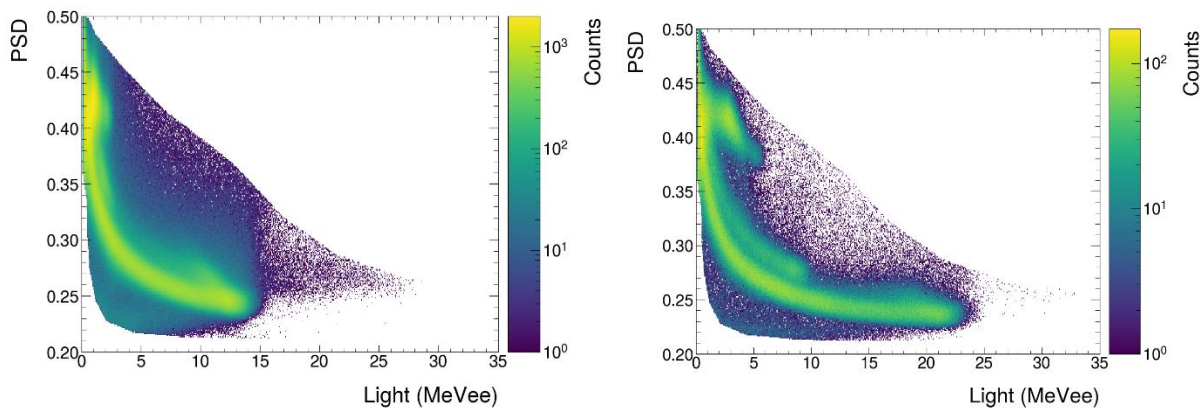


Figure 5. PSD vs light spectrum for neutrons of 20 (left) and 30 (right) MeV.

In the figure, three main different structures can be observed. The lower banana-like structure corresponds to events where the light has been produced by protons. The structure immediately above to the protons one corresponds to the light produced by deuterons and protons emitted in the reaction with carbon. In the figure, this contribution is clear for the case of neutrons of 30 MeV (right panel), but not for lower energy ones (left panel). Finally, at higher values of PSD, from 0.38 to 0.45, the contribution of α -particles can be observed as a third banana structure.

Efficiency

To obtain the efficiency curve of MONSTER detectors, the response function corresponding to each neutron energy considered will be integrated. The obtained values need to be corrected by the total current integrated during the measurement. After the experimental values of the efficiency are obtained, they will be compared to Monte Carlo simulations performed both with Geant4 and PHITS. Some preliminary results of the simulations performed are shown in Figure 6.

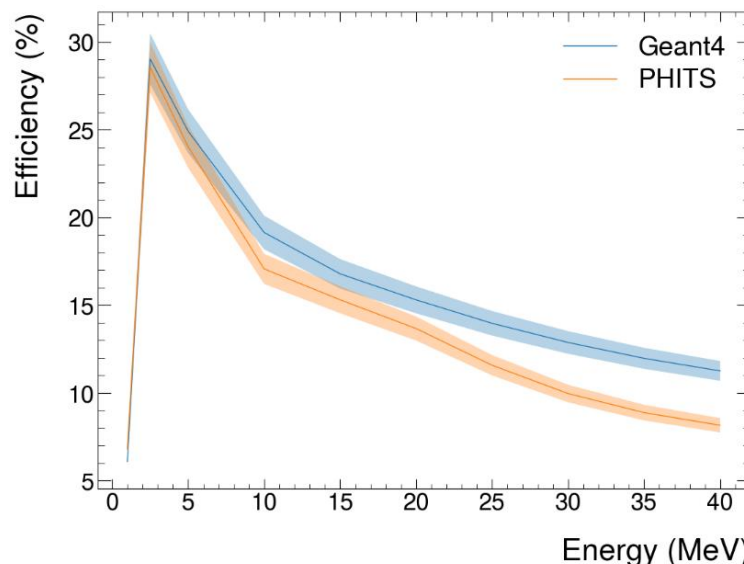


Figure 6. Simulated efficiency curves of a MONSTER module with Geant4 and PHITS.

As can be seen in the figure, both simulation codes produce results that are in agreement below 20 MeV, within the 5% of uncertainty that has been assigned to each curve. In this energy range, the small differences observed are due to differences in the simulated geometries. In the case of the simulation with PHITS, more geometrical

details need to be included. Above 20 MeV, the differences are mainly due to the fact that Geant4 uses models instead of data.

Conclusions

The analysis is still ongoing. A successful preliminary analysis of the data taken has been performed. There are still some difficulties to be addressed, such as the lack of a reliable current integration signal in some runs and the pileup caused by the high neutron yield and the difficulty of placing the second collimator on the beam line. Nonetheless, the results obtained so far look promising.

References

- [Sch02] D. Schmidt et al., Nucl. Instrum. Methods A, 476 (2002) 186-189.
- [Gar12] A. Garcia et al., J. Instrumentation, 7 (2023) C05012.
- [Mar14] T. Martinez et al., Nucl. Data Sheets, 120 (2014) 78
- [Gar17] A. Garcia et al., Nucl. Instrum. Methods A, 868 (2017) 73
- [Led21] X. Ledoux et al., Eur. Phys. J. A (2021) 57: 257
- [Vil23] D. Villamarin et al. Nucl. Instrum. Methods A, 1055 (2023) 168526.

5. Neutrons response determination of four LNE-IRSN (LMDN) scintillators in their operating energy range (i.e. between 100 keV-22 MeV)

Experiment number: LNE-IRSN scintillators test

Date: September 15-20, 2023

Spokeperson and co-authors

Michaël PETIT/IRSN (michael.petit@irsn.fr), Diane QUEVAUVILLERS (IRSN), Laurent OTTAVIANI (Aix-Marseille Université), Christelle REYNARD-CARETTE (Aix-Marseille Université)

Abstract

Between September 15th and 20th 2023, the Laboratory for micro-irradiation, neutron metrology and dosimetry (LMDN) of IRSN carried out an experiment on the neutron beam line NFS at GANIL. The aim of the experiment was to determine the neutron response functions for 4 scintillators between 100 keV and 22 MeV. The characteristics of the NFS beam - frequency, energy resolution and count rate - were perfectly compatible with the scientific and technical goal and the technical resources from NFS teams were excellent. Finally, it was possible to obtain completed data for the four detectors within 16 hours. The data are currently being analyzed, and an initial assessment suggests that the objectives have been achieved. NFS is a high-profile facility for this type of calibration, which is essential in neutrons metrology field. The LMDN would like to thank the NFS teams for their welcome, their availability and the quality of the neutrons beam. These scintillators will set LMDN's metrological references for years to come.

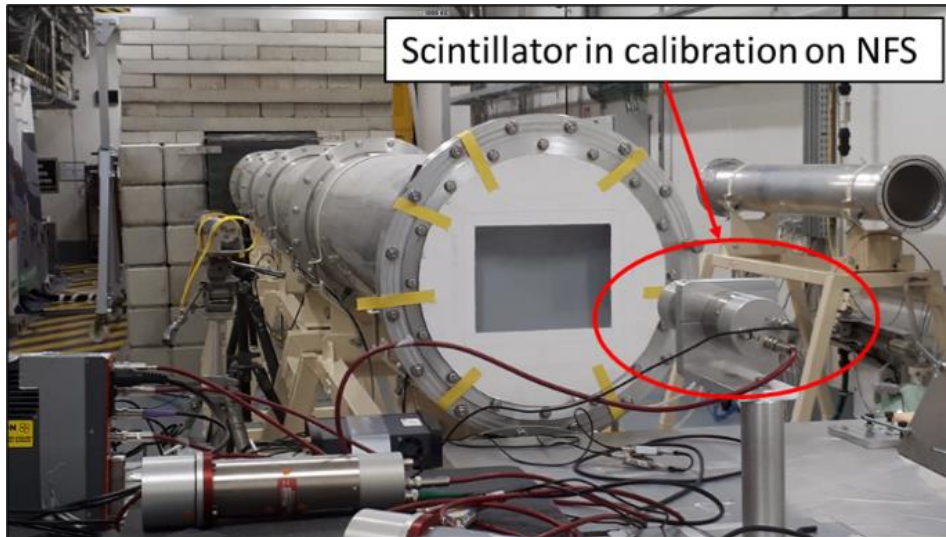
This work is supported by LNE, the French National Metrological Institute and is a part of Diane QUEVAUVILLERS' PhD (Characterization and use of stilbene scintillators at AMANDE and CEZANE for neutron metrology and spectrometry between 100 keV and 22 MeV)

Experiment report

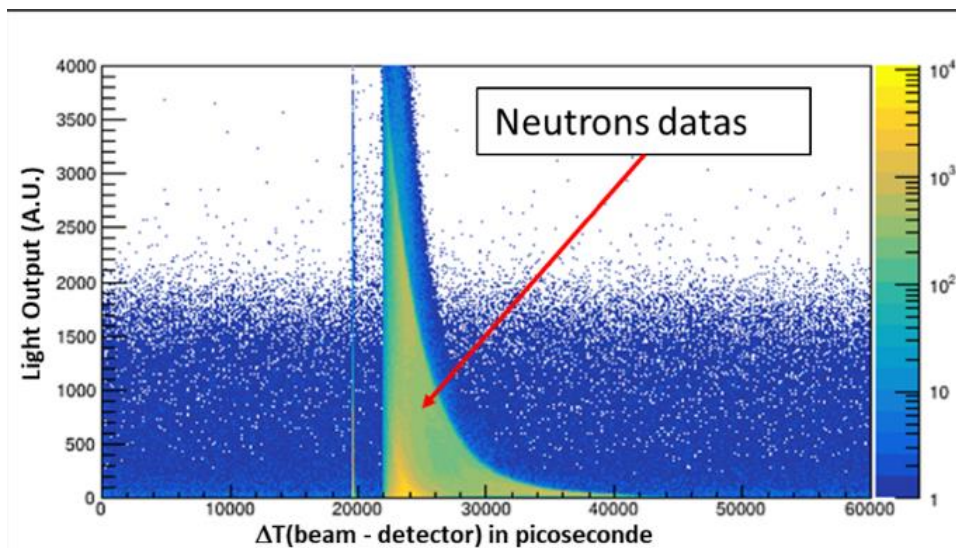
The four scintillators calibrated are two-inch orthocylindrical and are coupled to a DT5730 digital acquisition system driven by the commercial software COMPASS. The operating points of the scintillators had previously been determined by dedicated studies carried out on the AMANDE facility of the LMDN located on the Cadarache site. Neutron calibration of the 4 scintillators was carried out using a neutron beam from the reaction of 40 MeV deuterons pulsed beam on a thick ⁹Be target. This beam provides a neutron spectrum ranging from few keV up to 44 MeV, although the neutron spectrum below 1 MeV is not well known yet. The beam frequency was around 88 kHz, giving a period of 11 μs between two pulses. This delay means that the detector can be considered to have returned to its baseline between two pulses. The intensity of the beam resulted in a count rate of about 8,000 events per second for a background of about 200 events per second. Each detector was calibrated within 4 hours, so with about 100 million events per detector.

Neutron energy is determined by the time-of-flight method. The time resolution of the measurement is less than 1 ns for a flight distance of 29 m. More, the neutron energy was checked with a carbon filter which led to observe by transmission the resonances in the total effective cross-section of ¹²C. The uncertainty on the neutron energy is at most 30 keV for the highest energies, which is less than the intrinsic resolution of the detector. Photon calibration of the detectors was carried out on site using the NFS calibration sources (¹³⁷Cs, ²²Na, ⁸⁸Y, ²⁰⁷Pb). All of this data is currently being analyzed at LMDN.

This type of experiment, which is extremely simple to design and carry out, is nonetheless essential to the LNE-IRSN neutron metrology activities. Technical resources proposed were well suited to the task and the current lack of an equivalent alternative in Europe means that NFS is essential.



One of the four scintillators being calibrated on the NFS line.



Extract from the raw data for one of the scintillators.

6. Shedding new light on the structure of ^{56}Ni using $(n,3n)$ reaction at NFS

Experiment number: E838_21

Date: September 26-October 7, 2023

Spokeperson and co-authors

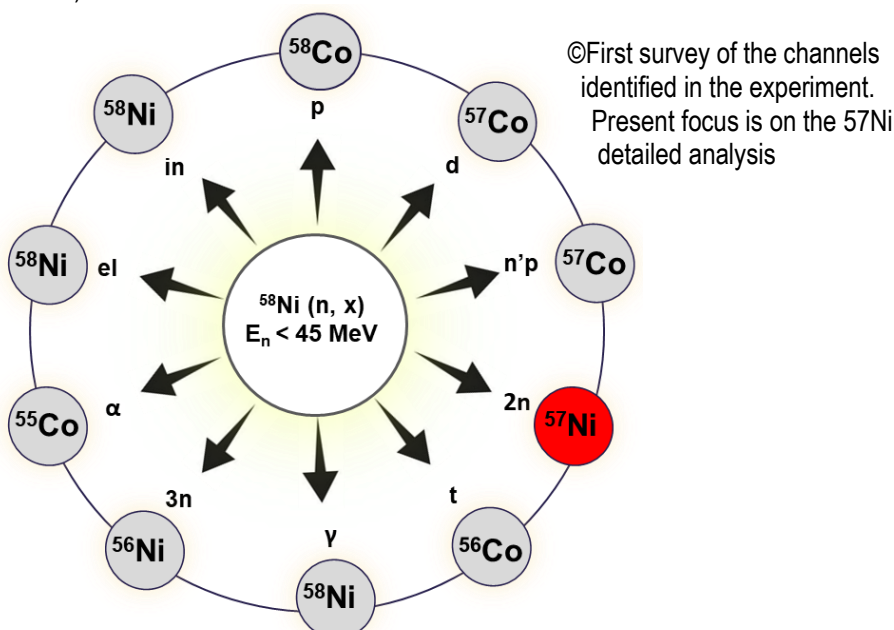
Emmanuel CLEMENT (GANIL) Maelle Kerveno (IPHC)

Abstract

We proposed to re-investigate the nuclear structure of the doubly magic nuclei ^{56}Ni using the $(n,3n)$ reaction from ^{58}Ni . The nuclei near ^{56}Ni are of particular interest as they are amenable to different microscopic theoretical treatments while studying the competition between single- particle and collective excitations. The collective states in ^{56}Ni involve multiparticle multihole excitations across the $N=Z=28$ shell gap. At high excitation energies, reaction studies have revealed evidence for hyperdeformed resonances in the ^{56}Ni compound. While the structure of ^{56}Ni has been intensively investigated using charge particle or heavy ions collision, the pure neutron probe was never used. The (n,xn) reactions are a long standing reaction mechanism used in the nuclear data evaluation but never used in the framework of nuclear structure. For the first time, using the unprecedented NFS neutron flux at $\sim 30\text{MeV}$, ^{56}Ni can be populated from ^{58}Ni in a $(n,3n)$ reaction with a cross section of 2 mb opening a new probe and possibly new aspect of the nuclear structure of this doubly magic nuclei. We propose to perform a prompt spectroscopy of ^{56}Ni using the EXOGAM array at NFS using the $(n,3n)$ reaction. Such new spectroscopic informations are also relevant for nuclear reaction mechanism formalism (like TALYS) and nuclear data evaluation. For nuclear structure, the main motivation is the search for low spin ($J=2$ or 4) states from 3 to 10 MeV excitation energy possibly populating the 0^+ states at 3956 keV, 6654 keV and 7903 keV observed only in $^{58}\text{Ni}(p,t)^{56}\text{Ni}$ reactions

Experiment report

EXOGAM was used for the first time to perform the in-beam spectroscopy of exotic nuclei using the (n,xn) reaction using fast neutron up to 40 MeV. The experiment was very successful and the analysis is led by a PhD student in the STARS group. Reaction products of $(n,2n)$, $(n,3n)$, (n,p) , (n,t) and (n,a) have been observed in prompt gamma gamma spectroscopy in coincidence with the fastest neutron. The in-depth analysis of the $^{58}\text{Ni}(n,2n)^{57}\text{Ni}$ channel led to the following first observations : the overall picture of the populated states is comparable to the heavy-ions fusion limited to low angular momentum, new states have been observed, the reaction is orienting the initial states, and excitation function can be measured. The analysis will be continued on the $(n,3n)$ and $(n, \text{charged particles})$ channel)





II. VAMOS

1. Damping of shell effects in nuclear fission

Experiment number: E850_21

Date: June 13-26, 2023

Spokeperson and co-authors (affiliation)

Julien Taieb (CEA), Pierre Morfouace (CEA), Diego Ramos (GANIL), Antoine Lemasson (GANIL), Audrey Chatillon (CEA), Benoit Mauss (CEA), Laurent Audouin (IJCLab), Lucas Bégué-Guillou (GANIL), Jose Luis Rodriguez (University of Coruna), Alex Cobo Zarzuelo (GANIL), Neeraj Kumar (IPHC), Christelle Schmitt (IPHC), Cyril Lenain (CEA), Théodore Efremov (CEA), Alexis Francheteau (GANIL), Indu Jangid (GANIL), Taiki Tanaka (GANIL), Manuel Caamano (Santiago), Bea Errandonea (Santiago), Owenn Syrett (CEA), Ron Malone (Livermore), Anton Tonchev (Livermore), Anthony Ramirez (Livermore), Charlène Surrault (CEA), Marius Godio (IJCLab), Alicia Munoz (USC-IGFAE), Deby Treasa (LP2IB), Igor Tsekhanovich (LP2IB), Emmanuel Clément (GANIL)

Abstract

The experiment aims at measuring isotopic fission-fragment yields as a function of excitation energy of the fissioning systems produced by transfer reaction. Using the newly-developed highly-segmented PISTA silicon array (Particle Identification Silicon Telescope Array), we aim at obtaining isotopic fission yields with high statistics per bin of about 1 MeV in excitation energy from 6 up to 20 MeV. Several fissioning systems of interest are populated such as ^{236}U , ^{240}Pu or ^{242}Pu . These data will bring new insights on the disappearance of shell effects with the excitation energy of the fissioning system and are of high relevance for the nuclear physics applications, in particular for Gen-IV reactors operating with fast neutrons.

Experiment report

The experiment took place in June 2023 with a planned beam time of 12 days to measure fission fragments at two angles of the VAMOS spectrometer: 14 and 20 degrees, for 6 days each. However, various issues in the production of the ^{238}U beam did not allow for 12 days of beam time, but only an effective time of about 6 days. For this reason, the measurement focused on a single VAMOS angle to obtain the necessary statistics. Consequently, the GANIL management agreed to grant us an additional 6 days to perform the measurement at 14 degrees. This additional beam time took place in April 2024. This experiment is part of Lucas Bégué-Guillou's thesis and will be the subject of further theses.

Despite the non-optimal performance of the accelerator, this was the first use of the new silicon detector array, PISTA. Very quickly, we were able to recognize the excellent performance of PISTA in terms of ejectile identification. Indeed, PISTA allows for a much better separation between ^9Be and ^{10}Be , as well as between different carbon isotopes, as shown in Figure 1. The quality of this particle identification spectrum clearly demonstrates the added value of PISTA for this experiment. Finally, the better granularity of PISTA, after fine calibration and alignment, will enable a resolution 2.9 times better than that obtained with SPIDER.

In this identification spectrum, we can also see that ^{14}C is produced ten times less frequently than ^{10}Be , which will make the study of the ^{236}U system less relevant compared to ^{240}Pu , where we have ten times more events.

In any case, it is clear that PISTA allows for better identification of the ejectile and will thus enable a much better characterization of the fissioning system in terms of mass, charge, and excitation energy. Its resolution in excitation energy will allow for a much finer probing of the evolution of shell effects with E^* .

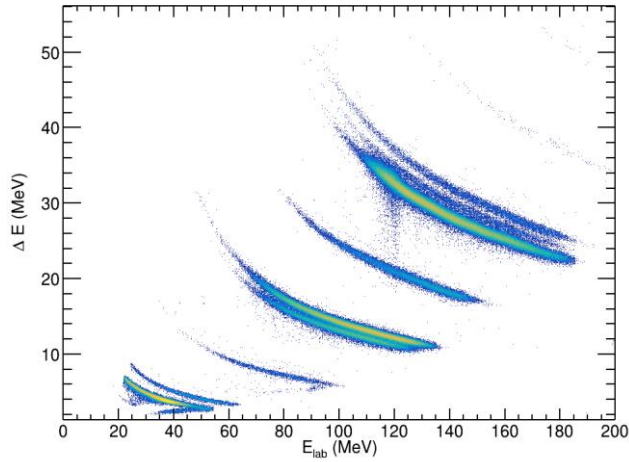


Figure 1: PISTA particle identification

Moreover, the VAMOS spectrometer is dedicated to the mass and charge identification of one of the fission fragments through its various multi-wire detectors and ionization chambers. This spectrometer enables the measurement of both charge and mass with adequate resolution across the entire distribution of fission fragments. The measurement of the mass of the fragments is provided through a time-of-flight measurement combined with a position measurement, thus giving the magnetic rigidity $B\rho$. A current preliminary analysis shows the mass distribution obtained for all excitation energies in the case of ^{240}Pu , where ^{10}Be has been selected in PISTA. This distribution is presented in Figure 2. This preliminary distribution shows a mass separation up to mass 150, that is, across the entire distribution of fission fragments as well.

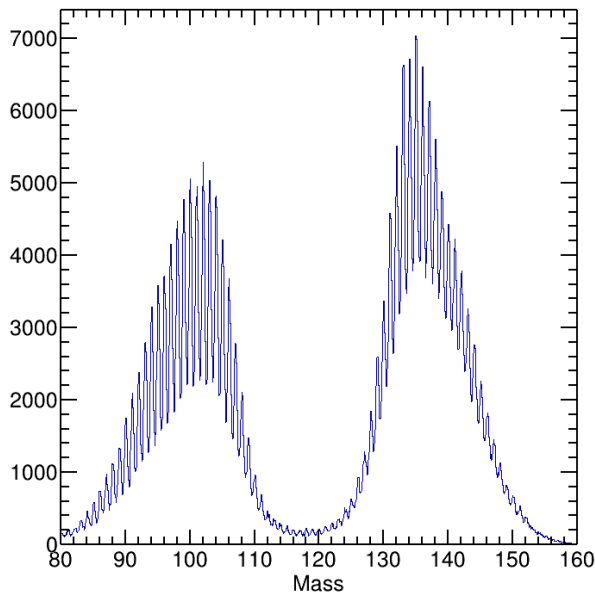


Figure 2: Fission fragment mass distribution for ^{240}Pu



III. LISE

1. How does deformation influence neutron-proton pairing? Study of the two-nucleon transfer reaction $^{48}\text{Cr}(p, ^3\text{He})^{46}\text{V}$

Experiment number: E805_20

Date: April 7-20, 2023

Spokeperson and co-authors

M. Assié¹, H. Jacob¹, V. Alcindor¹, Y. Blumenfeld¹, Ö. Aktas², D. Beaumel¹, J. Béquet¹, S. Bottoni³, E. Clément², G. De France², Q. Delignac⁴, F. De Oliveira², N. De Séréville¹, L. Dienis², S. Franchoo¹, F. Galtaross⁵, A. Gottardo⁶, F. Hammache¹, M. Kaci¹, S. Koyama², A. Lemasson², M. Lozano González⁷, A.O. Macchivelli², I. Matea¹, O. Nasr¹, C. Paxman⁹, S. Pigliapoco⁶, J. Piot², T. Roger², F. Rotaru¹⁰, O. Sorlin², M. Stanoiu¹⁰, I. Stephan¹, Ch. Stodel², J.C. Thomas², L. Zago⁶.

¹ Université Paris-Saclay, CNRS/IN2P3, IJCLab, Orsay, France

² GANIL, CEA/DRF-CNRS/IN2P3, Boulevard Henri Becquerel, Caen, France

³ INFN Sezione di Milano, Italy

⁴ University of Bordeaux, CNRS, LP2I Bordeaux, UMR 5797, Gradignan, France

⁵ INFN Sezione di Padova, Padova, Italy

⁶ LNL, Legnaro, Italy

⁷ IGFAE and Dpt. de Física de Partículas, Univ. of Santiago de Compostela, E-15758, Santiago de Compostela, Spain

⁸ Oak Ridge National Laboratory, USA

⁹ School of Maths and Physics, University of Surrey, Guildford, United Kingdom

¹⁰ IFIN-HH, Bucharest-Magurele, Romania

Abstract

Neutron-proton pairing manifests itself predominantly in nuclei with $N=Z$ and is expected to be maximum for open shell nuclei with high- j orbitals. Pair-transfer is one of the experimental signatures for pairing. The experiment aimed at studying the unstable ^{48}Cr nucleus that is the middle of the f -shell, the largest shell accessible experimentally for two-nucleon transfer and also a good rotor. By measuring the neutron-proton transfer reaction $^{48}\text{Cr}(p, ^3\text{He})^{46}\text{V}$, the interplay between pairing and deformation will be investigated. The goal was to determine the cross-sections to the ground state ($0^+, T=1$) and to the first $1^+, T=0$ state in order to: (i) determine the ratio of these cross-sections and put it in perspective with previous measurements in the f -shell; (ii) study the effect of deformation on each pairing channel by comparing with theoretical predictions. The experiment was run as part of the LISE2023 campaign, making use of CATS beam trackers, the MUST2 array, EXOGAM and the 0° degrees detection chamber (ZDD, see Fig. 1).

Experiment report

^{48}Cr was produced at 33.9 MeV/u in the fragmentation of a ~ 50 pnA ^{50}Cr stable beam at 72 MeV/u in a 1mm thick Be target. The secondary beam was purified using a 700 μm thick Be wedge shaped degrader and the LISE Wien Filter set to 1500 kV/m. Up to $2.5 \cdot 10^5$ pps of an almost pure beam (see Fig. 2) was sent to a 5 mg/cm² CH₂ secondary target.

First, the online analysis focused on the one-nucleon transfer reaction $^{48}\text{Cr}(p,d)^{47}\text{Cr}$ because of its larger cross-section than the $(p, ^3\text{He})$ reaction. Fig. 3 shows preliminary results for the (p,d) reaction with the kinematic lines and the gamma spectrum obtained by gating on a ^{47}Cr isotope in the ZDD.

Second, after proper calibration of the MUST2 and the CATS detectors, the excitation energy spectrum for the two-nucleon transfer reaction $^{48}\text{Cr}(p, ^3\text{He})$ have been extracted in coincidence with the detection of Vanadium ions in the ZDD (see insert on Fig. 4). The angular distribution for the ground state has also been determined and corresponds to an $L=0$ transfer as expected (see. Fig. 5). The extraction of the gamma-rays in coincidence is still on going.

Copyright

© IJCLab, GANIL

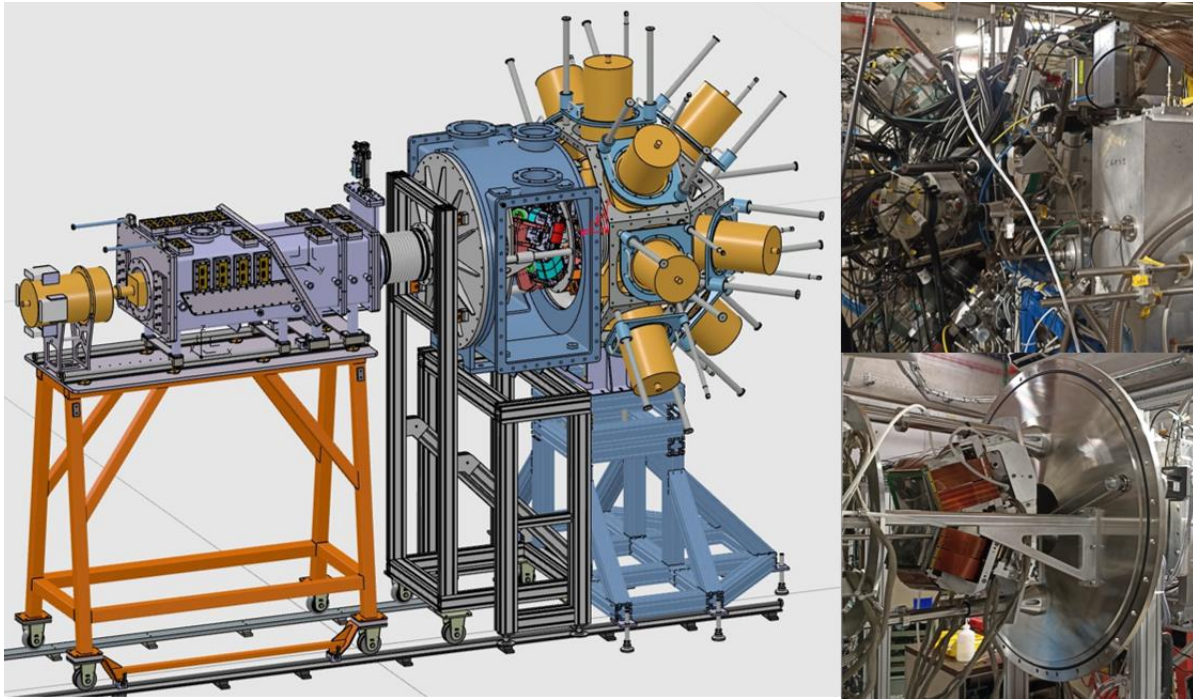


Figure 1: Technical drawing of the experimental setup used in the E805 experiment. On the right side, photographs of on the two CATS beam trackers (upper part) and of the MUST2 charged-particle detection array (bottom part) are shown.

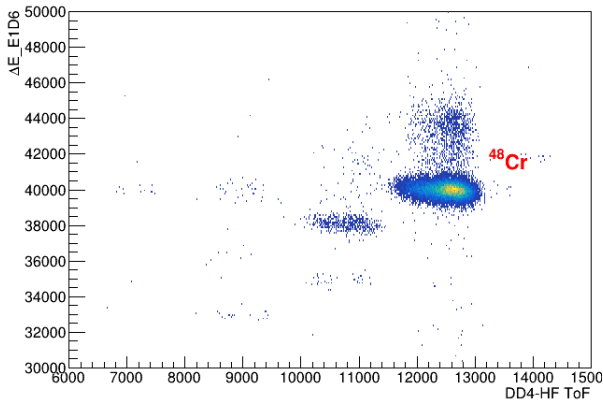


Figure 2: ΔE -ToF identification matrix of the ^{48}Cr secondary beam (97 % of the total) obtained after the F62 slits using the LISE Wien filter.

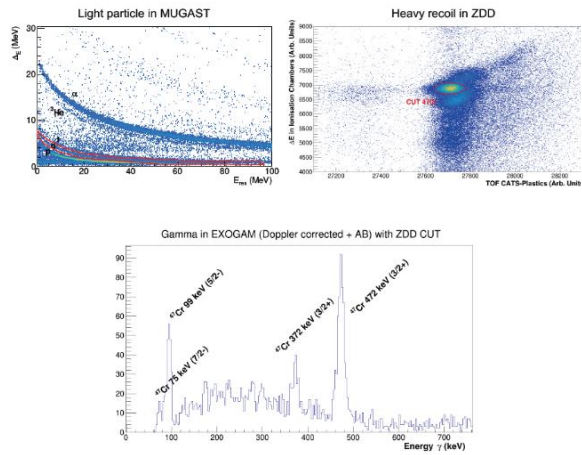


Figure 3: Online results obtained for the $^{48}\text{Cr}(p,d)^{47}\text{Cr}$ reaction, showing from left to right the kinematic lines associated with the detection of light particles in MUST2 and the identification of heavy recoiling ions in the ZDD, and in the bottom picture the gamma lines deexciting the states populated in ^{47}Cr .

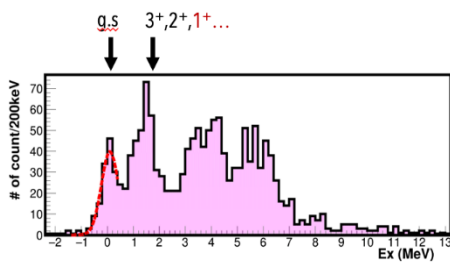


Figure 4 : Excitation energy spectrum for ^{46}V . The ground state is well separated from the other excited states. The $1+$ state (of interest in this experiment) is mixed with other contributions and will be disentangled by the coincidence with gamma-rays.

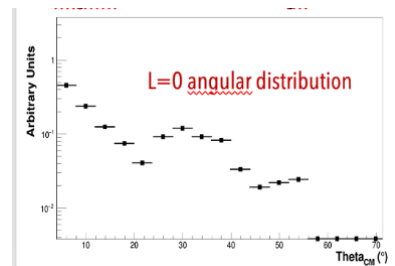


Figure 5 : Angular distribution for the two-nucleon transfer $^{48}\text{Cr}(p,^3\text{He})^{46}\text{V}$ g.s. It is peaked at 0 degree as expected for a $L=0$ transfer.

2. Search for tensor type interactions in nuclear beta decay

Experiment number: E815_20

Date: April 28 – May 1, 2023

Spokeperson and co-authors

O. Naviliat-Cuncic^{1,2}, X. Fléhard¹, G. Craveiro³, D. Etasse¹, T.E. Haugen², L. Hayen¹, M. Kanafani¹, S. Leblond³, F. Lebourgeois¹, E. Liénard¹, J. Lory¹, F. Marie-Saillenfest⁴, X. Mougeot³, J. Perronnel¹, J.C. Thomas⁴, Ch. Vandamme¹, V. Watt-Morel⁴

¹ Université de Caen Normandie, ENSICAEN, CNRS/IN2P3, LPC Caen, Caen, France

² National Superconducting Cyclotron Laboratory, Dep. Phys. and Astronomy, Michigan State University, USA

³ CEA, LIST, Laboratoire National Henri Becquerel, Gif-sur-Yvette, France

⁴ GANIL, CEA/DRF-CNRS/IN2P3, Boulevard Henri Becquerel, Caen, France

Abstract

The Fierz interference term is the most sensitive parameter in nuclear beta decay to probe the existence of exotic (scalar and tensor) interactions contributing to weak decays, involving left-handed neutrinos. The experiment aims at extracting the Fierz interference term from the precise measurement of the beta energy spectrum in the pure Gamow-Teller decay of ⁶He with a total uncertainty of 0.004. Such a level of sensitivity will provide the tightest constraint on the phenomenological tensor coupling from any low energy experiment. The possibility for improving this level of sensitivity by an additional factor of 4 is being considered as a second phase of the project. Precision measurements of the beta particle energy spectrum were performed using both, high energy (LISE - 2023) and low energy (LIRAT - 2021) ⁶He beams.

Experiment report

⁶He ions were produced in the fragmentation of a ¹³C beam at 60.2 MeV/u in a 2 mm thick Be target. The secondary beam was purified using a 1 mm thick Be wedge-shaped degrader and the LISE Wien filter set at 3000 kV/m. A collimator was used to further define the beam shape, which spot size and alignment was checked using a hodoscope consisting of four plastic scintillators.

The energy spectrum of beta particles was measured in a beam On/Off mode using a calorimetry technique. For each cycle, the beam was kept on during 3 seconds for implantation and switched off for 12 seconds to record data during the beta decay. The ⁶He nuclei, extracted in air at an energy of 52 MeV/u, were implanted about 9mm deep in the volume of a YAP scintillator. The beta particles emitted by the ⁶He ions do not escape the YAP detector, thus eliminating the main instrumental effect in beta spectroscopy, which is the scattering and backscattering of beta particles on materials. The implantation detector was surrounded (Fig. 1) by a high-purity Germanium detector to monitor possible secondary beam contamination and by another YAP detector to measure Bremsstrahlung radiations escaping the implantation detector.

YAP detectors of two different volumes were used during the measurement, and placed at short and large distance from the extraction window in order to study systematics effects. A total number of $\sim 10^8$ decay events were recorded with a FASTER acquisition system, split in four data sets. The analysis of the YAP spectrum during implantation (Fig. 2) shows only pileup events and no sign of beam contamination (above the 10^{-5} level). Figure 3 shows a typical spectrum obtained during the beam off period of the cycles. Background subtracted ⁶He energy spectra will be derived after baseline and gain corrections will be applied.

Copyright

© LPC Caen, GANIL

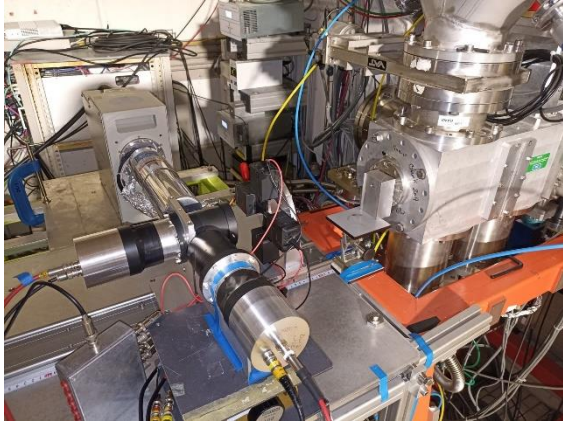


Figure 1: Experimental setup at the final focal point of the LISE spectrometer.

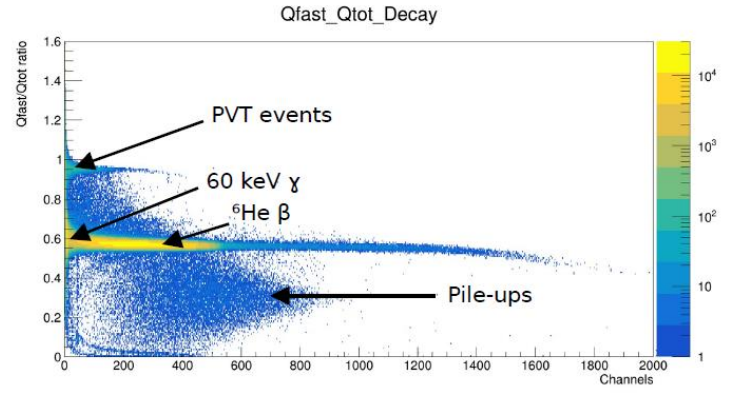


Figure 2: Time integration of the signal delivered by the implantation detector during the beam-off phase (${}^6\text{He}$ decay).

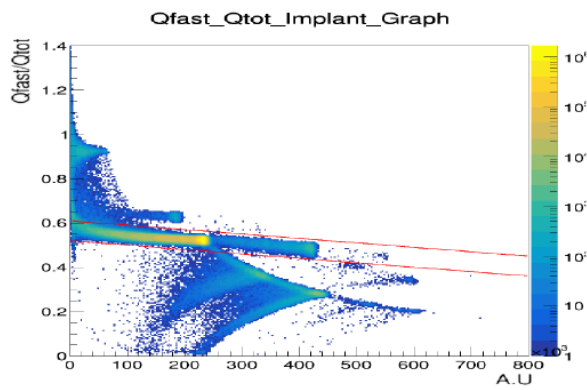


Figure 3: Time integration of the signal delivered by the implantation detector during the beam-on phase (${}^6\text{He}$ implantation).

3. Search for two-proton radioactivity and beta-delayed multi-particle emission in ^{39}Ti

Experiment number: E839_21

Date: March 9-16, 2023

Spokeperson and co-authors

V. Guadilla¹, F. de Oliveira², Z. Janas¹, L. Janiak³, O. Kamalou², G. Kamiński⁴, A. Korgul¹, A. Kubiela¹, C. Mazzocchi¹, K. Miernik¹, M. Pfützner¹, J. Piot², M. Pomorski¹, B. Rebeiro², A. Skruch¹, O. Sorlin², C. Stodel², M. H. Stodel², J. C. Thomas²

¹ Faculty of Physics, University of Warsaw, 02-093 Warsaw, Poland

² GANIL, CEA/DRF-CNRS/IN2P3, Boulevard Henri Becquerel, Caen, France

³ National Centre for Nuclear Research, 05-400 Otwock, Świerk, Poland

⁴ Heavy Ion Laboratory, University of Warsaw, 02-093 Warsaw, Poland

Abstract

The experiment aimed at measuring the decay of ^{39}Ti , a very neutron-deficient nucleus laying beyond the predicted di-proton dripline. This nucleus has been highlighted as an excellent candidate to undergo the very exotic two proton radioactivity. An Optical Time Projection Chamber (see Fig. 1.), was used to look for such two proton radioactivity emission at the focal point of the LISE spectrometer. Several beta-delayed multi-particle emission branches are energetically possible, but only beta-delayed two protons are known to be emitted from the isobaric analog state of the daughter nucleus, the proton unbound ^{39}Sc . The experiment should allow a clear determination of the energies and branching ratios of these beta-delayed two protons for the first time, as well as to identify unknown beta-delayed multi-particle channels. The clear determination of the energy of the beta-delayed two protons is expected to clarify the mass excess value of ^{39}Ti .

Experiment report

^{39}Ti was produced in the fragmentation of a ~ 100 pnA ^{58}Ni beam at 74.5 MeV/u in a 100 μm thick $^{\text{nat}}\text{Ni}$ target. The secondary beam was purified using a 220 μm thick Be wedge shaped degrader and the LISE Wien filter set at 1500 kV/m. Radioactive ions were slowed down and identified by ΔE and ToF measurements using active silicon detectors located before the OPTC entrance window and two DELICAT fast gas detectors located at the focal planes of the spectrometer. The implantation range distribution of ^{39}Ti was fine-tuned using a rotating, remotely controlled passive Aluminium slower. A double conditioning was set online on the ΔE and ToF measurements with MSCA modules in order to reduce the triggering rate of the optical system of the OPTC to a few Hz. The “active gate” was applied on ^{39}Ti ions and on the main contaminants (N=17 isotones), observed at similar ΔE and ToF values. Figure 2 shows a representative ΔE -ToF identification matrix after the double gate conditioning.

In the first part of the experiment, a low-density gas mixture was used to favour the observation of the direct two protons decay of ^{39}Ti ions. In the second part of the experiment, a higher-density gas mixture was used to implant ^{39}Ti ions in the middle of the OPTC chamber in order to observe its beta-delayed charge particle emission. Both gas mixtures were at 1 Atm. The measured ^{39}Ti production yield of ~ 0.1 particle/h/pnA was more than 10 times lower than the LISE++ expectations. Data are under analysis but no clear evidence of direct two proton radioactivity was found in the first part of the experiment, thus constraining the possible branch to less than 0.5%. For the higher-density gas mixture, events with fully stopped beta-delayed two protons are being analysed in order to determine the mass of ^{39}Ti , an important input value for two-proton radioactivity models. In addition, hints of previously unknown beta-delayed alpha (see Fig. 3) and alpha-proton emission are under study.

Copyright

© University of Warsaw, GANIL



Figure 176: OPTC setup at the end of the LISE beam line.

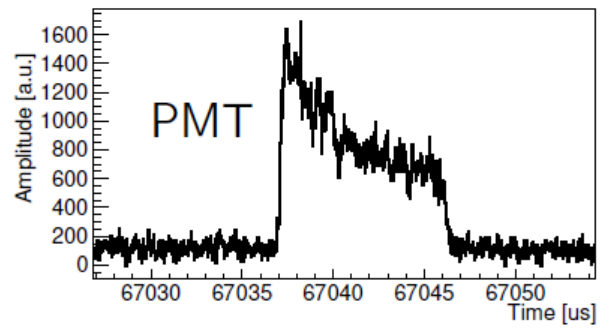
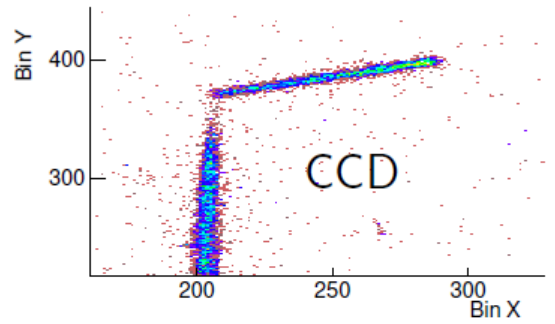


Figure 3: Observation of a possible beta-delayed alpha decay event.

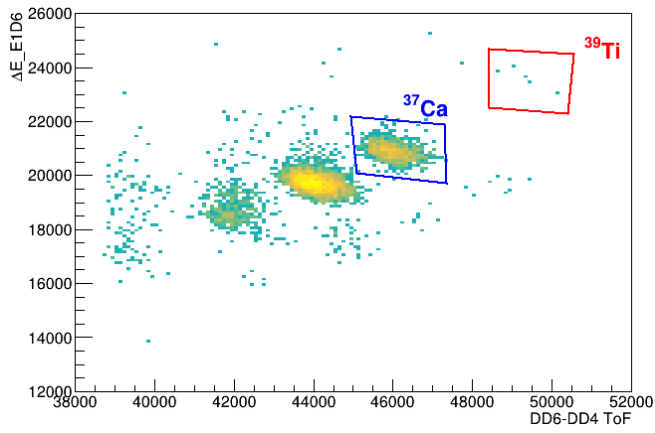


Figure2: ΔE -ToF selection of events triggering the OPTC DAQ

4. Study of ^{68}Ni by neutron adding and removing reactions

Experiment number: E843_21

Date: May 23 – June 3, 2023

Spokeperson and co-authors

S. Koyama^{1,2}, O. Sorlin¹, D. Mengoni^{3,4}, M. Assié⁵, O. Aktas¹, M. Balogh⁶, D. Beaumel⁵, Y. Blumenfeld⁵, S. Bottoni^{7,8}, D. Brugnara⁶, E. Clément¹, G. De Angelis⁶, G. de France¹, F. De Oliveira¹, Q. Delignac⁹, N. de Séréville⁵, L. Dienis¹, C.Aa. Diget¹⁰, B. Fernández-Domínguez¹¹, F. Galtarossa³, A. Goasduff⁶, A. Gottardo⁶, J. Ha^{3,4}, F. Hammache⁵, D.S. Harrouz⁵, O. Kamalou¹, A. Lemasson¹, A. Laird¹⁰, S.M. Lenzi^{3,4}, S. Leoni^{7,8}, M. Moukaddam¹², D. Napoli⁶, M. Niikura^{2,13}, J. Pellumaj^{6,14}, R.M. Pérez Vidal⁶, J. Piot¹, J.-C. Thomas¹

¹GANIL, CEA/DRF-CNRS/IN2P3, Boulevard Henri Becquerel, Caen, France

²RIKEN Nishina Center, Wako, Japan

³INFN Sezione di Padova, Padova, Italy

⁴Dipartimento di Fisica e Astronomia, Università di Padova, Padova, Italy

⁵Université Paris-Saclay, CNRS/IN2P3, IJCLab, Orsay, France

⁶INFN, Laboratori Nazionali di Legnaro (LNL), Legnaro, Italy

⁷Dipartimento di Fisica, Università degli Studi di Milano, Milano, Italy

⁸INFN Sezione di Milano, Milano, Italy

⁹University of Bordeaux, CNRS, LP2I Bordeaux, UMR 5797, Gradignan, France

¹⁰Department of Physics, University of York, York YO10 5DD, United Kingdom

¹¹IGFAE and Dpt. de Física de Partículas, University of Santiago de Compostela, Santiago de Compostela, Spain

¹²Institut Pluridisciplinaire Hubert Curien, 67037 Strasbourg, France

¹³Department of Physics, Faculty of Science, The University of Tokyo, Tokyo, Japan

¹⁴Dipartimento di Fisica e Scienze della Terra, Università degli Studi di Ferrara, Ferrara, Italy

Abstract

The shell structure of ^{68}Ni was investigated via neutron adding (d,p) and removal (p,d) reactions during the LISE2023 experimental campaign using the CATS+MUST2+EXOAM+ZDD setup (see E805 report). The measurement of the $d_{5/2}$ single particle state(s) in ^{69}Ni via (d,p) reactions with a slow-downed beam at 18 MeV/u will allow confirming its excitation energy and spin-parity, and to infer the size of the N=50 gap at ^{68}Ni . The complimentary measurement of neutron removing (p,d) and (d,t) reactions was also performed to investigate the neutron occupancies of ^{68}Ni . By combining the vacancy and occupancy of each neutron orbital in ^{68}Ni from the transfer reactions, the neutron Fermi surface at N=40 will be studied. These reactions should also enable to access the spin-orbit splitting of 2p 1f, and 1g orbitals in ^{68}Ni .

Experiment report

^{68}Ni was produced at ~38 and 18 MeV/u in the fragmentation of a ~40 pA ^{70}Zn stable beam at 62.5 MeV/u in a 560 μm thick Be target. The secondary beam setting was the same at the two energies up to D4 where the beam energy was 38 MeV/u after a 570 μm thick Be wedge. For the 18 MeV/u setting, an additional 530 μm thick Be slower was set at an angle of 25° after the F43 slits, and a transmission of about 60% was measured up to the D6 room. ^{68}Ni beams of up to $1.6 \cdot 10^5$ pps were used at the two energies to induce transfer reactions on CH_2 and CD_2 targets of 5 and 0.5 mg/cm², respectively.

For the $^{68}\text{Ni}(p,d)$ reaction, clear kinematics curves for the low-lying states in ^{67}Ni were observed online. The associated reconstructed excitation energy is shown in Fig.1 (a), compared with the data obtained with a 4 mg/cm² carbon target. Known gamma-rays at 694 and 1710 keV in the deexcitation of ^{67}Ni were observed in coincidence with EXOGAM (Fig.1 (b)), which absolute gamma-detection efficiency was of about 5% à 1.4 MeV. Fig. 2 shows a preliminary excitation energy spectrum obtained for ^{69}Ni in coincidence with the detection of protons in the MUST2 array.

Copyright

© GANIL

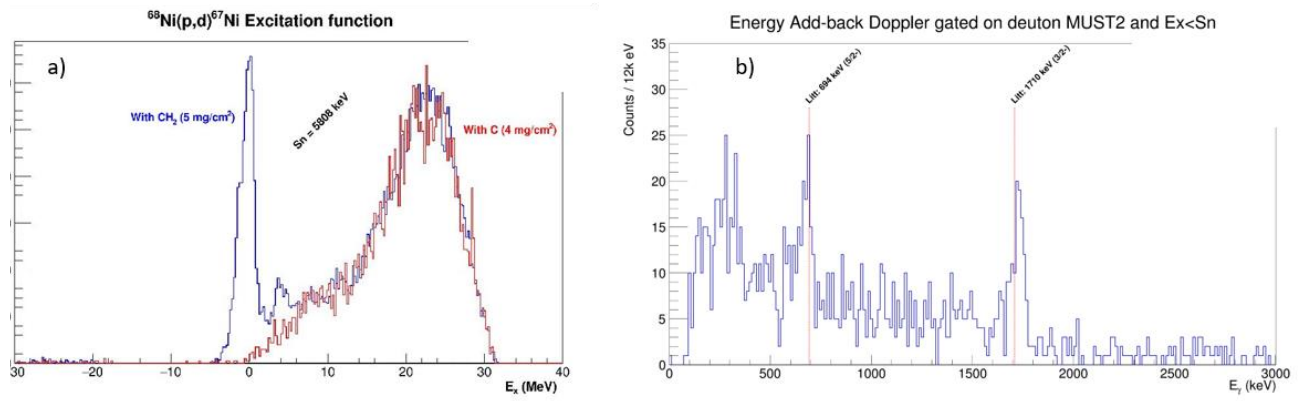


Figure 1: Excitation energy spectrum obtained in the $^{68}\text{Ni}(p,d)$ reaction (a), and coincident Doppler-corrected EXOGAM spectrum (b).

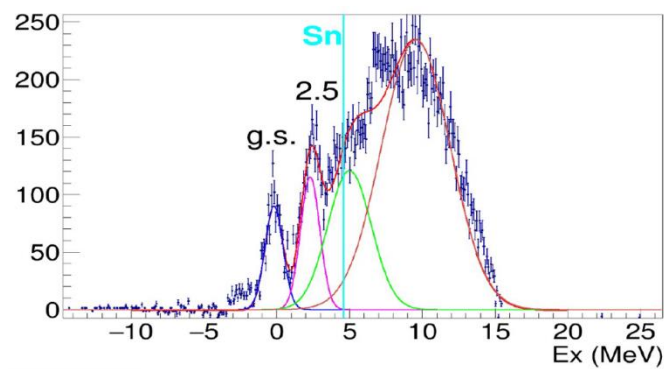


Figure 2: $^{69}\text{Ni}^*$ excitation energy spectrum obtained in the $^{68}\text{Ni}(d,p)$ reaction at 18 MeV/u.



IV. D1-HE

1. The immune system in Space – T-cell dysfunction mechanisms

Experiment number: P1211 and CORA

Date: July 10, 2023

Spokeperson and co-authors

Silvana Miranda^{1,2}, Randy Vermeesen¹, Ann Jansen¹, Emil Renhberg^{1,2}, Emre Etiloglu¹, Sarah Baatout^{1,2}, Kevin Tabury^{1,3}, and Bjorn Baselet^{1,*}

¹Radiobiology Unit, Nuclear Medical Applications Institute, Belgian Nuclear Research Centre SCK CEN, 2400 Mol, Belgium

²Department of Biotechnology, Faculty of Bioscience Engineering, Ghent University, 9000 Ghent, Belgium

³Department of Biomedical Engineering, College of Engineering and Computing, University of South Carolina, Columbia, SC, 29208, USA.

* Spokeperson

Abstract

The exposure to space stress factors such as cosmic radiation, altered gravity, and psychological stress leads to a disruption in various bodily systems. Dysfunction of the human immune system is caused by an alteration of the distribution of the cellular components and altered cytokine profiles, as well as cytoskeleton alterations and gene expression dysregulation. We irradiated CD4+ T-cells with iron ions, in combination with simulated altered gravity – microgravity, Mars gravity and Moon gravity – and stress hormone exposure. The effects of this exposure and possible causes were investigated with a transcriptomic, proteomic, flow cytometric and cytokine profiling approach. Our conclusion have the potential to enable the development and implementation of space-induced immune dysfunction countermeasures, with translational prospects for immune dysfunction pathologies which occur on earth.

Experiment report

CD4+ T cells were obtained from healthy individuals and subjected to Fe ion particle radiation (within European Space Agency Continuously Open Research Announcement for Investigating Biological and Physical Effects of space Radiation ESA CORA IBPER) GANIL, Photon irradiation, simulated microgravity, and hydrocortisone, either individually or in different combinations. Cytokine levels for Th1 and Th2 cells were determined using multiplex Luminex assays, and RNA sequencing was used to investigate gene expression patterns and identify essential genes and pathways impacted by these stressors.

Simulated microgravity exposure resulted in a Th1 to Th2 shift, evidenced on the level of cytokine secretion as well as altered gene expression. RNA sequencing analysis showed that several gene pathways were altered, particularly in response to Fe ions irradiation and simulated microgravity exposures. Individually, each space stressor caused differential gene expression, while the combination of stressors revealed complex interactions.

The research findings underscore the substantial influence of the space exposome on immune function, particularly in the regulation of T cell responses. Future work should focus expanding the limited knowledge in this field. Comprehending these modifications will be essential for devising effective strategies to safeguard the health of astronauts during extended space missions.

Results from this experiment was submitted as an original research manuscript to *Frontiers in Immunology* (04/06/2024)

Funding

Silvana Miranda is the recipient of an SCK CEN/UGent PhD grant. This work is supported by the ESA/BELSPO/Prodex IMPULSE-2 contract PEA4000140806. This project has received funding from the European Union's Horizon 2020 research and innovation program under grant agreement n°654002. Irradiations at GANIL were financed through the P1211-H IPAC and CORA Project.

2. Modulation of a tissue specific radiation-induced inflammatory response by high LET radiation

Experiment number: P1341-H

Date: July, 11 2023

Spokeperson and co-authors

I. Testard, S. Candéias, C. Rouichi, E. Chartier, A. Gattoni (CEA Grenoble, DRF / IRIG / DIESE / CBM)

Abstract

The physical properties of ionizing radiation (dose, dose rate, linear energy transfer) are important factors controlling the biological response of cells and tissues. In addition to DNA damage response (DDR) driven by the activation of the ATM kinase (p53 pathway), an inflammatory response is also induced by radiation. These NF κ -B-dependent immune signalling pathways can promote cell survival. Hence, the concurrent activation of p53 and NF κ -B in irradiated cells plays a key role in the determination of cell fate by regulating the balance between cell death or survival.

Since these responses can depend on radiation quality in model cancer cell lines, our proposal aimed at comparing the effects of high LET radiation and X-rays on the radiation-dose dependence, kinetics and tissue specificity of radio-induced inflammatory response in primary human endothelial cells and fibroblasts. Our recent unpublished results show that high dose X-rays exposure induces an early and transient NF κ -B-dependent inflammatory response in endothelial cells, with a kinetics and a radiation-dose dependence distinct than that of p53 activation after DDR initiation.

The preliminary results of one ^{12}C beam time experiment in July 2023 show that a similar inflammatory response, but at higher levels, is initiated in endothelial cells. In contrast, the modulation of the DDR pathway (DDB2 and p21 expression) is comparable in both low- and high-LET irradiations. In the next analysis steps, we plan to measure pro and inflammatory cytokines excreted in the irradiated cells medium taken up to 24 hours after exposure.

Experiment report

In July 2023, a first ^{12}C beam time (1 UT) was dedicated to our project. We exposed in D1 IRABAT normal human fibroblasts (HFPM) and endothelial cells (HUVEC) to native and/or degraded beam (95 and 26 MeV/u for HUVEC) to 4 different doses: 0, 2, 5 and 10 Gy. The corresponding LETs were 28 and 73 keV/ μm , respectively. Due to beam concerns, we were able to irradiate our HFPM cultures only with ^{12}C at one energy (26 MeV/u). Both cell types were irradiated in 25 cm 2 culture flasks. The cells and their conditioned culture media were harvested 6 h, 12 h and 24 h after irradiation. All doses and time points were realized in triplicates.

The cells were lysed for extraction of proteins and RNA to analyze the modulation of the expression of p53-dependent genes, involved in the DNA damage response (DDR) after ATM activation, and NF κ -B-dependent genes coding for inflammatory factors in the different exposure scenarios. The conditioned culture media harvested from control and irradiated cells were frozen (-20°C) and will be used later to compare the level of secreted cytokines (soluble inflammatory mediators) and their effects on non-irradiated bystander cells.

In parallel, we irradiated our two cell models (26 MeV/u only) in thin 96 wells plates (for microscopy) at the same doses and time points, in duplicate wells. They were used for in situ immunofluorescence analysis of p53 phosphorylation and NF κ -B nuclear translocation on the one hand, and RNA detection by ViewRNA $^{\text{®}}$ staining of p21 and MCP-1, two genes controlled by activated p53 and activated NF κ -B, respectively, on the other hand. In these analysis, p53 phosphorylation and p21 expression, signed the activation of the DDR pathway, whereas NF κ -B translocation and MCP-1 expression attest activation of inflammatory signaling pathways.

We performed the same analysis on the same cell cultures exposed to equivalent doses of X-rays in order to compare radio-induced responses at high and low LET at the cell level.

We compared the modulation of a set of genes induced during the DDR and inflammatory responses by RNA analysis (RT q-PCR) in HUVEC cells exposed at 26 MeV/u and X-rays. The results are showed in the figure below for MCP-1, as a typical NF κ -B target gene, and DDB2 and p21, as typical p53 target genes.

For both types of radiation, significant inductions were only observed at the higher 10 Gy dose. For low-LET X-rays, a peak in the expression of genes coding for inflammatory factors, such as the MCP-1 gene shown in A, is reached 3 to 6 hours after the irradiation at 10 Gy and the level returns to baseline 24 h after exposure (Figure below). The exposure to carbon ions results in a stronger induction of MCP1-expression measured 6 and 12 hours after exposure and, again, the expression returns to baseline after 24h. The same trend is observed for the lower doses (2 and 5 Gy) but no statistical significance is reached.

We next quantified the expression of genes involved in the DDR response. While we observed no significant difference in DDB2 induction with radiation quality, the expression of p21, coding for a protein involved in cell cycle regulation is induced with a more transient pattern in response to ^{12}C ions than to X-rays.

For the in situ approach, the analysis of the images acquired on a CX-7® High Content Analyzer shows no clear modulation of the inflammatory responses as assessed by the nuclear translocation of the NF κ -B protein, whatever the radiation type. In the same samples, the DDR activation, assessed by p53 phosphorylation, is greater and persists over time in HUVEC cells exposed at all doses of high LET compared to X-rays radiations, indicating that there is less repair of DNA lesions in response to C-ions. We measured similar initial levels and disappearance kinetics of p53 phosphorylation in HFPM irradiated in the same conditions. The assessment of in situ mRNA expressions (p21 for DDR and MCP-1 for inflammation) is still ongoing. We acquired 150-300 cells per duplicate wells on the CX7® but image analysis needs further developments to allow accurate quantification and conclusions.

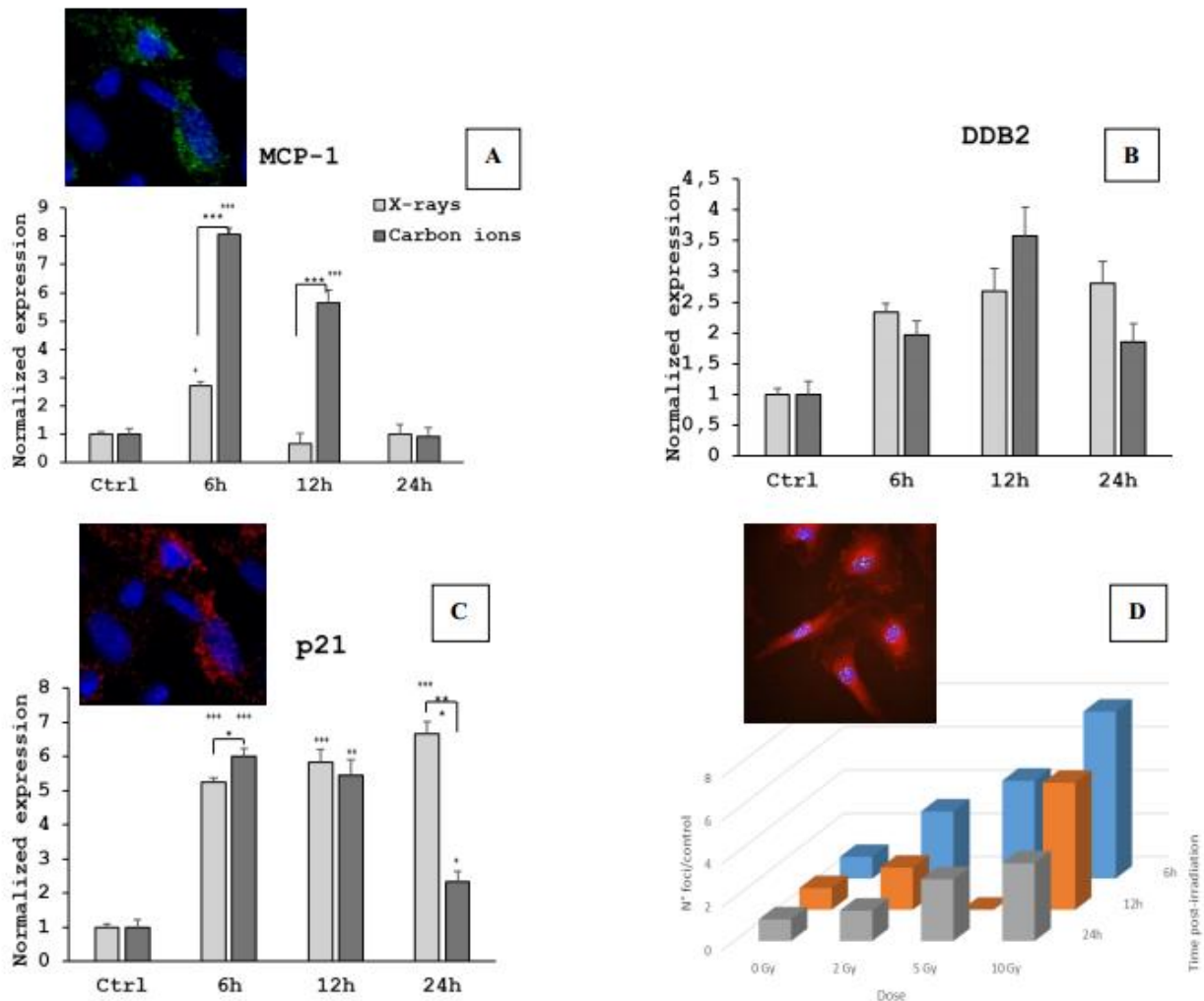
Inflammatory response is induced at a higher level and with a longer time course in endothelial cells exposed at high-LET carbon ions (26 MeV/u, 73 keV/ μm). The analysis of the pro- and anti-inflammatory cytokines in the cell culture medium taken 6 to 24 hours after exposure, would bring more information of downstream effectors of this response. At present, we have not initiated this part of the study.

The mRNA analysis (RT q-PCR) is currently ongoing for HFPM irradiated with ^{12}C at 26 MeV/u, and also for HUVEC at 95 MeV/u.

These first results show differences in the radioinduced responses initiated after the exposure of our cell models to different radiation type. A transient and strong inflammation activation is induced early after high LET exposure, whereas the DDR is activated later but lasts longer after X-rays. Thus, kinetics and radiation dose dependence confirm the measurements done after proton irradiation (unpublished results). However, the in situ approach applied here in addition to PCR analysis, does not totally confirm these trends. These experiments need to be repeated and comparisons established for the different LETs and cell types for significant conclusions.

As a result, an inflammatory state can be induced in normal healthy cells irradiated by accident or because of their vicinity of a treated tumor zone. The resulting pro- or anti-inflammatory processes can contribute to the orientation of the fate of these cells to a conservative or deleterious outcome. To better understand the involvement and interaction of both DNA damage and inflammatory responses, in our proposal, we want to use specific inhibitors of each pathways. To this aim, a second beam time in April 2024 allowed us to repeat the experiment at the higher LET (73 keV/ μm) with the use in our cell cultures of Ku 55933 a specific inhibitor the DDR via inactivation of the ATM kinase. In parallel, comparative experiments were performed with our X-rays generator for irradiation at low-LET of our cell culture models treated with Ku 55933 or with Bay 11-7082 for inhibition of the inflammatory pathway via NF κ -B inhibitor.

Legend



Modulation of stress and inflammatory signaling pathways in irradiated human umbilical vein endothelial cells (HUVEC). The expression of inflammatory (A) and DDR (B,C) genes was analyzed by RT-qPCR 6 to 24 hours after X-rays or carbon ions (26 MeV/u) 10 Gy irradiation. For each gene, the level of expression in control and exposed cells, and between irradiation modalities, were compared by an ANOVA test (n=3). When a value of $p < 0.05$ indicated significant differences in irradiated cells (vs Control: ‡ : p-value < 0,05, ‡‡ : p-value < 0,01, ‡‡‡ : p-value < 0,001), pairwise comparisons were performed with a Tukey's test (* : p-value < 0,05, ** : p-value < 0,01, *** : p-value < 0,001). Above MCP-1 and p21 graphs, a view of the in situ mRNA staining (green spots for MCP-1, red spots for p21, nucleus in blue).

The phosphorylation of p53 (green foci staining) and nuclear translocation of NFκ-B (red staining) was measured in HUVECs nucleus (blue staining) after in situ immunofluorescence detection (D). HUVECs were irradiated with 12C (26 MeV/u) at 0, 2, 5 and 10 Gy and fixed for analysis 6, 12 and 24h after the exposure (no data for 5 Gy, 12h). Histograms represent the mean number of phospho-p53 foci per nucleus, normalized to control non-irradiated cells, n=200-600. An ANOVA test showed that the data were not normally distributed then by a Kruskal-Wallis test, was applied for pairwise comparisons. All data are significantly different (**** : p-value < 0.0001).



V. D1-SME

1. Radiolysis of polymers: LET and temperature effects

Experiment number: P1343-M

Date: June 09-10, 2023

Spokeperson and co-authors (affiliation)

Stéphane Esnouf (CEA DES/ISAS/DRMP/SPC/LC2R)

Muriel Ferry (CEA DES/ISAS/DRMP/SPC/LC2R)

Solène Legand (CEA DES/ISAS/DRMP/SPC/LC2R)

Yvette Ngono (CEA DRF/IRAMIS/CIMAP)

Vincent Pacary (CEA DRF/IRAMIS/CIMAP)

Abstract

The present proposal is a contribution to the understanding of the influence of temperature and Linear Energy Transfer (LET) on mechanisms of hydrogen release from polymers under irradiation.

Different kind of polymers (polyethylene, polyurethane, polyvinyl chloride, cellulose and polystyrene) were ion (9.04 MeV/u ^{22}Ne) irradiated under various temperatures, from room temperature to 150°C, under inert or oxidative conditions. Gas release was measured in-situ using micro-gas chromatography. The results of this study provide data essential to elaborate of a relevant model predicting the gas release in nuclear waste for safety purpose.

Experiment report (Between 1000 and 1500 words)

Polymers are components of nuclear waste in intermediate level waste packages. In these packages, these materials are in contact with actinides and degradation upon alpha irradiation induces inflammable and corrosive gas release. The accumulation of these gases can affect the integrity of the waste container. For safety purpose, it is thus necessary to predict the quantity of gases released by the different organic materials.

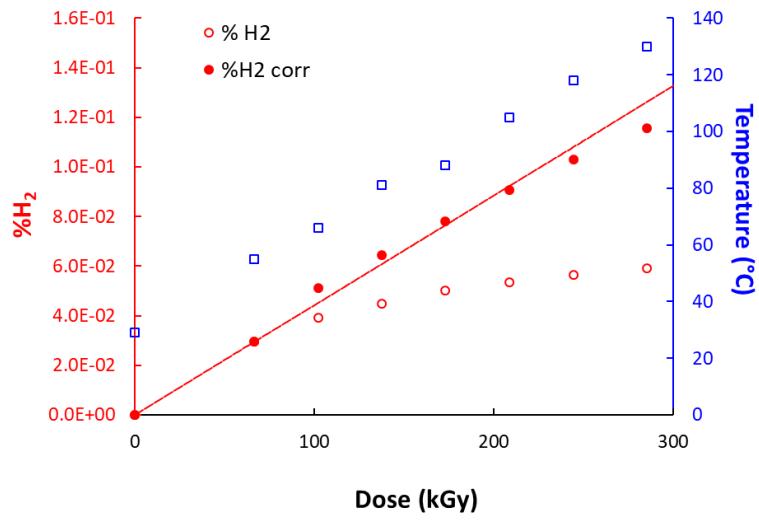
For the most common polymers, the influence of dose rate, dose, atmosphere and LET (Linear Energy Transfer) has been addressed. However, few studies have focused on the effect of temperature. This parameter is essentially relevant to transportation. The temperature inside nuclear waste packaging is supposed to be above room temperature (generally close to 50°C) and can increase up to 150°C during a short time in case of accidental conditions.

This work is dedicated to the influence of temperature on the radiolysis of polymers at high LET irradiation. The polymers of interest for this study are: polyethylene, aromatic polyester-urethane, polyvinyl chloride, cellulose and polystyrene. The impact of atmosphere (inert or oxidizing) was also evaluated.

The polymer samples were irradiated in a small chamber (CHIMERE2) designed by the CIMAP and the LC2R. A remotely controlled valve system enable gas sampling after or during irradiation and flushing the chamber. Gases were collected and analysed by μ -GC gas chromatography.

In addition to isothermal experiments, dynamical measurements were also performed. For this type of acquisition, the sample is heated at a rate of 2°C per minute from room temperature to 150°C and periodically the atmosphere is analysed. An increase of gas concentration is thus recorded as a function of the time or dose. After correction for successive sampling, the data are plotted as a function of the dose. If temperature accelerates gas release, the dose–response curve takes the form of a supralinear curve and an energy activation can be determined.

Our results show that temperature effect for ion irradiation is reduced compared to gamma irradiation (Furtak-Wrona K, Cornaton M, Durand D, Dauvois V, Roujou JL, Esnouf S, Ferry M, Temperature and LET effects on radiation-induced modifications in non-perfect polyethylenes, Polymer Degradation and Stability 162 (2019) 66-75). For example, hydrogen release upon ion irradiation of polyethylene is almost independent of temperature (energy activation equals to 0 kJ/mol) (see Figure below).



Legend

Evolution of hydrogen concentration and temperature as a function of the ion irradiation dose.

2. Ion radiation chemistry in poly allyl diglycol carbonate: assessing the influence of radical migration in the defect creation mechanisms

Experiment number: P1354

Date: June 4- 9, 2023

Spokeperson and co-authors

Spokesperson:

Tamon KUSUMOTO (National Institutes for Quantum Science and Technology (QST), Japan)

Deputy Spokesperson: Remi BARILLON (IPHC)

Co-authors:

Yvette NGONO-RAVACHE (CIMAP-GANIL)

Satoshi Kodaira (QST)

Quentin RAFFY (IPHC)

Tomoya YAMAUCHI (Kobe University)

Masato KANASAKI (Kobe University)

Shunto SADAMITSU, (Kobe University)

Daisuke KOHINATA (Kobe University)

Abstract

The aim of our study is to unveil chemical reactions of poly allyl diglycol carbonate (PADC) irradiated with heavy ions. To do so, PADC samples are exposed to 10 MeV/u Ne ions at 16 K under vacuum up to 2.0×10^{12} ions/cm², with a fluence increment of 2.0×10^{11} ions/cm², for minimizing the influence of the radical mobility. Then, PADC samples are annealed up to room temperature (RT) with an increment of 30 K. We have acquired IR spectra at each fluence and temperature step. In 2023, we focus on the absorbance around 3500 cm⁻¹, which is assigned to OH groups that form by radio-oxidation after the irradiation. Any changes in the absorbance are not seen during the irradiation. In comparison, the absorbance starts increasing above 200 K. This finding implies that the radical mobility plays important roles to decorate newly created ending groups after the irradiation.

Experiment report

Introduction

Poly allyl diglycol carbonate (PADC) is a well-known Polymeric Nuclear Track Detector (PNTD). This material has been used in various branches, e.g., space radiation dosimetry, laser driven ion acceleration experiments and dosimetry for the targeted radiation cancer therapy. The application field is spreading out, but there are unsolved issues concerning the creation mechanism of latent tracks formed in PADC. The chemical structure of PADC is modified under ionizing radiations through the fragmentation of typical functional groups in PADC (ether, carbonate ester and CH groups). Damages to these moieties lead to release CO₂ molecules and alkene molecules and to form OH groups. This phenomenon was seen in the previous study, but their formation mechanisms were largely unknown. In the present study, we investigate defects creation of PADC under vacuum to get rid of the oxidation process and to focus solely on effects of swift heavy ions that is the creation of latent tracks. The aim of the present work is to elucidate roles of molecular and radical mobility in the creation of these defects under ion irradiations.

A brief history of our project

Thanks to a strong international collaboration between Japan and France, our team has conducted a series of FT-IR spectrometric studies to investigate structure and generation mechanism of latent tracks in PADC irradiated with protons and heavy ions. Especially, the influence of radical-mobility and radical migration should be clarified to unveil the creation mechanism of latent tracks in PADC. In 2018, we performed 11 MeV/u C ion irradiations at 11, 100, 200 K and RT. The radiation chemical yield (G value) of carbonate ester lost in PADC at 11 K is lower than that of RT. The G values of 100 K and 200 K are in between. The G value of CO₂ molecules generated is smaller than that of carbonate ester lost. It is known that CO₂ molecules are formed by the decomposition of the

carbonate ester bond. This smaller G value of CO₂ molecules generated could be related to radical mobilities in PADC. Furthermore, no creation of OH groups is observed at the low temperatures. This finding would suggest that oxygen and radical mobility are necessary to form OH groups as new ending groups. We summarized results obtained in 2018 as a paper in Polymer Degradation Stability (Kusumoto et al., Polym. Degrad. Stab. 164 (2019) 102-108).

In 2019, we had beam time, but new data were not acquired due to the limitation of the beam time because of hit of the heat wave. From 2020 to 2022, we faced COVID diffusion, thereby it was not possible to travel GANIL from Japan for the beam time. Thus, we have no new experimental data during this period. We had difficult time for these 4 years, despite all that, our project re-started from 2023.

Experiments of 2023 beam time

We prepared PADC films with 15 μm thick by chemical etching with KOH solution. This PADC film was made from BARYOTRAK, which is obtained from a monomer with a purity higher than 99%. The prepared film was too thick to quantitatively evaluate damages to carbonate ester, which has the strongest IR absorption in PADC, but was appropriate to have a look the evolution of OH groups around 3500 cm⁻¹.

PADC samples were irradiated with 10 MeV/u Ne ions under vacuum at 16 K in the SME beamline. The fluence was up to 2.0×10^{12} ions/cm². IR spectra were acquired using CASIMIR set-up, which equipped an in-situ FT-IR spectrometer, at each fluence increment of 2.0×10^{11} ions/cm². After the irradiation, PADC samples were annealed up to RT with an increment of 30 K. We reduced temperature from each annealed temperatures to 16 K to minimize the influence of changes in the molar extinction coefficient with temperature. In the present study, we focused on the ether and CH groups lost and creation of OH groups.

Results of 2023 beam time

Damages to ether and CH groups and formation of OH groups during irradiation

The absorbance assigned to ether decreased linearly up to 7.0×10^{12} ions/cm². Then, the linearity was broken. This trend would suggest the track overlapping in a high-fluence region. In comparison to this, the absorbance assigned to CH groups decreased linearly in the examined fluence region and the trend is gentle compared to the ether. Thus, the ether is more radiation-sensitive moiety than CH groups. Seeing the absorbance of OH groups around 3500 cm⁻¹, the absorbance increased drastically above 7.0×10^{12} ions/cm², above which track overlapping became significant. It has been considered that OH groups were formed by the radio-oxidation. Therefore, oxygen molecules and “a certain level” of radical mobility would be necessary. However, the present study was performed under vacuum at 16 K, at which very low oxygen concentration and low radical mobilities were expected, thereby it would be hard to consider OH groups were formed by radio-oxidation. The other interpretation to form OH groups was reactions between oxygen radicals created by radiation damage to carbonate ester or ether moieties and hydrogen atoms released from CH groups. Below 7.0×10^{12} ions/cm², each latent track had enough distance. When the track overlapping becomes significant, the distance between some tracks became close. In that case, it could be possible that oxygen radicals sometimes reacted with hydrogen atoms, when they were in close locations due to the track overlapping. Thus, not only radical mobilities but also latent track structure was also an important factor to form OH groups as new ending groups.

Roles of radical and molecular mobility

The absorbance of OH groups was firstly constant up to 180 K. Above 180 K, the absorbance began increasing monotonically. This finding demonstrated that “a certain level” of radical mobility was mandatory to form OH groups, which were formed reactions between oxygen radicals and hydrogen atoms. We also confirmed the increase of CO₂ molecules with increasing annealed temperature. The absorbance assigned to CO₂ molecules increased monotonically with increasing the temperature. To quantitatively discuss the relation of intermediate species and yields for typical functional groups lost with yields of CO₂ molecules, additional experiments using thinner PADC film (< 3 μm) are crucial. This is because we can obtain unsaturated IR spectra for any functional groups in PADC when the thinner PADC films are used for experiments. However, unfortunately, we did not have enough beam time in 2023 due to the accelerator trouble. However, in the 2024 beam time (July 13th to 17th), we have successfully conducted experiments to give answers to the relation between yields of CO₂ molecules and typical functional groups lost in PADC. We are now carefully analyzing obtained spectra.

3. Determination of absolute singly and doubly cross-section of emitted electrons from biomolecules upon carbon ion collision

Experiment number: P1230

Date: April 22-24, 2023

Spokeperson and co-authors

Violaine VIZCAINO (CIMAP)

Suvasis SWAIN (CIMAP)

Alain MERY (CIMAP)

Jean-Yves CHESNEL (CIMAP)

Abstract

We measured ion-induced electron emission from DNA base Adenine and RNA base uracil using a newly developed experimental set-up based on velocity map imaging (VMI) technique. This technique allows measuring, at once, all electrons emitted in a solid angle of 4π steradians with energy as low as a few tenths of eV up to 200eV. By monitoring the target density, projectile ion beam intensity and the beams overlap with the use of a quartz crystal micro balance and an ion beam profiler, we were able to estimate absolute singly- and doubly-differential cross sections for electron emission. We measured these absolute cross sections for collision with carbon ion beam with energy from 0.95 MeV/u (IRRSUD beamline) to 13.7 MeV/u (SME beamline)

Experiment report

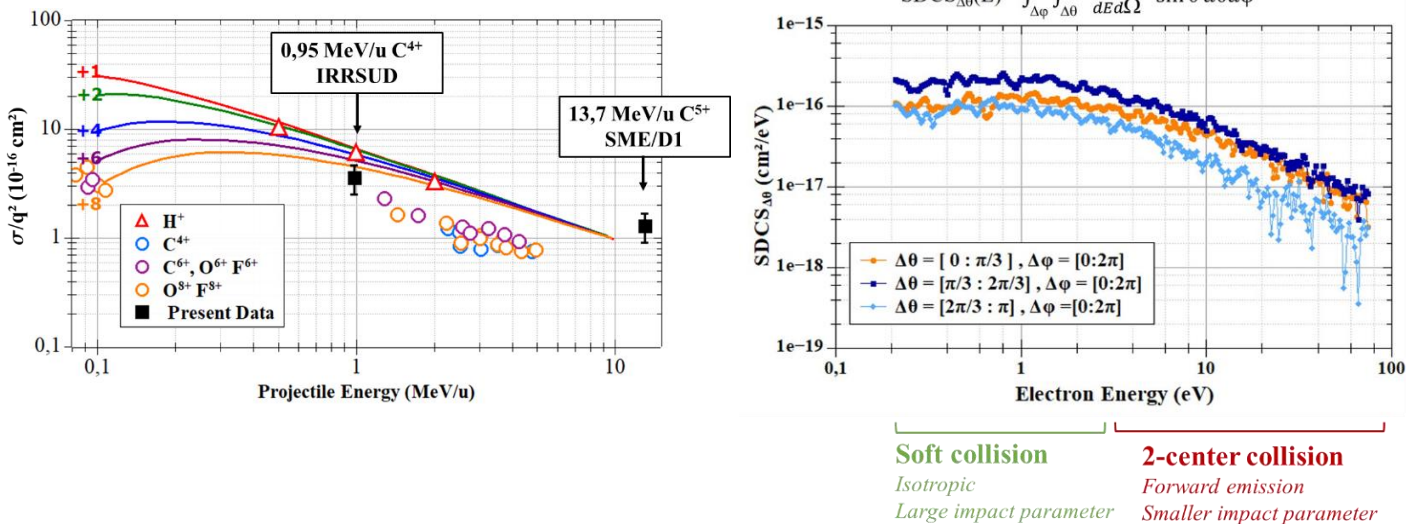
Electron emission following ion collisions with atoms or molecules has been studied for several decades. Electron emission from the target, projectile or both, electron transfer or electron interference have been the subject of numerous experimental and theoretical studies. Measuring the electron yield as a function of energy allows a better understanding of the main ionization mechanisms, from soft collisions producing low energy electrons to binary collisions or inner-shell ionization producing well defined peaks at high energy. In more recent years, ion collision with biologically relevant molecules has received increasing interest due to applications to radiation biology. Indeed, the use of ion beams (protons or carbon ions) is increasingly employed in medicine for the treatment of cancer. Ion beam therapy, unlike conventional radiotherapy, allows a better localization of the energy deposition in the tissue due to the intrinsic properties of ion propagation through matter. Studies of the collision between multiply charged ions and molecules in the gas phase help understanding the fundamental mechanisms involved at the molecular level (fragmentation, electron emission). With this experiment, we contributed to this general endeavour by measuring absolute cross section from DNA/RNA. With our new set-up based on the velocity map imaging technique, we were able to measure electrons with low energy and all emission angle (including forward and backward emission) unlike conventional technique using electrostatic analyser.

The projectile ion beam from either IRRSUD or SME beamlines is shaped by a series of slits before entering the collision chamber. Its intensity and position are monitored by a Faraday cup and an ion beam profiler, respectively, located after the collision chamber. The target beam is produced with a two-stage effusion cell and shaped by two consecutive skimmers before entering the collision chamber where it crosses orthogonally the projectile ion beam. A pneumatic push-pull shutter is placed between the two skimmers to block the target beam in order to measure the background (i.e. electrons from the residual gas) which is subtracted latter on. After crossing the collision chamber, a quartz crystal microbalance allows monitoring the mass flux of the target beam and thus obtaining the beam density. The electrons created in the collision region are extracted by a homemade multi-electrode VMI spectrometer and detected by a position sensitive detector constituted of two microchannel plates (MCPs) and a phosphor screen. The images are recorded with a camera: they represent the 2D projection of the electron cloud produced by the ionization of the target. Therefore, by applying an inverse Abel transform we can reconstruct the velocity distribution (kinetic energy and emission angle) of the emitted electrons. Absolute cross sections σ (expressed in cm^2 in the following) can be determined by normalizing the count rate of detected electrons N_e (electrons.s⁻¹) by the detector efficiency ε , the count rate of projectile ions N_p (ions.s⁻¹), the density of the target beam ρ (molecules.cm⁻³) and the length of the interaction region l (cm): $\sigma = N_e / (\varepsilon N_p \rho l)$. In order to study the kinetic energy (E) dependence and/or angular (Ω) dependence of electron emission, differential cross sections $d\sigma/dE$, $d\sigma/d\Omega$ or $d^2\sigma/dEd\Omega$ can be determined after analysis of the inverse Abel transform of the detector

image. The inverse Abel transform numerically reconstructs a cylindrically symmetric 3D object (emitted electrons) from its 2D projection on a plane (detector) parallel the axis of symmetry (projectile ion beam). Electron emission has indeed a cylindrical symmetry along the projectile beam, which means that it does not depend on the azimuthal angle φ . The angular dependence of the cross section is usually expressed as a function of θ , the polar angle defined with respect to the projectile ion beam.

Integral cross sections have been determined by integrating the single differential cross sections ($d\sigma/dE$ or $SDCS(E)$) between 0.2 eV and 100 eV for both Uracil and Adenine upon collision with both 0.95 MeV/u C^{4+} and 13.7 MeV/u C^{5+} . In the figure below (left panel), we compare our values (normalized by q^2 , q being the projectile charge state) for Uracil to both experimental and theoretical cross sections from the literature. As expected, the determined cross section is lower for 13.7 MeV/u C^{5+} than for 0.95 MeV/u C^{4+} . Indeed, as the projectile ion velocity increases, the interaction time between the target electron and the projectile ion and therefore the ionization cross section decreases as well. However the values measured seems to be a bit higher than the theoretical model or experimental results while the previous measurement on IRRSUD beamline with 0.95 MeV/u C^{4+} had reasonably good agreement with the literature. The same trend is also found for Adenine. For adenine we also have measured the cross section for 13.7 MeV/u C^{6+} using the stripper from SME beamline and confirm the q^2 dependence of the cross section.

To study the angular dependence of the electron emission, one can plot the absolute doubly differential cross sections $DDCS(E, \theta)$ i.e. $d^2\sigma/dEd\Omega(E, \theta)$ that can be deduced directly from the inverse Abel transform of the detector images. However, due to the poor statistics, we rather plot here the absolute $SDCS(E)$ integrated on a specific angular range $\Delta\theta$, noted $SDCS_{\Delta\theta}(E)$. In the figure below (right panel), the $SDCS_{\Delta\theta}(E)$ are determined for three angular ranges $\Delta\theta$ to highlight the forward emission $[0 : \pi/3]$, backward emission $[2\pi/3 : \pi]$ and orthogonal emission $[\pi/3 : 2\pi/3]$. In the figure, we can see that below 1 eV, the forward and backward emission are roughly of the same magnitude. Between 1 eV and 10 eV, we observe a break of the forward/backward symmetry as the forward emission increases to reach the orthogonal emission magnitude above 10 eV. This increase of forward emission is characteristic of two-center electron emission where ejected electrons are attracted by the outgoing projectile ions. At higher projectile energy (not shown here) the electron emission presents a similar angular distribution.



Legend

Absolute cross section for electron emission from Uracil in cm^2 determined for both 0.95 MeV/u C^{4+} and 13 MeV/u C^{5+} are compared with theoretical models as well as other experimental data (left panel). Single differential cross section $SDCS_{\Delta\theta}(E)$ in cm^2/eV for electron emission from uracil upon 0.95-MeV/u C^{4+} collision determined for three different angular ranges (right panel).

4. Flexible piezoelectric SHI-nanostructured composite generators undergoing large bulging deformation regime

Experiment number: P1358

Date: May 11-12, 2023

Spokeperson and co-authors

Marie Sigallon¹, E. Sarrey¹, A.-L. Hamon,² Adrien Baillard³, Vincent Consonni³, Florian Aubrit¹, Natalya Potrzebowska¹, Romain Grasset¹, Mohamed Tabellout³, Jean-Eric Wegrowe¹, Marie-Claude Clochard^{1*}

1. Laboratoire des Solides Irradiés, CEA/DRF/IRAMIS, Ecole Polytechnique, CNWS, Institut Polytechnique de Paris, F-91128 Palaiseau
2. Laboratoire de Mécanique Paris-Saclay, Université Paris-Saclay, CentraleSupElec, ENS Paris-Saclay, CNRS, F-91190, Gif-sur-Yvette, France
3. Laboratoire des Matériaux et du Génie Physique, Grenoble INP - CNWS, Minatec, 3, parvis Louis Néel, F-38016 Grenoble
4. IMMM, UMR CNWS 6283. Université du Maine - UFR Sciences et Techniques Avenue Olivier Messiaen 72085 Le Mans Cedex 9

*spokeperson

Abstract

There is a huge difference between piezoelectric polymer films and solid crystals for the application to piezoelectric generators. In the case of polymers, the optimal piezoelectric response imposes the large deformation regime. Starting from the linear Curie's constitutive equations, we have developed an analytical model under the assumption of the large bending and elongation regime. Such a regime resulted herein from bulge testing configuration that our newly mounted experimental set-up allows. This model showed a specific non-linear piezoelectric response, that followed a power 2/3 of the mechanical excitation:

$$|\hat{V}| = \mathcal{A}(\ell) \left| \mathcal{F}_t \left[\delta p^{\frac{2}{3}}(t) \right] (\omega) \right| \frac{\omega R}{\sqrt{1 + (\omega RC)^2}}$$

$$\text{with } \mathcal{A}(\ell) := A_p e_{31} \left(\frac{A_p}{\pi \ell^2} \right)^{\frac{1}{3}} \left(3 \frac{1 - \nu}{7 - \nu} \frac{1}{Y} \right)^{\frac{2}{3}}$$

in where ω is the angular frequency, R the load resistance, C the capacitance, δp the overpressure, A_p pressurized area, t time, ℓ the piezopolymer or composite thickness, e_{31} the piezoelectric constant, ν the Poisson's coefficient, Y the young modulus. The experimental results carried out on piezoelectric pure PVDF films and SHI-nanostructured Ni NWs/PVDF composites validated the model.

To test the validity domain of such a model, peculiar SHI-nanostructured PVDF-based ZnO composites was also successfully synthesized and tested under the bulge deformation applied by this new experimental set-up. The beneficial effect of hydrothermal process on the morphology and piezoelectric performance of zinc oxide/polyvinylidene fluoride (ZnO-PVDF) composite thin membranes (10 μ m thick) was demonstrated. Vertically aligned ZnO nanowires were epitaxially grown inside the cylindrical nanoporosity of an ion-track-etched polarized PVDF to form flexible ZnO-PVDF composite piezomembranes. Swift-Heavy Ions (SHI) were firstly used to irradiate polarized PVDF thin films. A subsequent chemical etching in alkaline media created dense and statistical arrays of cylindrical nanopores (10⁹ cm⁻²). These nanoporous piezoelectric PVDF membranes, before and after hydrothermal reaction, were characterized by scanning electron microscopy (SEM, TEM), atomic force microscopy (AFM), reflectance spectroscopy and dielectric measurements. Results demonstrated that under mild hydrothermal reaction conditions, produced ZnO nanowires exhibited an ideal microstructure for piezoelectric performances, *i.e.* hexagonal wurtzite structure. Such a structure plays an important role in the resulted piezoelectric capacity of ZnO-PVDF composite membranes. From piezoelectric analysis in bulging mode, the output power was plotted against 8 load resistances ranging from 10⁵ to 10⁷ Ω , exhibiting a maximum at 2.10⁶ Ω . It was found that the maximum of the output power can also be modelled using our analytical model and found to be 28% higher in presence of these embedded ZnO nanowires of high aspect-ratio in low mechanical excitation frequency region ranging from 4 to 26 Hz. It thus demonstrates a very promising potential in the renewable energy application of electromechanical energy conversion.

Experiment report

Beam-line	IRASME
Ion	${}_{86}\text{Kr}^{28+}$
Flux max	10^6 ions/($\text{cm}^2 \cdot \text{s}$)
Fluences	$10^7 - 10^8 - 10^9 - 10^{10}$ ions. cm^{-2}
Atmosphere	He [A 'tromblon' is needed to change the atmosphere of the irradiation chamber]
Holder	Classical aluminium plates
Surface	4x30= 120 cm^2 per plate
Number of polymer bands stacking max per plate	3 for 10 μm thick films, 1 for films > 10 μm (herein 28 to 100 μm)
Number of irradiation runs	22
Total of irradiated polymer bands	12x3+1x2+9x1=47 bands

IRASME line at GANIL is necessary to get sufficient energy to cross the entire thickness of piezoPVDF films (10 and 28 μm) without any difference in the deposited energy on both side. Superimposed polymer bands of 4x30 cmxcm are stuck on the sample holder for each irradiation run. No modification of existing holders was done. He atmosphere helped in limiting temperature increase during irradiation to avoid any depolarization of piezoelectric polymers.

For evaluation of piezoelectric performances, we have recently developed a dedicated experimental set-up at LSI (Fig. below). Its specificity is to apply cyclically a quasi-perfect sinusoidal deformation to the part of piezoPVDF membrane exposed to the strain. The tested polymer or composite films are clamped inside the circular chamber which provokes a bulge deformation under air overpressure.

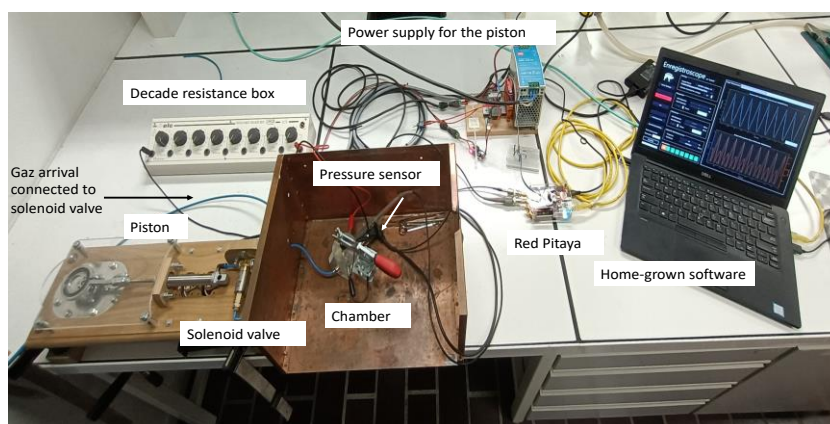
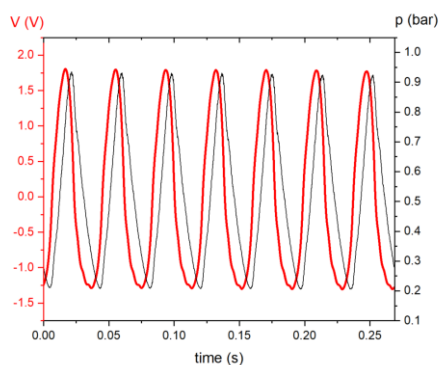
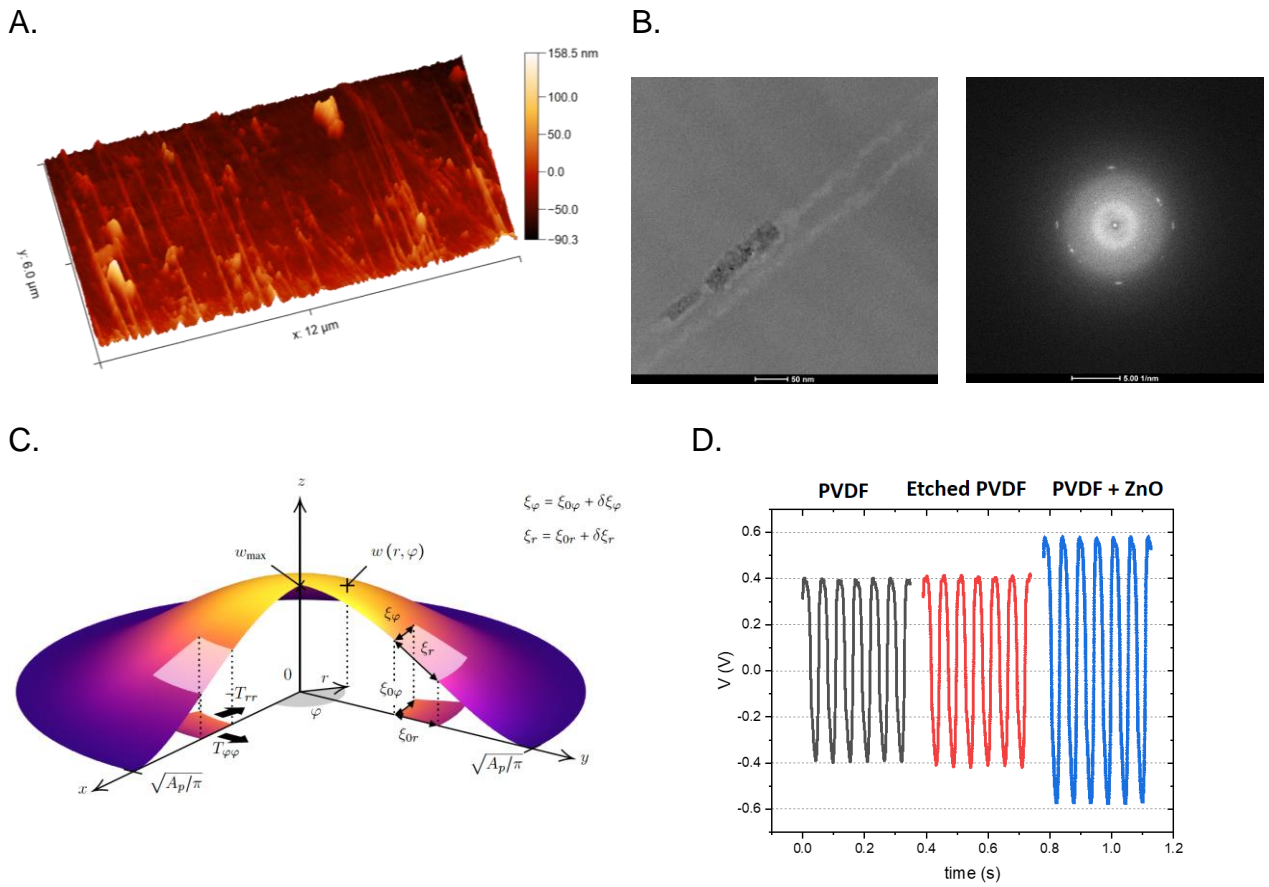


Photo of experimental set-up for piezoelectric study of PVDF-based piezomaterials in shape of thin films



Typical output voltage and pressure signal profiles obtained for a 10 μm -thick piezoPVDF film.

Figure



Legend

SHI-nanostructured ZnO NWs/piezoPVDF composite membranes synthesized by hydrothermal bath processing – A. 3D AFM image of a cross-section showing a completely-filled ion-track etched PVDF membrane with ZnO NWs; B. TEM image and its figure of diffraction of a piece of ZnO in an etched piezoPVDF track ; C. Scheme displaying the bulge testing configuration of our experimental set-up at LSI to measure piezoelectric response of flexible piezomaterials and the transformation of a circular membrane of radius $\sqrt{A_p/\pi}$ due to an overpressure δp inside the chamber. Cylindrical coordinates (r, φ, z) are used. w stands for the z-component of the displacement field for any point of polar coordinates (r, φ) , and w_{\max} its maximum value reached at the center $r = 0$; D. Output voltage time traces of the piezoelectric responses of piezoPVDF, track-etched piezoPVDF and nanostructured piezoPVDF with ZnO NWs.

A photograph of industrial machinery, possibly a robotic arm or a complex assembly line, with a teal overlay. The machinery is metallic and features various pipes, valves, and mechanical components. The teal overlay is a large, semi-transparent shape that covers the top and right portions of the image, creating a modern, technical aesthetic. The text 'VI. IRRSUD' is positioned to the right of the machinery, partially overlapping the teal overlay.

VI. IRRSUD

1. Chemical evolution of PAH astrophysical ices induced by heavy ion irradiations

Experiment number: P1319

Date: April 2023

Spokeperson and co-authors

Spokesperson: de Barros, Ana Lucia Ferreira (CEFET-RJ, Rio de Janeiro, Brazil)

Boduch, Philippe (CIMAP, UNICAEN)

Bychkova, Anna (CIMAP, UNICAEN)

Da SILVEIRA, Enio (Van de Graaff Lab, Physics Department, Rio de Janeiro, Brazil)

Domaracka, Alicja (CIMAP, CNRS)

Pires da Costa, Cintia (CIMAP, ENSICAEN)

Rothard, Hermann (CIMAP, CNRS)

Ricca, Alessandra (Carl Sagan Center, SETI Institute & NASA Ames Research Center)

Abstract

Samples of α -pinene ice were irradiated at 10 K by 61.3 MeV $^{84}\text{Kr}^{15+}$ ions to simulate the effects of heavy ion cosmic ray bombardment on chiral molecules in the interstellar medium. Their chemical evolution was monitored by mid-infrared Fourier transform (FTIR) spectroscopy to follow the reaction products and to determine the extent of racemization. This successful pinene irradiation experiment was started in 2022 with a Kr beam and pursued with a Fe beam in 2023.

Experiment report

Radiolysis of α -pinene by 61.3 MeV $^{84}\text{Kr}^{15+}$ ions was analysed with the scope to simulate the effects of heavy ion cosmic ray bombardment on chiral molecules in the interstellar medium. The α -pinene ice samples were irradiated at 10 K and their chemical evolution was monitored by mid-infrared Fourier transform (FTIR) spectroscopy to characterize the reaction products and to determine the extent of racemization. The integrated band strengths have been obtained for all the neutral α -pinene vibrational bands using the experimental band integrated absorbances and the theoretical absolute intensities calculated along the column densities.

In the current heavy ion bombardment experiments, small molecules were formed and the precursor, α -pinene, was destroyed instead of being racemized. Twelve hydrocarbons were produced (final fluence of 2.0×10^{12} ions cm^{-2}): methane (CH_4), acetylene (C_2H_2), ethylene (C_2H_4), propylene (C_2H_6), propane (C_3H_8), n-butane (C_4H_{10}), butene (C_4H_8), propyne (C_3H_4), benzene (C_6H_6), ethane (C_2H_6), vinylacetylene (C_4H_4), and 2-methyl-1,3-butadiene or isoprene (C_5H_8). The highest formation cross-section ($\sim 40 \times 10^{-15}$ cm^2) was observed for the C_3H_4 , and the lowest was for C_3H_8 ($\sim 3 \times 10^{-15}$ cm^2).

The radiochemical yields for these molecules follow the same trends as those of their cross-sections. The atom budget calculation confirms that all the expected products have been generated during the radiolysis and supports the conclusion that the proposed A values are accurate. The α -pinene sputtering yield for this ion beam was found to be $Y_0 = 1.84 \times 10^6$ molecules per impact.

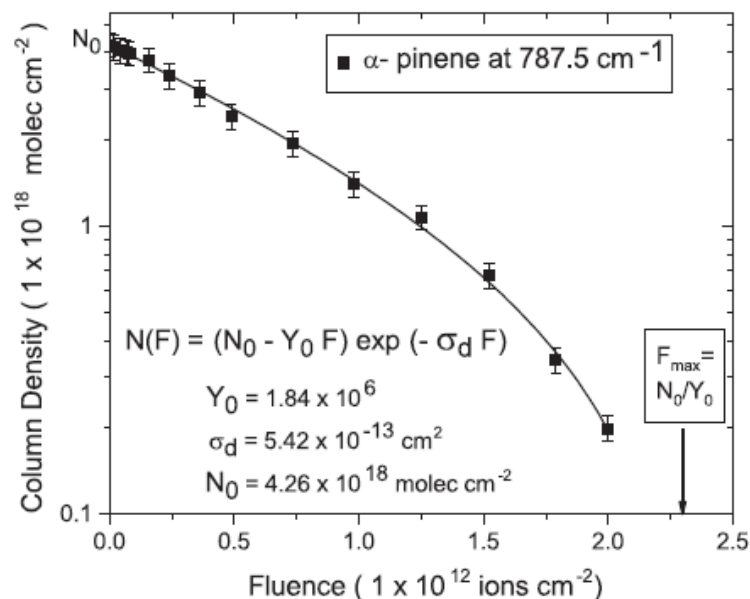


Fig. 1. The column density N of pinene as a function of projectile fluence F follows the function $N(F) = (N_0 - Y_0 F) \exp(-\sigma_d F)$. The values of the destruction cross section σ_d , of the sputtering yield Y_0 and of the initial column density N_0 are given in the figure 1.

ACKNOWLEDGEMENTS

ALF de B and EF da S acknowledge the Brazilian organizations CAPES, CNPq (Bolsa de Produtividade 307418/2021-9 and 30.4511/2022-6) and FAPERJ (E-26-210.965/2021, E-26-210.801/2021, E-26-245.307/2019, E-26-202.549/2019, E-26/201.934/2019, E-26-200.320/2023, and E-26/201.622/2023). AR acknowledges support from the NASA's Solar System Workings program (SSW; 80NSSC21K0776). We also acknowledge support by the Region Normandie (RIN SCHINOBI) including a post grant for CAPdC. The experiment was performed at Grand Accélérateur National d'Ions Lourds (GANIL) by means of CIRIL Interdisciplinary Platform, part of CIMAP laboratory, Caen, France.

Reference: A. L. F. de Barros, A. Ricca, A. Bychkova, Cíntia Pires da Costa, P. Boduch, H. Rothard, E. F. da Silveira, A. Domaracka, Heavy ion radiolysis of the chiral terpene α -pinene, Monthly Notices of the Royal Astronomical Society MNRAS 530 (2024) 2181–2198 doi: 10.1093/mnras/10.1093/stae757

2. Self-healing of nuclear glass alteration gels under irradiation

Experiment number: P1254, P1263

Date: May and June 2023

Spokeperson and co-authors

de Laharpe Pierre, Deschanel Xavier (UMR 5257 ICSM/LNAR)

Abstract

In the context of elucidating the role of water in the long-term behavior of vitrified nuclear waste, understanding the microstructural evolution of the glass alteration gel under irradiation remains necessary. In particular, the porous network present in the gel may collapse when irradiated. Concomitantly, the collapse of mesoporous silica under various irradiation regimes was recently monitored using X-ray scattering techniques. In this study, mesoporous silica thin films derived from the synthesis of SBA-15 and MCM-41 were prepared via sol-gel dip-coating. Some were immersed for several days in silica-enriched water and irradiated in the electronic regime by Xe ($E = 92$ MeV) and Ne ($E = 20$ MeV) ions. Results exhibit a mild reduction of pore collapse when samples with thinner pore walls are immersed prior to irradiation compared to dry samples, suggesting some degree of interaction between water and pore walls. Further experiments and analysis tools are called for.

Experiment report

Deep geological disposal of high-level nuclear waste is envisioned for the French CIGEO future repository site, where glass was chosen to compose the immobilization matrix of radionuclides. The parameters affecting its long-term durability include self-irradiation and aqueous alteration due to groundwater. Studies conducted on simplified borosilicate compositions found that ballistic damage tends to increase the formation of the alteration gel [1], which can feature nanometer scale pores and open channels [2]. Other recent results combining irradiation after alteration showed a possible competing phenomenon, as the gel's porous microstructure collapsed when irradiated [3]. The mechanisms surrounding this process, especially the possible role of water, are yet to be determined. Monitoring the collapse of a gel's random porous microstructure is experimentally challenging, as it typically requires TEM imaging throughout the irradiation episode. In this work, we address this point by using SBA-15 and MCM-41 as model materials.

Mesoporous silica thin films were dip-coated on silicon substrates. Initial solutions were prepared from tetraethylorthosilicate (TEOS) in two steps according to reference [4]. They were later aged at 80°C and calcinated at 400°C for 7 h. Calcinated thin films using P123 and CTAB were respectively noted IPc and ICc. The essential structural descriptors of mesoporous silica thin films are d_{inter} , defined as the distance between two layers of pores in the film (with $d_{\text{inter}} = d_{\text{pore}} + t_{\text{wall}}$, respectively the pore diameter and the pore wall thickness), and d_{tot} the total thickness of the film, they were extracted from Kiessig fringes and pseudo-Bragg peaks measured by X-Ray Reflectivity at, according to method from reference [5]. IPc films feature a 2D hexagonal network of cylindrical pores, while in ICc films they are spheres arranged hexagonally in 3D [4]. Dissolution processes in the immersion water were kept to a minimum by cooling down and filtering a $[\text{Si}] = 200$ mg/L solution prepared at 90°C , $\text{pH}90^\circ\text{C} = 9$ to ensure near saturation at 25°C . Samples of thin films (ICc, IPc) were immersed in 1.75 mL individual volumes of this solution for durations ranging from 2 to 5 days. Before irradiation, they were left to dry for 1h in open air and characterized. Because additional drying is expected from the vacuum in the irradiation chamber, "control" immersed samples were placed in the chamber but not irradiated. One series of IPc samples immersed 4 and 5 days was also enclosed in an airtight sealed cell behind a $8\ \mu\text{m}$ thick Al foil in the irradiation chamber to retain a few drops of the immersion water while irradiated by Xe ions. They are indicated by semi-hollow symbols on Fig. 1. In this series, the presence of water could be visually confirmed after irradiation for fluences $1\text{-}2 \times 10^{13}$ ions. cm^{-2} . Irradiations were performed at room temperature on the IRRSUD beamline of GANIL in a $\approx 10^{-6}$ mbar vacuum chamber. The beams were respectively Xe-92 MeV and Ne-20 MeV. Due to a specific experimental design and in order to maintain comparable damage across the experiment, all samples (except "dry non-immersed" samples in Ne irradiations) were shielded by $9\ \mu\text{m}$ -thick (for Ne irradiation) and $8\ \mu\text{m}$ -thick (for Xe irradiation) aluminum foil screens. For all samples the ion beam is perpendicular to the surface, and therefore perpendicular to the cylindrical pores. The effective projectile energy and the corresponding stopping powers in $2.2\ \text{g}\cdot\text{cm}^{-3}$ SiO_2 (representing the density of the silica walls, which is considered the same as amorphous silica), after traversing

the screens were calculated using data available in the SRIM/TRIM 2013 software. In both cases, the electronic contribution is largely dominant. Due to the very small thickness of material traversed by the beam, the total stopping power is assumed to be constant and the deposited energy is estimated as : deposited energy = total stopping power \times fluence. Table 2 summarizes the ion beams' characteristics, including sputtered ion yields obtained by calculations on 10^4 ion projectiles accumulated in TRIM (mode: monolayer collision steps/surface sputtering, with surface, binding and displacement energies as tabulated in the software).

Figure 1 summarizes the variation of structural descriptors for all experiments, displayed on a common axis accounting for the deposited energy. Since the chosen immersion duration range did not allow a clear discrimination between immersed samples series, they were grouped for readability and compared to the dry ones. An asymptotic exponential function is fitted on the d_{tot} variation plots to help qualitatively discriminate the sample series. This fit is made under the assumptions that the thickness variation reaches a saturation value (equal to the initial porosity, typically 40 % for IPc and 35 % for ICc [4]) and that the change in thickness is proportional to the damaged volume (Marples model [6]). This fit was not performed on the d_{tot} plots due to insufficient data outside the uncertainty range. For all sample series, pore collapse does not significantly occur before $\approx 1-2 \cdot 10^{21}$ keV.cm $^{-3}$, consistent with previous observations made on such samples [7-8]. Both immersed and non immersed IPc samples show similar collapse, reaching up ≈ 30 % d_{tot} at $\approx 10^{22}$ keV.cm $^{-3}$ and ≈ -40 % d_{inter} at $\approx 10^{22}$ keV.cm $^{-3}$. In the Xe irradiation series, ICc dry samples exhibit up to 25 % d_{tot} and 11 % d_{inter} decreases at 3×10^{21} keV.cm $^{-3}$ of deposited energy, against 15 % d_{tot} and negligible d_{inter} decreases for immersed ICc samples at the same energy. The fitted curves for the Ne irradiation series suggest a similar tendency.

Based on the evolution d_{tot} and d_{inter} , the collapse of the porous structure under irradiation seems mildly mitigated for ICc immersed samples. The absence of such a phenomenon for IPc samples might be primarily due to their greater pore wall thickness (typically 2-3nm against 1nm), rendering them less sensitive to the immersion prior to irradiation. Three IPc and two ICc samples above 10^{21} keV.cm $^{-3}$ of deposited energy irradiated by Xe ions (against only on ICc for Ne ions) did not allow the extraction of d_{inter} , indicating that the structure is too damaged, therefore limiting the interpretation from the d_{inter} plots. This is unlikely a result of sputtering, as fluctuations of the ratio (estimating the number of porous layers) are comparable between the ion beams despite much higher sputtering yields for Xe (Table 2). However, the electronic stopping power of Xe (4.71×10^7 keV.cm $^{-1}$) being well above the track formation threshold [9] could better explain this stability discrepancy. Both structural descriptors show an overall increase for control samples. While it suggests a swelling of thin films upon immersion and vacuum drying, it doesn't exceed 5% in value, rendering the preimmersion and post-immersion structures quite comparable. Under irradiation, the various immersion durations sample series could not be distinguished one from another. Additional immersion throughout irradiation (samples enclosed with water in the airtight cell) did not appear a relevant parameter either. The observed collapse reduction is overall greater when the deposited energy (and time spent in the vacuum chamber, thus eliminating any remaining water of samples that were only immersed before irradiation) increases. Albeit difficultly interpretable with only the descriptors and the experimental conditions used in this study, these observations preferably indicate an interaction effect of pore walls with water prior to irradiation over an energy dissipation by remaining pore water. Mesoporous silica are metastable materials and can continue to evolve even in saturation conditions. Gouze et al. [10] identified several possible mechanisms while studying the aqueous alteration of MCM-41 and SBA-15 powders at 50°C. It is well conceivable that a higher degree of hydration (increased time and temperature) on both types of samples might better highlight the reported phenomenon and allow its quantification.

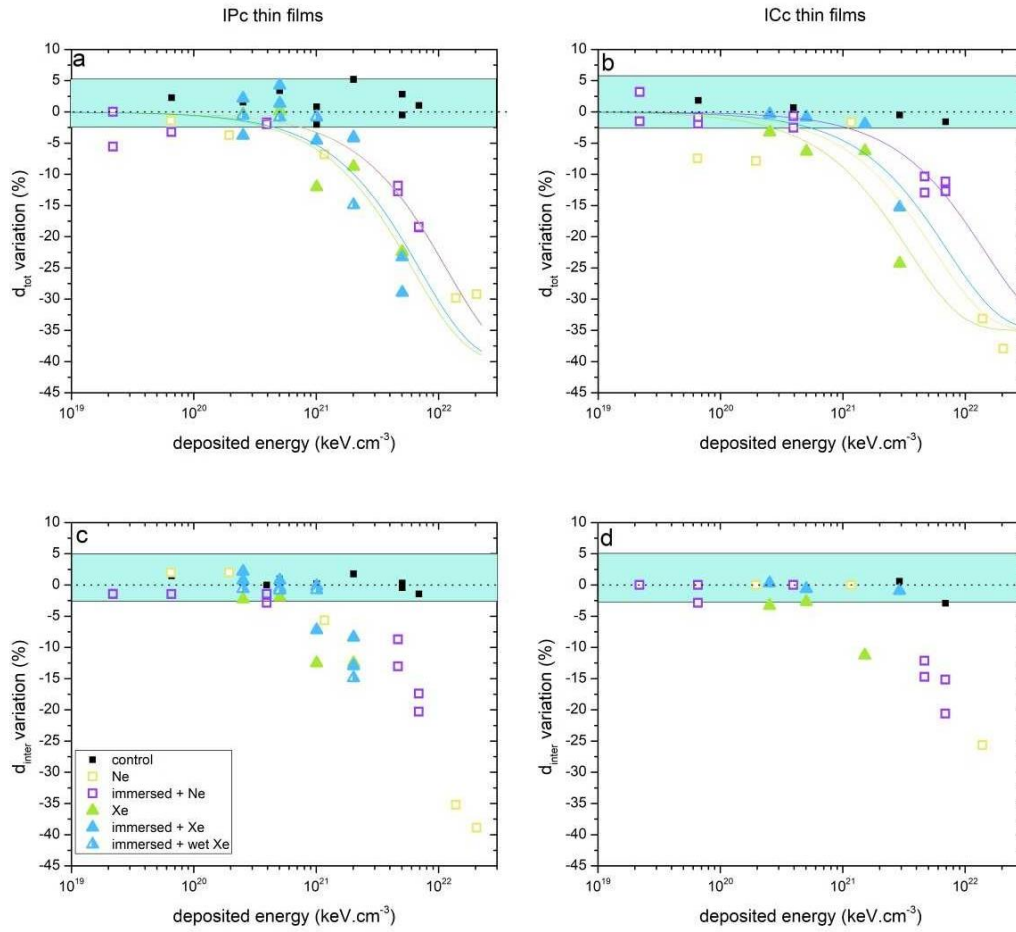


Fig. 1. Evolution of the (a) total thickness d_{tot} and (b) interlayer distance d_{inter} of IPc thin films and (c) total thickness d_{tot} and (d) interlayer distance d_{inter} of ICc thin films under irradiation. For Xe immersed samples of graph (b) and (d), variations are calculated between the final state and the initial pre-immersion state. The area filled in light blue indicates the estimated uncertainty range from fluctuations of control samples, which were immersed and placed in the irradiation chamber but not irradiated. Missing data points at high deposited energies on graphs (c) and (d) correspond to sample for which d_{inter} could not be extracted from the XRR profile.

Thin film	Initial structure				Morphology of pores
	d_{tot} (nm)	d_{inter} (nm)	d_{pore} (nm)	t_{wall} (nm)	
ICc	85-100	3.3-3.9	~2-3	~1	3D, spheres
IPc	50-65	5.5-7.0	~4	~2-3	2D, cylinders

Table 1 – Thin films characteristic

Ion beam	Average flux (ions.cm ⁻² .s ⁻¹)	Min. and max. fluences (ions.cm ⁻²)	Beam energy (MeV)			Stopping (keV.cm ⁻¹)	power	Sputtered ion yield (atoms.ion ⁻¹)	
			Before Al foil	After Al foil	Al			Electroni c	Ballistic
Ne (non immersed)	6x10 ⁹	3.0x10 ¹² 9.4x10 ¹⁴	–	20		2.16x10 ⁷	2.98x10 ⁵	0.006	0.018
Ne	6x10 ⁹	3.0x10 ¹² 9.4x10 ¹⁴	–	20	0.61	6.84x10 ⁶	4.76x10 ⁵	0.083	0.274
Xe	4-5x10 ⁹	5.0x10 ¹² 1.0x10 ¹⁴	–	92	17.7	4.71x10 ⁷	3.3x10 ⁶	0.446	1.37

Table 2 - Characteristics of the ion beams

Legend

- [1] A. Jan, J. Delaye, H. Kaya, S.H. Kim, A.H. Mir, T. Charpentier, F. Angeli, S. Gin, *Int. J. Appl. Glass Sci.* 14 (2023) 113–132. <https://doi.org/10.1111/ijag.16618>.
- [2] S. Gin, M. Collin, P. Jollivet, M. Fournier, Y. Minet, L. Dupuy, T. Mahadevan, S. Kerisit, J. Du, *Nat. Commun.* 9 (2018) 2169. <https://doi.org/10.1038/s41467-018-04511-2>.
- [3] A.H. Mir, A. Jan, J.-M. Delaye, S. Donnelly, J. Hinks, S. Gin, *Npj Mater. Degrad.* 4 (2020) 11. <https://doi.org/10.1038/s41529-020-0115-0>.
- [4] Sandrine Dourdain“ Caractérisation structurale, poreuse et mécanique de films minces de silice mésoporeuse : influence de la fonctionnalisation”, thèse 2006. <http://www.theses.fr/2006LEMA1020>.
- [5] A. van der Lee, *Solid State Sci.* 2 (2000) 257–278. [https://doi.org/10.1016/S1293-2558\(00\)00119-9](https://doi.org/10.1016/S1293-2558(00)00119-9).
- [6] J.A.C. Marples, *Nucl. Instrum. Methods Phys. Res. B* 32 (1988) 480–486. <https://doi.org/10.1016/>.
- [7] Y. Lou, S. Dourdain, C. Rey, Y. Serruys, D. Simeone, N. Mollard, X. Deschanel, *Microporous Mesoporous Mater.* 251 (2017) 146–154. <https://doi.org/10.1016/j.micromeso.2017.05.057>.
- [8] J. Lin, G. Toquer, C. Grygiel, S. Dourdain, Y. Guari, C. Rey, J. Causse, X. Deschanel, *Microporous Mesoporous Mater.* 328 (2021) 111454. <https://doi.org/10.1016/j.micromeso.2021.111454>.
- [9] S. Klaumünzer, *Nucl. Instrum. Methods Phys. Res. Sect. B Beam Interact. Mater. At.* 225 (2004) 136–153. <https://doi.org/10.1016/j.nimb.2004.05.014>.
- [10] B. Gouze, J. Cambedouzou, S. Parrès-Maynadié, D. Rébiscoul, *Microporous Mesoporous Mater.* 183 (2014) 168–176. <https://doi.org/10.1016/j.micromeso.2013.08.041>

3. Energetic ion processing of carbonaceous molecule icy mantles: destruction and formation of new species

Experiment number P1322

Date April 2023

Spokeperson and co-authors

Alicja Domaracka (CIMAP, Caen France)
 Anna Bychkova (CIMAP, Caen, France)
 Philippe Boduch (CIMAP, Caen, France)
 Hermann Rothard (CIMAP, Caen, France)
 Cintia Aparecida Pires da Costa (CIMAP, Caen, France)
 Ana Lucia Ferreira de Barros (CEFET-RJ, Rio de Janeiro, Brazil)

Abstract

Over the last decades it became clear that we live in a "molecular universe". Carbon forms the basis of the majority of the molecular species so far having been identified in space. Although small carbon-based molecules, like CO and CO₂, are among the most abundant molecules in space, only a small fraction of carbon is expected to be locked up in such species. It was proposed that a large fraction (up to 20%) of the interstellar carbon is built in polycyclic aromatic hydrocarbons (PAHs) and fullerenes. Several laboratory studies were carried out to investigate the effects of vacuum ultraviolet photolysis on PAH:H₂O ices. However, data about interaction of energetic ions (cosmic rays) with PAH ices are very scarce. Therefore, we investigated effects induced by ion irradiation of pure pyrene ice at 10 K and of its mixtures with water. The aim is to obtain molecule destruction cross sections and to identify formation of new species.

Experiment report

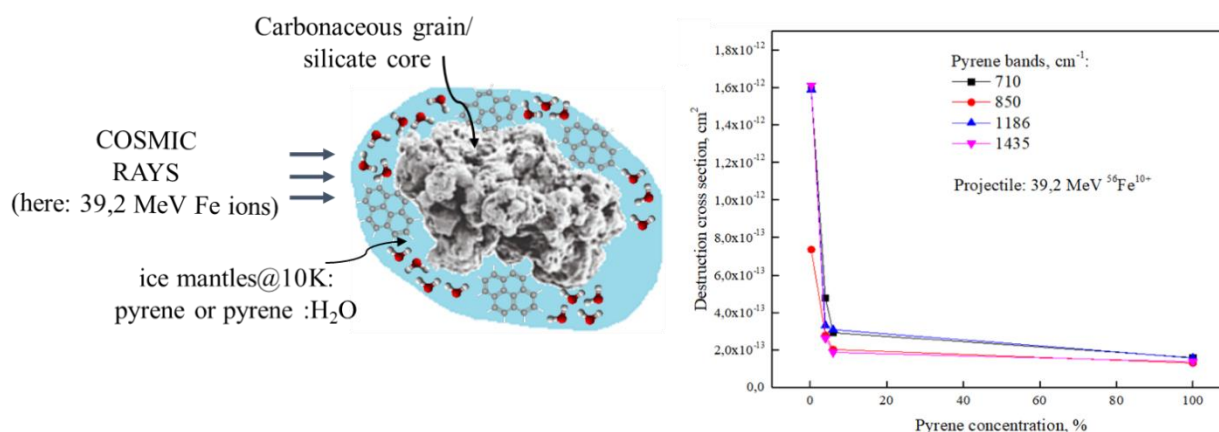
PAHs are important carbon carriers in space, playing a significant role in galaxy evolution and planets formation. Although PAHs with sizes ranging from C₅₀ to C₁₀₀ are reported to be the most common in space (Allamandola, et al., 1989), smaller PAHs may also survive in icy grain mantles. In the present studies, pyrene molecule (C₁₆H₁₀) was selected as a PAH representative. Pyrene was commonly detected in meteorites (Elsila, et al., 2005), (Basile, et al., 1984) and identified in the UV spectra of P/Halley comet (Clairemidi, et al., 2004). The possible formation pathway of pyrene from the reaction of 4-phenanthrenyl radical ([C₁₄H₉][•]) with acetylene (C₂H₂) in carbon-rich circumstellar environment was demonstrated in the work (Zhao, et al., 2018).

Samples of pure pyrene ice and mixed pyrene-water ices were irradiated at 10 K by 39.2 MeV ⁵⁶Fe¹⁰⁺ ions to simulate the effects of heavy ion cosmic ray bombardment of carbonaceous molecules in the interstellar medium (for experimental details see table below). The experiments were conducted with the UHV IGLIAS set-up. Pyrene films were prepared by an evaporation of the commercial pyrene power (Merk) in a home made oven kept between 120-190°C. To prepare mixed ices, water vapor were injected in to main UHV chamber during pyrene deposition.

Percentage of pyrene, %	Ion	Energy, MeV	T _{dep} , K	T _{irr} , K	Electronic stopping power, keV/μm	Nuclear stopping power, keV/μm	Penetration depth, μm	Column density of pyrene (10 ¹⁷ cm ⁻²)	Column density of water (10 ¹⁷ cm ⁻²)	Initial thickness of the sample, μm
0,3	⁵⁶ Fe ¹⁰⁺	39,20	10	10	4360	13,86	16,60	0,057	17,13	0,56
2,3					4342	13,68	16,36	0,291	7,26	0,31
5					4572	14,23	15,58	0,196	3,07	0,15
100					5449	16,50	12,02	3,57 0,82	-	0,95 0,22

The chemical evolution under irradiation of samples was monitored by mid-infrared Fourier transform (FTIR) spectroscopy to characterize the reaction products and to determine destruction cross sections of pyrene. The destruction cross section of pyrene varies as a function of water concentration (see figure). Formation of several small hydrocarbons was observed: methane (CH_4), acetylene (C_2H_2), ethylene (C_2H_4), ethane (C_2H_6), allene (C_3H_4), benzene (C_6H_6), cyclopropane ($\text{c-C}_3\text{H}_6$), propane (C_3H_8), propylene (C_3H_6), propyne (C_3H_4). Additionally, in water mixed ices CO and CO_2 formation occurred.

The present results will be compared with data obtained with lighter projectiles like protons, He, C and S ions at ATOMKI facility (Debrecen, Hungary). This experiment was conducted in the frame of Anna Bychkova's thesis (defence mid of October 2024).



Legend

The aim of the experiment is to investigate pyrene evolution in pure and water mixed ices at 10K under analog of cosmic rays. On the right evolution of pyrene dissociation cross sections as a function of water concentration in the ice.

ACKNOWLEDGEMENTS

ALF de B acknowledges the Brazilian organizations CAPES, CNPq (Bolsa de Produtividade 307418/2021- 9 and 30.4511/2022-6) and FAPERJ (E-26-210.965/2021, E- 26-210.801/2021, E-26-245.307/2019, E-26-202.549/2019, E- 26/201.934/2019, E-26-200.320/2023, and E-26/201.622/2023). We also acknowledge support by the Region Normandie (RIN SCHINOBI) including a post grant for CAPdC. The experiment was performed at Grand Accélérateur National d'Ions Lourds (GANIL) by means of CIRIL Interdisciplinary Platform, part of CIMAP laboratory, Caen, France.

4. Processing of amino acids by swift ion beams/ Processing of amorphous and crystalline pyridine ices by MeV ion irradiation

Experiment number: P1337

Date: May 2023

Spokeperson and co-authors

Cintia Pires da Costa

Alicja Domaracka (CIMAP, Caen France)

Anna Bychkova (CIMAP, Caen, France)

Philippe Boduch (CIMAP, Caen, France)

Hermann Rothard (CIMAP, Caen, France)

Abstract

The occurrence of amino acids in meteorites and comets raises questions about how they have been formed in cosmic environments, as well as how long they can survive in outer space; radioresistance is essential information to predict half-lives and make advances on the origins of life studies. Furthermore, amino acid radiolysis is of Medical Physics interest. The main objective of the current work is to analyze, via infrared spectrometry, how destruction cross section of pure and water mixed amino acids exposed to energetic ion radiation depends on projectile's energy and sample temperature. We propose then, to examine the degradation of pure amino acids (e.g., glycine, phenylalanine and cysteine) by swift ions. The main goal is to verify the destruction cross section dependence on the beam stopping power and its possible applications for Astrochemistry and Medical Physics.

The radioresistance of pyridine ice was probed under MeV ion beams irradiation by investigating the dependence of radiolysis and structural modifications as a function of projectile stopping power. The structural and chemical evolution of the samples as a function of projectile fluence was followed using infrared spectroscopy. All apparent destruction cross sections σ_d^{ap} , which incorporate the effects of radiolysis induced molecule dissociation as well as the ejection of particles by sputtering, were measured. Initially crystalline pyridine ices present apparent destruction cross sections four times higher than amorphous ices. However, after amorphization is completed, the cross sections σ_d^{ap} of initially crystalline samples are equal to those of initially amorphous ices. At 130 K, pyridine is more radioresistant than at 10 K, with smaller destruction cross sections.

Experiment report

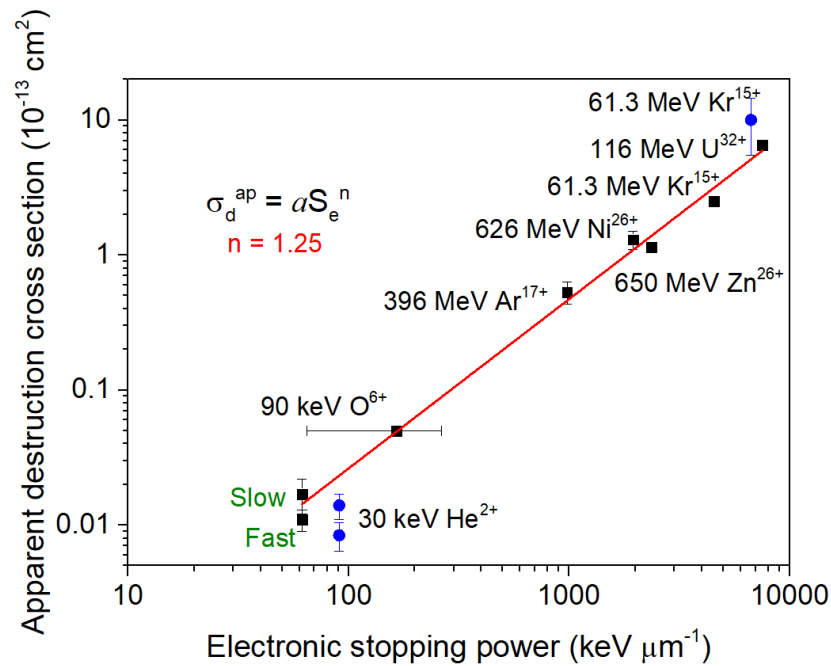
Organic materials have been detected in meteorites and comets. The amino acid glycine was observed in comet 67P/Churyumov–Gerasimenko by the Rosetta mission. This calls for inquiries into their formation processes within cosmic environments and their durability in outer space. Understanding the radioresistance of amino acids, for instance, is needed for estimating their lifespans and crucial for advancing research in fields such as astrobiology. Additionally, the radiolysis of amino acids holds significance in the realm of Medical Physics. We therefore propose to investigate the processing of pure and water mixed amino acids by swift ions, which are constituents of the radiation field in space. We focus on the dependence on the stopping power of the incoming ions. We intend to explore the degradation of various amino acids by infrared spectroscopy.

The experiments were planned to be conducted with the UHV IGLIAS set-up. Unfortunately, a technical problem with the oven of IGLIAS did not allow the production of amino acid films in situ for the measurements at the time. We spent hours trying to make a deposition of an amino acid film of glycine over a ZnSe substrate, thickness should be controlled by Fourier Transform Infrared spectroscopy – FTIR). We noticed that the oven was making the sample (which was in powder form) sublimate, because the blank window behind it became white after some time of “deposition”. However, those gas phase molecules never arrived the substrate to form a film, probably due to some clogging in the tube between the oven and the substrate sample holder. We decided, then, to not waste the beam time and switched to the irradiation of ices of pyridine.

Amorphous and crystalline pyridine films were irradiated in the IGLIAS set-up. The evolution of column densities as a function of beam fluence (i.e. the accumulated number of projectiles per surface area irradiating the sample) was followed by FTIR in transmission mode. The measured pressures went from 1×10^{-8} to 5×10^{-10} mbar, where the first value represents the residual gas pressure during irradiation. Spectra were acquired at the Mid-IR regions (range $4000 - 600 \text{ cm}^{-1}$). Pyridine films, with thicknesses between ~ 0.2 and $10 \mu\text{m}$ (according to amorphous and

crystalline A-values measured by Hudson & Yarnall (2022) for the band 1031 cm^{-1}), were deposited onto ZnSe substrates at 10 and 130 K to make amorphous and crystalline pyridine ices, respectively. A commercially supplied sample of pyridine (liquid of 99.8% purity from Sigma Aldrich) was purified before using it in a series of freeze-pump-thaw cycles to remove air and other impurities volatile at liquid N_2 temperature.

The figure shows the dependence of the apparent destruction cross section, σ_d^{ap} , on the electronic stopping power, S_e , for seven different projectiles impinging on amorphous pyridine at low temperatures (10 - 15 K). As expected, the apparent destruction cross section of amorphous and crystalline pyridine samples increases with the increasing electronic stopping power. Compiling data from the present work, and from published studies [33, 10], a scaling law where $\sigma \sim a S_e^n$, with $n = 1.25$ is found. These data should help to estimate half-lives of pyridine ices in various cosmic environments.



Legend

Amorphous (black squares) and crystalline (blue dots) pyridine apparent destruction cross section dependence on the electronic stopping power for different ion beams. The red line is a fitting of only amorphous data with the expression $\sigma_d^{\text{ap}} = a S_e^n$, where $n = 1.25$ and $a = 8.1 \times 10^{-5} \text{ cm}^2 \mu\text{m}^{1.25} \text{ keV}^{-1.25}$.

5. Surface microstructuring of single-crystal strontium titanate using swift heavy ions.

Experiment number: P1331

Date: June 14, 2023

Spokeperson and co-authors

RAHALI Radia, GRYGIEL Clara, LEBIUS Henning, BENYAGOUB Abdenacer.

Abstract

The modification of materials and the formation of defects caused by ion irradiation are the focus of several studies aimed at managing and improving their properties for various technological applications. Irradiation with ions of energy greater than 0.1 MeV/u gives rise to various modifications ranging from defects to amorphisation. At low fluence, where single ions prevail, each incident ion induces modifications that can be observable at the surface as craters, nano-hillocks, or chains of nano-hillocks, depending on the material characteristics and angle of irradiation [1-2]. As the intensity increases, we enter a regime of multiple ion impacts involving overlapping tracks. In the latter case, surface amorphization occurs in single crystal strontium titanate [3]. Previously, during other experiments conducted at the IRRSUD beamline at GANIL facility, wave-like structures on single-crystalline strontium titanate were observed [4]. The aim of this study was to assess the reproducibility of this phenomenon and, if it could be demonstrated to be reproducible, to identify the characteristics of these structures that could be controlled.

Experiment report

In this study, swift heavy ions (SHI) at high fluences with a grazing incidence geometry were used to induce surface modifications on single crystal strontium titanate (STO). The analysis of the morphological change of the surface by means of atomic force microscopy (AFM) has shown a surface reorganisation with the formation of wave-like structures oriented perpendicular to the ion beam for the first for this material [4].

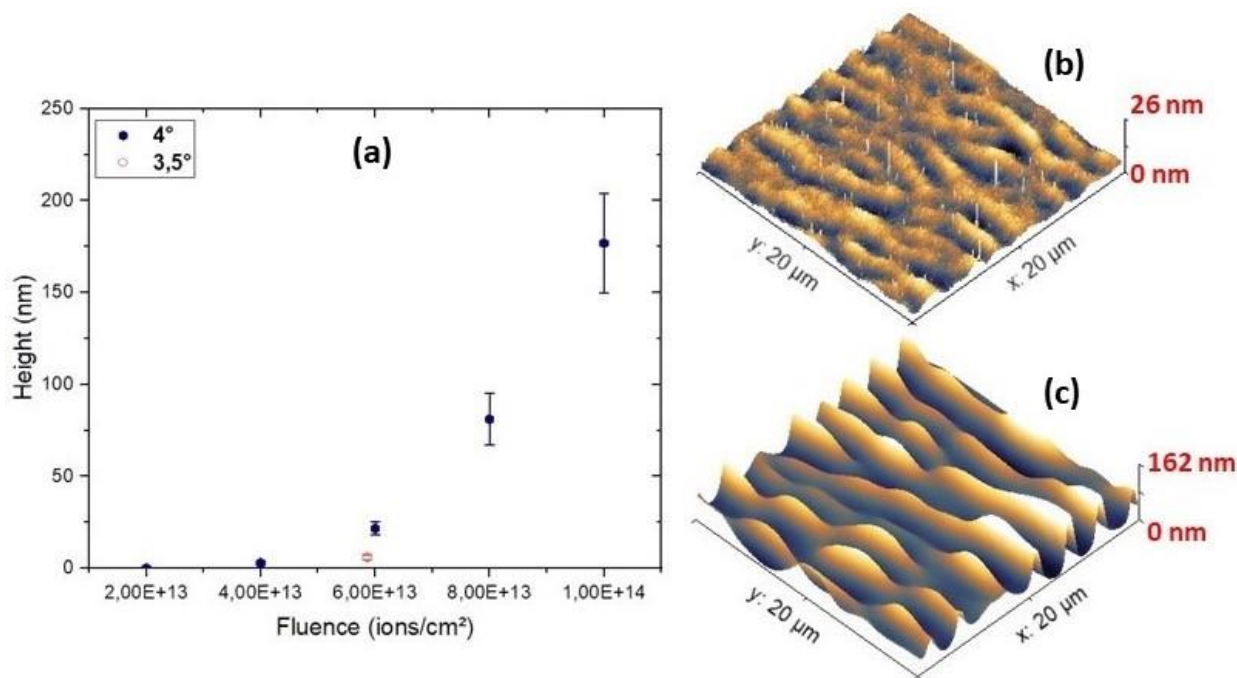
In order to investigate the effect of the different irradiation parameters on the modification of the strontium titanate (STO), a serie of irradiation were peromred where the angle of irradiation and the fluence were varied.

92 MeV $^{129}\text{Xe}^{23+}$ ions beam on the IRRSUD beam-line were used. It correspond to an electronic energy loss at the surface to 21 keV/nm, which is well above the stopping power threshold of 12 keV/nm needed for track formation on the strontium titanate (SrTiO_3) sample [5].

The irradiation angle extends from the surface normal, decreasing until grazing incidence. The results showed that the angle affects the periodicity (λ) of the waves-like structures. While the angle increases towards the surface normal, the periodicity increases. Control over surface wave density is therefore possible with the angle.

The width of these structures is also impacted by the irradiation geometry. So, as the angle increases towards the surface normal, the waves grow larger (with an increasing period) and the more they extend parallel to the ion beam, the more they fill the area of a given surface. This has a direct impact on the valleys, whose size will therefore be reduced as the angle increases. At this point, the impact of the fluence is unclear since it was modified each time for the varied angles employed. Given this, research into the effect of fluence (the number of ions per unit area) was required to better understand the mechanism underlying this phenomenon and learn how to control it. During this beam time, intermediate fluences were used as a baseline to compare the evolution of the surface wave structure obtained. The ion fluence at various grazing irradiation angles ranged from 1×10^{13} ions cm^{-2} to 4×10^{14} ions cm^{-2} .

The analysis of the evolution of these structures with fluence indicated that the waves increased in height. The periodicity was unaffected by the fluence ; thus, the number of waves remained constant while their size varied. In this approach, using higher fluences appears to increase wave growth, which can even result in very tiny pillar-shaped structures. To achieve a relatively thin structure and prevent its widening while increasing the irradiation angle towards the surface normal, it is necessary to increase the fluence.



Evolution of the height (a) of waves of SrTiO₃ (100) surfaces irradiated with 92 MeV Xe ions at 4° as a function of fluence. AFM image of SrTiO₃ (100) surfaces irradiated at 4° with 92 MeV Xe ions at (b) $\phi = 4 \times 10^{13}$ ions cm⁻² and (c) $\phi = 1 \times 10^{14}$ ions cm⁻².

- [1] E. Akcöltekin, T. Peters, R. Meyer, A. Duvenbeck, M. Klusmann, I. Monnet, H. Lebius, M. Schleberger. Nature Nanotechnology 2 (2007) 290, 10.1038/nnano.2007.109.
- [2] E. Akcöltekin, S. Akcöltekin, O. Osmani, A. Duvenbeck, H. Lebius, and M. Schleberger. New Journal of Physics, 10:053007, 2008.
- [3] C. Grygiel, H. Lebius, S. Bouffard, A. Quentin, J. M. Ramillon, T. Madi, S. Guillous, T. Been, P. Guinement, D. Lelièvre, and I. Monnet. Review of Scientific Instruments, 83:013902, 2012.
- [4] R. Rahali, H. Lebius, A. Benyagoub, E. Gardes, S. Guillous, I. Monnet, M. Sall, M.P. Chauvat, D. Marie, C. Grygiel. Materialia 27 (2023) 101696, 10.1016/j.mta.2023.101696.
- [5] M. Karlusic, S. Akcöltekin, O. Osmani, I. Monnet, H. Lebius, M. Jaksic, M. Schleberger New J. Phys. 12 (2010) 043009, 10.1088/1367-2630/12/4/043009.

6. Ion irradiation on solid phase silicate and organic matter, application for grain evolution in protoplanetary disks.

Experiment number: P1295-S-A

Date: March 8-10, 2023

Spokeperson and co-authors

VINOGRADOFF Vassilissa (spokeperson)	PIIM, UMR CNRS 7345 - Centre Saint-Jérôme - case 252, Université d'Aix-Marseille, 13397 Marseille, France
DANGER Grégoire	PIIM, UMR CNRS 7345 - Centre Saint-Jérôme - case 252, Université d'Aix-Marseille, 13397 Marseille, France
DUVERNAY Fabrice	PIIM, UMR CNRS 7345 - Centre Saint-Jérôme - case 252, Université d'Aix-Marseille, 13397 Marseille, France
MINISSALE Marco	PIIM, UMR CNRS 7345 - Centre Saint-Jérôme - case 252, Université d'Aix-Marseille, 13397 Marseille, France
BODUCH Philippe	CIMAP-CIRIL-GANIL, BP5133, 14070 Caen Cedex 05, France
ROTHARD Hermann	CIMAP-CIRIL-GANIL, BP5133, 14070 Caen Cedex 05, France
SALL Mamour	CIMAP-CIRIL-GANIL, BP5133, 14070 Caen Cedex 05, France
DJOUADI Zahia	IAS-Université Paris Saclay, UMR CNRS 8617, Bât 120 – 121 Univ. Paris-Saclay, 91405 ORSAY CEDEX
BRUNETTO Rosario	IAS-Université Paris Saclay, UMR CNRS 8617, Bât 120 – 121 Univ. Paris-Saclay, 91405 ORSAY CEDEX
BAKLOUTI Donia	IAS-Université Paris Saclay, UMR CNRS 8617, Bât 120 – 121 Univ. Paris-Saclay, 91405 ORSAY CEDEX
HENault Elsa	IAS-Université Paris Saclay, UMR CNRS 8617, Bât 120 – 121 Univ. Paris-Saclay, 91405 ORSAY CEDEX

Abstract

We propose in this new project to investigate the interaction of the silicate phase of interstellar dust grains with organic ices exposed to cosmic rays by a laboratory simulation with swift ion irradiation. The main objective of the project is to approach the evolution encountered by dust grains from interstellar medium to protoplanetary disk: is the organic matter in solid phase modified by the silicate phase? What are the main chemical modifications on the produced organic residue, leftover of the experimental process at room temperature? This project joins three laboratories that have different knowledge on the silicate or organic matter evolution in astrophysical environments. Such experiments will be performed for the first time and will bring new constraints to the organic-mineral interface/system that could exist in different solar system objects (comets, asteroids).

Experiment report

The experiments have been discussed by the team prior the beginning of the beam time, in order to define properly which experiments will be performed, the distribution of the samples afterwards and the analysis. We decided that to start 3 days of experiments are enough, and the allocated time was in March 2023 due to covid restrictions and delay.

The experiments have been performed by Elsa Henault, Zahia Djouadi, Philippe Boduch, Hermann Rothard, Alicia Domaracka, Mamour Sall. Vassilissa Vinogradoff was not able to attend because she was sick.

During the three days of experiments, a series of experiments have been investigated with and without silicate on the windows, for future comparison. Before the arrival the 8th of march, thin films of silicate (olivine composition) were synthesized on 8 ZnSe windows. Two of them were used as reference or blanks and have not been used for the experiments.

The formation of the ice and its chemical evolution during and after irradiation have been monitored by IR spectroscopy. Table 1 presents the experiments performed and the fluence of the beam calculated for each experiment. The ions beam was iron (Fe) at 39.2 MeV/ions, the temperature of the sample order 15k, and the temperature ramp set at 3k/min from 15 to 100 K, 5K/min from 100 to 200 K, and 10K/min from 200 to 300K.

Day	window	Composition (gaz phase)	Mbar pressure deposited	Final fluence (ions/cm ²)
20230408	W1 ZnSe	H ₂ O:CH ₃ OH (1:1)	1 mbar in 38 min	6.862x10 ¹²
20230408	W2 ZnSe + olivine1	H ₂ O:CH ₃ OH (1:1)	1 mbar in 19 min / ~0.8 μm	6.862x10 ¹²
20230408	W3 ZnSe + olivine2			6.862x10 ¹²
20230409	W1 ZnSe	H ₂ O:NH ₃ :CH ₃ OH (3:1:1)	5 mbar	1x10 ¹³
20230409	W2 ZnSe + olivine3	H ₂ O:NH ₃ :CH ₃ OH (3:1:1)	5 mbar	1x10 ¹³
20230409	W3 ZnSe + olivine4	H ₂ O:NH ₃ :CH ₃ OH (3:1:1)	~0.7 mbar / ~0.5 μm	6.862x10 ¹²
20230410	W1 ZnSe			
20230410	W2 ZnSe + olivine8	H ₂ O:NH ₃ :CH ₃ OH (3:1:1)	< 0.1 mbar	1x10 ¹³
20230410	W3 ZnSe + olivine7	H ₂ O:NH ₃ :CH ₃ OH (3:1:1)	2 mbar	1x10 ¹⁴

Different mixtures have been tested (table 1), but as a first series of experiments, we wished to investigate the role of the silicate on the formation of the organic residue and its composition. Hence, we made ices containing water, ammonia and methanol, all together irradiated by ions at low temperature.

7. Ion induced electron emission from radiosensitizing agents

Experiment number: P1302

Date: July 2023

Spokeperson and co-authors

Violaine VIZCAINO (CIMAP)

Suvasis SWAIN (CIMAP)

Alain MERY (CIMAP)

Jean-Yves CHESNEL (CIMAP)

Abstract

In ion beam therapy, radiosensitizers are used in order to enhance, locally, the ionizing radiation damage in biological matter. Much effort has still to be made to understand the basic mechanism and physical processes explaining this enhancement effect. One of the explanation is the important release of electrons from such agents. Therefore, we have measured ion-induced electron emission from two radiosensitizing agents molecules (Iodouracil and bromouracil) using a newly developed experimental set-up based on velocity map imaging (VMI) technique. This technique allows measuring, at once, all electrons emitted in a solid angle of 4π steradians with energy as low as a few tenths of eV up to 200eV. We provide absolute cross sections (total or as a function of energy and/or angle) and compare them to the one from uracil in order to determine the sensitizing factors.

Experiment report

Ion collision with biologically relevant molecules has received increasing interest due to applications to radiation biology. Studies of the collision between multiply charged ions and molecules in the gas phase help understanding the fundamental mechanisms involved at the molecular level (fragmentation, electron emission). In the past years, absolute total or differential cross-sections for electron emission have been measured for nucleobases and amino acids. Experiments were mainly performed with bare ions such as proton, C₆⁺ or O₈⁺ with a kinetic energy of a few MeV.

Enhancement of ionizing radiation damage in biological matter due to the presence of radiosensitizer has been shown but much effort has still to be made to understand the basic mechanism and physical processes explaining this effect. With this experiment, we are helping to answer the question by measuring absolute electron emission cross section from halogenated nucleobases.

To do so, we have used new crossed beam experimental set-up dedicated to the measurement of absolute cross-sections for ion-induced electron emission from atoms, molecules and nanoparticles that has been recently be built. With the previous allocated beamtime, we have validated our methodology by measuring the first absolute cross section from DNA/RNA bases (Uracil and Adenine) with this set-up on the IRRSUD beamline as well as SME beamline (P1230).

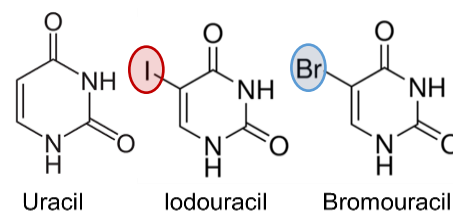
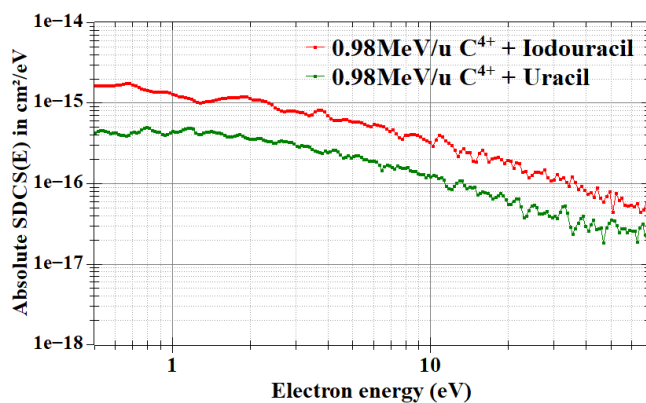
Absolute cross section are directly estimated from the number of emitted electrons N_e , the number of projectile ion beam N_p , the density ρ of the target beam (measured with a quartz crystal microbalance), the detector efficiency ε and the length l of the collision volume due to the beams overlap. Electrons are detected using a Velocity Map Imaging (VMI) spectrometer that allows collecting, at once, electrons with different kinetic energies emitted in a solid angle of 4π steradians without the need to rotate an energy analyser spectrometer. The image on the detector represent the 2D projection of the electron cloud produced by the ionization of the target and by applying an inverse Abel transform we can reconstruct the full momentum (energy and emission angle) of the emitted electrons in order to get the electron yield as a function of angle (θ), energy (E) or both. This method, using direct determination of absolute cross section rather than normalization to known scattering processes and VMI technique rather than standard electron spectrometer, is new but has been proven accurate.

We have measured the absolute cross sections for two 5-halouracil molecules. 5-halouracil molecules have the same structure than the RNA base uracil but one the H atoms is replaced by an halogen atom such as bromine (Br) or iodine (I) as seen in the figure below. These molecules are in powder form at room temperature and are put in the gas phase thanks to an oven that has two independent cavities: the effusion cell in which the powder of molecules is inserted, and the hot lip which allows shaping the beam thanks to an aperture tube (length = 30 mm,

diameter = 3 mm). The hot lip is held at higher temperature than the effusion cell to avoid condensation in the small exit aperture. The temperatures are chosen to be below any thermal decomposition of the molecules.

Total σ , single ($d\sigma/dE$, $d\sigma/d\theta$) and double differential ($d^2\sigma/dE d\theta$) cross sections have been determined and compared them to the Uracil in order to determine the sensitizing factors, i.e. the increase of the cross section due to the presence of the halogen atom.

In the Figure below, we show the single differential cross section (SDCS(E) or $d\sigma/dE(E)$) as a function of the emitted electron energy for both Uracil and Iodouracil. At low energy (around 1 eV), the cross section is almost a factor 3 higher for iodouracil. This ratio decreases as the energy of the emitted electron increases but still it remains higher than 2 up to a few tenths of eV. Such massive increase in the cross section cannot be explained by the number of valence electrons in each molecule. Indeed, according to theoretical calculations taking into account 29 orbitals for Uracil and 55 for Iodouracil (A. Mandal *et al.* Phys Rev A 102, 062811 (2020)) an average enhancement of 1.15 is expected for the energy range of 1 to 30 eV. Our observation would rather indicate a collective excitation (atomic giant resonances) of 4d correlated electrons in I atom. Theoretical calculation needs to be implemented to better quantify such collective processes and further experiments should be performed to confirm some observation for the angular dependence of the enhancement factor.



Absolute single differential cross section $d\sigma/dE(E)$ in cm^2/eV as a function of electron energy from Iodouracil and Uracil upon 0.98 MeV/u C^{4+} collision

8. Heavy Ion Irradiation of Scaffolded DNA Nanostructures

Experiment number: 1344 P1327-H

Spokeperson and co-authors

Jaroslav Kočišek, Leo Sala, Agnes Zerolová

J. Heyrovský Institute of Physical Chemistry of the CAS, Dolejškova 3, Prague, 182 23, Czech Republic

Dominik Pinkas

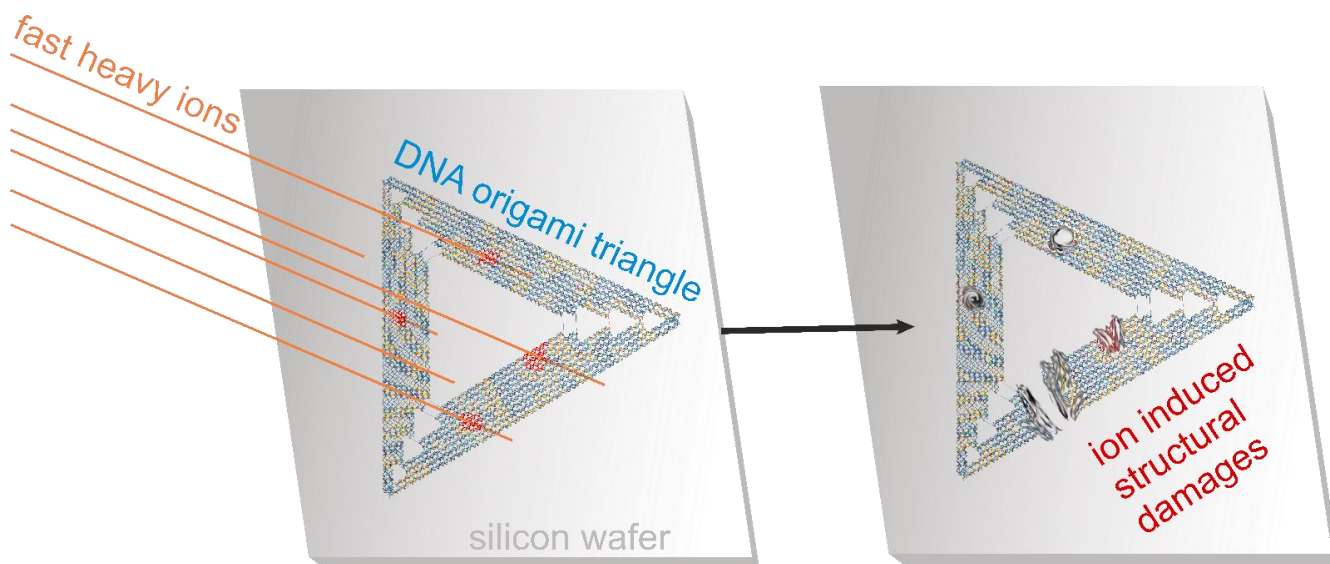
Institute of Molecular Genetics of the CAS, Vídenská 1083, 142 20, Prague, Czech Republic

Violaine Vizcaino, Alain Mery, Alicja Domaracka, Hermann Rothard, Philippe Boduch

Normandie Univ, ENSICAEN, UNICAEN, CEA, CNRS, CIMAP, Boulevard Henri Becquerel, BP 5133, 14070, Caen cedex 5, France

Abstract

In a series of experiments, we explored the structural damage induced by heavy ions to DNA origami nanostructures deposited on silicon surfaces. These pilot experiments provide a base for further exploration of unique combinations of top-down ion beam processing techniques with bottom-up self-assembly in nano-tech applications. The experiments also provide a valuable set of data for our ongoing research towards elucidating the details of the multiscale processes during radiation interaction with living tissue.



Experiment

DNA origami are nanostructures made by folding DNA into precisely defined shapes. The starting material is a long single strand consisting of several thousands of interconnected DNA bases that can be produced naturally. This scaffold strand is complemented by a set of designed staples. Under precisely defined conditions, the staples self-assemble with scaffold DNA to form double helix DNA folded into a desired shape.¹ Since the position of every single molecule in the final structure is well known from the design step, the specific DNA sequences can be used to bind other components to DNA origami at precise locations at their surface. This makes DNA origami superior to any other type of nanoparticle. Additionally, the nanoparticles possess several more advantages arising from DNA as a material that can be useful for a variety of applications.²

In our group, we are using the nanostructures to study fundamentals of radiation interaction with DNA. In these experiments, we can use the DNA origami as a platform for the precise positioning of molecules for single-molecule studies³ or we can use the DNA origami as a tiny dosimeter to explore the radiation effects on the structure⁴. The ultimate goal of our current efforts is to provide experimental verification for multiscale processes in radiation interaction with materials, such as shock waves.⁵ While the DNA origami sensitivity to damage via radicals or low-energy electrons seems to be low, its susceptibility to mechanical stress is high, and therefore, we believe origami is the ideal probe for this process. However, the shock-wave hypothesis represents a significant paradigm shift,

and therefore experiments for its proof must be performed with special care. The current experiments at GANIL allowed us to test several interaction regimes and provide a ... valuable base for further experiments in this direction, however the full test of the hypothesis will require much more experiments. However, the performed experiments are not interesting only for the fundamental radiation chemistry and physics. The range of projectiles and conditions, which we were able to explore during two planned experiments, allowed us to disentangle structural damages to the DNA origami deposited on surfaces, that could be interesting for nanotechnology.

Thanks to a spread of the software to design DNA origami and commercial availability of synthetic DNA strands, the DNA origami technique has become very popular in many fields including in nanotechnology. Examples include the use of these structures as a precisely shaped form for creating organometallic conducting nanostructures or their application in lithography.⁶ We have shown already that the nanostructures are very stable with respect to ionizing radiation damage, however at high doses the shape of the origami can be distorted.⁴ The current experiments with DNA origami deposited on silicon surface, performed at laboratory conditions at IRABAT platform with Fe²⁵⁺ ions at 60 MeV/u and under vacuum at IRRSUD platform with Fe¹⁰⁺ ions at 0.7 MeV/u enabled us to answer if the structures remain stable in typical material processing techniques such as ion implantation, ion beam deposition, or milling.

Results of these experiments were, already published in the journal BJSANO⁷ and therefore we will describe them only briefly. The main observation is that the nanostructure-to-surface interaction is strong allowing for high doses of radiation or cutting the nanostructure by ion beam without significant changes in the shape of the nanostructures. Typically, only a region of approximately 10nm around the ionization track was influenced, also limited by the resolution of the used AFM (atomic force microscopy) for the analysis. In some cases, profile heights change which means some components of the origami could be evaporated from the structure and probably the heavy atoms such as phosphorus remain on the substrate. Such change can be used to deposit the metal structures on the surface of a well-controlled shape of DNA origami. The observations opens the doors for novel applications, where DNA origami nanostructures could be used as an active component in lithographic techniques and as a part of nanoelectronics.

- (1) Rothmund, P. W. K. Folding DNA to Create Nanoscale Shapes and Patterns. *Nature* **2006**, *440* (7082), 297–302. <https://doi.org/10.1038/nature04586>.
- (2) Wang, P.; Meyer, T. A.; Pan, V.; Dutta, P. K.; Ke, Y. The Beauty and Utility of DNA Origami. *Chem* **2017**, *2* (3), 359–382. <https://doi.org/10.1016/j.chempr.2017.02.009>.
- (3) Sala, L.; Lyshchuk, H.; Šáchová, J.; Chvátíl, D.; Kočíšek, J. Different Mechanisms of DNA Radiosensitization by 8-Bromoadenosine and 2'-Deoxy-2'-Fluorocytidine Observed on DNA Origami Nanoframe Supports. *J. Phys. Chem. Lett.* **2022**, *13* (17), 3922–3928. <https://doi.org/10.1021/acs.jpcllett.2c00584>.
- (4) Sala, L.; Zerolová, A.; Rodríguez, A.; Reimtz, D.; Davidková, M.; Ebel, K.; Bald, I.; Kočíšek, J. Folding DNA into Origami Nanostructures Enhances Resistance to Ionizing Radiation. *Nanoscale* **2021**, *13* (25), 11197–11203. <https://doi.org/10.1039/D1NR02013G>.
- (5) Solov'yov, A. V.; Verkhovtsev, A. V.; Mason, N. J.; Amos, R. A.; Bald, I.; Baldacchino, G.; Dromey, B.; Falk, M.; Fedor, J.; Gerhards, L.; Hausmann, M.; Hildenbrand, G.; Hrabovský, M.; Kadlec, S.; Kočíšek, J.; Lépine, F.; Ming, S.; Nisbet, A.; Ricketts, K.; Sala, L.; Schlathöller, T.; Wheatley, A. E. H.; Solov'yov, I. A. Condensed Matter Systems Exposed to Radiation: Multiscale Theory, Simulations, and Experiment. *Chem. Rev.* **2024**. <https://doi.org/10.1021/acs.chemrev.3c00902>.
- (6) Heuer-Jungemann, A.; Linko, V. Engineering Inorganic Materials with DNA Nanostructures. *ACS Cent. Sci.* **2021**, *7* (12), 1969–1979. <https://doi.org/10.1021/acscentsci.1c01272>.
- (7) Sala, L.; Zerolová, A.; Vizcaino, V.; Mery, A.; Domaracka, A.; Rothard, H.; Boduch, P.; Pinkas, D.; Kocišek, J. Ion Beam Processing of DNA Origami Nanostructures. *Beilstein J. Nanotechnol.* **2024**, *15* (1), 207–214. <https://doi.org/10.3762/bjnano.15.20>.



VII. ARIBE

1. Low energy ion detection system for the FISIC project

Experiment number: P1328

Date: June 19-30, 2023

Spokeperson and co-authors

M JOLLY, Emily Lamour, Christophe Prigent, Martino Trassinelli, Stéphane Macé, Sebastien Steydli, Dominique Vernhet (INSP, Sorbonne Université, CNRS UMR 7588, Paris), Alain Méry, Jimmy Rangama, Patrick Rousseau, Jean-Marc Ramillon, Jean-Yves Chesnel (CIMAP, CEA/CNRS/ENSICAEN, Université de Caen Normandie, Caen)

Abstract

In this experiment, we characterized the modified version of the low-energy detection system of the FISIC project. This system consists of a 90° electrostatic ion charge state analyzer, constructed with two deviation plates enclosed by Matsuda plates. The analyzer is connected to a custom-built detection device that combines a Faraday cup and a position-sensitive detector. Experiments conducted in November 2021 at ARIBE revealed a significant contribution of background ions due to scattering on the electrode walls or ionization of the residual gas. Consequently, several modifications were made to the analyzer geometry to reduce these contributions to acceptable levels. In June 2023 the updated setup was connected to an OMEGA-shaped beam purifier, that had been previously characterized at ARIBE in 2018. Estimates of well-known capture cross-sections as well as less established ionization cross-sections in the literature at these collision energies were obtained. Some of the background contributions seen in 2021 were successfully reduced with the modified setup. However, the noise level, although better controlled, remains too high for future experiments at higher energies. Therefore, we must consider modifying the detection system by decoupling the Faraday Cup (FC) from the Microchannel Plates (MCPs).

Experiment report

The requested beam time was part of the preparatory phase for the FISIC (Fast Ion Slow Ion Collisions) project. The primary goal of this project is to establish a unique crossed beam ion-ion experiment to measure absolute cross-sections of electronic processes in the velocity range where ion stopping power is at its maximum. The initial phase involves conducting experiments on ion-atom and ion-ion collisions at low velocities in the INSP lab in Paris, utilizing the SIMPA and FISIC ion sources. The collision zone of the FISIC project comprises three parts (see Figure 1). Upstream of the collision chamber, the ion beam undergoes “cleaning” to ensure that the ions with the desired charge state enter the collision chamber. This is necessary because the incoming ion beam may contain a small fraction of undesired charge states formed in collisions with residual gas along the beamline. To address this, a dedicated electrostatic purification system, known as “Omega,” was designed and successfully tested at ARIBE [1]. Downstream of the collision chamber, the low-energy ion products are q-analyzed and collectively detected. The initial version of this analyzer was tested in November 2021 at ARIBE, and the results led to design modifications that were further tested during the 2023 beam time [2].

The charge state analyzer consists of a cylindrical 90° electrostatic analyzer coupled with a detection system developed in collaboration between CIMAP and INSP. A portion of the upper plate of the analyzer is drilled to install a transparent grid, allowing ions that could otherwise contribute to background noise to escape. This experiment aimed to test the new version of the ion spectrometer and to evaluate the effect of the charge state purifier. The spectrometer was directly connected to the Omega purifier, and both were linked to the ARIBE L4 beamline (see Figure 2). The experiment utilized 10 qkeV beams of O³⁺, Ar⁹⁺, and Ar¹²⁺ with currents ranging from a few picoamperes (pA) to a few tens of nanoamperes (nA) at the level of the detection system. Two detector positions were employed: one to measure secondary beams produced by capture on the residual gas and another for secondary beams produced by ionization (Figure 3 and see also Figure 4 for SIMION simulations).

Multiple runs were conducted with systematic variations in parameters such as the omega ON or OFF, voltage changes on inner and outer omega plates, deflectors, Matsuda plates, and detector voltages. For an Ar¹²⁺ primary beam, the new design of the ion spectrometer successfully eliminated the parasitic peak observed in 2021 (see Figure 5). In all capture configuration runs, the omega's effect was consistent with predictions, significantly reducing secondary beams. Runs with Ar⁹⁺ and Ar¹²⁺ as primary beams allowed the estimation of three capture cross-sections, which were found to be in good agreement with Müller-Salzborn cross-sections [3].

Process	Estimations from measurements	Müller-Salzborn cross sections
$\text{Ar}^{12+} \rightarrow \text{Ar}^{11+}$	$(1.4 \pm 0.7) \times 10^{-14} \text{ cm}^2$	$1.3 \times 10^{-14} \text{ cm}^2$
$\text{Ar}^{12+} \rightarrow \text{Ar}^{10+}$	$(2 \pm 1) \times 10^{-15} \text{ cm}^2$	$2.9 \times 10^{-15} \text{ cm}^2$
$\text{Ar}^{9+} \rightarrow \text{Ar}^{8+}$	$(8 \pm 6) \times 10^{-15} \text{ cm}^2$	$9.5 \times 10^{-15} \text{ cm}^2$

In the ionization configuration, the O^{3+} runs revealed a distinct semi-circular background, which was replicated using SIMION simulation software and attributed to elastic collisions within the analyzer (Figure 6). Additionally, ions resulting from the ionization of Ar^{9+} were detected (Figure 4), and the estimated cross-section for $\text{Ar}^{9+} \rightarrow \text{Ar}^{10+}$ was found to be $(3 \pm 2) \times 10^{-17} \text{ cm}^2$. This value, while larger by several orders of magnitude than expected, was consistent with values reported in the literature [4].

Overall we found that the transmission of the beam through the whole system (omega + ion spectrometer + detector) is 100%, and the ion spectrometer has the expected charge state separation power. The omega is effectively fulfilling its function by reducing the intensity of secondary beams by a factor of 10. However, despite reducing and eliminating some background contributions, the expected performance for ion detection was not fully achieved. High background noise from beams with currents up to the microampere (μA) range prevented the use of higher current ion beams. Further modifications to the spectrometer to eliminate background from elastic collisions may be necessary, along with a redesign of the detector. A proposed solution involves spatially separating the detection of the primary beam using a Faraday Cup and the secondary beams using MCPs, to prevent secondary electrons emitted from the Faraday Cup from reaching the MCPs. This experiment provided valuable insights into the setup and its performance, and the results will be crucial in guiding future design changes for the spectrometry and detection system.

[1] Schury, D et al, RSI 90 083306 (2019)

[2] Jolly, M et al, Atoms, 10, 146 (2022)

[3] Müller, A and Salzborn, E, Phys. Lett.A, 62, 6 (1977)

[4] A Diehl et al 2001 J. Phys. B: At. Mol. Opt. Phys. 34 4073

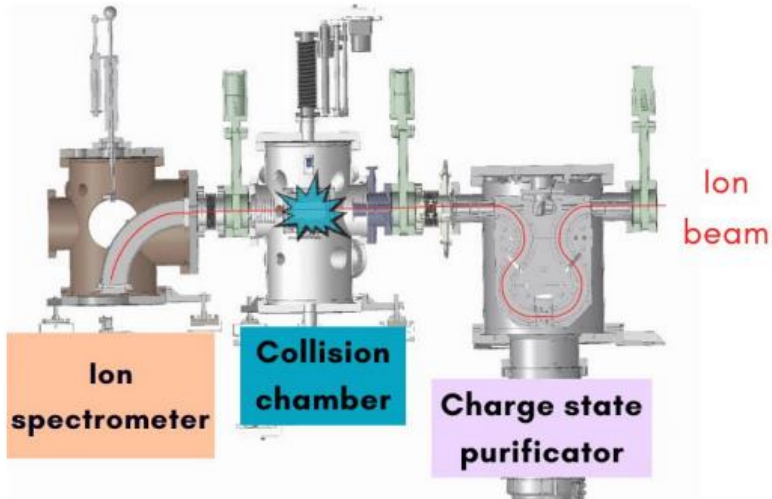


Figure 1: Overview of the FISIC collision zone with the Omega charge state purificator, the Collision chamber and the ion spectrometer.

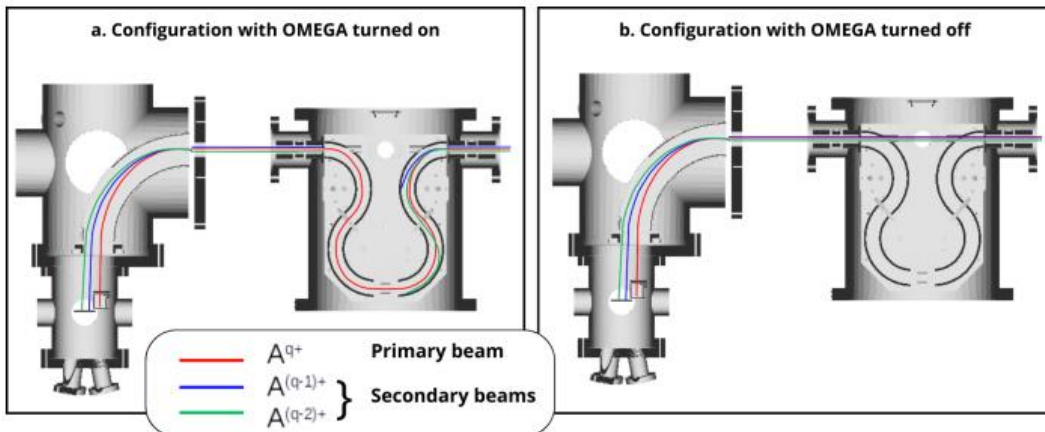


Figure 2: Trajectories of the primary and secondary beams from capture in the spectrometer and the OMEGA when it is turned on (a) and off (b)

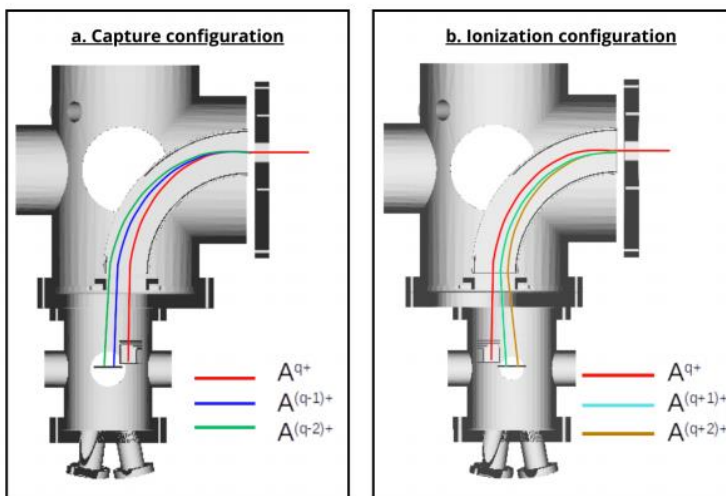


Figure 3: Trajectories of the secondary beams originating from capture and ionization in the ion spectrometer and the ion detector

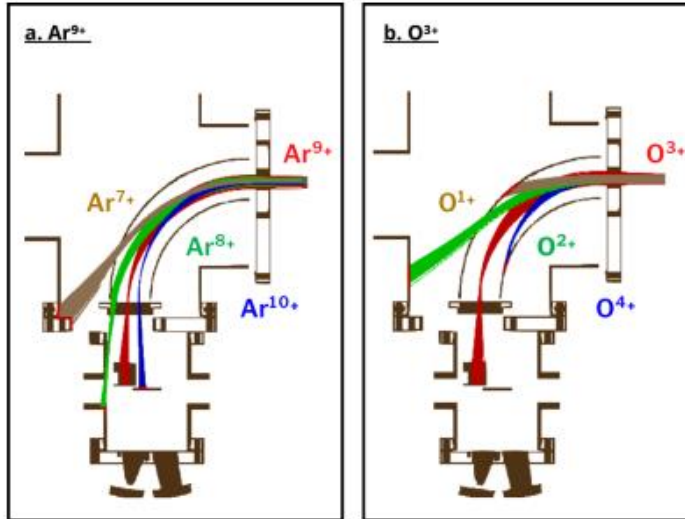


Figure 4: SIMION simulations of trajectories of the primary and secondary beams (produced by capture and ionization) in the spectrometer with the detector position to measure secondary beams only produced by ionisation for an Ar^{9+} (a) and O^{3+} (b) primary beam

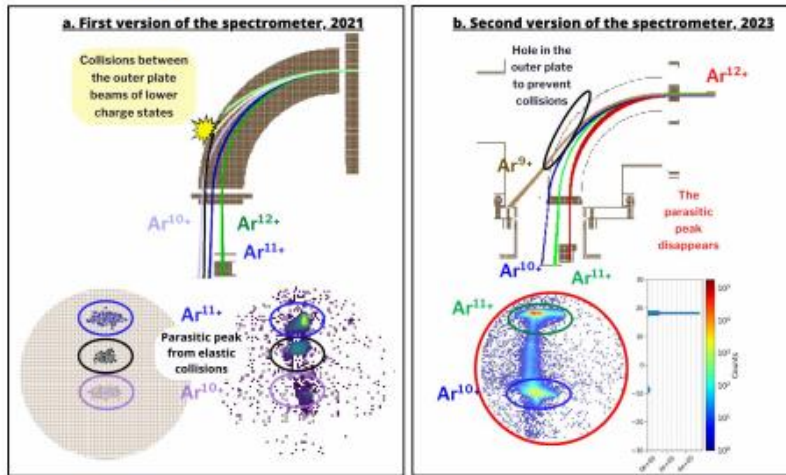


Figure 5: Comparison showing the effect of the spectrometer modifications on the parasitic peak background

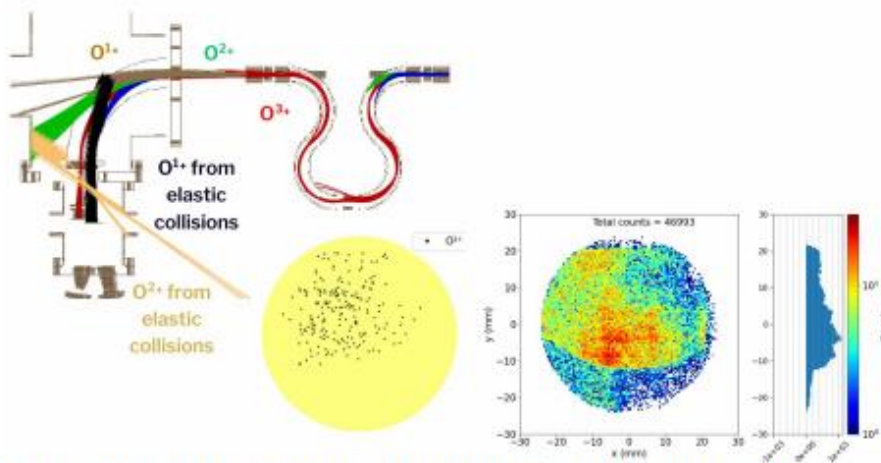


Figure 6: Simulated trajectories of capture beams from an O^{3+} primary beam in ionization configuration, showing the trajectories of the elastic collisions beams

2. Ion collision induced excitation dynamics in PAHs

Experiment number: P1342-A

Date: June 11-17, 2023

Spokeperson and co-authors

Najeeb Punnakayathil (NASA Ames Research Center, CA, USA)

Andrew L Mattioda (NASA Ames Research Center, CA, USA)

Patrick Rousseau (Université de Caen Normandie – CIMAP, GANIL, France)

Alicja Domaracka (Université de Caen Normandie – CIMAP, GANIL, France)

Abstract

Low energy radiation interaction with polycyclic aromatic hydrocarbons (PAHs) causes local electronic energy loss and thus excitation of electrons, one such prominent mode of collective excitation in PAHs are known as plasmon excitation. Previous studies of photo-ion yield measurements performed over a large range of PAH has clearly shown plasmon excitation at 17 eV, but the ion collision-induced excitation process in PAHs is less studied. Unlike in the photoexcitation which are governed by selection rule, it is not possible to assess how strong the ion induced excitation in these molecules considering the complexity of interaction dynamics and consequences. The collective excitation states due to inner valence shell electrons are expected to couple with intramolecular vibrational distributions via single-particle states. Such coupling is strongly dependent on the symmetry, size, and aromaticity of the molecule. We have investigated the ion-induced coupling mechanism in the electronic states of PAHs molecules particularly tetracene ($C_{18}H_{12}$), its isomers chrysene ($C_{18}H_{12}$) and triphenylene ($C_{18}H_{12}$) in collision with low energy He^{2+} and Xe^{20+} ions in the energy range of 5 - 20 qkeV

Experiment report

We studied the ion-PAH interaction by using the time-of-flight mass spectrometer set-up (COLIMACON) at ARIBE facility, GANIL. We use the multihit data acquisition system to measure the multi-ionization and multi fragmentation/dissociation of the PAH molecules, Tetracene ($C_{18}H_{12}$) - carcinogenic PAH and its isomers Chrysene and Triphenylene. As for the range of energies of projectiles, the low energy ions where electronic stopping dominant and low charge state, He^{2+} and high charge state Xe^{20+} at 5 and 20 qkeV were used. The excitation/ionisation/fragmentation mechanisms of PAHs in this energy range of radiation are also important as the supernova explosion will release radiation this range will interact with PAHs in the colder region in ISM. This energy range covers different excitations in PAHs, including the outermost $\pi-\pi^*$ excitations at $\sim 7 - 8$ eV as well as $\pi-\sigma^*$, $\sigma-\pi^*$ and $\sigma-\sigma^*$ excitations, which peak at ~ 17 eV. The projectile ion beams (He^{2+} , Xe^{20+}) were produced in the ECR source and accelerated to the interaction region of a Wiley-McLaren time-of-flight (ToF) mass spectrometer. The neutral target molecules are produced by heating the PAH powders in a resistively heated oven (tetracene ($125^\circ C$), chrysene ($95^\circ C$) and triphenylene ($70^\circ C$)) and the isolated gas phase molecules are introduced in the interaction region through a nozzle, where the sample undergo collisions with the projectile. The experiment was performed on two energies (5, 20 qkeV) of projectile with ion beam flux of about 1 particle nano amperes. In total, to perform experiment with three isomers with He and Xe ion beams at two different energies, the experiment took 6 days of beam time (2 days for Xe ion beams and 4 days of He ion beams). In addition, we took need 2 days between two ion beams for change of the target molecule.

The experiment were successful and we are currently working on the data analysis, we found some interesting correlation in the decay dynamics and molecular structural fragmentation and isomerisation in case of ion-PAH collision mechanism. Once the results are concluded we will publish in the peer reviewed journals. By realizing the complexity of interaction dynamics, along with the experimental studies, we are also working on Monte Carlo simulation for the ion-molecule collision which provides projectile energy loss and relative fragmentation cross-section for molecular targets.

Report to beam time of 90keV O^{6+} on organic molecules: benzonitrile and mixtures of acetonitrile and benzene.

Wania Wolff, Physics Institute of the Federal University of Rio de Janeiro

3. Radiate project: 23003101-ST

June 2023

In this work, reflection-absorption IR spectra were collected in the 5000–600 cm^{-1} range for acetonitrile, benzene, benzonitrile and the mixtures of acetonitrile and benzene.

For the sake of comparison first measurements of the infrared spectrum benzonitrile were performed to compare it with the database supplied by Wiley. The benzonitrile sample was purchased from Sigma Aldrich with a purity of (99.9%), HPLC, with water content of 0.03%. The appropriate sample we find out should be benzonitrile 99% anhydrous with water content of 0.003%, ten times less than the HPLC sample. The freeze-pump-thaw method was applied on the liquid sample to degas solvents and water. Thick and thin samples were deposit varying the delta ramp pressure for approximately 5 and 9 minutes onto a ZnSe subtract. The temperature of deposition was 10K. Unfortunately, the IR spectrum showed very clearly the IR band of water superimposed to the benzonitrile bands and it is difficult to analyze the data considering the spectra shown from the database (see Figure 1)

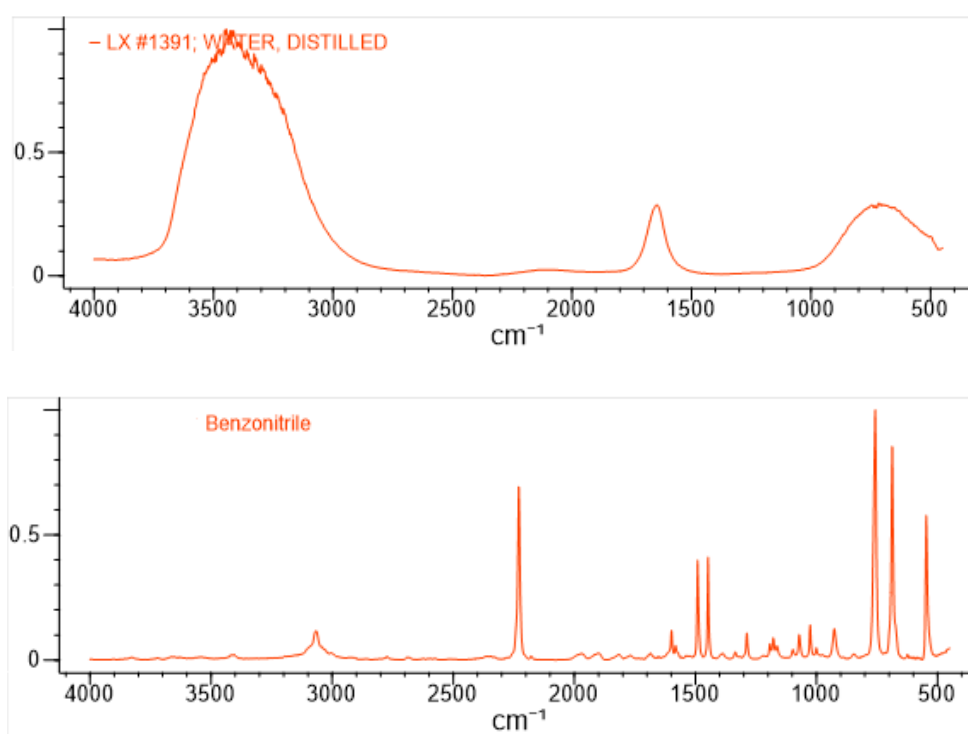


Figure 1 IR spectra of water and benzonitrile extracted from Wiley database.

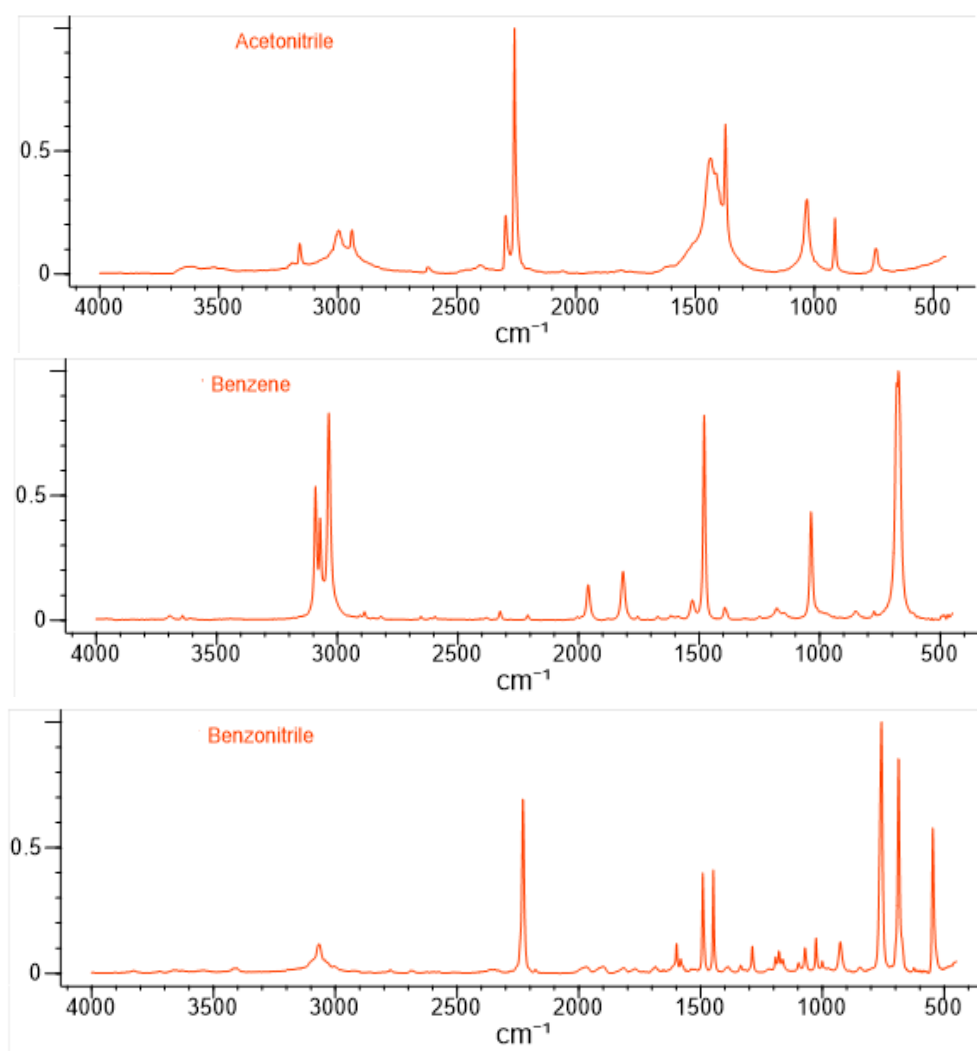


Figure 2 IR spectra of acetonitrile, benzene and benzonitrile extracted from Wiley data base.

Figure 2 show the IR spectra of acetonitrile, benzene and benzonitrile extracted from Wiley data base.

It is essential to reduce the water contribution to the spectra for all compounds. The ramp line was heated before new injection, but it turned out that most of the water contents derived from the sample itself. The benzonitrile liquid was treated for almost 24h in molecular sieves 4A to adsorb the water molecules, but the procedure did not reduce the water presence significantly as verified in the next IR spectra. It was imperative to collect the IR spectra of pure condensed benzonitrile. The only efficient method to suppress the water presence would have been distillation, but the time and means did not allow this option (proposal of distillation of the sample was not included in the project). Afterwards in a chemistry laboratory of the Federal University of Rio de Janeiro the distillation procedure was done, and it turned out to be very efficient, eliminating most of the water contents. At home time of flight mass spectra were collected under impact of 2.3 keV electrons before and after distillation to probe the effectiveness of the process. The thick and thin samples were exposed to O₆⁺ at currents of μA with fluences starting at 2×10^{13} ions/cm² and reaching a total accumulated fluence of 1×10^{15} ions/cm². The damage induced in the films are presented in figure 3.

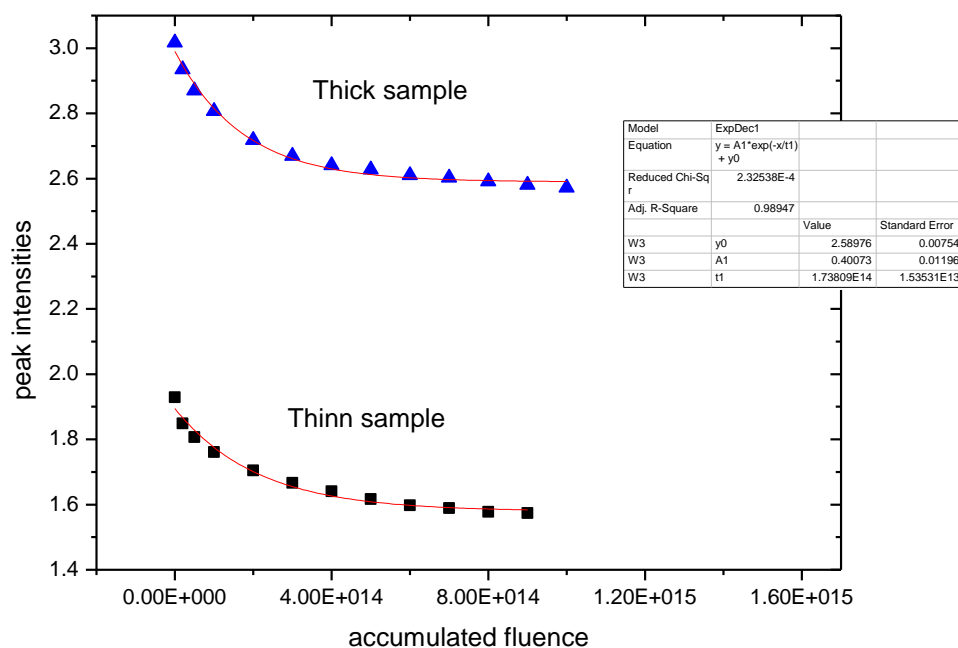


Figure 3 show representative the damage induced in the thick and thin samples of benzonitrile.

Following the proposal, a mixture of acetonitrile and benzene was prepared. For comparison prior to the mixture experiment acetonitrile and benzene pure samples were exposed to the oxygen beam and IR spectra collected. The molar fraction of the compound's acetonitrile and benzene in the mixture was fixed to 1:4. The molar fraction that showed the possible formation of benzonitrile was previously establish in the chemistry laboratory of the Federal University of Rio de Janeiro. The injection was monitored by a quadrupole mass spectrometer, which did not show the expected ratio, but measured equal amounts of the compounds. The mixture did not show any trace of benzonitrile IR bands. It was difficult to compare the mixture IR spectra to the benzonitrile spectra. New samples of the mixture heated to 110K followed by a cooling down to 10 K to increase the interaction of the compounds were also tried. Under electron impact the experience showed that after heating the films slightly below its sublimation more aggregates are formed. All measurements were negative with respect to the aggregate's formation in the mixture. The negative results are partly explained by the stopping powers for ninety keV oxygen ions of the acetonitrile, benzene and benzonitrile. The nuclear stopping power for 90keV O⁶⁺ are than the electronic one. Previous experiments with pyridine had already shown that daughter products are not formed for ions at this energy range. Water molecules trap acetonitrile molecules or segregate distinct species in mixtures by weakening the interaction between the molecules [Souda, 2016]. In the case of the benzonitrile formation in ice c-C₆H₆:CH₃CN mixture the presence of water inhibits its formation [Maksyutenko et al. 2022]. Therefore, particular care needs to be taken to avoid water contamination in the anhydrous samples and the deposition should be free of water.

At present calculations were performed to get the structures of benzonitrile cations and possible aggregates and next the IR spectrum of neutral and cationic benzonitrile in crystalline phase will be obtained.

Conclusion and perspectives

These preliminary data with low energy (around hundred keV) charged oxygen ions delivered at ARIBE (Ganil-Caen) beamline impinging anhydrous acetonitrile and benzene ice mixtures resulted negative with respect to the benzonitrile formation mostly suggested as due to low production of secondary electrons and subsequent radicals in the sample. On the other hand, very recent experiments on c-C₆H₆:CH₃CN binary ice mixtures upon the incidence of two keV electrons and Lyman alpha photons suggest its formation [Maksyutenko et al. 2022]. Very tiny structures, at 2230 cm⁻¹ and 1495 cm⁻¹ were assigned to benzonitrile produced in the acetonitrile-benzene mixture as shown in figure 4. The bands indicated in black solid line were assigned to pure benzonitrile.

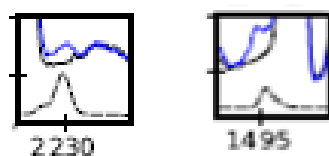


Figure 4 Data extracted from Maksyutenko 2022

As the ice processing is dependent on collision parameters, as charge, mass and energy of heavy ions, electronic stopping power of the projectiles, ionization, and dissociative cross sections, absorbed energy acquired by the reactants, and penetration depth in the ice sample we have proposed the impact of swift heavy ions. High velocity projectiles in the electronic stopping regime with masses ranging from Carbon-Ne, or Ar-Kr, (Iron, Niquel) or Xe with energies from 0.3 up to 1 MeV/u. These ions can reach a penetration depth around 10-20 microns depositing almost constant amounts of energy along the track since the thickness of the sample, d , is smaller than the penetration (around 10 times the d) so that the full length of the ice sample is processed inducing the production of much more radicals due to the enhanced secondary ionization by high energy delta electrons. along the track within a track radius much larger than for the slower projectiles delivered by ARIBE beamline. The measurements of the IR bands intensity through Fourier transform spectroscopy with the IGLIAS setup as function of the projectile fluence would allow to follow the physical and chemical radiolytic modifications of the pure and mixed samples and estimate the apparent destruction cross section, the radiation resistance, determine the survival time of the molecule and suggest the appearance of new and expected absorption features. Irradiation times of 4-5 hours need to be set for the mixtures with varying composition ratios of benzene and acetonitrile to allow the expected new bands corresponding to new daughter species to emerge with intensity as product of the interaction between benzene and acetonitrile, like the bands of benzonitrile and biphenyl, respectively [Lemmens et al. 2022]. The setup to be used is IGLIAS from CIMAP and beam line at IRRSUD. They both are best adequate for the project. References with impact in astrochemistry suggest the relevance of the investigation.

Reggie L. Hudson, Yukiko Y. Yamall, 2022 *Icarus* 377, 114899.

Radha Gobinda Bhuin, Rabin Rajan J. Methikkalam, Bhalamurugan Sivaraman, and Thalappil Pradeep 2015 *The Journal of Physical Chemistry C*, 119, 11524.

Ada Bian, Prudence C.J. and Agnihotri, Aditya N. and Boduch, Philippe and Domaracka, Alicja and Kanuchova, Zuzana and Rothard Hermann, 2021 *European Physical Journal D* 75, 57.

J. Cui, R.V. Yelle, V. Vuitton, J.H. Waite Jr., W.T. Kasprzak, D.A. Gell, H.B., Niemann,

Maksyutenko, Pavlo, Rafael Martín-Doménech, Elettra L. Piacentino, Karin I. Öberg and Mahesh Rajappan. 2022 *The Astrophysical Journal* 940, 113.

Alexander K Lemmens, Daniël B Rap, Sandra Brünken, Wybren Jan Buma, Anouk M Rijs, Van't Hoff Phys. 2022 *Physical Chemistry Chemical Physics*, 24, 14816.

B. Augé; T. Been; P. Boduch; M. Chabot; E. Dartois; T. Madi; J. M. Ramillon; F. Ropars; H. Rothard; P. Voivenel, 2018 *Review Scientific Instruments*. 89, 075105.

R. Souda, 2016, *JPC C120*, 934

4. Radiolysis of Complex Organic Molecules (COMs) in the condensed Phase

Experiment number: 19001773-ST

Date: June 6, 2023

Spokeperson and co-authors (affiliation)

Z. Kanuchova, Astronomical Institute of SAS, 05960 T. Lomnica, Slovakia

P. Boduch, A. Domaracka, H. Rothard, C. A. P. da Costa, CIMAP-CIRIL-Ganil, Normandie Univ, ENSICAEN, UNICAEN, CEA, CNRS, Caen, France

Abstract

Ices are omnipresent in cold regions in space. Examples include comets, dust grains, trans-Neptunian objects, surfaces of planets and their satellites. Although such ices are mainly formed from small molecules with two to five atoms (e.g., water, carbon oxides, nitrogen, methane), larger, complex organic molecules (COMs) may be present. Ionizing radiation (UV photons, electrons, ions from cosmic rays or solar wind) induces several physico-chemical processes such as radiolysis and subsequent formation of new molecules including COMs. The radioresistance of pyridine ice was probed under MeV ion beams irradiation by investigating the dependence of radiolysis and structural modifications as a function of projectile stopping power.

Experiment report

Pyridine (C_5H_5N) is an important complex organic molecule (COM). It has a similar structure as benzene, but with a nitrogen atom (N) replacing a methine bridge ($=CH-$), giving the ring the heterocyclic feature. It is proposed that pyridine also represents the key building block of nitrogen-substituted polycyclic aromatic hydrocarbons.

The radioresistance of pyridine ice was probed under MeV ion beams irradiation by investigating the dependence of radiolysis and structural modifications as a function of projectile stopping power. In recent years, amorphous and crystalline pyridine films (Fig. 1) were irradiated at different beam lines of the Grand Accélérateur d'Ions Lourds (GANIL). Different projectiles were used: i) 396 MeV Ar^{17+} and 626 MeV Ni^{26+} at SME, ii) 61.3 MeV Kr^{15+} at IRRSUD. The latest experiments of the series were conducted in 2023, using 30 keV He^{2+} ions of the ARIBE beam line of the GANIL for energetic processing of pyridine. Experiments were performed using the high vacuum setup IGLIAS (Auge et al., 2018) mounted as the end station of the ARIBE beam line.

The evolution of column densities as a function of beam fluence (i.e. the accumulated number of projectiles per surface area irradiating the sample) was followed by Fourier Transform Infrared spectroscopy (FTIR) in transmission mode.

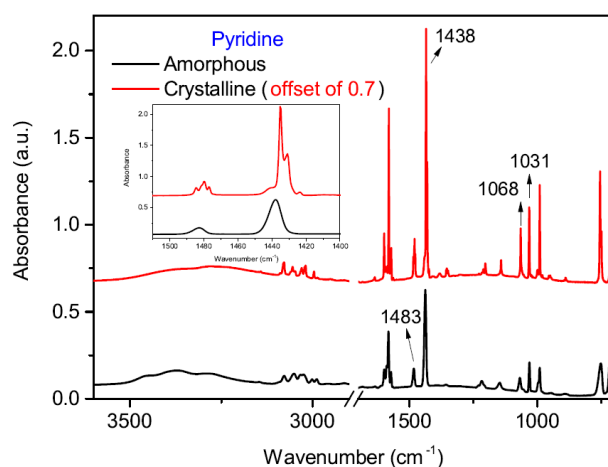


Figure 1: Crystalline (top red curve) and amorphous (bottom black curve) pyridine infrared spectra at 15 K. Inset graph highlights differences between amorphous and crystalline bands in the region of 1550 to 1400 cm^{-1} . Offsetting of the red curve for better visualization. Pyridine vibration modes are highlighted: 1031 cm^{-1} (ν_{12} C_5H_5N trigonal ring breathing), 1068 cm^{-1} (ν_{18a} C_5H_5N C-H deform), 1438 cm^{-1} (ν_{19b} C_5H_5N ring stretch), and 1483 cm^{-1} (ν_{19b} C_5H_5N ring stretch).

Based on previous experiments we can say, that energetic processing of crystalline pyridine with heavy MeV ions induce its amorphization. In contrast to these findings, the complete amorphization of crystalline pyridine was not achieved by irradiation 30 keV He⁺ ions (Fig. 2). However, amorphization was expected at the achieved fluences, and further experiments are needed to elucidate this ambiguity.

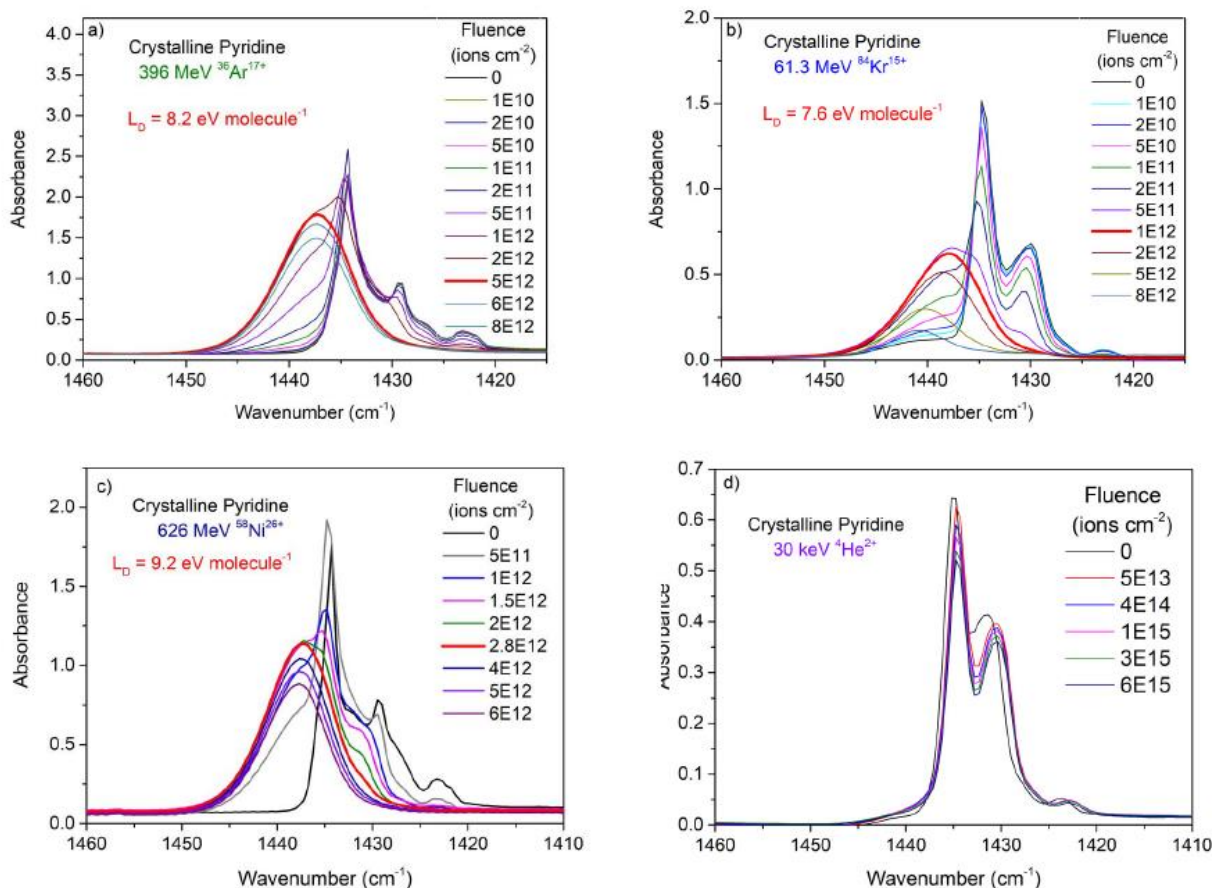


Figure 77 Evolution of infrared spectra of crystalline pyridine at 15 K with fluence of various energetic ions.

Results of the latest irradiation experiments of crystalline and amorphous pyridine with 30 keV He⁺ ions, as well as MeV heavy ions, are currently under detailed analysis and are being prepared for a publication in a peer-reviewed scientific journal.

5. Investigation of ion-induced fragmentation of diatomic molecules as a function of projectile charge

Experiment number: P1179A

Date: May 21 – June 3, 2023

Spokeperson and co-authors

Zoltán Juhász, Béla Sulik, Péter Herczku

(HUN-REN Institute for Nuclear Research, Hungary, 4026 Debrecen, Bem square 18/c)

Jean-Yves Chesnel, Violaine Vizcaïno, Jimmy Rangama, Alain Méry, Suvasis Swain

(CNRS CIMAP, Caen, France)

Sándor Demes

(Institute of Physics of Rennes (IPR), University of Rennes, 263 avenue du Général Leclerc

35042 Rennes CEDEX, France ; HUN-REN Institute for Nuclear Research)

Abstract

We have studied the fragmentation of O_2 and N_2 by multiply charged ions of the same atomic species, which are relevant for atmospheric sciences. The aim was to obtain results beyond the ones presently available for singly charged projectiles by measuring with projectiles of higher charge states. The results may find an application e.g., in the modelling of chemical processes in the atmospheres of Jupiter's moons, since highly charged ions continuously bombard these celestial objects. The planned program was to study collisions of O^+ , O^{2+} , O^{3+} and O^{4+} projectiles collisions with O_2 molecules, as well as the similar collision systems by replacing O (oxygen) by N (nitrogen) in both collision partners.

Experiment report

Energy/charge spectra of the fragment ions for the different collision systems were recorded by means of an electrostatic ion spectrometer available at ARIBE facility. We started the experiment with 20 keV $O^{2+} + O_2$ collisions. This spectrometer provides reliable data for fragments of kinetic energy larger than 1 eV. Below 1 eV, the trajectories of the fragments may be affected by spurious fields induced by surface charges and/or contact potentials. Therefore, the same collisions were investigated in ATOMKI with a field free time of flight (TOF) setup, which is ideal for investigation of the low energy fragments (< 1 eV). The two datasets are complementary and give full picture of the fragment emission. In the overlapping region the results agree well (see Figure 1.)

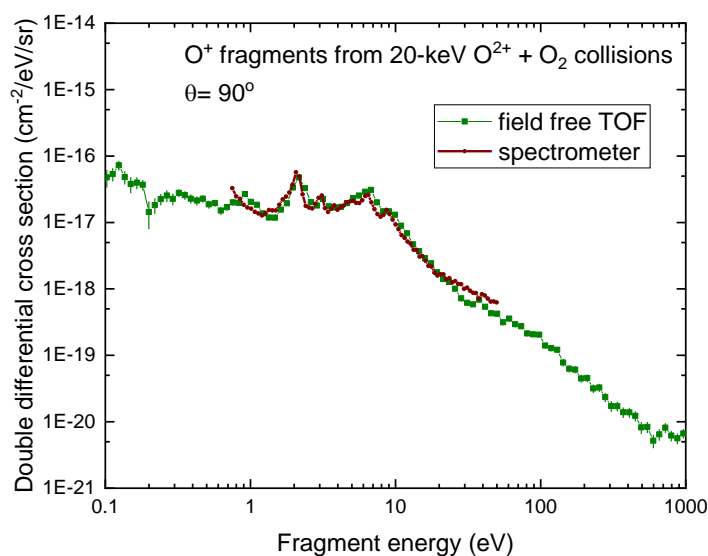


Figure 1

The fragment energy spectra were dominated by low energy O^+ ions, for which characteristic peaks appeared at 2.2, 3.3, 6.6, and 9.0 eV. These peaks were found to be isotropic. To identify the various charge-states of the ionic species contributing to each peak, we measured the time of flight of these different species within the spectrometer (see Fig. 2). To do so, it was necessary to pulse the beam. Besides the dominating O^+ fragments, some O^{2+} and O^{3+} were detected (with decreasing amount with increasing charge state). Surprisingly, the molecular ion O_2^+ was also detected. Even more surprising is the fact that the molecular ion could be identified at relatively large emission energies, up to 20 eV, too. The question arises as to how an intact molecular ion can get such a large momentum transfer without breaking. This question needs to be answered by model calculations including the molecular nature of the target by *ab initio* or at least semi-classical level. At forward angles, high energy peaks of several keV due to recoiled fragment ions from binary collisions were also detected. These peaks show a steep angular dependence and O^+ , O^{2+} , O^{3+} contributions were all detected.

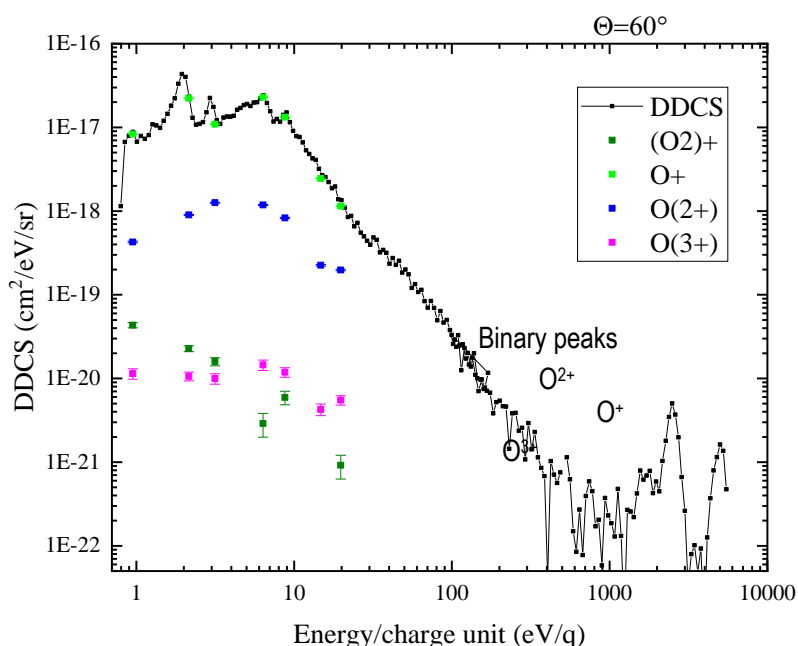


Figure 2

Anion contributions were checked also but we did not find significant contribution for this collision system. Then we changed the projectile energy to 30 keV so as to check the projectile-energy dependence of the fragmentation process. Moreover, at 30 keV all the other projectile charge states up to 4 could be delivered by the ECR ion source, which allowed us to study the effect of charge state purely, without changing other parameters. No significant energy dependence was found, but the effect of the charge state is dramatic (see Fig. 3). At higher projectile charge states, the fragment emission concentrated at higher energies and the contribution of multiply charged fragments becomes significant. One may expect that the total fragmentation cross section integrated in the energy scale significantly increases with the charge state since higher charge state projectile can remove electrons from the target more efficiently and from larger internuclear distance by electron capture processes. We have found that the total cross section for triply charged projectile is about one order of magnitude higher than for doubly charged projectile. However, the difference between quadruply and triply charged projectile is less than a factor of two.

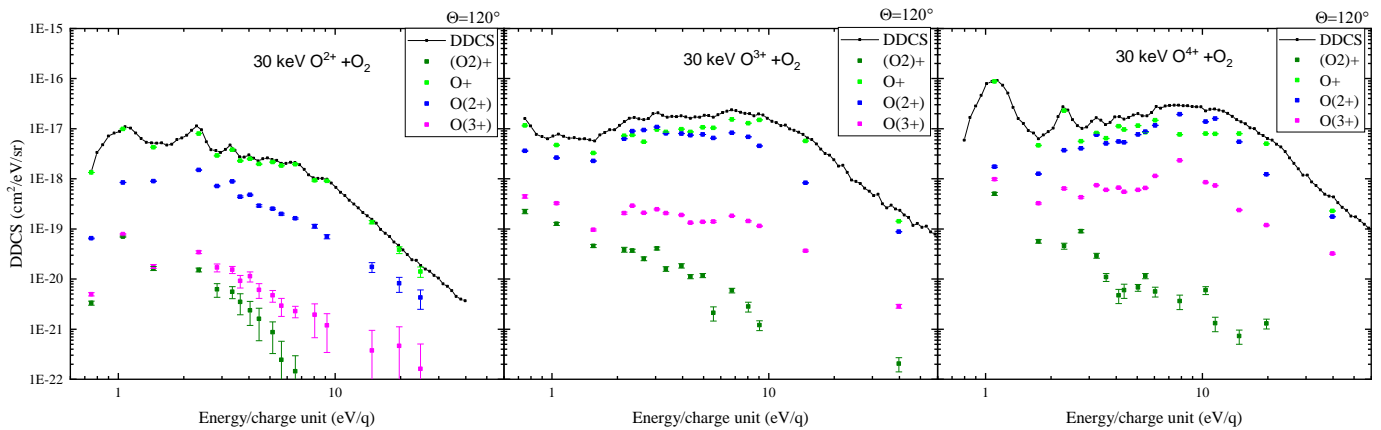


Figure 3

For the binary peaks, systematic changes are observed: the O^+ contribution decrease with increasing projectile charge state, the O^{2+} does not change significantly, while the O^{3+} contribution increases with the projectile charge state. After the experiments in Ganil, in a recent campaign we have measured some of the same collision systems ($30 \text{ keV } O^{3+} + O_2$, $7.8 \text{ keV } O^+ + O_2$) by means of the field free TOF setup, in order to extend the measured fragment energy range energy below 1 eV. These result are partially evaluated so far (see Fig. 4). Above 2 eV the two results are similar (note that the results are not absolutely calibrated yet). Below 2 eV, the TOF results show significantly larger cross section. This is the range, where the spectrometer transmission usually declines due to surface charges. This range is quite important, however, which is indicated by the high cross section values measured by means of the field free TOF apparatus in the range below the lower limit of the spectrometer. Above 400 eV, the spectra reported in Fig. 4 do not match to each other. This is due to the fact that the field-free TOF setup is limited in TOF resolution, thus making it less reliable for high emission energies. In contract, the electrostatic spectrometer available in Caen is an ideal system for detection of high-energy fragments. Therefore, the two setups are complementary.

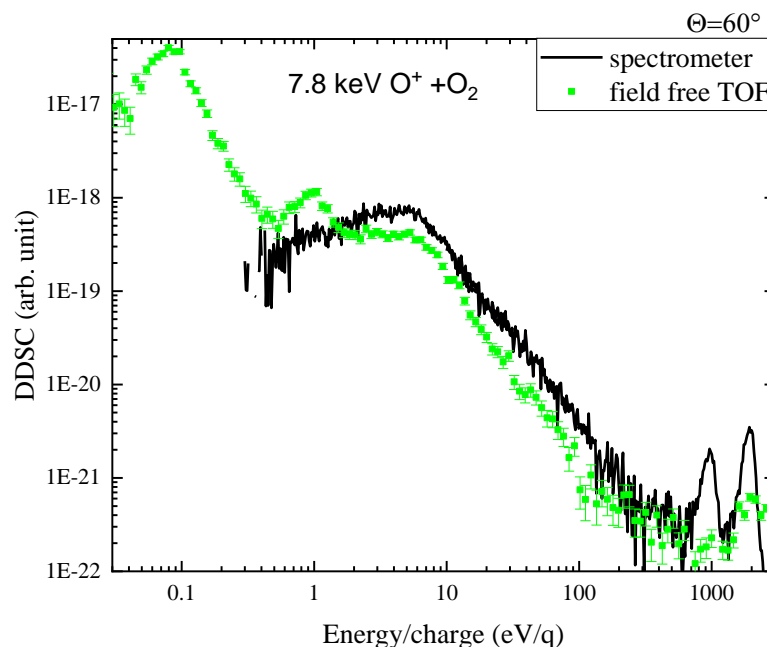


Figure 4

During this beamtime, very small time remained for measuring the collision systems of nitrogen ion projectiles colliding on N_2 molecules. However, we had already had some results from a previous beamtime. In this project we just made some supplementary measurements for the missing results from previous measurement, particularly

but not exclusively the binary peaks were measured for 5 keV $N^+ + N_2$ collisions (see Fig. 5). For this collision system, we also pulsed the beam in order to be able to measure the TOF of the various fragments through the spectrometer. We have observed a significant contribution of molecular ions emitted at low energies as one can accept for the strongly bonded nitrogen molecule. We would like to complete the nitrogen results during another beamtime at ARIBE with the electrostatic spectrometer, as well as at ATOMKI with the field-free TOF setup, so that the differences compared to the oxygen results could be studied in detail.

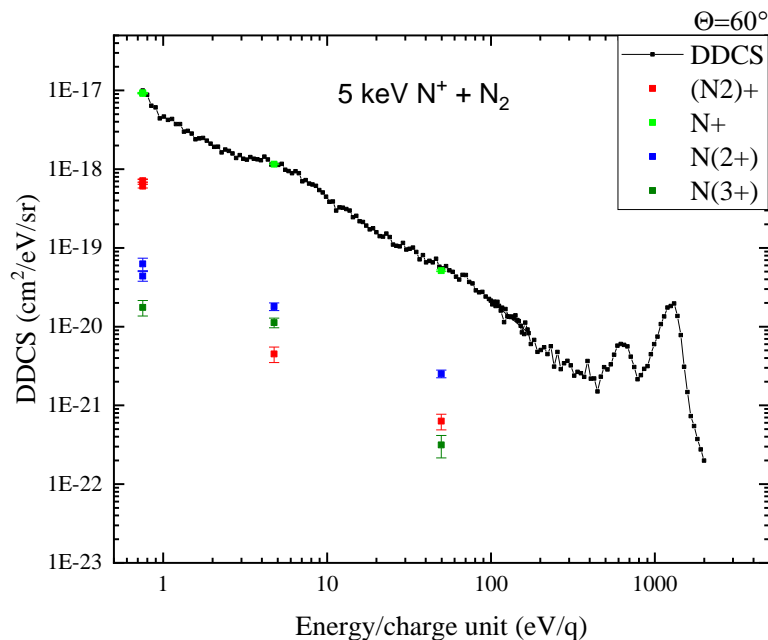


Figure 5

Legend

Figs 1 to 5: Doubly differential cross sections for fragment emission at the indicated emission angle θ (with respect to the beam direction) and as a function the emission kinetic energy per charge unit for different collision systems indicated in the figures.

We note that the singly charged projectiles (Figs. 4-5) do not lead to characteristic peak structures in the fragment energy distribution between 1 and 10 eV like in the case of multiply charged projectiles (Fig. 3). This is triggering theoretical investigation. We also note that for the triply charged projectiles the structure is less prominent than for doubly and quadruply charged projectiles.

From the oxygen results we have a complete set of data that we would like to publish in *Phy. Rev. A*. The results may have some astrophysical implications on the exospheres of icy moons of Jupiter and Saturn. We plan to study these by model calculations, which may also be published in a thematic journal in astrophysics.

Acknowledgments

The authors are grateful to Claire Feierstein-Plancq and Dr. Patrick Rousseau for beam tuning and technical assistance at the ECR ion source.



05 | ANNEXES



I. PUBLICATION LIST

1. ARTICLES & PROCEEDINGS

- [1] Zanon, E. Cle´ment, A. Goasduff, J. Mene´ndez, T. Miyagi, M. Assie´, M. Ciemala, F. Flavigny, A. Lemasson and A. Matta, *et al.* “High-Precision Spectroscopy of ^{20}O Benchmarking *Ab Initio* Calculations in Light Nuclei,” *Phys. Rev. Lett.* **131** (2023) no.26, 262501 doi:10.1103/PhysRevLett.131.262501 [arXiv:2405.14305 [nucl-ex]].
- [2] M. Ley, L. Knafla, J. Jolie, A. Esmaylzadeh, A. Harter, A. Blazhev, C. Fransen, A. Pfeil, J. M. Re´gis and P. Van Isacker, “Life-time measurements in ^{92}Mo : Investigation of seniority conservation in the $N=50$ isotones,” *Phys. Rev. C* **108** (2023) no.6, 064313 doi:10.1103/PhysRevC.108.064313
- [3] M. Sguazzin, B. Jurado, J. Pibernat, J. A. Swartz, M. Grieser, J. Glorius, Y. A. Litvinov, J. Adamczewski-Musch, P. Alfaut and P. Ascher, *et al.* “First measurement of the neutron-emission probability with a surrogate reaction in inverse kinematics at a heavy-ion storage ring,” [arXiv:2312.13742 [nucl-ex]].
- [4] E. Ahlgren Cederlo´f, T. Ba´ck, J. Nyberg, C. Qi, A. Atac, H. Badran, T. Braunroth, T. Calverley, D. M. Cox and M. Doncel, *et al.* “Lifetime measurement of the yrast 2^+ state in ^{118}Te ,” *Eur. Phys. J. A* **59** (2023) no.12, 300 doi:10.1140/epja/s10050-023-01212-3
- [5] Q. Fable *et al.* [INDRA and INDRA-FAZIA], “Isospin diffusion from $\text{Ca}40,48+\text{Ca}40,48$ experimental data at Fermi energies: Direct comparisons with transport model calculations,” *Phys. Rev. C* **109** (2024) no.6, 064605 doi:10.1103/PhysRevC.109.064605 [arXiv:2312.01763 [nucl-ex]].
- [6] J. Lois-Fuentes, B. Fern´andez-Dom´inguez, X. Pereira-Lo´pez, F. Delaunay, W. N. Catford, A. Matta, N. A. Orr, T. Duguet, T. Otsuka and V. Soma´, *et al.* “Low-lying structure of ^{15}C : Information on the $N=8$ shell gap,” *EPJ Web Conf.* **290** (2023), 09008 doi:10.1051/epjconf/202329009008
- [7] D. Fern´andez, M. Caama˜o, D. Ramos, A. Lemasson, M. Rejmund, H. A´lvarez-Pol, L. Audouin, J. D. Frankland, B. Fern´andez-Dom´inguez and E. Galiana-Baldo´, *et al.* “Experimental study of high-energy fission and quasi-fission with fusion-induced fission reactions at VAMOS+,” *EPJ Web Conf.* **290** (2023), 02012 doi:10.1051/epjconf/202329002012
- [8] M. Lozano-Gonz´alez, B. Fern´andez-Dom´inguez, J. Lois-Fuentes and T. Roger, “Event reconstruction in ACTAR TPC: Adaptation for transfer experiments,” *EPJ Web Conf.* **290** (2023), 01006 doi:10.1051/epjconf/202329001006
- [9] Vite´z-Szeiczzer, A. Algora, G. G. Kiss, B. Rubio, A. I. Morales, P. Sarriguren, G. de Angelis, F. Recchia, S. Nishimura and J. Agramunt, *et al.* “The β -decay of ^{71}Kr : Precise measurement of the half-life,” *EPJ Web Conf.* **290** (2023), 02021 doi:10.1051/epjconf/202329002021
- [10] J. L. Rodr´iguez-Sa´nchez, M. Feijoo, J. Benlliure, A. Chatillon, J. Ta´ieb, L. Audouin, H. Alvarez-Pol, Y. Ayyad, G. Be´lier and G. Boutoux, *et al.* “Fragmentation-induced fission reactions of ^{236}U in inverse kinematics to investigate the pre-fragment angular momentum parameterizations,” *EPJ Web Conf.* **290** (2023), 02016 doi:10.1051/epjconf/202329002016
- [11] Le Fe`vre, M. Colonna, G. Verde, K. Agarwal, J. Aichelin, T. Aumann, A. Chbihi, M. D. Cozma, E. De Filippo and H. Elfner, *et al.* “Long range plans to study the nuclear equation-of-state from sub- to supra-saturation densities with heavy-ion collisions,” *EPJ Web Conf.* **290** (2023), 10004 doi:10.1051/epjconf/202329010004
- [12] W. Urban, M. Czerwiński, G. de France, M. Jentschel, U. Ko´ster, P. Mutti, T. Rzaca-Urban and J. Wis´niewski, “Directional-polarization correlations using EXILL,” *JINST* **18** (2023) no.11, P11031 doi:10.1088/1748-0221/18/11/P11031
- [13] A. Leviatan, N. Gavrielov and F. Iachello, “Intertwined quantum phase transitions in odd-mass Nb isotopes,” [arXiv:2311.17127 [nucl-th]].
- [14] M. Markova, P. von Neumann-Cosel and E. Litvinova, “Systematics of the low-energy electric dipole strength in the Sn isotopic chain,” [arXiv:2311.14525 [nucl-ex]].
- [15] C. Agodi, F. Cappuzzello, G. Cardella, G. A. P. Cirrone, E. De Filippo, A. Di Pietro, A. Gargano, M. La Cognata, D. Mascalci and G. Milluzzo, *et al.* “Nuclear physics midterm plan at LNS,” *Eur. Phys. J. Plus* **138** (2023) no.11, 1038 doi:10.1140/epjp/s13360-023-04358-7
- [16] J. L. Wood and P. Van Isacker, “Remembering David J. Rowe,” *SciPost Phys. Proc.* **14** (2023), 013 doi:10.21468/SciPostPhysProc.14.013
- [17] G. Pasqualato, S. Ansari, J. S. Heines, V. Modamio, A. Go´rgen, W. Korten, J. Ljungvall, E. Cle´ment, J. Dudouet and A. Lemas-son, *et al.* “Shape evolution in even-mass $^{98-104}\text{Zr}$ isotopes via lifetime measurements using the γ -coincidence technique,” *Eur. Phys. J. A* **59** (2023) no.11, 276 doi:10.1140/epja/s10050-023-01172-8
- [18] M. Markova, A. C. Larsen, P. von Neumann-Cosel, E. Litvinova, A. Choplin, S. Goriely, S. Martinet, L. Siess, M. Guttormsen and F. Pogliano, *et al.* “Systematic study of the low-lying electric dipole strength in Sn isotopes and its astrophysical implications,” *Phys. Rev. C* **109** (2024) no.5, 054311 doi:10.1103/PhysRevC.109.054311 [arXiv:2311.08864 [nucl-ex]].
- [19] A. Rebillard-Soulie´, R. Bougault, H. Pais, B. Borderie, A. Chbihi, C. Ciampi, Q. Fable, J. Frankland, E.

- Galichet and T. Ge'nard, *et al.* "Isoscaling in dilute warm nuclear systems," *J. Phys. G* **51** (2024) no.1, 015104 doi:10.1088/1361-6471/ad0edd [arXiv:2311.05392 [nucl-ex]].
- [20] A. Savalle and O. Kamalou, "History and Prospectives of GANIL," *JACoW CYCLOTRONS2022* (2023), TUAO01 doi:10.18429/JACoW-CYCLOTRONS2022-TUAO01
- [21] D. Berverge, P. Leconte, B. Geslot, G. Kessedjian, P. Mutti, F. Rodiac, E. Pirovano, B. Lutz, X. Ledoux and L. Mathieu, *et al.* "New experiment for measuring the delayed neutron yields of 238U fission in the range 1 MeV to 19 MeV," *EPJ Web Conf.* **288** (2023), 04016 doi:10.1051/epjconf/202328804016
- [22] P. Van Isacker, A. Algora, A. Vite'z-Sveiczer, G. G. Kiss, S. E. A. Orrigo, B. Rubio and P. Aguilera, "Gamow–Teller Beta Decay and Pseudo-SU(4) Symmetry," *Symmetry* **15** (2023) no.11, 2001 doi:10.3390/sym15112001
- [23] L. Nies, L. Canete, D. D. Dao, S. Giraud, A. Kankainen, D. Lunney, F. Nowacki, B. Bastin, M. Stryczyk and P. Ascher, *et al.* "Further Evidence for Shape Coexistence in Zn79m near Doubly Magic Ni78," *Phys. Rev. Lett.* **131** (2023) no.22, 222503 doi:10.1103/PhysRevLett.131.222503 [arXiv:2310.16915 [nucl-ex]].
- [24] S. Hudan, H. Desilets, R. Kumar, R. T. deSouza, C. Ciampi, A. Chbihi and K. W. Brown, "Influence of additional neutrons on the fusion cross section beyond the N=8 shell," *Phys. Rev. C* **109** (2024) no.1, L011601 doi:10.1103/PhysRevC.109.L011601 [arXiv:2310.06776 [nucl-ex]].
- [25] A. Khandelwal, J. E. Ducret, L. Maunoury and L. Garrigues, "Simulation modeling and electron energy distribution function studies of an electron cyclotron resonance source with a new magnetic topology," *Phys. Rev. Accel. Beams* **26** (2023) no.10, 103501 doi:10.1103/PhysRevAccelBeams.26.103501
- [26] P. Pawlowski, J. Brzychczyk, N. Buyukcizmeci, H. T. Johansson, W. Trautmann, A. Wieloch, P. Adrich, T. Aumann, T. Barczyk and S. Bianchin, *et al.* "Neutrons from projectile fragmentation at 600 MeV/nucleon," *Phys. Rev. C* **108** (2023) no.4, 044610 doi:10.1103/PhysRevC.108.044610 [arXiv:2310.00409 [nucl-ex]].
- [27] M. Di Giacomo, C. Barthe-Dejean, B. Jacquot, S. Leloir and A. K. Orduz, "Upgrade of the medium energy dump geometry for the SPIRAL2 single bunch selector," *JACoW IPAC2023* (2023), THPA190 doi:10.1088/1742-6596/2687/8/082041
- [28] M. H. Moscatello, D. Ackermann, M. Di Giacomo, J. Dumas, A. Fournier, C. Haquin, C. Jamet, M. Michel, G. Normand and C. Peaucelle, *et al.* "NEWGAIN project at GANIL-SPIRAL2 : design of the new heavy ion injector for the superconducting linac," *JACoW IPAC2023* (2023), TUPA193 doi:10.18429/JACoW-IPAC2023-TUPA193
- [29] G. Normand, J. M. Lagniel and A. Orduz, "Strategies for SPIRAL2 linac heavy-ion beam tuning," *JACoW IPAC2023* (2023), TUPA192 doi:10.18429/JACoW-IPAC2023-TUPA192
- [30] J. Dumas, O. Kamalou, A. Orduz and E. Traykov, "Beam dynamics in the NEWGAIN project at GANIL-SPIRAL2," *JACoW IPAC2023* (2023), WEPL035 doi:10.18429/JACoW-IPAC2023-WEPL035
- [31] A. Orduz, P. E. Bernaudin, M. Di Giacomo, C. Jamet, J. M. Lagniel, G. Normand, A. Savalle and D. Uriot, "Commissioning and operation of the SPIRAL2 SC linac," *JACoW IPAC2023* (2023), FRXD3 doi:10.18429/JACoW-IPAC2023-FRXD3
- [32] Chance, T. Da Silva, B. Dalena and A. Ghribi, "Status and plans for the high energy booster of the future electron-positron collider FCC-ee," *JACoW IPAC2023* (2023), MOPL070 doi:10.18429/JACoW-IPAC2023-MOPL070
- [33] F. Osswald, E. Traykov, J. C. Thomas, J. Michaud, M. Heine and T. Durand, "Beam loss monitoring through emittance growth control and feedback with design," *JACoW IPAC2023* (2023), TUPA082 doi:10.18429/JACoW-IPAC2023-TUPA082
- [34] R. Abukeshek, H. Abualrob, A. Stocchi, L. Perrot, A. Fomin, J. Michaud, A. Bogacz, J. Benesch and B. Jacquot, "Magnetic Design of the Commutational Magnet and Quadrupoles for PERLE Accelerator," *JACoW IPAC2023* (2023), MOPA023 doi:10.1088/1742-6596/2687/2/022023
- [35] Dalena, T. Da Silva, A. Chance' and A. Ghribi, "Definition of tolerances and corrector strengths for the orbit control of the High-Energy Booster ring of the future electron-positron collider," *JACoW IPAC2023* (2023), MOPL054 doi:10.1088/1742-6596/2687/2/022004
- [36] A. Esper, M. H. Stodel, H. Savajols, M. Authier, M. Aburas, F. Carville, A. Drouart, B. Jacquot, A. Lefevre and F. Esnault, "Superconducting multipole triplet field measurements," *JACoW IPAC2023* (2023), THPA043 doi:10.1088/1742-6596/2687/7/072027
- [37] L. G. Sarmiento, T. Roger, J. Giovinzano, B. A. Brown, B. Blank, D. Rudolph, A. Kankainen, H. Alvarez-Pol, A. Arokia Raj and P. Ascher, *et al.* "Elucidating the nature of the proton radioactivity and branching ratio on the first proton emitter discovered ^{53m}Co," *Nature Commun.* **14** (2023) no.1, 5961 doi:10.1038/s41467-023-39389-2
- [38] M. Q. Hlatshwayo, J. Novak and E. Litvinova, "Quantum benefit of the quantum equation of motion for the strongly coupled many-body problem," *Phys. Rev. C* **109** (2024) no.1, 014306 doi:10.1103/PhysRevC.109.014306 [arXiv:2309.10179 [nucl-th]].
- [39] N. Gavrielov, J. E. Garcia-Ramos, P. Van Isacker and A. Leviatan, "Persistent vibrational structure in ^{110–116}Cd," *Phys. Rev. C* **108** (2023) no.3, L031305 doi:10.1103/PhysRevC.108.L031305 [arXiv:2309.09285 [nucl-th]].
- [40] N. Saneesh, D. Arora, A. Chatterjee, N. Kumar, A. Parihari, C. Kumar, I. Ahmed, S. Kumar, M. Kumar and A. Jhingan, *et al.* "Impact of multichance fission on fragment-neutron correlations in Pa227," *Phys. Rev. C* **108** (2023) no.3, 034609 doi:10.1103/PhysRevC.108.034609
- [41] G. Rucher, K. Prigent, C. Simard, A. M. Frelin, M. Coquemont-Guyot, N. Elie, N. Delcroix, N. Perzo, R. Guinamard

- and L. Berger, *et al.* "Targeted Radiation Exposure Induces Accelerated Aortic Valve Remodeling in ApoE^{-/-} Mice," *Journal of Clinical Medicine* **12** (2023) no.18, 5854 doi:10.3390/jcm12185854
- [42] A. Bahini, P. von Neumann-Cosel, J. Carter, I. T. Usman, N. N. Arsenyev, A. P. Severyukhin, E. Litvinova, R. W. Fearick, R. Neveling and P. Adsley, *et al.* "Fine structure of the isoscalar giant monopole resonance in Ni58, Zr90, Sn120, and Pb208," *Phys. Rev. C* **109** (2024) no.1, 014325 doi:10.1103/PhysRevC.109.014325 [arXiv:2309.04016 [nucl-ex]].
- [43] H. D. Thi, A. F. Fantina and F. Gulminelli, "Light clusters in the liquid proto-neutron star inner crust," *Eur. Phys. J. A* **59** (2023) no.12, 292 doi:10.1140/epja/s10050-023-01199-x [arXiv:2309.01533 [nucl-th]].
- [44] H. Dinh Thi, A. F. Fantina and F. Gulminelli, "The proto-neutron star inner crust in a multi-component plasma approach," *Astron. Astrophys.* **677** (2023), A174 doi:10.1051/0004-6361/202346606 [arXiv:2309.01527 [astro-ph.HE]].
- [45] Blank, J. C. Thomas, M. Gerbaux, P. Ascher, D. Atanasov, F. Cresto, Q. De'ignac, A. de Roubin, M. Flayol and Q. Gendre, *et al.* "Precise mass measurement of the ³²S member of the (A=32, T=2) quintet of analogue states," *J. Phys. Conf. Ser.* **2586** (2023) no.1, 012060 doi:10.1088/1742-6596/2586/1/012060
- [46] N. Goyal, S. Daumas-Tschopp, F. De Oliveira Santos, P. Delahaye, X. Flechard, J. M. Fontbonne, E. Lienard, L. M. Motilla, J. Perronnell and G. Quemener, *et al.* "Detection of recoil ion in the beta decay of laser oriented trapped radioactive isotopes for the MORA Project," *J. Phys. Conf. Ser.* **2586** (2023) no.1, 012142 doi:10.1088/1742-6596/2586/1/012142
- [47] M. Forge, O. Dorvaux, A. Lopez-Martens, K. Kessaci, B. J. P. Gall, K. Hauschild, Z. Asfari, R. Chakma, A. V. Yeremin and M. L. Chelnokov, *et al.* "New results on the decay spectroscopy of ²⁵⁴No with GABRIELA@SHELS," *J. Phys. Conf. Ser.* **2586** (2023) no.1, 012083 doi:10.1088/1742-6596/2586/1/012083
- [48] A. F. Fantina and F. Gulminelli, "Nuclear physics inputs for dense-matter modelling in neutron stars. The nuclear equation of state," *J. Phys. Conf. Ser.* **2586** (2023) no.1, 012112 doi:10.1088/1742-6596/2586/1/012112 [arXiv:2311.07144 [astro-ph.HE]].
- [49] Brugnara, A. Gottardo, M. Assie', D. Mengoni, A. Lemasson, E. Clement, F. Flavigny, D. Ramos, F. Galtarossa and A. Matta, *et al.* "The ⁴⁶Ar(³He, d)⁴⁷K direct reaction as a probe of the ⁴⁶Ar proton wavefunction," *J. Phys. Conf. Ser.* **2586** (2023) no.1, 012073 doi:10.1088/1742-6596/2586/1/012073
- [50] L. M. Donaldson, P. Adsley, A. Banu, S. Bassauer, B. Bastin, C. A. Bertulani, J. W. Bru"mmer, J. Carter, G. R. J. Cooper and R. W. Fearick, *et al.* "Nuclear-structure experiments at iThemba LABS to investigate discrepancies between (p, p') and (γ, xn) data," *J. Phys. Conf. Ser.* **2586** (2023) no.1, 012068 doi:10.1088/1742-6596/2586/1/012068
- [51] A. Ciampi *et al.* [INDRA-FAZIA], "Nuclear symmetry energy at work in heavy ion reactions: new results from the INDRA-FAZIA apparatus," *J. Phys. Conf. Ser.* **2586** (2023) no.1, 012039 doi:10.1088/1742-6596/2586/1/012039
- [52] M. Sguazzin, J. A. Swartz, B. Jurado, J. Pibernat, M. Grieser, J. Glorius, Y. A. Litvinov, R. Reifarth, K. Blaum and P. Alfaut, *et al.* "Determining neutron-induced reaction cross sections through surrogate reactions at storage rings," *J. Phys. Conf. Ser.* **2586** (2023) no.1, 012082 doi:10.1088/1742-6596/2586/1/012082
- [53] M. Le Joubiou, H. Savajols, W. Mittig, X. Fle'chard, L. Hayen, Y. E. Penionzhkevich, D. Ackermann, C. Borcea, L. Caceres and P. Delahaye, *et al.* "Search for a Neutron Dark Decay in He6," *Phys. Rev. Lett.* **132** (2024) no.13, 132501 doi:10.1103/PhysRevLett.132.132501 [arXiv:2308.16536 [nucl-ex]].
- [54] Y. Kondo, N. L. Achouri, H. A. Falou, L. Atar, T. Aumann, H. Baba, K. Boretzky, C. Caesar, D. Calvet and H. Chae, *et al.* "First observation of ²⁸O," *Nature* **620** (2023) no.7976, 965-970 [erratum: *Nature* **623** (2023) no.7988, E13] doi:10.1038/s41586-023-06352-6
- [55] C. Ciampi *et al.* [INDRA-FAZIA], "Quasiprojectile breakup and isospin equilibration at Fermi energies: Potential indication of longer projectile-target contact times," *Phys. Rev. C* **108** (2023) no.5, 054611 doi:10.1103/PhysRevC.108.054611 [arXiv:2308.15077 [nucl-ex]].
- [56] A. Jaries, M. Stryczyk, A. Kankainen, L. Al Ayoubi, O. Beliuskina, P. Delahaye, T. Eronen, M. Flayol, Z. Ge and W. Gins, *et al.* "High-precision Penning-trap mass measurements of Cd and In isotopes at JYFLTRAP remove the fluctuations in the two-neutron separation energies," *Phys. Rev. C* **108** (2023) no.6, 064302 doi:10.1103/PhysRevC.108.064302 [arXiv:2308.15270 [nucl-ex]].
- [57] E. Litvinova, "On the dynamical kernels of fermionic equations of motion in strongly-correlated media," *Eur. Phys. J. A* **59** (2023) no.12, 291 doi:10.1140/epja/s10050-023-01198-y [arXiv:2308.07574 [nucl-th]].
- [58] M. Ballan, S. Bottoni, M. Caamaño, A. Caciolli, M. Campostrini, M. Cicerchia, F. C. L. Crespi, S. Cristallo, D. Dell'Aquila and R. Depalo, *et al.* "Nuclear physics midterm plan at Legnaro National Laboratories (LNL)," *Eur. Phys. J. Plus* **138** (2023) no.8, 709 doi:10.1140/epjp/s13360-023-04249-x
- [59] J. Wis'niewski, W. Urban, T. Rzaca-Urban, K. Sieja, A. Blanc, M. Jentschel, C. Micheagnoli, P. Mutti, U. Ko"ster and G. de France, *et al.* "Structure of N=56 isotones with 36≤Z≤42 protons," *Phys. Rev. C* **108** (2023) no.2, 024302 doi:10.1103/PhysRevC.108.024302
- [60] T. Rzaca-Urban, W. Urban, A. Blanc, M. Jentschel, P. Mutti, U. Ko"ster, G. de France, G. S. Simpson and C. A. Ur, "Low-spin excitations in Zr95," *Phys. Rev. C* **108** (2023) no.1, 014324 doi:10.1103/PhysRevC.108.014324
- [61] A. Camaiani, S. Barlini, A. A. Stefanini, G. Casini, H. Alvarez-Pol, A. Arokiajaraj, L. Baldesi, R. Bolzonella, G. Cardella and C. Ciampi, *et al.* "Energy loss profile measurements using the ACTAR TPC demonstrator active target,"

- Nucl. Instrum. Meth. B **542** (2023), 188-194 doi:10.1016/j.nimb.2023.07.001
- [62] E. Cle'ment, A. Bracco, A. Gadea and J. Simpson, "Organisation of the AGATA collaboration and physics campaigns," Eur. Phys. J. A **59** (2023) no.7, 152 doi:10.1140/epja/s10050-023-01057-w
- [63] Thisse, M. Lebois, D. Verney, J. N. Wilson, N. Jovančević, M. Rudigier, R. Canavan, D. Etasse, P. Adsley and A. Algora, et al. "Study of $N = 50$ gap evolution around $Z = 32$: new structure information for ^{82}Ge ," Eur. Phys. J. A **59** (2023) no.7, 153 doi:10.1140/epja/s10050-023-01051-2
- [64] Rey-herme et al. [IGISOL], "Level structure of $\text{Ac}221$ and $\text{Fr}217$ from decay spectroscopy, and reflection asymmetry in $\text{Ac}221$," Phys. Rev. C **108** (2023) no.1, 014304 doi:10.1103/PhysRevC.108.014304
- [65] M. Colonna and A. Navin, "EURO-LABS: Europe's Super Community of Subatomic Researchers," Nucl. Phys. News **33** (2023) no.2, 3-4 doi:10.1080/10619127.2023.2198906
- [66] S. Chakraborty, S. Bhattacharyya, R. Banik, S. Bhattacharya, G. Mukherjee, C. Bhattacharya, S. Biswas, S. Rajbanshi, S. Dar and S. Nandi, et al. "Search for the origin of wobbling motion in the $A \approx 130$ region: The case of $\text{Xe}131$," Phys. Rev. C **107** (2023) no.6, 064318 doi:10.1103/PhysRevC.107.064318 [arXiv:2311.09713 [nucl-ex]].
- [67] D. A. Nesterenko, J. Ruotsalainen, M. Stryczyk, A. Kankainen, L. Al Ayoubi, O. Beliuskina, P. Delahaye, T. Eronen, M. Flayol and Z. Ge, et al. "High-precision measurements of low-lying isomeric states in $\text{In}120-124$ with the JYFLTRAP double Penning trap," Phys. Rev. C **108** (2023) no.5, 054301 doi:10.1103/PhysRevC.108.054301 [arXiv:2306.11505 [nucl-ex]].
- [68] Wang, M. Yasuda, Y. Kondo, T. Nakamura, J. A. Tostevin, K. Ogata, T. Otsuka, A. Poves, N. Shimizu and K. Yoshida, et al. "Intruder configurations in ^{29}Ne at the transition into the island of inversion: Detailed structure study of ^{28}Ne ," Phys. Lett. B **843** (2023), 138038 doi:10.1016/j.physletb.2023.138038 [arXiv:2306.16189 [nucl-ex]].
- [69] A. Lemasson, J. Dudouet, M. Rejmund, J. Ljungvall, A. Go'rgen and W. Korten, "Advancements of γ -ray spectroscopy of isotopically identified fission fragments with AGATA and VAMOS+," Eur. Phys. J. A **59** (2023) no.6, 134 doi:10.1140/epja/s10050-023-01053-0 [arXiv:2306.10818 [nucl-ex]].
- [70] J. Collado, S. Capra, A. Pullia, N. Karkour, C. Houarner, V. Gonzalez, G. Wittwer, A. Boujrad, M. Kogimtzis and J. Lawson, et al. "AGATA phase 2 advancements in front-end electronics," Eur. Phys. J. A **59** (2023) no.6, 133 doi:10.1140/epja/s10050-023-01045-0
- [71] J. D. Ovejas, I. Martel, D. Dell'Aquila, L. Acosta, J. L. Aguado, G. de Angelis, M. J. G. Borge, J. A. Briz, A. Chbihi and G. Colucci, et al. "Suppression of Coulomb-nuclear interference in the near-barrier elastic scattering of ^{17}Ne from ^{208}Pb ," Phys. Lett. B **843** (2023), 138007 doi:10.1016/j.physletb.2023.138007
- [72] N. Michel, W. Nazarewicz and M. Płoszajczak, "Description of the Proton-Decaying 0_2^+ Resonance of the α Particle," Phys. Rev. Lett. **131** (2023) no.24, 242502 doi:10.1103/PhysRevLett.131.242502 [arXiv:2306.05192 [nucl-th]].
- [73] J. P. Linares Fernandez, N. Michel, M. Płoszajczak and A. Mercenne, "Description of $\text{Be}7$ and $\text{Li}7$ within the Gamow shell model," Phys. Rev. C **108** (2023) no.4, 044616 doi:10.1103/PhysRevC.108.044616 [arXiv:2306.05215 [nucl-th]].
- [74] A. Lemasson and M. Rejmund, "Fast trajectory reconstruction techniques for the large acceptance magnetic spectrometer VAMOS+," Nucl. Instrum. Meth. A **1054** (2023), 168407 doi:10.1016/j.nima.2023.168407 [arXiv:2307.03752 [physics.ins-det]].
- [75] S. Raeder, B. Andelic, J. Auler, M. Block, P. Chauveau, P. Chhetri, A. Claessens, A. de Roubin, C. E. Du'Ilmann and R. Ferrer, et al. "Opportunities and limitations of in-gas-cell laser spectroscopy of the heaviest elements with RADRIS," Nucl. Instrum. Meth. B **541** (2023), 370-374 doi:10.1016/j.nimb.2023.04.044
- [76] Brunet, M. Michel, G. De France, V. Desmezie'res, B. Jacquot, C. Hocini, S. Ferey, J. Gueret, L. Rossard and M. Morisset, et al. "Design of a high power solid target for ^{211}At ," EPJ Web Conf. **285** (2023), 07001 doi:10.1051/epjconf/202328507001
- [77] P. Jardin, V. Bosquet, S. Damoy, G. Fre'mont, F. Perocheau and M. MacCormick, "Ni target development for the TULIP project," EPJ Web Conf. **285** (2023), 08001 doi:10.1051/epjconf/202328508001
- [78] A. Korichi, E. Cle'ment, N. Dosme, E. Legay, O. Ste'zowski, A. Goasduff, Y. Aubert, J. Dudouet, S. Elloumi and P. Gauron, et al. "AGATA DAQ-box: a unified data acquisition system for different experimental conditions," Eur. Phys. J. A **59** (2023) no.9, 211 doi:10.1140/epja/s10050-023-01091-8 [arXiv:2305.18653 [physics.ins-det]].
- [79] Y. Cho, Y. H. Kim, S. Choi, J. Park, S. Bae, K. I. Hahn, Y. Son, A. Navin, A. Lemasson and M. Rejmund, et al. "Particle identification at VAMOS+ with machine learning techniques," Nucl. Instrum. Meth. B **541** (2023), 240-242 doi:10.1016/j.nimb.2023.05.053 [arXiv:2311.07103 [physics.ins-det]].
- [80] R. M. Pe'rez-Vidal, F. Galtarossa, T. Mijatović, S. Szilner, I. Zanon, D. Brugnara, J. Pellumaj, M. Ciemala, J. J. Valiente-Dobó'n and L. Corradi, et al. "Nuclear structure advancements with multi-nucleon transfer reactions," Eur. Phys. J. A **59** (2023) no.5, 114 [erratum: Eur. Phys. J. A **59** (2023) no.6, 143] doi:10.1140/epja/s10050-023-01027-2
- [81] Michaud, P. Alfaut, A. Balana, B. Blank, L. Daudin, T. Kurtukian-Nieto, B. Lachacinski, L. Serani, J. C. Thomas and F. Varenne, "Commissioning of the DESIR high-resolution mass separator," Nucl. Instrum. Meth. B **541** (2023), 161-164 doi:10.1016/j.nimb.2023.05.013
- [82] P. Jardin, M. MacCormick, V. Bosquet, P. Chauveau, S. Damoy, P. Delahaye, M. Dubois, M. Fadil, M. Lalande and C. Michel, et al. "Sub-millisecond atom-to-ion transformation in the TULIP ISOL system," Nucl. Instrum. Meth. A **1055**

- (2023), 168332 doi:10.1016/j.nima.2023.168332
- [83] P. Chauveau, V. Bosquet, S. Damoy, P. Delahaye, M. Dubois, P. Jardin, M. Lalande, L. Maunoury and J. C. Thomas, "Latest improvements of the SPIRAL1 facility at GANIL," Nucl. Instrum. Meth. B **541** (2023), 61-64 doi:10.1016/j.nimb.2023.05.003
- [84] Y. Son, Y. H. Kim, Y. Cho, S. Choi, S. Bae, K. I. Hahn, J. Park, A. Navin, A. Lemasson and M. Rejmund, *et al.* "CATLIFE (Complementary Arm for Target Like Fragments): Spectrometer for Target like fragments at VAMOS++," Nucl. Instrum. Meth. B **540** (2023), 234-236 doi:10.1016/j.nimb.2023.04.024 [arXiv:2311.16165 [physics.ins-det]].
- [85] V. Bosquet, P. Jardin, M. MacCormick and C. Michel, "The TULIP project: First on-line result and near future," Nucl. Instrum. Meth. B **541** (2023), 106-108 doi:10.1016/j.nimb.2023.04.046 [arXiv:2304.14416 [physics.ins-det]].
- [86] A. Ajayakumar, J. Romans, M. Authier, Y. Balasmeh, A. Brizard, F. Boumard, L. Caceres, J. F. Cam, A. Claessens and S. Damoy, *et al.* "In-gas-jet laser spectroscopy with S³-LEB," Nucl. Instrum. Meth. B **539** (2023), 102-107 doi:10.1016/j.nimb.2023.03.020
- [87] J. Valiente-Dobón, R. Menegazzo, A. Goasduff, D. Aguiaro, P. Aguilera, F. Angelini, M. Balogh, D. Bazzacco, J. Benito and G. Benzoni, *et al.* "Conceptual design of the AGATA 2π array at LNL," Nucl. Instrum. Meth. A **1049** (2023), 168040 doi:10.1016/j.nima.2023.168040
- [88] H. Dinh Thi, A. F. Fantina and F. Gulminelli, "The proto-neutron star inner crust in the liquid phase," Astron. Astrophys. **672** (2023), A160 doi:10.1051/0004-6361/202245061 [arXiv:2304.01584 [astro-ph.HE]].
- [89] M. Kanafani, X. Flechard, O. Naviliat-Cuncic, G. D. Chung, S. Leblond, E. Lénard, X. Mougeot, G. Quémerner, A. S. D. Filippo and J. C. Thomas, "Precision measurements in the beta decay of ⁶He," EPJ Web Conf. **282** (2023), 01010 doi:10.1051/epjconf/202328201010
- [90] B. Dalena, T. Da Silva, A. Chance and A. Ghribi, "Definition of tolerances and corrector strengths for the orbit control of the High-Energy Booster ring of the future electro-positron collider," [arXiv:2303.17996 [physics.acc-ph]].
- [91] G. Lhersonneau, P. Jones, M. Fadil, T. Malkiewicz and W. H. Trzaska, "Experimental cross sections in fission of natural uranium induced by a neutron spectrum of 12.4-MeV average energy," Eur. Phys. J. Plus **138** (2023) no.3, 303 doi:10.1140/epj/s13360-023-03912-7
- [92] C. Frosin *et al.* [INDRA-FAZIA], "Examination of cluster production in excited light systems at Fermi energies from new experimental data and comparison with transport model calculations," Phys. Rev. C **107** (2023) no.4, 044614 doi:10.1103/PhysRevC.107.044614 [arXiv:2303.17390 [nucl-ex]].
- [93] S. Piantelli *et al.* [FAZIA], "Characterization of the breakup channel in the asymmetric systems Ca40,48+C12 at 25 and 40 MeV/nucleon," Phys. Rev. C **107** (2023) no.4, 044607 doi:10.1103/PhysRevC.107.044607 [arXiv:2303.13215 [nucl-ex]].
- [94] Á. Koszorús, M. Block, P. Campbell, B. Cheal, R. P. de Groot, W. Gins, I. D. Moore, A. Ortiz-Cortes, A. Raggio and J. Warbinek, "High-precision measurements of the hyperfine structure of cobalt ions in the deep ultraviolet range," Sci. Rep. **13** (2023) no.1, 4783 doi:10.1038/s41598-023-31378-1
- [95] F. Osswald, E. Traykov, T. Durand, M. Heine, J. Michaud and J. C. Thomas, "Challenges in low losses and large acceptance ion beam transport," [arXiv:2303.06969 [physics.acc-ph]].
- [96] M. Urquiza-González, M. Au, C. Bernerd, M. Bissell, B. van den Borne, K. Chrysalidis, T. E. Cocolios, V. N. Fedosseev, K. T. Flanagan and R. G. Garcia Ruiz, *et al.* "Benchmark evaluation for a single frequency continuous wave OPO seeded pulsed dye amplifier for high-resolution laser spectroscopy," doi:10.1117/12.2646665
- [97] O. Steżowski, J. Dudouet, A. Goasduff, A. Korichi, Y. Aubert, M. Balogh, G. Baulieu, D. Bazzacco, S. Brambilla and D. Brugnara, *et al.* "Advancements in software developments," Eur. Phys. J. A **59** (2023) no.5, 119 doi:10.1140/epj/a/s10050-023-01025-4 [arXiv:2303.01275 [physics.ins-det]].
- [98] D. Ackermann, "Nuclear Isomers in the Heaviest Nuclei — the Odd Nucleon as a Sensitive Probe of Low-lying Nuclear Structure," Acta Phys. Polon. Supp. **16** (2023) no.4, 9 doi:10.5506/APhysPolBSupp.16.4-A9
- [99] N. Cieplicka-Oryńczak, B. Fornal, M. Ciemała, M. Kmiecik, A. Maj, J. Łukasik, P. Pawłowski, B. Sowicki, B. Wasilewska and M. Ziebliński, *et al.* "M4 Resonances in Light Nuclei Studied at CCB," Acta Phys. Polon. Supp. **16** (2023) no.4, A4 doi:10.5506/APhysPolBSupp.16.4-A4
- [100] J. Romero, K. Auranen, M. Block, A. D. Briscoe, T. Eronen, W. Gins, T. Grahn, P. T. Greenlees, A. Illana and R. Julin, *et al.* "Nuclear Reaction Studies and Prospects for the New MARA-LEB Facility," Acta Phys. Polon. Supp. **16** (2023) no.4, A12 doi:10.5506/APhysPolBSupp.16.4-A12
- [101] A. Utepov, D. Ackermann, C. Stodel, A. Lemasson, D. Ramos, M. Rejmund, E. Clement, B. Jacquot, J. Piot and J. E. Ducret, *et al.* "Multinucleon Transfer Reactions in the ²³⁸U + ²³⁸U System Studied with the VAMOS+AGATA+ID-Fix," Acta Phys. Polon. Supp. **16** (2023) no.4, A11 doi:10.5506/APhysPolBSupp.16.4-A11
- [102] J. P. Linares Fernandez, M. Płoszajczak and N. Michel, "Gamow Shell Model Description of ⁷Li and Elastic Scattering Reaction ⁴He(³H,³H)⁴He," Acta Phys. Polon. Supp. **16** (2023) no.4, 22 doi:10.5506/APhysPolBSupp.16.4-A22 [arXiv:2304.00602 [nucl-th]].
- [103] P. E. Georgoudis, "A + 2n compound nuclei and the unitary limit in nuclear physics," J. Phys. Conf. Ser. **2453** (2023) no.1, 012023 doi:10.1088/1742-6596/2453/1/012023 [arXiv:2304.02400 [nucl-th]].
- [104] D. Simon, T. Cadoux, E. Fernandez Mora, B. Hervieu, C. Berriaud, M. Segreti, G. Minier, E. Rochepault, R. Vallcorba and A. Sinanna, *et al.* "Design of ASTERICS: A Superconducting 28 GHz ECR Ion Source Magnet for GANIL,"

- IEEE Trans. Appl. Supercond. **33** (2023) no.5, 4002905 doi:10.1109/TASC.2023.3260779
- [105] Sguazzin, B. Jurado, J. Pibernat, J. A. Swartz, M. Grieser, J. Glorius, Y. A. Litvinov, R. Reifarth, K. Blaum and P. Alfaut, *et al.* "Indirect measurements of neutron-induced reaction cross sections at storage rings," EPJ Web Conf. **279** (2023), 11006 doi:10.1051/epjconf/202327911006
- [106] Lalanne, O. Sorlin, A. Poves, M. Assie, F. Hammache, S. Koyama, D. Suzuki, F. Flavigny, V. Girard-Alcindor and A. Lemasson, *et al.* "*N=16* Magicity Revealed at the Proton Drip Line through the Study of *Ca35*," Phys. Rev. Lett. **131** (2023) no.9, 092501 doi:10.1103/PhysRevLett.131.092501 [arXiv:2302.14382 [nucl-ex]].
- [107] D. P. Carrasco-Rojas, M. Williams, P. Adsley, L. Lamia, B. Bastin, T. Faestermann, C. Fouge`res, F. Hammache, D. S. Harrouz and R. Hertzenberger, *et al.* "Searching for resonance states in *Ne22(p,γ)Na23*," Phys. Rev. C **108** (2023) no.4, 045802 doi:10.1103/PhysRevC.108.045802 [arXiv:2302.12939 [nucl-ex]].
- [108] C. Haquin, O. Delahaye, C. Patard, F. Pillon, J. Pivard and G. Se`ne`cal, "How GANIL Plan to Use Web Technologies to Update the Control System User Interfaces," JACoW **PCaPAC2022** (2023), THO14 doi:10.18429/JACoW-PCaPAC2022-THO14
- [109] J. Lois-Fuentes, B. Fernandez-Dominguez, X. Pereira-Lopez, F. Delaunay, W. N. Catford, A. Matta, N. A. Orr, T. Duguet, T. Otsuka and V. Soma, *et al.* "Cross-shell states in *15C*: A test for *p-sd* interactions," Phys. Lett. B **845** (2023), 138149 doi:10.1016/j.physletb.2023.138149 [arXiv:2302.08382 [nucl-ex]].
- [110] A. Doudard, A. Corroyer-Dulmont, C. Jaudet, M. Bernaudin, S. Valable, X. Ledoux and A. Frelin-Labelme, "Application of a new spectral deconvolution method for in vitro dosimetry in assessment of targeted alpha therapy," Med. Phys. **50** (2023) no.6, 3762-3772 doi:10.1002/mp.16279
- [111] D. Ramos, M. Caamaño, F. Farget, C. Rodríguez-Tajes, A. Lemasson, C. Schmitt, L. Audouin, J. Benlliure, E. Casarejos and E. Clement, *et al.* "Experimental evidence of the effect of nuclear shells on fission dissipation and time," Phys. Rev. C **107** (2023) no.2, L021601 doi:10.1103/PhysRevC.107.L021601 [arXiv:2302.13856 [nucl-ex]].
- [112] B. Bastin, J. Kiener, I. Deloncle, A. Coc, M. Pospelov, J. Mrazek, L. Lamia, D. Ackermann, P. Adsley and C. O. Bacri, *et al.* "Investigation of a light Dark Boson existence: The New JEDI project," EPJ Web Conf. **275** (2023), 01012 doi:10.1051/epjconf/202327501012
- [113] D. Godos-Valencia, L. Acosta, P. Ascher, B. Blank, J. Giovinazzo, F. de Oliveira Santos, C. Fouge`res and A. M. Sa´nchez- Ben´itez, "Experimental studies of the ^{46}Mn β^+ -decay channel and spectroscopy of ^{46}Cr at LISE-GANIL," EPJ Web Conf. **275** (2023), 02005 doi:10.1051/epjconf/202327502005
- [114] E. Cle´ment, A. Lemasson, M. Rejmund, B. Jacquot, D. Ralet, C. Michelagnoli, D. Barrientos, P. Bednarczyk, G. Ben-zoni and A. J. Boston, *et al.* "Spectroscopic quadrupole moments in *Xe124*," Phys. Rev. C **107** (2023) no.1, 014324 doi:10.1103/PhysRevC.107.014324
- [115] A. Sorensen, K. Agarwal, K. W. Brown, Z. Chajecski, P. Danielewicz, C. Drischler, S. Gandolfi, J. W. Holt, M. Kaminski and C. M. Ko, *et al.* "Dense nuclear matter equation of state from heavy-ion collisions," Prog. Part. Nucl. Phys. **134** (2024), 104080 doi:10.1016/j.pnpnp.2023.104080 [arXiv:2301.13253 [nucl-th]].
- [116] J. Angot, O. Tarvainen, P. Chauveau, S. Kosonen, T. Kalvas, T. Thuillier, M. Migliore and L. Maunoury, "The longitudinal en-ergy spread of ion beams extracted from an electron cyclotron resonance ion source," JINST **18** (2023) no.04, P04018 doi:10.1088/1748- 0221/18/04/P04018 [arXiv:2301.07395 [physics.acc-ph]].
- [117] A. Mercenne, N. Michel, J. P. Linares Fern´andez and M. Płoszajczak, "Gamow shell model description of the *Ca40(d,p)* transfer reaction," Phys. Rev. C **107** (2023) no.1, L011603 doi:10.1103/PhysRevC.107.L011603 [arXiv:2301.05419 [nucl-th]].
- [118] Sguazzin, B. Jurado, J. Pibernat, J. A. Swartz, M. Grieser, J. Glorius, Y. A. Litvinov, R. Reifarth, K. Blaum and P. Alfaut, *et al.* "Indirect measurements of neutron-induced reaction cross sections at heavy-ion storage rings," EPJ Web Conf. **284** (2023), 01008 doi:10.1051/epjconf/202328401008
- [119] L. T. Bott, K. Go`bel, M. Heil, A. Kelic`-Heil, R. Reifarth, M. Aliotta, T. Almusidi, H. Alvarez-Pol, L. Atar and L. Atkins, *et al.* "Coulomb dissociation of ^{16}O into ^4He and ^{12}C ," EPJ Web Conf. **279** (2023), 04003 doi:10.1051/epjconf/202327904003
- [120] D. Fern´andez, M. Caamaño, D. Ramos, A. Lemasson, M. Rejmund, H. A´lvarez-Pol, L. Audouin, J. D. Frankland, B. Fern´andez-Dom´inguez and E. Galiana-Baldo´, *et al.* "Experimental study of high-energy fission and quasi-fission dynamics with fusion-induced fission reactions at VAMOS+," EPJ Web Conf. **284** (2023), 04009 doi:10.1051/epjconf/202328404009
- [121] A. Chatillon, G. Boutoux, T. Gorbinet, L. Grente, J. F. Martin, E. Pellereau, J. Taieb, H. Alvarez-Pol, L. Audouin and Y. Ayyad, *et al.* "Fission-fragment yields measured in Coulomb-induced fission of $^{234,235,236,238}\text{U}$ and $^{237,238}\text{Np}$ with the $R^3\text{B}/\text{SOFIA}$ setup," EPJ Web Conf. **284** (2023), 04002 doi:10.1051/epjconf/202328404002

II. CONFERENCE LIST

In 2023, GANIL hosted or organized different workshops and schools:

- “WS SOURCES” organised by Mickael Dubois, 18-19 May, 87 participants
- “Colloque GANIL” organised by Pierre Delahaye & Muriel Fallot, 25-29 September, 111 participants
- “19th Russbach School on Nuclear Astropysics” organised by Olivier Sorlin, 12-18 March, 64 participants
- “The 4th French-Czech “Barrande” Nuclear Research workshop” organised by François de Oliveira, Véronique Debord-Lazar and Jaromír Mrázek, 10-12 October, 37 participants.

III.COMMITTEES

1. MEMBERS OF THE GANIL USERS EXECUTIVE COMMITTEE (GUEC)

Beatriz Fernandez Dominguez (USC, Spain) - chair
Franco Galtarossa (Padova, Italy)
Michal Ciemala (Krakow, Poland)
Hervé Savajols (GANIL, France)
Iolanda Matea (IJCLab, France)
John Frankland (GANIL, secretary and management liaison)
Marika Schleberger (University Duisburg-Essen, Germany)
Jose Lay (University of Sevilla, Spain)

2. MEMBERS OF THE PROGRAM ADVISORY COMMITTEE (PAC)

Mandate – March 2019-July 2024

DE OLIVEIRA François – GANIL, Caen, France
JUNGHANS Arnd - HZDR Dresde, Germany
LACROIX Denis – IJCLab, Paris Saclay, France
OBERTELLI Alexandre - TU Darmstadt, Germany
RIDIKAS Danas- IAEA Vienna, Austria

Mandate – February 2022 to February 2026

ASAI Masato - JAEA, Ibaraki, Japan
GAUDEFROY Laurent - CEA DAM, Bruyères-le-Châtel, France
LEIFELS Yvonne - GSI, Darmstadt, Germany
MORO Antonio - University Sevilla, Sevilla, Italy
OBERSTEDT Stephan - JRC Geel, Geel, Belgium
PETRI Marina - University York, Heslington, United Kingdom
TUMINO Aurora - University Kore, Enna, Italy

3. MEMBERS OF THE INTERDISCIPLINARY PROGRAM ADVISORY COMMITTEE (IPAC)

LORENZ Katharina - Instituto Superior Técnico (IST), Universidade de Lisboa, Instituto de Plasmas e Fusão Nuclear/Laboratório de Aceleradores e Tecnologias de Radiação, Lisbon, Portugal
MANTI Lorenzo - University of Naples Federico II, Naples, Italy
MCCOUSTRA Martin R. S. - Heriot-Watt University,Edimburg, Scotland
SICARD-ROSELLI Cécile - Laboratoire de Chimie Physique, Université de Paris-Sud, Orsay, France
SIMS* Ian, Institut de Physique de Rennes, UMR 625 - Université de Rennes 1, Rennes, France
TOIMIL-MOLARES Maria Eugenia - GSI Helmholtzzentrum für Schwerionenforschung GmbH Materials Research, Darmstadt, Germany

4. MEMBERS OF THE ACCELERATOR ADVISORY COMMITTEE (AAC)

Maud Baylac (IN2P3/LPSC)
Romuald Duperrier (DRF/Irfu)
Daniela Kiselev (PSI)
Marco Calviani (CERN)
Nancy Postiau (University Louvain)
Udo Weinrich (GSI/FAIR)

5. MEMBERS OF THE SCIENTIFIC COUNCIL

Mandate 2022-2026

Amine Cassimi - CIMAP, France
Anna Corsi - Irfu/DPhN, France
Anne-Marie Frelin - GANIL, France
Fabiana Gramegna - LNL INFN, Italy
Ferid Haddad - ARRONAX, France
Michal Kowal - NCBJ, Varsovie, Poland
Alain Letourneau - Irfu/DPhN, France
Nathalie Moncoffre - IP2IL EMIR&A, France
Iain Moore - Jyfl, Finland
Jaromir Mrazek - NPI, Czech Republic
Christoph Scheidenberger - GSI Darmstadt, Germany
David Verney - IJCLab France

Mandate 2019-2023

Ani Aprahamian - Univ Notre Dame, USA
Jerome Giovinazzo - CENBG, France
Rituparna Kanungo - Triumpf, Canada
R.G. Pillay - TIFR Mumbai, India
Bob Tribble - TAMU, USA

Ex-officio members:

Chairperson GANIL PAC
Chairperson GANIL GUEC
Chairperson Interdisciplinary PAC

6. REPORT OF THE SCIENTIFIC COUNCIL

INTRODUCTION

The GANIL Scientific Council (SC) met January 17-18, 2023, in a hybrid format. During the first day of the meeting, the SC heard an update detailing on-going activities from Director Patricia Chomaz, which was followed by presentations of possible future initiatives. Attending the meeting for the SC in person were Amine Cassimi, Anna Corsi, Anne-Marie Frelin, Fabiana Gramegna, Férid Haddad, Michal Kowal, Alain Letourneau, Jaromír Mrázek, Nathalie Moncoffre, Iain Moore, David Verney, and Robert Tribble (chair). On-line were Rituparna Kanungo and R.G. Pillay. Also attending was the PAC Chair, Stephan Oberstedt.

The previous SC meeting was held via zoom early in February, 2021, during the height of COVID-19. Much has happened at GANIL during the intervening two years. The progress on commissioning the LINAC in 2021 and then using it for a very successful campaign of research at NFS was a highlight for the facility. Indeed, the success of this campaign is a major step forward toward more routine SPIRAL2 operations. In addition to the work at NFS, the accelerator team produced the first heavy-ion beam in the LINAC in September, 2022. This was another major milestone in the development of SPIRAL2. Today, only NFS is available for SPIRAL2 operations but this will change over the next few years. Next to come on line should be S³. This spectrometer system will be a powerful tool for developing secondary beams of radioisotopes. A report on the commissioning activities associated with S³ was given at the meeting. Detailed comments on the report are included below. Two other major efforts related to SPIRAL2 are also progressing—DESIR and NEWGAIN. The DESIR facility will complement the capabilities of S³ and will greatly expand the program of research on rare isotopes. Both S³ and DESIR will benefit from the higher heavy-ion beam intensities that will be made available from NEWGAIN, which will be optimized to produce beams of A/Q=7 rather than A/Q=3 for the existing injector. With all of these facilities in operation, SPIRAL2 will be able to carry out the world-leading nuclear science program that led to its initiation.

The cyclotrons at GANIL continue to generate new science. The SC notes that they are in high demand by GANIL users. During 2022, cyclotron operations provided new data for several major collaborations. However, problems with unscheduled maintenance limited their overall performance. The cyclotrons now are more than four decades old and are in need of maintenance to reduce lost time due to water leaks inside the vacuum vessels. A plan has been developed—CYREN—to carry out a program of maintenance by replacing resonator cavities. Funding for this work will be crucial to maintain routine operations of the cyclotrons.

Looking ahead, GANIL management is now developing plans to have simultaneous operation of the cyclotrons and the LINAC. This will be very important for the future program as it could provide a path for carrying out science with the LINAC while using cyclotron beams for both science and applications. The GANIL facility is one of the best infrastructures in the EU for carrying out irradiations of electronics for space applications. Today a relatively small amount of time is used for this work. In the future, a larger share of time could be used, but this requires a business plan with a charging scheme that provides the resources for staff to maintain such a broader program, and support for maintenance that would be needed to make a larger amount of beam time available.

At our session on January 18, Director Chomaz gave an overview of the labs future plans, which included a discussion of the report about GANIL's future that was authored by a committee chaired by Professor Michel Spiro. The SC looks forward to continued discussion of GANIL's long term vision and its goals both near and far term at future meetings.

With the change of management and the lapse of two years in SC meetings, some of the recommendations from the 2021 report of the SC were lost. One in particular is sufficiently important that the SC puts it back into this report. In 2021, the recommendation was prompted by the discussion of the workforce needed to carry out simultaneous operation of the LINAC and cyclotrons. As this is an ongoing effort, **the council recommends that a session devoted to workforce concerns and development at all levels, including theory, be included in the next SC meeting.**

Following a discussion of each initiative presented to the SC, a list of recommendations from the 2023 meeting are summarized here:

- The SC recommends that a session devoted to workforce concerns and development at all levels, including theory, be included in the next SC meeting.
- The SC recommends that the collaboration [(NA)2STARS] specify the niche experiments that can be done at the GANIL facility as they develop an MoU with GANIL. It further suggests the addition of GANIL collaborators within the project.
- The SC recommends that an MOU is needed to organize the collaboration [REPARE] among GANIL and medical and biology centers of the Caen region, and to clearly identify commitments of its members. Clear identification of needed investment is mandatory for GANIL and other partners that will take care of the chemistry, radiobiology and radiolabeling as well as preserving the option to move GANIL to SPIRAL2 Phase 2 as recommended in the recent report on GANIL's future.
- The SC notes that it is planned to install this platform [MIRRPLA] in the D2 room of GANIL. This room is currently cluttered and it will be necessary to clear it, make it clean and equip it to receive this new equipment. The workforce and budget requirements on the part of GANIL to allow this installation in D2 seem to be very limited. However, technical adaptations necessary to install MIRRPLA in the D2 room need to be further specified and quantified. The effort from GANIL for the platform installation in the D2 room needs to be estimated.
- The SC recommends to continue the support for the [NEW JEDI] project with respect to the following points:
 - The collaboration maintains a reasonably low-medium material/financial demand;
 - Workforce (students) requirements that are justified (also in the case of a negative outcome of the analysis);
 - The experimental equipment obtained during the project remains in GANIL;

- If a positive result is found for X17, the SC recommends that the [NEW JEDI] collaboration **define the strategy** for the follow-up experiment(s), since GANIL may find itself in a unique position in this potentially new branch of research.

The SC has the following recommendations for S³ commissioning.

- We recommend that GANIL management prioritize a rapid commissioning of the S³ spectrometer.
- We recommend that the S³ scientific collaboration work out a plan for first exploratory physics runs simultaneously while commissioning the spectrometer and the focal plane detectors. The physics cases to be studied during commissioning should evolve through consensus from the collaboration and should be factored into the time allotted for S³ commissioning.
- In particular, physics cases that are easily feasible from already demonstrated beams should be chosen. A list of three possible LEB experiments during commissioning was presented. The physics outcome from each needs to be specifically reviewed for international competitiveness. This was not clearly presented. One experiment each with ⁴⁰Ar and ⁵⁰Cr beams could be planned. Although the latter is expensive the structure information around ¹⁰⁰Sn will be of high scientific value.
- It was not clear if the possible commissioning experiments with SIRIUS were only to verify published results or if they will also have the potential for some new physics information, too. It is recommended that the collaboration work out a strategy for first experiments. The ²²Ne+Pt → ²¹⁶⁻²²⁰Ra → ²¹⁰⁻²¹⁴Ra has a large cross section, hence might be a simpler case to start with if sufficient new physics information can be derived.
- The standalone cryogenic plants and the cryogenic distribution lines need to be fully tested and should be very robust and trouble-free. This aspect needs to be simultaneously ensured, as stable cryogenics is critical for the operation of the spectrometer as a whole and can more often than not, derail the schedule during the commissioning phase.

Below the SC provides reports on the presentations and associated write-ups for (NA)²STARS, REPARE in LHE, MIRPLA, NEW JEDI, and S³ Commissioning.

(NA)²STARS

The goal of the (NA)²STARS project is the development of a second-generation Total Absorption Spectrometer (TAS), combining efficiency as a calorimeter, segmentation as well as very good energy resolution and timing. The latter characteristics differ from existing spectrometers and will be realized by the addition of (up to 16) LaBr₃ crystals. The project will oversee the upgrade of both DTAS (as originally designed for DESPEC, NUSTAR) as well as Rocinante.

The TAGS technique uniquely addresses limitations in high-resolution gamma-ray spectroscopy by accessing the full beta decay strength within the Q-value window, solving the so-called Pandemonium effect. It is the best method of accessing the beta-decay strength, providing critical constraints on theoretical models of nuclear structure, complementary (and yet more sensitive) to integral observables such as half-lives and P_n values.

A compelling physics program that can be addressed by the TAS technique is outlined. Regions of nuclear structure interest include ¹⁰⁰Sn, ¹³²Sn and ⁷⁸Ni. For each region, the advantages of the new spectrometer are presented including improved energy resolution, gamma-neutron

resolution, as well as potential gamma-gamma correlations. Nuclear astrophysics plays an important role with relevant beta decays in the mass A~80 region, the r-process region around ¹³²Sn and ⁷⁸Ni, and accurate measurements of the gamma component of the neutron/gamma ratio to constrain neutron capture rates. These regions are also favorable for the study of low-lying collective modes through beta decay. Additional topics include core-collapse supernovae, ⁴⁴Ti nucleosynthesis and the origin of p-nuclei. A third main scientific focus relates to neutrino physics and applications with nuclear reactors, including reactor and shape anomalies, as well as the reactor decay heat.

The device can be flexibly used at LISE, S³-LEB, and DESIR, and thus the timetable is adaptable to the expected commissioning of these facilities. Letters of Intent were originally proposed for DESIR, combining the TAS with the Piperade Penning trap to achieve isobaric cleanliness. Possibilities to couple the TAS after the multi-reflection time-of-flight (MR-TOF) mass spectrometer at S³-LEB are encouraging, as well as more immediate implications with the LISE spectrometer. The SC noted that complementary activities are underway at several other facilities, e.g., RIKEN, Jyväskylä, GSI and ISOLDE. Due to a lack of access to neutron-rich nuclei, aspects of the physics program cannot currently be performed at GANIL, and it was not clear from the proposal what the niche experiments would be in the immediate and longer-term.

The proposed instrumentation is discussed regarding the current state-of-the-art worldwide, also noting the potential disadvantage that arises from the large intrinsic radioactive background from the LaBr₃ crystals and how this is mitigated via tagging. It is mandatory to understand the response of the crystals and studies of prototypes have been performed and compared with Monte Carlo simulations. Design studies of the STARS setup based on the DTAS have been started by the Subatech group with GEANT4. The SC would have appreciated additional simulations to illustrate the added advantage of the LaBr₃ crystals. This would have afforded an evaluation of whether they bring a major improvement to the capabilities of existing segmented TAS devices, or a more incremental improvement. In connection to this aspect, the SC noted that the granularity of the proposed TAS detectors offers flexibility in the funding timeline for implementing the full 16 crystals. Nevertheless, an opportunity was missed to address the impact on the scientific program with a reduced number of crystals should the project be de-scoped.

The collaboration within (NA)²STARS gathers the leading experts of the TAGS technique in Europe. The IFIC team of Valencia have the expertise to build the detectors and have developed the rigorous analysis codes necessary to extract the requisite data. The IFIC partners will play a critical role at every step of the project. Other partners include CIEMAT Madrid, who have contributed to the analysis methods, have developed tools to address neutron interactions with matter in GEANT4, co-developed and built the MONSTER neutron detector and have general expertise in nuclear instrumentation. IP2I Lyon have expertise in gamma-ray simulations and will oversee the design of STARS with GEANT4 for in-beam cross-section measurements at Neutrons for Science (NFS). The scientific coordinator, Muriel Fallot, is from Subatech. Fallot has been the spokesperson for several TAGS experiments motivated by neutrino physics and Pygmy modes. The Subatech group has excellent visibility as shown by several published articles, and has the expertise needed to analyze and estimate the impact of the TAGS measurements on antineutrino spectra.

The project has a clear management structure, with annexes including details of nine work packages, the institutional breakdown with requisite responsibilities as well as the timeline projected from the various tasks for the upgrade of both DTAS and Rocinante.

Recommendations and summary

The SC recommends that the collaboration specify the niche experiments that can be done at the GANIL facility as they develop an MoU with GANIL. It further suggests the addition of GANIL collaborators within the project. Given the opportunity to use this device at other facilities to optimize the scientific output, the Council recommend that the GANIL management weigh the options of purchasing the required LaBr₃ detectors with asking the partners to explore funding opportunities through national funding agencies and other funding calls, e.g., ANR.

In summary, the SC members are positive towards the (NA)²STARS project.

REPARE in the LHE

The goal of the project “REPARE in the LHE” is to install a high-power target system for the production of innovative radioelements for targeted alpha therapy (TAT) in the high energy line (LHE) of the SPIRAL2 building. The target system is developed within the REPARE project financed by the French Research Agency ANR, and is planned to be used starting in 2023 to produce ²¹¹At using the alpha beam from SPIRAL2 at NFS. The ANR REPARE is part of a larger project that aims to develop the full chain from the synthesis of ²¹¹At up to clinical trials in

collaboration with medical and biology centers of the Caen region. In addition to the direct production of ^{211}At , the collaboration wants to investigate the production of a ^{211}Rn generator that will decay to ^{211}At . This may be a way to allow distribution in a larger area and therefore easier exploitation. The installation of a high-power target in a dedicated zone in the LHE will allow to efficiently carry on this research plan without interfering with other experiments foreseen in the SPIRAL2 building.

The context of the REPARE project follows a worldwide increasing interest for targeted radionuclide therapy (TRT) which has proven to be particularly effective to treat specific kinds of cancer which resist conventional therapies, minimizing the collateral effects. Among TRT, TAT is a modality that is of great potential thanks to the high linear energy transfer of alpha particles and their high relative biological effectiveness. Only few alpha emitters can be used for TAT among which are ^{225}Ac and ^{211}At , which can be produced using accelerators. Alpha or ^7Li beams, as provided by the SPIRAL2 accelerator, are necessary to produce ^{211}At directly or through ^{211}Rn . Thanks to the availability of an intense alpha (^7Li) beam, only few hours of beam time will be needed to obtain the activity necessary for a patient dose to perform clinical trials.

A budget of 1.116 M€ has been estimated to build the new beam line, plus 221 k€ for the new casemate. The PI intends to apply to funding agencies to finance this construction, and requests that GANIL grants scientific support, a dedicated space in the LHE, manpower and beam at the rate of 4 hours per week to the project.

The SC thinks that GANIL will benefit from such a research program with very high potential societal impact and great interest from the local government. Furthermore, this program fits very well with the activity assigned for GANIL (more specifically, the development of innovative techniques for hadron therapy and radiobiology) and is recommended in the report of the “Spiro committee” for the future of GANIL.

At the GANIL level, the construction of a third hall in the SPIRAL2 building may be an opportunity also for other experiments because it will allow for the possibility to switch more quickly from one experiment to another and make more efficient use of the beam time. The SC suggests that the design of the new beam line needs to be optimized to minimize the costs. It also points out that a special care on radioprotection is needed as it is a non-conventional activity on the GANIL site temporarily producing a high level of radioactivity around the target station.

To be able to play a role in medical research, one production run per week (preferably at the beginning of the week to let people have time for follow-up mice or patient procedures) is mandatory.

It is important that this project not impact the other main projects of GANIL (S^3 , DESIR and NEWGAIN). For this reason, after the R&D phase is concluded, the radioisotope production has to be handed to industrial companies. The goal of GANIL and the consortium around this project is the study of new production methods and the validation of the full chain up to clinical trials. In this sense, the SC recommends that the collaboration work towards a portfolio of new radioisotope studies beyond ^{211}At that may benefit from the specificity of this new installation in the SPIRAL2 facility.

- The SC recommends that an MOU is needed to organize the collaboration among GANIL and medical and biology centers of the Caen region and to clearly identify commitments of its members. Clear identification of needed investment is mandatory for GANIL and others for partners that will take care of the chemistry, radiobiology and radiolabeling as well as preserving the option to move GANIL to SPIRAL2 Phase 2 as recommended in the recent report on GANIL’s future.

MIRRPLA (Multiple-beam IRRadiation PLAtform to investigate the origin of organic matter) project

MIRRPLA is part of the PEPR Origins, from planets to life – technological, societal and epistemic breakthroughs, with a budget of 45.5 million euros over 7 years. It is included in a Work Package of the axis 4, on the emergence of life. MIRRPLA is already funded (equipment of about 800 k€ and personnel costs around 270 k€). The scientific value of the project has also been evaluated positively in the framework of this accepted PEPR Origins.

The MIRRPLA platform consists of a unique ultrahigh vacuum chamber, combining three types of irradiation sources (UV photons, keV electrons and keV-GeV ions), equipped with in situ

infrared and mass spectrometers. This device meets the challenge of the PEPR to build the most efficient and appropriate tools to understand the complex mechanisms at the origin of life.

The selected ionizing beams, including those of GANIL available in a wide range of particle type and energy, are very relevant to simulate the processes that occur in space such as the solar wind and cosmic rays. These ionizing radiations will be used independently or in combination. For the first time it will be possible to study potential synergistic effects, where there is no data yet. It is very interesting to mention the possibility to irradiate with heavy ions, which, even if they are a minority in space compared to electrons and photons, have a great impact on the behavior of space matter, either organic or inorganic.

This field of research has been very active in GANIL for several years. The beginning of this project is linked to the work on polymers carried out at CIMAP for many years, which gradually led to the design of this very original device. The PEPR origins provides an excellent opportunity for the CIMAP teams to benefit from the skills and expertise acquired in this field to upgrade experiment capabilities in this research field with the MIRRPLA Platform. This expertise will be complemented by the collaboration of the PIIM laboratory, partner of the PEPR Origins, expert in photon and electron irradiations.

The field of investigation is huge and complex. The first experiments will use 1 μm thick ice samples made of simple carbonaceous molecules, to simulate icy mantles. The targets will be progressively made more complex.

The committee wishes to emphasize the unique character of this new setup which should make GANIL highly attractive for the astrophysics community and to new external collaborations. The platform will be open to the whole scientific community via GANIL-CIMAP-CIRIL user's facility. This project will certainly contribute to the international visibility of GANIL and CIMAP.

Recommendations

It is planned to install this platform in the D2 room of GANIL. This room is currently cluttered and it will be necessary to clear it, make it clean and equip it to receive this new equipment. The workforce and budget requirements on the part of GANIL to allow this installation in D2 seem to be minimal. However, technical adaptations necessary to install MIRRPLA in the D2 room need to be further specified and quantified. The effort from GANIL for the platform installation in the D2 room needs to be estimated.

NEW JEDI

The main goal of the NEW JEDI project is to find a signal verifying the existence of a light X boson with a mass of 17 MeV that has been hypothesized from recent measurements of ^8Be decay. Studies planned to be carried out at GANIL and iThemba LABS were triggered by the experimental observations reported in a Physical Review Letters article by A. Krasznahorkay (so-called ATOMKI ANOMALY). Although this is a high-risk project, signal confirmation, which would indicate physics beyond the standard model, will be crucial for all modern physics.

The project's current state is in the data analysis phase, and the results will be reported in 2023. There are three possible outcomes of the analysis:

(1) The reported effect is confirmed. Since the detection setup is different from that of ATOMKI ANOMALY, this would be an independent confirmation that would exclude uncertainties connected to the original experimental approach. In such a case, a new physics field would experience a boom and strong competition would start. It will be a meaningful confirmation (not a discovery) of the existence of a particle beyond the standard model; it seems natural to continue supporting and investing in the project, as with the beams, detectors, and workforce involved are already available, GANIL would be in a favorable position for the competition.

(2) **The reported effect is not confirmed by a significant factor.** If the collected data allows rejection of the announced effect, the collaboration publishes the negative results, adds a new exclusion zone to the systematics, and further investigations should conform to GANIL and PAC standard rules.

(3) **The experimental result is inconclusive.** In the case of a measurement that is not definitive, it should be clarified by the collaboration whether this situation is under control, given the amount of accumulated data (500 expected X-bosons/week, four weeks of data), the expected statistical error, and the statistical significance of the original claim as well as the possibility that nuclear structure effects may lead to this situation.

The SC had several observations on this effort during the meeting:

- The ratio of the possible profit, i.e., finding a light boson (the first BSM signal) - a new interaction, to the effort involved (people, even if they are not too young, money, etc...) is very favorable. We note the possible scientific profit with possible outcomes: positive: triggers all community to pursue X17; negative: new exclusion zone, further search needs reconsiderations.
- It is not clear how the project is situated among the competition. Other experimental efforts were mentioned but few details were provided.
- The decision to support the next beam campaign should be taken after the knowledge of the analysis of current results is obtained.
- The necessity and reasoning for measurements of other light systems was briefly mentioned in the presentation (J.L. Feng et al., Phys. Rev. D 102 (2021) 036016.) The plan for potential future experiments should be prepared by the collaboration that allows for changes in direction based on an informed decision from analysis of previous measurements.
- Questions on workforce issues and long term experimental support were touched upon in the presentation. While this is a rather internal organizational issue, it is possible to look for a synergy in other GANIL projects such as remote experiment control.

Ending the support for this project now might result in a loss of one year amid a very competitive environment that can be expected in the case the effect is confirmed. Realizing this, the SC recommends to continue the support for the project with respect to the following points:

- The collaboration maintains a reasonable material/financial demand;
- Workforce (students) requirements that are justified (also in the case of negative outcome of the analysis);
- The experimental equipment obtained during the project remains in GANIL

If a positive result is found for X17, the SC recommends that the collaboration **define the strategy** for the follow-up experiment(s), since GANIL may find itself in a unique position in this potentially new branch of research due to its intensive stable beams available from the LINAC, an existing, fine-tuned and tested detector system accompanied by simulation and analysis codes, and a local and international team, that has acquired the necessary experience to carry out this research.

The project has lost a key senior co-spokesperson(s) due to his retirement. GANIL may consider creating a position for a temporary/partial involvement of this person with a plan to transfer his knowledge to a young team member(s).

S³ Commissioning

The S³ spectrometer is a flagship facility of GANIL that will bring unique science capabilities at GANIL for stopped beam physics, such as laser spectroscopy and mass measurements as well as for super-heavy element research. S³ will have the combined advantage of high-resolution laser spectroscopy, Mr-ToF-MS (PILGRIM) and a high-performance alpha and conversion electron decay detector (SEASON) for the study of the ground and isomeric states of nuclei along the N=Z line and of heavy refractory elements, heavy actinides and super heavy elements. Laser spectroscopy and mass measurements of neutron deficient nuclei, especially in the vicinity of ¹⁰⁰Sn has the potential of strong scientific impact. The absence of ⁴⁸Ca beam impacts the SIRIUS experimental program, therefore the first phase science program needs to be reconsidered.

There are two detector configurations in the focal plane, the SIRIUS detector setup used mainly for heavy element decay studies and LEB for laser spectroscopy and mass measurements. The committee appreciates the SWOT analysis that was presented.

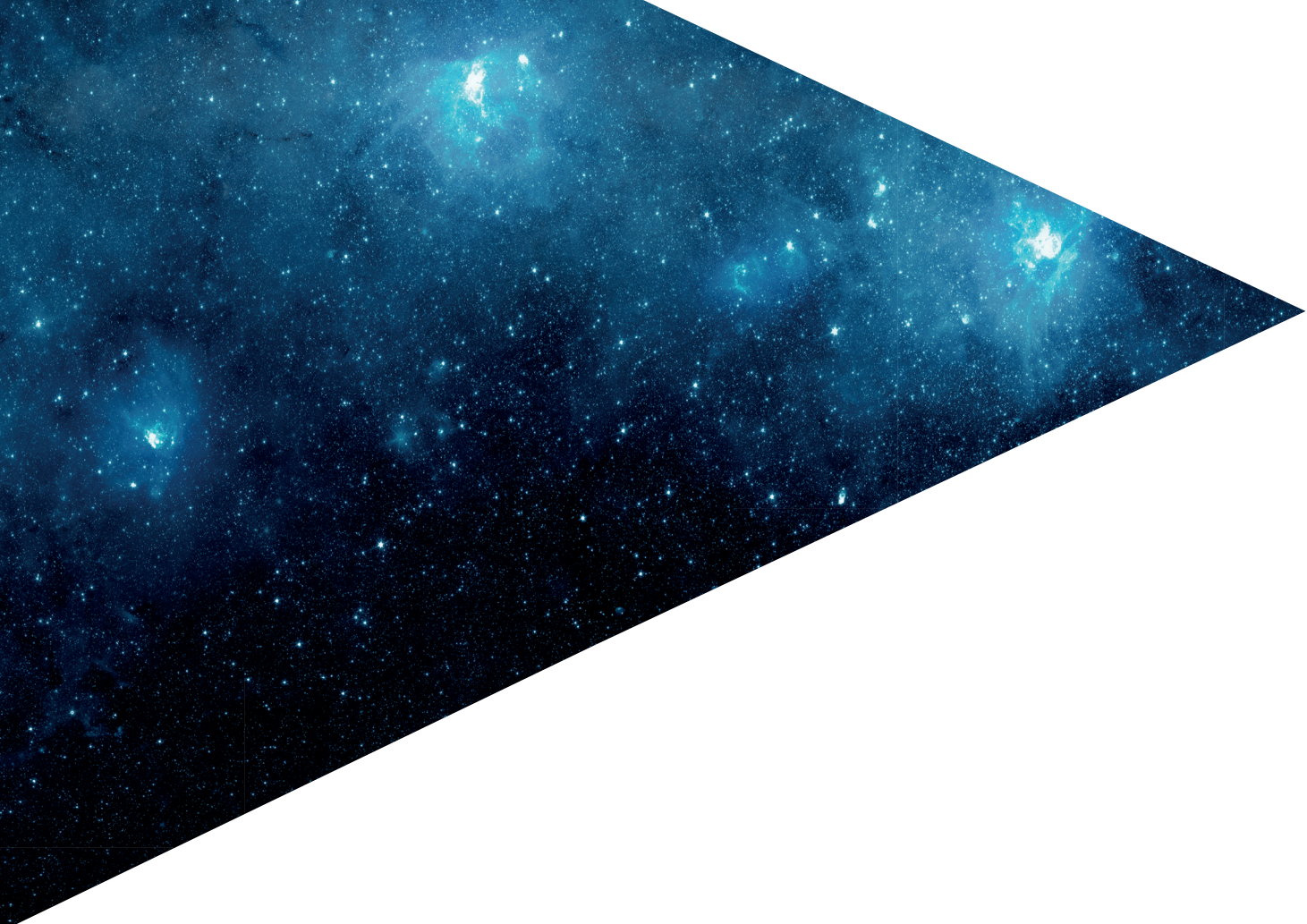
The committee has the following recommendations:

- We recommend that GANIL management prioritize a rapid commissioning of the S³ spectrometer.
- We recommend that the S³ scientific collaboration work out a plan for first exploratory physics runs simultaneously while commissioning the spectrometer and the focal plane detectors. The physics cases to be studied during commissioning should evolve through a consensus from the collaboration and should be factored into the time allotted for S³ commissioning.
- In particular, physics cases that are easily feasible from already demonstrated beams should be chosen. A list of three possible LEB experiments during commissioning was presented. The physics outcome from each needs to be specifically reviewed for international competitiveness. This was not clearly presented. One experiment each with ⁴⁰Ar and ⁵⁰Cr beams could be planned. Although the latter is expensive the structure information around ¹⁰⁰Sn will be of high scientific value.
- It was not clear if the possible commissioning experiments with SIRIUS were only to verify published results or if they will also have the potential for some new physics information, too. It is recommended that the collaboration work out a strategy for first experiments. The ²²Ne+Pt → ²¹⁶⁻²²⁰Ra → ²¹⁰⁻²¹⁴Ra has a large cross section, hence might be a simpler case to start with if sufficient new physics information can be derived.
- The standalone cryogenic plants and the cryogenic distribution lines need to be fully tested and should be very robust and trouble-free. This aspect needs to be simultaneously ensured, as stable cryogenics is critical for the operation of the spectrometer as a whole and can more often than not, derail the schedule during the commissioning phase.

IV. ORGANISATION CHART



Mise à jour du 1er juillet 2024



GANIL

BP 55027 - 14076 CAEN CEDEX 5 - FRANCE

TEL. 02 31 45 46 47 - <https://www.ganil-spiral2.eu/fr/>

Directrice de la publication : Patricia Chomaz
Directrice de la rédaction : Fanny Farget
Conception graphique : Stéphanie Pupin
Coordination éditoriale : Stéphanie Pupin et Magali Tencé

The logo for CEA (Commissariat à l'énergie atomique et aux énergies alternatives), consisting of the lowercase letters 'cea' in a serif font with a horizontal line underneath.The logo for CNRS (Centre national de la recherche scientifique), consisting of the lowercase letters 'cnrs' in a bold, sans-serif font inside a white circle.